

Final Research Report
Agreement T2695, Task 66 Liquefaction Phase III

EVALUATION OF LIQUEFACTION HAZARDS IN WASHINGTON STATE

WA-RD 668.1

Professor Steven L. Kramer
University of Washington

December 2008



Final Research Report
Agreement T2695, Task 66
Liquefaction Phase III

EVALUATION OF LIQUEFACTION HAZARDS IN WASHINGTON STATE

By

Steven L. Kramer
Professor
Department of Civil and Environmental Engineering
University of Washington, Box 352700
Seattle, Washington 98195

Washington State Transportation Center (TRAC)
University of Washington, Box 354802
1107 NE 45th Street, Suite 535
Seattle, Washington 98105-4631

Washington State Department of Transportation Technical Monitor
Tony Allen
Chief Geotechnical Engineer, Materials Laboratory

Prepared for
Washington State Transportation Commission
Department of Transportation
and in cooperation with
U.S. Department of Transportation
Federal Highway Administration

December 2008

TECHNICAL REPORT STANDARD TITLE PAGE

1. REPORT NO. WA-RD 668.1	2. GOVERNMENT ACCESSION NO.	3. RECIPIENT'S CATALOG NO.	
4. TITLE AND SUBTITLE EVALUATION OF LIQUEFACTION HAZARDS IN WASHINGTON STATE		5. REPORT DATE December 2008	
7. AUTHOR(S) Steven L. Kramer		6. PERFORMING ORGANIZATION CODE	
9. PERFORMING ORGANIZATION NAME AND ADDRESS Washington State Transportation Center (TRAC) University of Washington, Box 354802 University District Building; 1107 NE 45th Street, Suite 535 Seattle, Washington 98105-4631		8. PERFORMING ORGANIZATION REPORT NO.	
12. SPONSORING AGENCY NAME AND ADDRESS Research Office Washington State Department of Transportation Transportation Building, MS 47372 Olympia, Washington 98504-7372 Kim Willoughby, Project Manager, 360-705-7978		10. WORK UNIT NO.	
15. SUPPLEMENTARY NOTES This study was conducted in cooperation with the U.S. Department of Transportation, Federal Highway Administration.		11. CONTRACT OR GRANT NO. Agreement T2695, Task 66	
16. ABSTRACT This report describes the results of a detailed investigation of improved procedures for evaluation of liquefaction hazards in Washington State, and describes the development and use of a computer program, WSliq, that allows rapid and convenient performance of improved analyses. The report introduces performance-based earthquake engineering (PBEE) concepts to liquefaction hazard evaluation. PBEE procedures have been developed and implemented for evaluation of liquefaction potential, lateral spreading displacement, and post-liquefaction settlement. A new model for estimation of the residual strength of liquefied soil was also developed. The WSliq code was developed to have broad capabilities for evaluation of liquefaction susceptibility, liquefaction potential, and the effects of liquefaction. It provides new methods for dealing with the magnitude-dependence inherent in current procedures, and makes the common "magnitude selection" problem moot via a new multiple-scenario approach and through the use of PBEE procedures.		13. TYPE OF REPORT AND PERIOD COVERED Final Research Report	
17. KEY WORDS Earthquake engineering, liquefaction, lateral spreading, settlement, residual strength, response spectrum, performance-based engineering		14. SPONSORING AGENCY CODE	
19. SECURITY CLASSIF. (of this report) None		18. DISTRIBUTION STATEMENT No restrictions. This document is available to the public through the National Technical Information Service, Springfield, VA 22616	
20. SECURITY CLASSIF. (of this page) None		21. NO. OF PAGES	22. PRICE

DISCLAIMER

The contents of this report reflect the views of the authors, who are responsible for the facts and the accuracy of the data presented herein. The contents do not necessarily reflect the official views or policies of the Washington State Transportation Commission, Washington State Department of Transportation, or Federal Highway Administration. This report does not constitute a standard, specification, or regulation.

CONTENTS

Chapter 1 Evaluation of Liquefaction Hazards in Washington State	1
1.1 Introduction	1
1.2 Soil Liquefaction.....	2
1.2.1 Terminology.....	5
1.2.2 Background.....	6
1.3 Organization of Manual	7
Chapter 2 Earthquake Ground Motions in Washington State.....	9
2.1 Introduction	9
2.2 Earthquake Sources.....	9
2.3 Ground Motions.....	11
2.3.1 PSHA-Based Ground Motions.....	12
2.4 Implications for Liquefaction Hazard Evaluation	19
Chapter 3 Performance Requirements	20
3.1 Introduction	20
3.2 Randomness and Uncertainty	21
3.3 Treatment of Uncertainties in Liquefaction Hazard Evaluation.....	22
3.3.1 Historical Treatment	22
3.3.2 Current Treatment.....	23
3.3.2.1 PSHA-Based Loading.....	23
3.3.2.2 Resistance	24
3.3.3 Emerging Treatment	25
3.3.4 Model Uncertainty	26
3.4 The Magnitude Issue.....	26
3.4.1 Single-Scenario Approach	28
3.4.2 Multiple-Scenario Approach.....	28
3.4.3 Performance-Based Approach	29
3.4.4 Recommendations.....	29
3.5 Performance Criteria.....	30
3.5.1 Conventional Analyses	30
3.5.2 Performance-Based Analyses	31
Chapter 4 Susceptibility to Liquefaction	32
4.1 Introduction	32
4.2 Deposit-Level Susceptibility Evaluation	33
4.2.1 Liquefaction History Factor.....	34
4.2.2 Geology Factor	35
4.3.2 Compositional Factor.....	37
4.3.2 Groundwater Factor	38
4.3 Examples	39
Example 1: Sodo District, Seattle.....	39
Example 2: Andresen Road Interchange, Vancouver	40

Example 3: Capitol Boulevard Undercrossing, Olympia	41
Example 4: Yakima River Site	42
Example 5: Bone River Site.....	43
4.4 Layer-Level Susceptibility Evaluation	43
4.4.1 Boulanger and Idriss (2005)	44
4.4.2 Bray and Sancio (2006)	46
4.4.3 Discussion.....	48
4.5 Susceptibility Index	49
4.5.1 Combination of S_{BI} and S_{BS}	49
4.5.2 Effects of Parametric Uncertainty.....	50
4.6 Recommendations.....	52
4.7 Examples	53
Chapter 5 Initiation of Liquefaction	55
5.1 Introduction	55
5.2 Background	56
5.3 Required Information.....	57
5.4 Procedures	59
5.4.1 Characterization of Loading	59
5.4.2 Characterization of Resistance.....	64
5.4.2.1 SPT-Based Resistance	65
5.4.2.2 CPT-Based Resistance.....	67
5.4.3 Evaluation of Liquefaction Potential	71
5.5 Discussion	71
5.6 Recommendations.....	72
5.6.1 Single-Scenario Analyses	73
5.6.2 Multiple-Scenario Analyses.....	73
5.6.3 Performance-Based Analyses	74
5.7 Other Considerations	74
5.7.1 Behavior of Plastic Silts and Clays.....	75
5.7.2 Liquefaction of Gravelly Soils.....	75
5.7.2.1 Becker Penetrometer.....	75
5.7.2.2 Short-Interval SPT	76
5.7.2.3 Shear Wave Velocity	76
5.8 Examples	77
5.8.1 Single-Scenario Analyses	78
5.8.2 Multiple-Scenario Analyses.....	80
5.8.3 Performance-Based Analyses	82
Chapter 6 Lateral Spreading	86
6.1 Introduction	86
6.2 Background	86
6.3 Required Information.....	89
6.4 Procedures	90
6.4.1 Youd et al. (2002) Model.....	90
6.4.2 Kramer and Baska (2006) Model.....	93

6.4.3	Zhang et al. (2004) Model	95
6.4.4	Idriss and Boulanger (2008) Model	97
6.5	Discussion	98
6.6	Recommendations.....	99
6.6.1	Single-Scenario Analyses	100
6.6.2	Multiple-Scenario Analyses.....	100
6.6.3	Performance-Based Analyses	101
6.7	Other Considerations	101
6.7.1	Subsurface Deformations.....	101
6.7.2	Pore Pressure Redistribution.....	102
6.8	Examples	103
6.8.1	Single-Scenario Analyses	103
6.8.2	Multiple-Scenario Analyses.....	104
6.8.3	Performance-Based Analyses	105
Chapter 7 Post-Liquefaction Settlement.....		106
7.1	Introduction	106
7.2	Background	106
7.3	Required Information.....	109
7.4	Procedure	110
7.4.1	Determination of Cyclic Stress Ratio	111
7.4.2	Tokimatsu and Seed Model	111
7.4.3	Ishihara and Yoshimine Model.....	112
7.4.4	Shamoto et al. Model.....	113
7.4.5	Wu and Seed Model.....	115
7.5	Discussion	116
7.6	Recommendations.....	117
7.6.1	Single-Scenario Analyses	117
7.6.2	Multiple-Scenario Analyses.....	118
7.6.3	Performance-Based Analyses	118
7.7	Other Considerations	119
7.8	Examples	119
7.8.1	Single-Scenario Analyses	120
7.8.2	Multiple-Scenario Analyses.....	121
7.8.3	Performance-Based Analyses	121
Chapter 8 Residual Strength of Liquefied Soil		123
8.1	Introduction	123
8.2	Background	123
8.3	Required Information.....	130
8.4	Procedure	131
8.4.1	Idriss Model	131
8.4.2	Normalized Strength Model—Olson and Stark.....	133
8.4.3	Normalized Strength Model—Idriss and Boulanger	134
8.4.4	Kramer-Wang Hybrid Model.....	135
8.5	Discussion	136

8.6	Recommendations.....	138
8.7	Other Considerations	138
	8.7.1 Pore Pressure Redistribution.....	139
	8.7.2 High SPT Values.....	139
	8.7.3 Consideration of Uncertainty.....	140
8.8	Examples	141
Chapter 9 Discussion		142
9.1	Introduction	142
9.2	Benefits	143
9.3	Final Comments.....	144
Acknowledgments		146
References		147
Appendix A SPT Corrections.....		A-1
Appendix B Performance-Based Earthquake Engineering		B-1
Appendix C Performance-Based Procedure for Initiation of Liquefaction.....		C-1
Appendix D Probabilistic Model for Estimation of Lateral Spreading Displacement		D-1
Appendix E Performance-Based Procedure for Lateral Spreading Displace- ment		E-1
Appendix F Performance-Based Settlement Analysis		F-1
Appendix G Residual Strength of Liquefied Soil		G-1
Appendix H WSliq User’s Manual.....		H-1
Appendix I WSliq Database Update Instructions.....		I-1

FIGURES

<i>Figure</i>	<i>Page</i>
1.1	(a) Paleo-evidence of liquefaction in the form of a buried sand boil, (b) lateral spreading damage to Showa Bridge from the 1964 Niigata earthquake, (c) bearing failure of foundations for Kawagishi-cho apartment buildings in the 1964 Niigata earthquake, (d) subsidence of a waterfront area in the 1999 Turkey earthquake.....	3
1.2	Examples of liquefaction-related damage from the 1949 Olympia earthquake.....	4
1.3	Examples of liquefaction-related damage from the 1965 Seattle-Tacoma earthquake.....	4
1.4	Examples of liquefaction-related damage from the 2001 Nisqually earthquake.....	5
2.1	Main geologic provinces of Washington State.....	11
2.2	Seismic hazard curve for Seattle, Washington based on USGS National Seismic Hazard Mapping Program analyses.....	13
2.3	Seismic hazard curve for eight cities in Washington State based on USGS National Seismic Hazard Mapping Program analyses.....	14
2.4	Contour maps of peak ground acceleration for soft rock outcrop conditions: (a) 475-year return period (10 percent probability of exceedance in 50 years), and (b) 2,475-year return period (2 percent probability of exceedance in 50 years). Colored acceleration scales are in percent of gravity	15
2.5	Magnitude and distance deaggregation of 475-year peak acceleration hazard for site in Seattle, Washington.....	16
2.6	Distributions of magnitude contributing to peak rock outcrop acceleration for different return periods in Seattle, Washington (a) $T_R = 108$ years, (b) $T_R = 224$ years, (c) $T_R = 475$ years, (d) $T_R = 975$ years, (e) $T_R = 2,475$ years, and (f) $T_R = 4,975$ years.....	17
2.7	Seismic hazard curves for Seattle, Washington deaggregated on the basis of magnitude. The total hazard curve is equal to the sum of hazard curves for all magnitudes.....	18
4.1	Transition from sand-like to clay-like behavior with plasticity index for fine-grained soils.....	45
4.2	Relationship between S_{BI} and Boulanger and Idriss (2005) transition zone boundaries.....	46
4.3	Ranges of w_c/LL and plasticity index for various susceptibility categories according to Bray and Sancio (2006).....	47
4.4	Illustration of variation of S_{BS} with plasticity index and w_c/LL ratio based on Equation 4.2.....	48

4.5	Variation of SI based on equal weighting of Boulanger-Idriss and Bray-Sancio susceptibility models. Effects of parametric uncertainty not included.....	51
5.1	Variation of magnitude scaling factor with earthquake magnitude for NCEER and Idriss and Boulanger models.....	62
5.2	Subsurface profile for idealized site	78
5.3	Variation of FS_L with depth for NCEER, Idriss-Boulanger, and Cetin et al. procedures, assuming mean and modal magnitudes for 475-year peak ground acceleration.....	79
5.4	Variation of FS_L with depth for Idriss-Boulanger procedure at different locations in Washington State, assuming mean magnitudes for 475-year peak ground acceleration	80
5.5	Variation of FS_L with depth for NCEER, Idriss-Boulanger, and Cetin et al. procedures using multiple-scenario approach for 475-year peak ground acceleration.....	81
5.6	Variation of FS_L with depth for Idriss-Boulanger procedure at different locations in Washington State using multiple-scenario approach for 475-year peak ground acceleration	82
5.7	Factor of safety hazard curves for various depths in hypothetical soil profile located in Seattle	83
5.8	Variation of 475-year factor of safety with depth for hypothetical soil profile located in Seattle	84
5.9	Variation of return period of liquefaction with depth for hypothetical soil profile located in Seattle	84
5.10	Variation of return period of liquefaction with depth for hypothetical soil profile at different locations within Washington State	85
6.1	Slope geometry notation	91
6.2	Variation of maximum cyclic shear strain with factor of safety and relative density	96
6.3	Variation of limiting strain with SPT resistance and variation of maximum shear strain with SPT resistance and cyclic stress ratio.....	98
6.4	Subsurface profile for idealized site	103
6.5	Lateral spreading hazard curve for hypothetical soil profile located in Seattle.....	105
7.1	Variation of volumetric strain with corrected SPT resistance and cyclic stress ratio	108
7.2	Variation of volumetric strain with relative density, SPT and CPT resistance, and factor of safety against liquefaction	108
7.3	Variation of maximum residual volumetric strain with corrected SPT resistance and cyclic stress ratio for clean sands	109
7.4	Variation of volumetric strain with corrected SPT resistance and cyclic stress ratio	109

7.5	Variation of maximum residual volumetric strain with corrected SPT resistance and cyclic stress ratio for sands with 10 percent fines.....	115
7.6	Variation of maximum residual volumetric strain with corrected SPT resistance and cyclic stress ratio for sands with 20 percent fines.....	115
7.7	Subsurface profile for idealized site	120
7.8	Seismic hazard curve for post-liquefaction settlement	122
8.1	Estimation of residual strength from SPT resistance.....	126
8.2	Estimation of residual strength from SPT resistance.....	127
8.3	Estimation of residual strength ratio from SPT resistance	128
8.4	Estimation of residual strength ratio from SPT resistance	129
8.5	Variation of residual strength ratio with SPT resistance and initial vertical effective stress using Kramer-Wang model.....	130
8.6	Comparison of back-calculated residual strengths with residual strength values predicted by (a) Idriss model, (b) Olson-Stark model, and (c) deterministic hybrid model	137
8.7	Probability density functions for residual strength: (a) different uncertainties in SPT resistance, and (b) different uncertainties in initial vertical effective stress.....	138
8.8	Hypothetical soil profile for residual strength calculation	141
8.9	Variation of computed residual strength with depth for hypothetical soil profile.....	141

TABLES

<i>Table</i>	<i>Page</i>
2.1	USGS peak acceleration (soft rock outcrop) and deaggregated magnitude data for various sites in Washington State..... 19
3.1	Advantages, disadvantages, and recommended use of different analysis approaches 30
4.1	Characterization of overall site susceptibility to liquefaction hazards 33
4.2	Historical observation factors 34
4.3	Past seismicity history factors..... 34
4.4	Geologic classification factors..... 36
4.5	Classification quality factors 37
4.6	(a) gradation factors, (b) particle shape factors, (c) fines content factors, (d) fines plasticity factors, (e) water content factors, and (f) impermeable cap factors 38
4.7	Groundwater factors 39
5.1	Calculation of magnitude scaling factor by methods of NCEER and Idriss and Boulanger. Cetin/Moss models do not make use of magnitude scaling factor 61
5.2	Coefficients for estimation of peak ground surface acceleration amplification factor 63
5.3	Depth correction factor calculation..... 64
5.4	Clean sand SPT value calculation..... 66
5.5	Calculation of cyclic resistance ratio at 1 atm 66
5.6	Calculation of overburden stress correction factor, K_{σ} 67
5.7	Calculation of overburden stress adjustment factor, C_N 68
5.8	Calculation of fines correction factor, K_c 69
5.9	Calculation of cyclic resistance ratio at 1 atm vertical effective stress ... 70
5.10	Calculation of overburden stress correction factor, K_{σ} 70
6.1	Recommended range of variable values for the Youd et al. (2002) predictive equation..... 92
6.2	Coefficients for Youd et al. (2002) model 92
6.3	Fines content correction variables 93
6.4	Recommended range of variable values for the predictive equation..... 94
6.5	Coefficients for Kramer and Baska (2006) model..... 95
6.6	Default weighting factors for lateral spreading models in W_{slq} 100
6.7	Computed lateral spreading displacements for various scenarios, assuming mean and modal magnitudes and distances associated with 475-year Seattle <i>PGA</i> values 104

6.8	Computed lateral spreading displacements for multiple-scenario magnitudes and distances associated with 475-year Seattle <i>PGA</i> values	104
6.9	Computed lateral spreading displacements of 475-yr and 975-yr hazard levels from performance-based lateral spreading analysis	105
7.1	Default weighting factors for post-liquefaction settlement models in <i>W_{sliq}</i>	118
7.2	Computed post-liquefaction settlements for various scenarios assuming mean and modal magnitudes and distances associated with 475-year Seattle <i>PGA</i> values.....	120
7.3	Computed post-liquefaction settlements for multiple-scenario magnitudes associated with 475-year Seattle <i>PGA</i> values	121
7.4	Computed post-liquefaction settlements for various scenarios associated with 475-year and 975-year ground motions	122
8.1	Variation of fines content correction with fines content.....	132
8.2	Weighting factors for residual strength estimation.....	138

Chapter 1

Evaluation of Liquefaction Hazards in Washington State

1.1 INTRODUCTION

This Manual is intended to provide the Washington State Department of Transportation (WSDOT) with guidance on the most practical, reliable, and consistent methods for evaluating liquefaction hazards in Washington State. It is the result of an ongoing research project conducted at the University of Washington under the direction of Prof. Steven L. Kramer, and represents the combined efforts of Prof. Kramer and several of his graduate students over an extended period of time. Through Prof. Kramer's involvement with the Pacific Earthquake Engineering Research (PEER) Center, several important topics in this Manual also reflect the efforts of PEER researchers. The approach to the entire research project has been to obtain and/or develop, as efficiently as possible, the best possible information on which to base recommended procedures for evaluation of liquefaction hazards.

The Manual is accompanied by a software package, the WSDOT Liquefaction Hazard Evaluation System, which will be hereafter referred to as WSliq. The WSliq program is a unique computational tool that allows users to perform multiple sophisticated analyses with less effort than is currently expended on less sophisticated, less accurate, and less consistent analyses. The program implements several new methods of analysis developed at the University of Washington under WSDOT support and a number of widely used existing methods of analysis. The Manual provides recommendations on how to use each of these analyses, but the WSliq program allows the user to combine their results in a manner that allows the attributes of each to be realized.

The WSliq program comes with a built-in database of earthquake ground motion hazards across Washington State. By entering the latitude and longitude of any site, the

program will automatically compute ground motion hazard data, including relevant deaggregation data, produced by U.S. Geological Survey probabilistic seismic hazard analyses. The program also provides mechanisms for expanding and/or updating the ground motion hazard database. These analyses consider all major earthquake sources (i.e., faults or other source zones), the rates of recurrence of all possible magnitude earthquakes from those sources, the distributions of potential earthquake locations, and the distributions of the resulting ground motions. WSliq allows users to utilize this information in the manner commonly applied in practice, but also in more advanced ways that produce substantially more consistent estimates of actual liquefaction hazards than conventional procedures. This capability is unique and represents an important step forward in the practice of liquefaction hazard evaluation.

1.2 SOIL LIQUEFACTION

Liquefaction is a term used to describe a range of phenomena in which the strength and stiffness of a soil deposit are reduced as a result of the generation of porewater pressure. While it is possible for liquefaction to be caused by static loading, it is most commonly induced by earthquakes. Liquefaction occurs most commonly in loose, saturated, clean to silty sands but has also been observed in gravels and non-plastic silts. Failures with characteristics similar to liquefaction failures have been observed in low-plasticity silty clays. Liquefaction can produce damage ranging from small slumps and lateral spreads to massive flow slides with displacements measured in tens of meters. It can cause foundations and retaining structures to settle and/or tilt, or can tear them apart through large differential displacements.

Liquefaction has occurred in numerous earthquakes and has left its mark in the geologic and historical record. Evidence of past liquefaction (Figure 1.1a), termed paleoliquefaction, has been used to evaluate seismic hazards in areas where instrumental and historical data are sparse. The subject of liquefaction came to the forefront of geotechnical earthquake engineering with the 1964 earthquakes in Niigata, Japan, and Alaska. In Niigata, liquefaction caused lateral spreading (Figure 1.1b) and loss of bearing capacity (Figure 1.1c). More recently, strong earthquakes in California, such as

Loma Prieta (1989) and Northridge (1994), Japan (1995), Turkey (1999), and Taiwan (1999) have provided additional evidence of the damaging effects of liquefaction (Figure 1.1d).

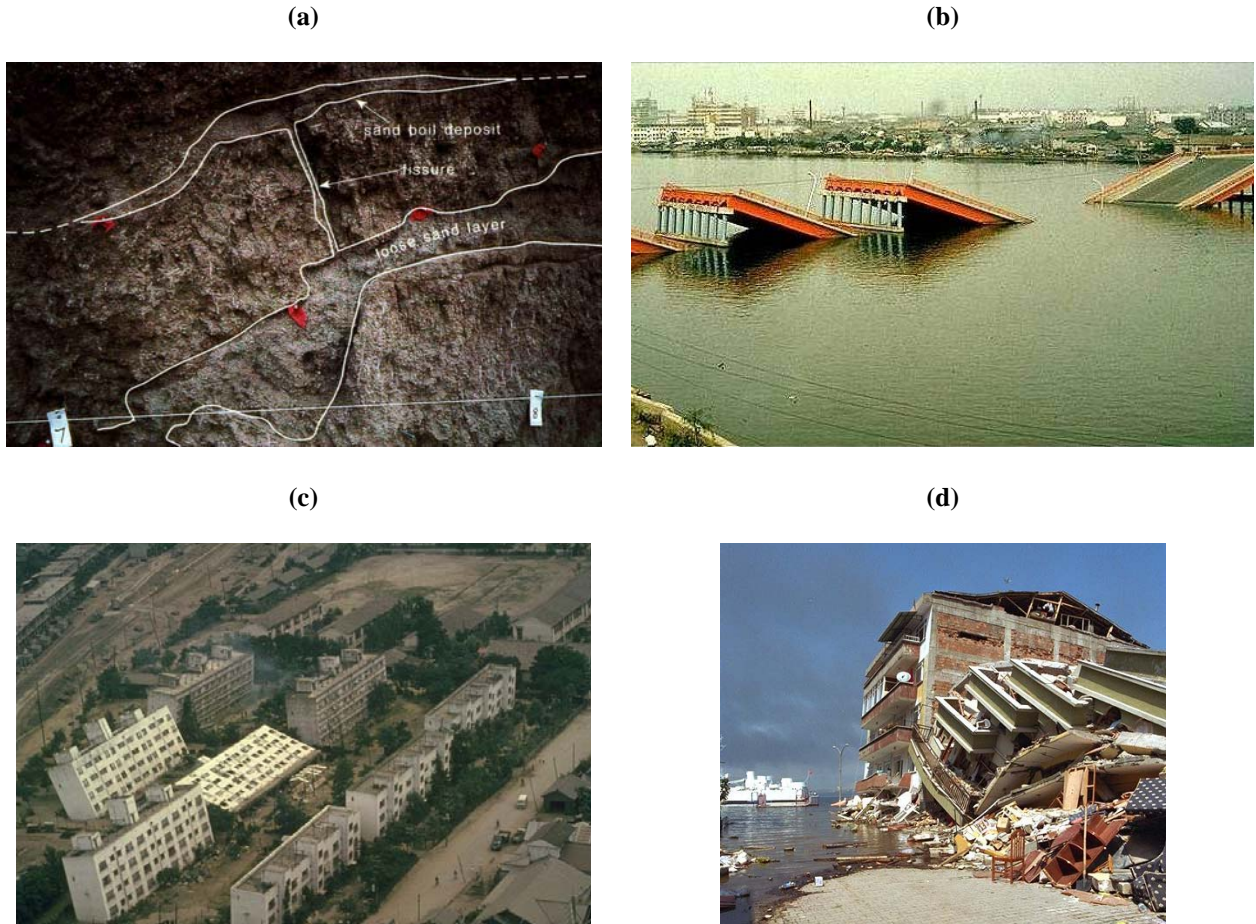


Figure 1.1 (a) Paleo-evidence of liquefaction in the form of a buried sand boil, (b) lateral spreading damage to Showa Bridge from the 1964 Niigata earthquake, (c) bearing failure of foundations for Kawagishi-cho apartment buildings in the 1964 Niigata earthquake, (d) subsidence of a waterfront area in the 1999 Turkey earthquake.

Liquefaction has also been observed in Washington state in previous earthquakes, including earthquakes that did not produce exceptionally strong ground motions. Figure 1.2 shows examples of liquefaction effects in the 1949 Olympia earthquake. At Pier 66, this earthquake resulted in the seaward displacement of the transit shed by up to about 9 inches. Retaining walls were also observed to have tilted and moved along the Duwamish waterway and in other areas south of downtown Seattle.



Figure 1.2 Examples of liquefaction-related damage from the 1949 Olympia earthquake.

The 1965 Seattle-Tacoma ($M_w = 6.5$) earthquake also caused liquefaction at a number of locations within the Puget Sound region (Figure 1.3). Breaks in water lines due to lateral soil movements were observed near Piers 64 through 66 in Seattle and in other areas. The fact that this type of damage occurred under the moderate levels of ground shaking levels produced by this earthquake underscores the high liquefaction hazards that exist in the Puget Sound region.



Figure 1.3 Examples of liquefaction-related damage from the 1965 Seattle-Tacoma earthquake.

The 2001 Nisqually earthquake caused liquefaction in locations from Olympia to Seattle. Figure 1.4 shows examples of lateral spreading damage in Olympia and Tumwater. The fact that the photos on the left sides of Figures 1.3 and 1.4 look similar is not coincidental: liquefaction occurred at the same location in both the 1965 Seattle-Tacoma and 2001 Nisqually earthquakes.



Figure 1.4 Examples of liquefaction-related damage from the 2001 Nisqually earthquake.

1.2.1 Terminology

The basic mechanisms that produce liquefaction behavior can be divided into two main categories. Flow liquefaction can occur when the shear stresses required to maintain static equilibrium of a soil mass is greater than the shear strength of the soil in its liquefied state. If liquefaction is triggered by earthquake shaking, the inability of the liquefied soil to resist the required static stresses can cause large deformations, or flowslides, to develop. The second mechanism, cyclic mobility, occurs when the initial static stresses are less than the shear strength of the liquefied soil and happens more frequently than flow liquefaction. Cyclic mobility leads to incremental deformations that develop during earthquake shaking; the deformations may be small or quite large, depending on the characteristics of the soil and the ground shaking. In the field, cyclic mobility can produce lateral spreading beneath even very gentle slopes and in the vicinity of free surfaces such as river beds.

1.2.2 Background

In all cases, there are three primary aspects of a liquefaction hazard evaluation. It is frequently helpful to think of them in terms of three questions that a geotechnical engineer must answer in order to complete the evaluation. In proper order, the questions are as follows:

1. *Is the soil susceptible to liquefaction?* Some soils are susceptible to liquefaction and others are not. If the answer to this question is no, liquefaction hazards do not exist and the liquefaction hazard evaluation is complete. If the answer is yes, the geotechnical engineer must move on to the next question.
2. *Is the anticipated loading sufficient to initiate liquefaction?* In some areas, the seismicity is low enough that the anticipated level of ground shaking is not strong enough to trigger liquefaction. If that is the case, the answer to this question is no, and the liquefaction hazard analysis is complete. If the anticipated level of shaking is strong enough to trigger liquefaction, however, the geotechnical engineer must answer yes to this question and move on to the next question.
3. *What will the effects of liquefaction be?* Liquefaction can affect the nature of ground shaking and can cause flow slides, lateral spreading, settlement, and other problems. It is important to recognize, however, that initiation of liquefaction does not necessarily mean that severely damaging effects will occur. The majority of the effort expended in this project, in fact, has been directed toward developing procedures for estimating the effects of liquefaction more accurately and reliably.

This three-part approach – susceptibility, initiation, and effects – to the problem of liquefaction hazard evaluation is reflected in the manner in which the research has been performed, and the manner in which this Manual and the WSliq program are organized.

1.3 ORGANIZATION OF MANUAL

The Manual comprises nine chapters, the first three of which present background material that supports the more technical, problem-focused topics of the next five chapters. The final chapter presents a summary and some concluding comments.

Chapter 2 presents a brief description of the seismicity of Washington State and of the resulting ground motion hazards; the focus of the chapter is on factors that influence soil liquefaction. Chapter 3 presents a discussion of performance requirements and the various factors that define and influence “performance” from the standpoint of liquefaction. The nature of uncertainties, the manner in which they are handled in current practice, and an emerging manner in which they can more consistently and accurately be handled are also described.

Chapters 4 through 8 contain the “meat” of the Manual and the research it describes. These chapters deal with the previously described questions of liquefaction susceptibility, initiation, and effects. Chapter 4 presents new procedures for evaluating the susceptibility of a soil to liquefaction based on historical, geologic, compositional, and groundwater criteria. The procedures result in the assignment of a numerical susceptibility rating factor, which can be used to compare, rank, and prioritize different sites. Chapter 5 describes procedures to evaluate the potential for initiation of liquefaction under different assumed loading conditions and presents recommendations for WSDOT practice in this area, both in the short- and long-term.

Chapters 6 through 8 deal with the effects of liquefaction. Chapter 6 covers lateral spreading, Chapter 7 covers post-liquefaction settlement, and Chapter 8 covers the residual strength of liquefied soil. Chapters 6 through 8 are organized similarly in that three approaches – single-scenario, multiple-scenario, and performance-based – to the problem of interest are presented in each. Chapter 9 summarizes the Manual and presents some concluding comments.

This Manual is accompanied by a computer program, WSliq, that implements the various analyses described herein. WSliq is also organized according to the susceptibility-initiation-effects paradigm and allows analyses to be performed in three different ways. The first, single-scenario analysis, represents the type of analysis most

commonly used in contemporary geotechnical earthquake engineering practice. The second, multiple-scenario analysis, integrates response over the many magnitudes (and, in some cases, distances) that contribute to ground motion hazard at a given location; multiple-scenario analyses eliminate the controversy of “which magnitude” to use in current, single-scenario analyses. The third, performance-based analysis, fully integrates the results of a probabilistic seismic hazard analysis with a probabilistic response analysis. This type of analysis is new to geotechnical earthquake engineering, but it represents the future of practice in this field. It has numerous important advantages, primary among which is the ensurance of consistent performance levels across regions of variable seismicity. This is particularly important for Washington State, in which consistent application of conventional procedures is shown to produce highly inconsistent (particularly along the Pacific Coast) actual liquefaction hazards. The technical bases for the various performance-based analyses described in chapters 6 through 8 are described in a series of appendices. A user’s manual for the WSliq program is also presented in an appendix.

Chapter 2

Earthquake Ground Motions in Washington State

2.1 INTRODUCTION

Washington State lies in an active and complex tectonic region about which much has been learned in the past 20 years and about which more will likely be learned in the near future. The level of seismic activity varies dramatically across the state, from high in the west to low in the east. Furthermore, the Pacific coast of Washington is subject to extremely large ($M > 9$) earthquakes, the likes of which are not even possible in other areas of the conterminous United States, including California.

The Washington State Department of Transportation (WSDOT) is responsible for the design, construction, operation, and maintenance of bridges, roads, and other facilities across the entire state. As stewards of the public trust, it is obligated to spend available resources in a manner that produces *the highest and most uniform level of safety possible for all citizens*. Achieving this goal requires an understanding of ground shaking hazards across the entire state.

This chapter provides a brief review of ground motion hazards across Washington State, with emphasis on those characteristics that affect soil liquefaction. It is not intended, and should not be viewed, as a comprehensive description of ground motion hazards in Washington. Its purpose is to provide background information for the liquefaction hazard evaluation procedures described in subsequent chapters and a context within which to better understand the new performance-based liquefaction hazard evaluation procedures described in those chapters.

2.2 EARTHQUAKE SOURCES

The seismicity of Washington State is dominated by two primary tectonic processes. The state lies on the North American plate, which is composed of a series of “blocks” that experience similar modes of movement. Northward movement of the

Sierra Nevada block in northern California produces north-south compression in much of Washington, which is bounded to the north by the relatively stationary British Columbia block. To the west, the Juan de Fuca plate is moving eastward and subducting beneath the North American plate. These movements produce a complex set of stress conditions – north-south compression in the upper crust transitioning to east-west compression at depth – and a correspondingly complex pattern of seismicity.

Figure 2.1 shows the main geologic provinces of Washington State. The Northern Washington Pre-Tertiary Highlands has many faults but negligible evidence that any are active (in Quaternary time). The largest known crustal earthquake in the state, however, occurred in a sparsely populated region (probably near Lake Chelan) in 1872. The Columbia basin province in southern and southeastern Washington has a number of Quaternary faults in the Yakima fold belt, along the Washington-Oregon border, and in the southeastern corner of the state. The faults in this province are, relative to western Washington, relatively small and dormant but are important for certain critical facilities located in that region. The Cascade Volcano arc produces some seismicity associated with volcanic activity, particularly in the vicinities of Mt. St. Helens and Mt. Rainier, but evidence for surface-rupturing earthquakes has not been found in either zone. As a result, the Cascade Volcano arc does not contribute significantly to ground motion hazards in Washington State.

The remaining three provinces are all affected by the Cascadia Subduction Zone, the 1,100-km-long boundary between the subducting Juan de Fuca plate and the overlying North American plate. Subduction zones are known to produce the largest earthquakes, known as interplate earthquakes, in the world; the Cascadia Subduction Zone is now known to have produced at least six great earthquakes (i.e., magnitudes likely greater than 9) in the past 3,500 years. Large magnitude earthquakes are particularly notable with respect to liquefaction hazards because the process by which liquefaction occurs is sensitive to ground motion duration, which increases with increasing magnitude. The Cascadia Subduction Zone also produces intraplate earthquakes expressed as extensional (normal faulting) events in the portion of the Juan de Fuca plate to the east (and hence deeper) than the portion involved in interplate events. The 1949 Olympia, 1965 Seattle-Tacoma, and 2001 Nisqually earthquakes are examples

of intraplate earthquakes; all were relatively large events (magnitudes of 6.5 to 7.1) but occurred so deep (about 40-60 km) that ground shaking levels were only moderately strong. Nevertheless, each of these events did produce liquefaction and damage to constructed facilities. The Puget Lowland is also known to be traversed by a number of shallow crustal faults, the number, location, and seismicity of which much is currently being learned. The best-known of these is the Seattle Fault, which runs in an east-west direction from Bainbridge Island, through Seattle, and into the Cascade foothills, and is now known to have produced several large, shallow earthquakes, most recently about 1,100 years ago.

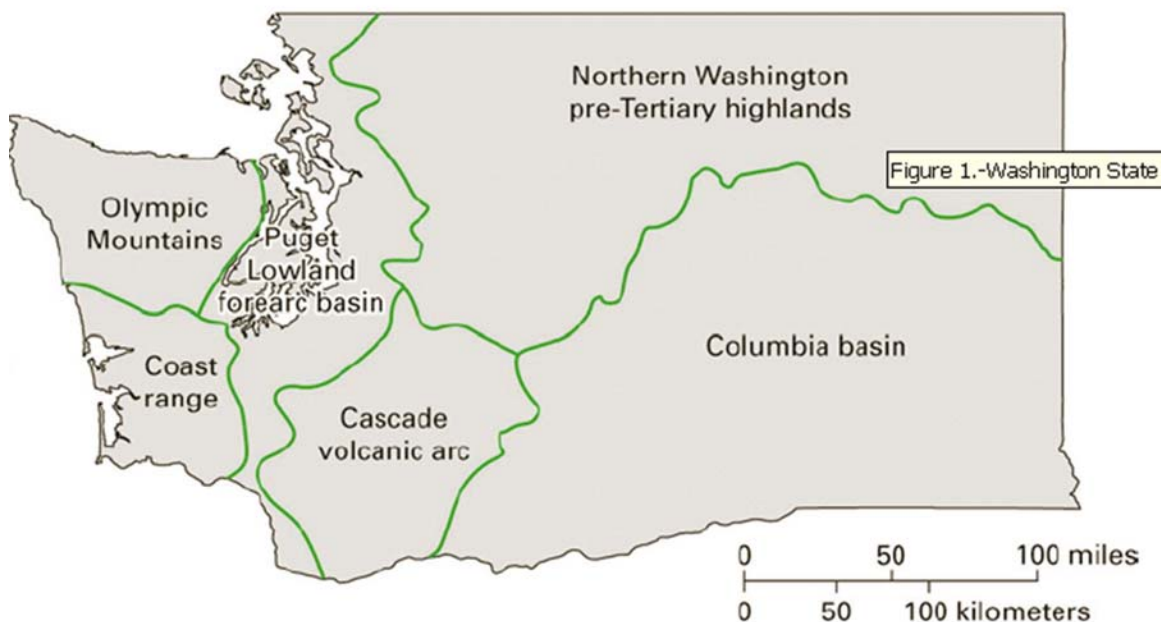


Figure 2.1. Main geologic provinces of Washington State (Lidke et al., 2003)

2.3 GROUND MOTIONS

The sources described in the preceding section are all capable of producing earthquakes of various magnitudes. Small (low magnitude) earthquakes are known to occur more frequently than large (high magnitude) earthquakes, but different faults produce earthquakes of different sizes at different rates. Attempts at actually predicting earthquakes have not been successful, so seismologists and engineers use knowledge of fault locations and historical seismicity with probabilistic analyses to predict expected

levels of shaking from future earthquakes – these methods are probabilistic seismic hazard analyses (PSHAs)

2.3.1 PSHA-Based Ground Motions

In a typical PSHA (Cornell, 1968), earthquake sources are identified and characterized with respect to their geometries (i.e., probability distributions of source-to-site distance), earthquake generation potentials (i.e., probability distributions of earthquake magnitudes), and seismicities (i.e., rates of recurrence of earthquakes of various magnitudes). The probability distributions of potential ground motion for all possible combinations of magnitude and distance are described by means of attenuation relationships. Details of the PSHA process are available in Kramer (1996) and McGuire (2004).

By combining the uncertainties in magnitude, distance, and ground motions (for some combination of magnitude and distance) with uncertainties in recurrence rates for all sources capable of affecting a particular site, a relationship between ground motion levels and the mean annual rates at which those ground motion levels are exceeded can be described. Graphically, this information is described in terms of a seismic hazard curve, an example of which is shown in Figure 2.2. Loading associated with some desired probability of exceedance can be specified. For example, loading with 10 percent probability of exceedance in a 50-year period can be shown (with common assumptions) to have a mean annual rate of exceedance (λ_{PGA}) of 0.0021 year^{-1} , or a return period, $T_R = 1/\lambda_{PGA} = 475 \text{ years}$. For the seismic hazard curve shown in Figure 2.2, the *PGA* with that hazard level is 0.330 g. Specifying loading in this way produces a more uniform means of describing earthquake loading than previous scenario-based analyses. In effect, the PSHA considers *all* possible scenarios and weights the contribution of each according to its relative likelihood of occurrence.

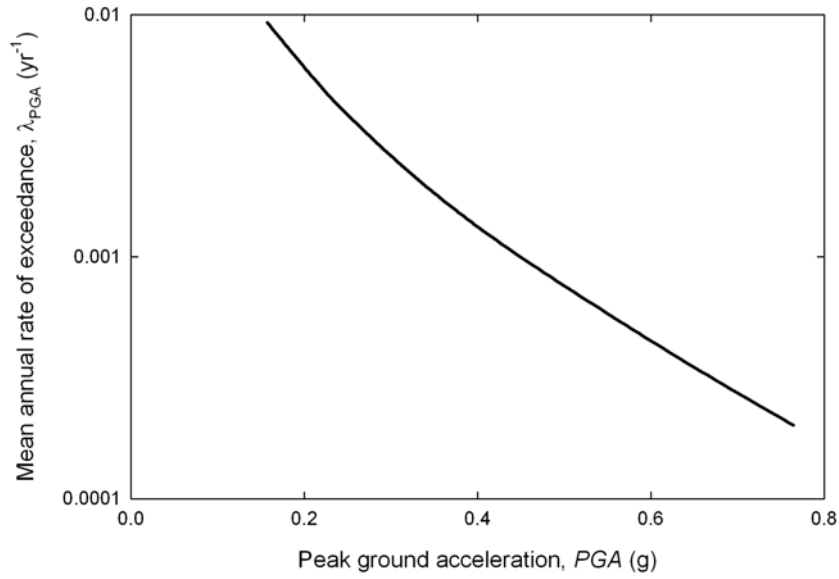


Figure 2.2. Seismic hazard curve for Seattle, Washington based on USGS National Seismic Hazard Mapping Program analyses.

By virtue of their different locations relative to active seismic sources and the different earthquake-generating characteristics of those sources, seismic hazard curves vary dramatically across Washington. As would be expected, the mean annual rate of exceeding a particular level of shaking is higher in the western part of the state than the central and eastern parts. Figure 2.3 shows seismic hazard curves for peak ground acceleration in eight selected cities across the state. The curves show that the peak ground acceleration with a 0.0021 yr^{-1} mean annual rate of exceedance (or a return period of 475 years) would range from 0.07 g in Spokane to 0.33 g in Seattle. Put differently, the peak acceleration with a 10 percent probability of being exceeded in a 50-year period is 0.33 g in Seattle but only 0.07 g in Spokane; a PGA -sensitive structure in Seattle would have to be built nearly 5 times stronger than one in Spokane to produce the same level of seismic risk.

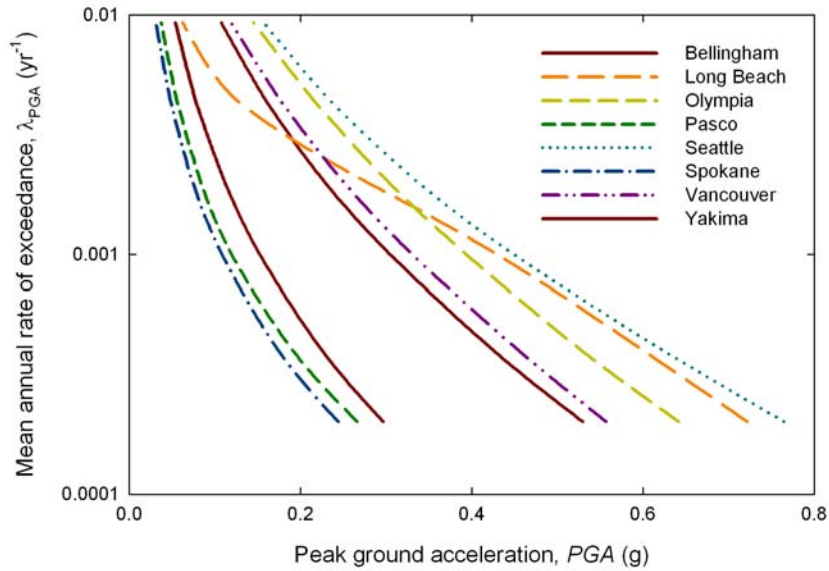


Figure 2.3. Seismic hazard curve for eight cities in Washington State based on USGS National Seismic Hazard Mapping Program analyses.

By performing PSHAs at points on a grid across some geographic region, contour maps of selected ground motion parameters with a given period can be drawn. Figure 2.4 shows contours of peak ground acceleration across Washington State for return periods of 475 years (10 percent probability of exceedance in a 50-year period) and 2,475 years (2 percent probability of exceedance in 50 years). Such maps reflect local and regional seismicity; only a cursory examination is required to confirm that the peak acceleration values are much higher in western Washington than in the central and eastern parts of the state. The 2,475-year peak acceleration values can also be seen to be higher than the 475-year values (stronger motions can be expected to occur in the longer return period), but, less obviously, the ratio between the two is higher on the coast than farther inland. The latter observation results from the differences in recurrence rates for the coastal and inland sources and shows that *complete characterization of ground motion potential requires consideration of motions at all return periods.*

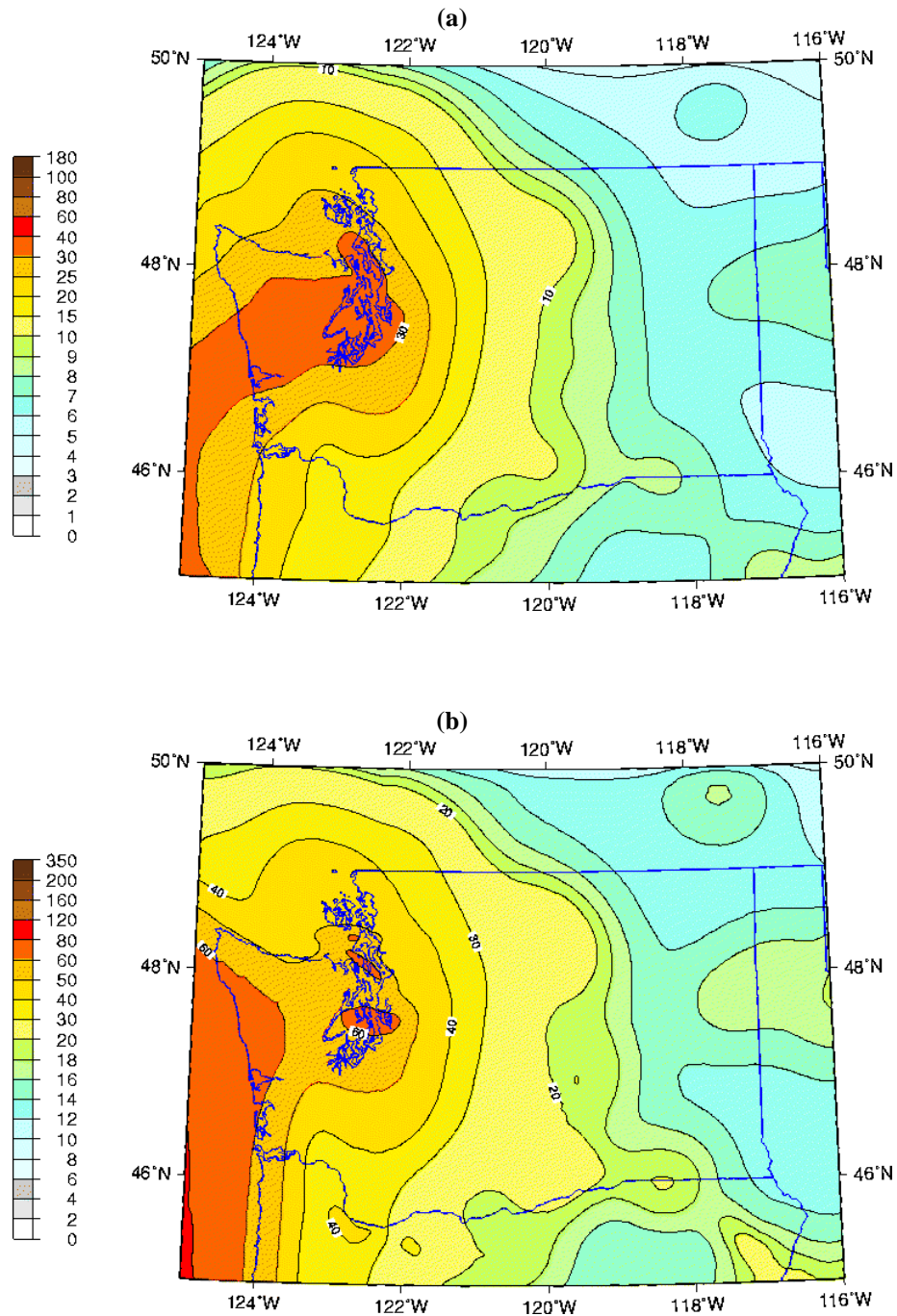


Figure 2.4. Contour maps of peak ground acceleration for soft rock outcrop conditions: (a) 475-year return period (10 percent probability of exceedance in 50 years), and (b) 2,475-year return period (2 percent probability of exceedance in 50 years). Colored acceleration scales are in percent of gravity.

A seismic hazard curve represents the aggregate contributions of all possible combinations of magnitude and distance from all sources, each weighted by their relative likelihoods of occurrence – in essence, all feasible scenarios (instead of just one) are

considered. This is a particularly important departure from scenario-based practice for liquefaction hazard evaluation because there is no single magnitude or distance associated with a given level of ground motion; rather, the ground motion is affected by a distribution of magnitudes and distances. The ground motion level is affected by multiple scenarios, the relative contributions of which can be quantified by means of a deaggregation analysis. Figure 2.5 shows a USGS deaggregation plot for *PGA* in Seattle for a mean return period of 475 years; the heights of the columns in the figure illustrate the relative contributions of each magnitude-distance combination to the 475-year peak acceleration of 0.33 g. The distribution of magnitude values contributing to peak acceleration is particularly important for liquefaction hazard evaluations because magnitude is taken as a proxy for duration in the most commonly used procedures for evaluation of liquefaction potential.

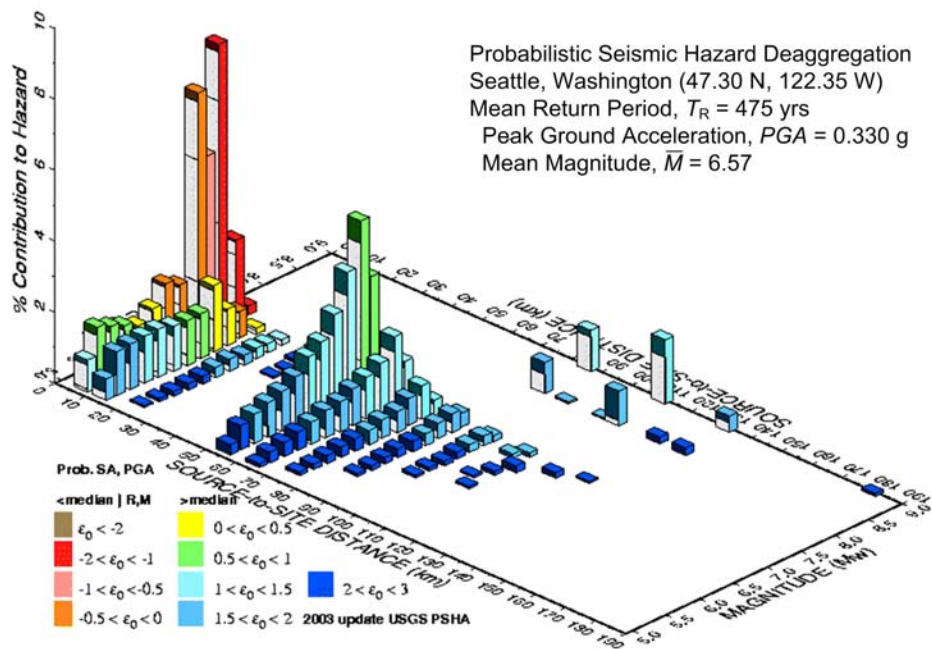


Figure 2.5. Magnitude and distance deaggregation of 475-year peak acceleration hazard for site in Seattle, Washington.

By integrating the results of a deaggregation analysis over all distances, a marginal distribution of magnitude can be constructed. This distribution shows the relative contributions of all magnitudes to the computed hazard. Figure 2.6 shows such

distributions for six return periods at the Seattle site; the distributions of magnitude can be seen to vary with return period. Given that liquefaction is sensitive to ground motion duration, which is correlated to magnitude, *complete characterization of ground motion potential requires consideration of all magnitudes at all return periods* for evaluation of liquefaction hazards.

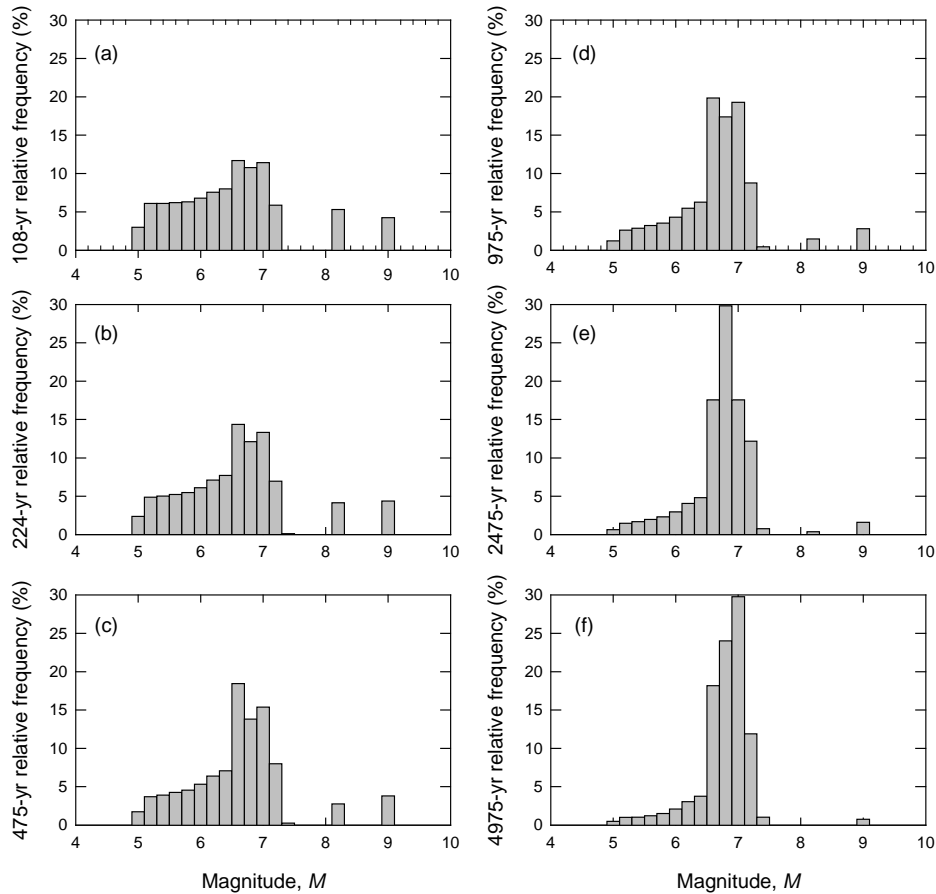


Figure 2.6. Distributions of magnitude contributing to peak rock outcrop acceleration for different return periods in Seattle, Washington (a) $T_R = 108$ years, (b) $T_R = 224$ years, (c) $T_R = 475$ years, (d) $T_R = 975$ years, (e) $T_R = 2,475$ years, and (f) $T_R = 4,975$ years.

Since the *PGA* values at each return period result from contributions from earthquakes of different magnitude, the *PGA* hazard curve can be broken down into contributions from different magnitudes. This allows magnitude deaggregation data to be displayed in a different way: as a series of magnitude-dependent hazard curves, the sum of which is equal to the total hazard curve, as shown in Figure 2.7.

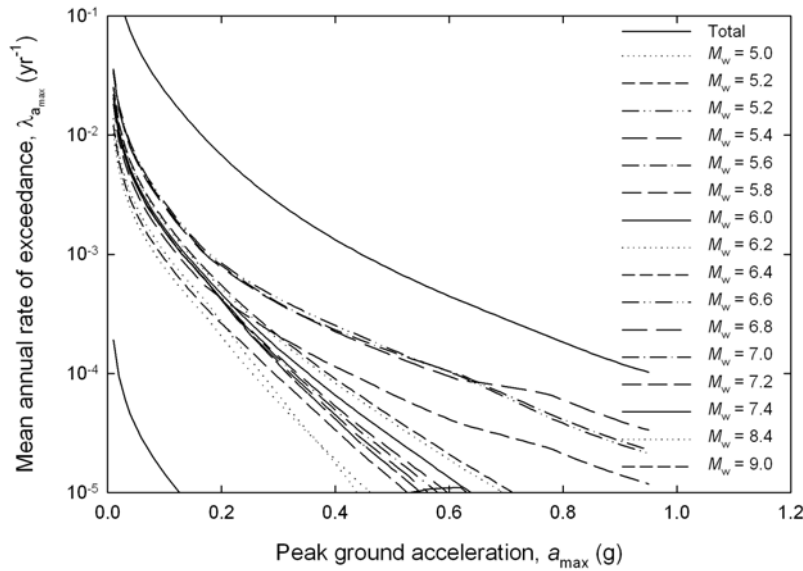


Figure 2.7. Seismic hazard curves for Seattle, Washington deaggregated on the basis of magnitude. The total hazard curve is equal to the sum of hazard curves for all magnitudes.

Because different sources are capable of producing earthquakes of different magnitudes, the type of distributions shown in figures 2.6 and 2.7 will vary across the state. Table 2.1 shows mean magnitudes for 475-year and 2,475-year return periods for the cities for which hazard curves are shown in Figure 2.2. Note that although the mean magnitudes are generally higher in the west than in the east because of the presence of the Cascadia Subduction Zone along the coast, the locations with highest mean magnitudes do not necessarily correspond to the locations with highest *PGAs*. For example, Seattle has a *PGA* of 0.330 g and mean magnitude of 6.57, while the coastal city of Long Beach has a lower *PGA* (0.266 g) but a higher mean magnitude (8.37). Because of the manner in which duration effects are accounted for in typical liquefaction analyses, the 475-year level of loading in Long Beach is actually *greater* than that in Seattle from the standpoint of liquefaction potential.

Table 2.1. USGS peak acceleration (soft rock outcrop) and deaggregated magnitude data for various sites in Washington State.

Location	Coordinates		$T_R = 475$ yrs		$T_R = 2,475$ yrs	
	Lat	Long	PGA (g)	\bar{M}	PGA (g)	\bar{M}
Bellingham	48.78	-122.40	0.223	6.40	0.424	6.39
Long Beach	46.35	-124.06	0.266	8.37	0.598	8.61
Olympia	47.04	-122.90	0.297	6.77	0.526	6.81
Pasco	46.25	-119.13	0.082	6.08	0.190	6.11
Seattle	47.62	-122.35	0.330	6.57	0.621	6.67
Spokane	47.67	-117.41	0.072	5.88	0.173	5.91
Vancouver	48.64	-122.64	0.246	6.49	0.453	6.51

2.4 IMPLICATIONS FOR LIQUEFACTION HAZARD EVALUATION

The seismo-tectonic environment of Washington is varied and complex, which results in a wide range of ground motion hazards across the state. Some portions of the state experience small-to-moderate size earthquakes relatively frequently and some only rarely. Some are exposed to extremely large potential earthquakes, and others to only smaller earthquakes. Ground motion hazards are controlled by small, frequent, nearby earthquakes in some parts of the state and by large, distant earthquakes in other areas.

The likelihood of liquefaction occurring at a given site depends strongly on the amplitude and duration of ground motions at that site. Some areas very near small-to-moderately sized faults may experience motions of relatively high amplitude but short duration. Other areas may experience motions with low amplitudes but very long durations. The fact that liquefaction can be triggered by both types of motions indicates that liquefaction hazard evaluation should consider all possible combinations of ground motion amplitude and duration. As discussed in subsequent chapters, earthquake magnitude is frequently used as a proxy for duration in liquefaction analyses. Therefore, accurate and consistent evaluation of liquefaction hazards requires consideration of ground motions at all hazard levels and of the underlying distributions of earthquake magnitudes that contribute to those motions.

Chapter 3

Performance Requirements

3.1 INTRODUCTION

The evaluation of liquefaction hazards and the process of designing to mitigate them must be based on some criterion for achieving successful “performance” of a structure or facility. The concept of performance can be interpreted in different ways, and recent trends in earthquake engineering point toward the adoption of more formal procedures for quantifying and estimating the performance of engineered structures in the future. This chapter describes the evolution of liquefaction hazard evaluation procedures and the criteria used to establish acceptable levels of performance. Because current criteria lead to inconsistent actual hazard levels (i.e., variable probabilities of achieving some desired performance level), alternative criteria that eliminate those inconsistencies are also described. The intent is to provide background information in support of the following chapters, which describe tools that will allow WSDOT to transition from current criteria to more objective and consistent criteria. Such criteria *will allow the more efficient use of WSDOT funds for construction of new structures and retrofit of existing structures, and will produce a more uniform and consistent level of safety for the traveling public across the state.*

An important part of the implementation of performance criteria is the treatment of uncertainty. As in all aspects of geotechnical engineering, uncertainty exists and plays an important role in analysis and design. Geotechnical engineers have historically treated uncertainty in a relatively informal manner by using factors of safety. More recently, practice has moved toward more formal treatment of uncertainty as the underpinning of load and resistance factor (LRFD) design (AASHTO, 2004; Allen, 2005). The following sections describe the primary uncertainties involved in liquefaction hazard evaluation, their historical treatment, and their future treatment. The intent is to provide a background for the recommendations presented in the chapters that follow.

3.2 RANDOMNESS AND UNCERTAINTY

The term “uncertainty” is frequently used to describe all deviations from pure determinism, i.e., all differences from perfect knowledge of a perfectly understood system. In order to better understand some of the concepts and recommendations that follow, it is useful to break these deviations down into two categories and define each more accurately.

The term “randomness” is often used in geotechnical engineering to describe natural processes that are inherently unpredictable (Baecher and Christian, 2003). Geotechnical engineers are well aware of the inherent variability – in geometry, composition, and properties – of geotechnical materials and deal with the implications of that variability on a daily basis. In seismic hazard analysis, the term “aleatory uncertainty” is often used to describe randomness, i.e., unknowable variability that is treated as being caused by chance.

The term “uncertainty” can also be used to describe processes that are predictable but unknown because of a lack of information or knowledge. For a particular site, a geotechnical engineer may have limited subsurface data with which to characterize the site; the uncertainty in subsurface conditions could be reduced, however, with additional (or improved) information. In seismic hazard analysis, the term “epistemic uncertainty” is frequently used to describe uncertainty due to lack of knowledge or information. Model uncertainty and parametric uncertainty are other common contributors to epistemic uncertainty in geotechnical engineering.

The division between aleatory and epistemic uncertainty is not always clear, and uncertainty that is actually epistemic is frequently treated as aleatory as a matter of practicality. Subsurface conditions at a particular site, for example, are often characterized by spatially variable aleatory uncertainty when, for example, much of that uncertainty could actually be eliminated by drilling borings at a 12-inch spacing across an entire site – obviously, an impractical solution to the uncertainty problem. For the purposes of this document, epistemic uncertainty will be referred to as that which can be reduced with the acquisition of *practical amounts* of additional information; the rest will be attributed to aleatory uncertainty.

3.3 TREATMENT OF UNCERTAINTIES IN LIQUEFACTION HAZARD EVALUATION

The evaluation of liquefaction hazards involves evaluation of both loading and resistance (or demand and capacity) terms. Uncertainties of different types exist in both. In the classical geotechnical interpretation of “failure” occurring when loading exceeds resistance, the probability of failure is equal to the probability that loading, L , exceeds resistance, R , i.e.,

$$P[F] = P[L > R] \quad (3.1)$$

If the possible values of L and R range over some intervals that can be discretized into a finite number of increments, the probability of failure can be obtained (approximately) by adding the contributions from all combinations of L and R , i.e.,

$$P[F] = \sum_{i=1}^{N_L} \sum_{j=1}^{N_R} P[L_i > R_j] P[L_i, R_j] \quad (3.2)$$

where N_L and N_R are the numbers of loading and resistance increments, respectively. Accurate evaluation of this probability of failure, therefore, requires understanding of the probability distributions of both loading and resistance. It also involves additional computational effort; as Equation 3.2 implies, computing the probability of failure requires $N_L \times N_R$ liquefaction evaluations. Such an increase in effort would be judged by many engineers to be unreasonable, but if implemented in an efficient computer program, the additional calculations need not be burdensome.

3.3.1 Historical Treatment

Liquefaction hazard analyses, like nearly all other earthquake engineering analyses, were initially accomplished by means of scenario analysis. In this approach, which originated from the nuclear power industry in the 1960s, a scenario event, usually described (as a *maximum probable* or *maximum credible earthquake*) by some combination of magnitude and distance, was postulated to define earthquake loading.

The scenario event was treated deterministically; attenuation relationships were used to predict relevant ground motion parameters (principally, peak acceleration, a_{\max}) at the site of interest for the scenario event. Uncertainty in resistance was accounted for by the use of a factor of safety (interpreted in the classical sense as a ratio of capacity to demand, or of resistance to loading) whose minimum acceptable value reflected both uncertainty and the consequences of “failure.”

Historical liquefaction evaluations were oriented toward evaluation of liquefaction potential, i.e., the potential for the initiation of liquefaction. Acceptable factors of safety for liquefaction potential were generally on the order of 1.5. When such evaluations indicated that liquefaction was expected, separate evaluations of the potential effects of liquefaction (e.g., slope instability, settlement, lateral spreading displacements) were undertaken, also in a deterministic manner with another factor of safety applied to the quantity of interest.

3.3.2 Current Treatment

Current practice treats loading in a different manner than the previously employed scenario analyses, but resistance is generally treated similarly. The procedures used to identify earthquake scenarios in the early days of geotechnical earthquake engineering did not account for the likelihood of that scenario actually occurring, which in reality is only one of many possible scenarios that could cause unsatisfactory performance. As a result, designs in different areas were frequently based on loading levels with very different probabilities of occurrence. In contemporary practice, loading is defined by means of probabilistic seismic hazard analysis (PSHA). Resistance is usually handled deterministically, but probabilistic descriptions of resistance have recently become available.

3.3.2.1 PSHA-Based Loading

In a typical PSHA (Section 2.2), earthquake sources are identified and characterized with respect to their geometries (i.e., probability distributions of source-to-site distance), earthquake generation potentials (i.e., probability distributions of earthquake magnitudes), and seismicities (i.e., rates of recurrence of earthquakes of

various magnitudes). The probability distributions of potential ground motion for each combination of magnitude and distance (and, in some cases, other variables) are described by means of attenuation relationships. Details of the PSHA process are available in Kramer (1996) and McGuire (2004). These uncertain variables are combined to produce a seismic hazard curve, which therefore represents the aggregate contributions of all possible combinations of magnitude and distance from all sources, each weighted by their relative likelihoods of occurrence; in essence, all feasible scenarios (instead of just one) are considered. This is a particularly important departure from scenario-based practice for liquefaction hazard evaluation because there is no single magnitude or distance associated with a given level of ground motion; rather, the ground motion is affected by a distribution of magnitudes and distances. Put differently, the ground motion level is affected by multiple scenarios, the relative contributions of which can be quantified by means of a deaggregation analysis. Figure 2.5 showed a USGS deaggregation plot for peak acceleration with a mean return period (reciprocal of mean annual rate of exceedance) of 475 years; the heights of the columns in the figure illustrate the relative contributions of each magnitude-distance pair to the 475-year peak acceleration of 0.335g. The distribution of magnitude values contributing to peak acceleration is particularly important for liquefaction hazard evaluations because magnitude is taken as a proxy for duration in the most commonly used procedures for evaluation of liquefaction potential.

3.3.2.2 Resistance

In current practice, liquefaction resistance is typically treated deterministically by using empirical correlations to field observations of the conditions under which soils have and have not liquefied in previous earthquakes. Uncertainty is typically accounted for through the use of factors of safety; acceptable values with PSHA-based loading are usually on the order of 1.2 to 1.5. When such evaluations indicate that liquefaction is expected, separate evaluations of the potential effects of liquefaction are undertaken; those evaluations are generally performed deterministically.

The recent development of probabilistic liquefaction models allows estimation of a probability of liquefaction, but that estimate corresponds to some assumed level of

loading (typically expressed in terms of a peak acceleration and magnitude). In practice, the loading (though obtained from a PSHA) is usually treated deterministically, i.e., as a single peak acceleration-magnitude pair. The results of the evaluation should therefore be recognized as being conditional upon the selected level of loading.

3.3.3 Emerging Treatment

An important goal of earthquake-resistance design and earthquake hazard mitigation is to achieve consistency and uniformity in safety and reliability. This is particularly important for agencies, like WSDOT, that are responsible for structures and facilities that are spread out over a large geographic area in which seismicity levels may be very different. As discussed in Chapter 2, seismicity in Washington varies from high west of the Cascades to low east of the Cascades, but also varies significantly within each of those regions. The design of structures in Seattle may be dominated by potential $M = 7.4$ Seattle fault earthquakes, while structures along the coast may be dominated by $M = 9$ Cascadia Subduction Zone earthquakes. At other locations, design may be controlled by potential earthquakes from several different sources, each of which may produce earthquakes of different sizes with different frequencies.

The concept of performance-based earthquake engineering, as developed by the Pacific Earthquake Engineering Research (PEER) Center, provides a rational framework for uniform and consistent evaluation of liquefaction hazards in all seismic environments. It accounts for all possible levels of ground motion (rather than motions with a single return period, as in current practice) and all magnitudes that contribute to each of those levels of ground motion. Implementation of the performance-based approach effectively involves mining through large PSHA databases and performing millions of individual liquefaction evaluations – tasks that would normally be costly and time-consuming. The WSliq software package that accompanies this Manual, however, automates this process so that it can be performed as easily as a conventional liquefaction analysis.

The performance-based approach can be formulated to directly predict the probability of some performance level being reached or exceeded. It does this by considering the uncertainty in ground motion intensity (through a PSHA), the uncertainty in response given ground motion intensity, and the uncertainty in damage given the

response. These analyses represent the state-of-the-art to which the state-of-practice is moving.

3.3.4 Model Uncertainty

An element of epistemic uncertainty that is frequently neglected in practice is model uncertainty. Different models are available for prediction of liquefaction potential, residual strength of liquefied soil, lateral spreading displacement, and post-liquefaction settlement. The models generally have different forms and are frequently calibrated against different data; as a result, they often produce similar, but somewhat different, results. Geotechnical engineers usually select one model on the basis of apparent applicability to the problem of interest—ease of use, perceived conservatism, or other reasons—and use that model alone. In effect, they are implicitly assigning a probability of 1.0 to the notion that the selected model is the most appropriate (or “best”) model, and probabilities of 0.0 to the other models. In reality, there is seldom a technical basis for justifying such a decision; using subjective (but rational) means, it is frequently more appropriate to assign “degrees of belief,” interpreted as probabilities that each model is the “most appropriate” in the form of weighting factors. The WSliq software package that accompanies this report provides the means for assigning such weighting factors to alternative models so that the final result of an analysis reflects the contributions of more than one appropriate model.

3.4 THE MAGNITUDE ISSUE

Liquefaction results from the generation of excess porewater pressure in loose, saturated soils; the porewater pressure is known to build up gradually in response to the series of cyclic shear stresses imposed on the soil by earthquake shaking. For a given element of soil in the field, the final porewater pressure is a function of the amplitude, frequency, and number of loading cycles. Therefore, earthquake loading, for the purposes of liquefaction analysis, is a function of ground motion amplitude, frequency content, and duration.

Since the early days of liquefaction hazard evaluation, the duration of a ground motion has been correlated to earthquake magnitude. This approach was logical and

quite workable at the time it was developed, since actual ground motion duration data at case history sites were rare and because earthquake loading was characterized by a scenario, i.e., a single magnitude-distance pair. With this approach, magnitude could easily be used as an unambiguous proxy for ground motion duration.

However, with the advent of PSHA-based characterization of loading, the use of magnitude as a proxy for duration became more difficult in many cases. As previously described, a PSHA accounts for ground motions resulting from all possible earthquake magnitudes, and so the ground motion with a particular return period comprises contributions from many different magnitudes; for a conventional liquefaction hazard evaluation, the geotechnical engineer must choose a single magnitude to represent all of these contributions. For sites affected by a single seismic source (i.e., fault), the choice is usually straightforward because one magnitude will typically dominate the hazard. For other locations, however, contributions may come from different seismic sources with different recurrence behavior; at these locations, different magnitudes may contribute nearly equally to the ground motion with a particular return period. Figure 2.5, for example, showed the relative contributions to 475-year peak ground acceleration for Seattle broken down by magnitude and distance in a deaggregation plot. The peak acceleration value of 0.33 g can be seen to be affected by magnitudes ranging from 5.0 to 9.0. The mean and modal magnitudes for Seattle are 6.57 and 6.64, respectively – not a large difference. In Tacoma, however, the 475-year mean and modal magnitudes are 6.54 and 7.00, respectively – a much more significant difference. In fact, use of the modal magnitude in a liquefaction evaluation for a site in Tacoma would produce loading 20 percent stronger (and hence a factor of safety 20 percent lower) than that based on use of the mean magnitude.

In current practice, selection of the appropriate magnitude value is controversial. Some engineers use mean magnitudes, some use modal magnitudes, and some use the larger of the two in an effort to be “conservative.” However, the use of any of these approaches will produce inconsistent actual risks of liquefaction because of the nonlinear relationship between duration and liquefaction potential. The correct way to handle the “magnitude issue” is to repeat the calculations for all magnitudes that contribute to significant ground motions and weight the calculated results by the relative contribution

of each magnitude. The cost of this approach is the increased computational burden. For a site in Seattle, for example, one would likely perform 20 analyses (covering the range of $M = 5.0$ to $M = 9.0$ in magnitude increments of 0.2) to implement this approach.

To allow the benefits of increased uniformity and consistency associated with accurate representation of magnitude contributions to be realized conveniently, the WSliq software package that accompanies this report allows liquefaction evaluations to be performed in three user-selected manners. The basic philosophy and use of each are described in the following sections.

3.4.1 Single-Scenario Approach

A single scenario analysis can be performed with user-defined data (e.g., peak acceleration and magnitude for liquefaction potential) or with PSHA-based data (e.g., peak acceleration for a user-defined return period and, at the user's choice, either mean or modal magnitude). A PSHA database for Washington State is built into the WSliq package, so all of the required data are available for any latitude and longitude within the state. This option lets the user control the required input parameters in a way that allows convenient sensitivity analyses, comparison of different models, and more.

The results of a single-scenario analysis must be recognized as being conditional upon the occurrence of that scenario. The fact that other scenarios capable of causing unsatisfactory performance may also occur should also be recognized.

3.4.2 Multiple-Scenario Approach

Multiple scenario analyses can be performed for ground motions with any return period. In this type of analysis, the results are computed for all magnitude values with weighting factors proportional to the relative contribution of each magnitude to the ground motion parameter used to compute the expected value of the result (for lateral spreading analyses, the contributions of all magnitudes *and distances* are considered). In WSliq, this option makes use of the built-in Washington State PSHA database so that the analyses are no more difficult to perform than the single-scenario analyses. The multiple-scenario analyses eliminate the controversial issue of using mean, modal, or other magnitudes in liquefaction hazard evaluations.

The results of a multiple-scenario analysis must be recognized as being conditional upon the level of ground motion associated with the selected return period. The fact that unsatisfactory performance could be caused by weaker, more frequent motions, and/or by stronger, less frequent motions should also be recognized.

3.4.3 Performance-Based Approach

Performance-based analyses consider ground motions with all return periods and the contributions of magnitude (and, for lateral spreading, all distances) to all of those return periods. They represent the most complete, consistent, and uniform method possible for evaluation of liquefaction hazards. The performance-based analysis can return a seismic hazard curve for the parameter of interest. Knowing the return period of a particular hazard is equivalent (with a common and appropriate assumption) to knowing the probability of that hazard in a given exposure period. For lateral spreading, for example, the performance-based option can compute the lateral spreading displacement with a particular return period (or, equivalently, a particular probability of a particular level of displacement being exceeded in a given exposure period). By keying performance criteria to return periods (or probabilities of exceedance), uniform and consistent levels of risk can be achieved in all seismic environments across the state.

3.4.4 Recommendations

One of the important goals of the research described in this report was the development of procedures and tools that will allow WSDOT engineers to evaluate liquefaction hazards consistently and uniformly, and to do so as easily as possible. The WSliq program, therefore, was designed to allow different single-scenario, multiple-scenario, and performance-based evaluations. Table 3.1 summarizes the recommended uses of each of these approaches; the recommendations anticipate that the trend of moving toward performance-based design and evaluation will accelerate in the next few years.

Table 3.1 Advantages, disadvantages, and recommended use of different analysis approaches.

Item	Single-Scenario	Multiple -Scenario	Performance-Based
Advantages	Simple approach, allows investigation of single hypothetical scenario; no site-specific hazard data required.	Straightforward extension of single-scenario approach; considers all magnitudes from all seismic sources weighted by relative contribution to hazard; consistent with, but improved upon, current practice.	Considers all levels of ground motion (all return periods) and all magnitudes from all sources, all weighted by relative likelihoods; gives most complete, consistent indication of hazard.
Disadvantages	Only considers one of many possible scenarios; no indication of likelihood of selected scenario.	Time-consuming, in that single-scenario calculations must be repeated many times; considers only one level of ground motion (one return period); requires site-specific hazard and deaggregation data at return period of interest.	Time-consuming, in that multiple-scenario calculations must be repeated many times; requires site-specific hazard and deaggregation data at multiple return periods.
Recommended Use	Use for sensitivity analyses – check sensitivity of results to different scenarios, e.g., most likely or worst case earthquake from each seismic source.	Use for design practice with WSliq; check results against performance-based results to determine return period associated with computed performance level.	Use with WSLIQ to check results of multiple-scenario analyses; develop return period database to begin transition to performance-based design.

3.5 PERFORMANCE CRITERIA

The field of earthquake engineering is in the early stages of a transition toward performance-based design and evaluation concepts. The performance-based procedures described in the following chapters represent the profession’s first implementation of performance-based liquefaction hazard evaluation procedures. In that context, WSDOT is now ahead of the curve and has the opportunity to play a leading role in the development and adoption of suitable performance criteria.

3.5.1 Conventional Analyses

For conventional (i.e., not performance-based) analyses, performance criteria should still be based on a factor of safety given a ground motion with some return period.

Criteria based on single scenario procedures are not recommended. In such cases, performance should be evaluated by using the results of multiple-scenario analysis, which can be performed easily with the WSliq software package.

As previously discussed, model uncertainty can be significant in several areas of liquefaction hazard evaluation. In conventional practice, the geotechnical engineer typically selects one method of analysis and accounts for model and all other uncertainty through the use of a factor of safety. If model uncertainty is addressed, for example by using multiple models, the reduction of uncertainty should, in principle, justify the use of a lower factor of safety for design. For design purposes, the use of weighted average response values can justify the use of factors of safety that are 5 percent to 10 percent lower than the standard factor of safety levels of 1.3 to 1.5.

3.5.2 Performance-Based Analyses

The move toward performance-based analyses means that performance-based criteria will need to be established for various liquefaction hazards. Such criteria will need to be established in terms of acceptable return periods for various performance levels; as an example, the results of this research show that conventional deterministic analyses of liquefaction potential produce a level of “safety” that is consistent with a 400-year return period for liquefaction (of an element of soil in a reference profile) in Seattle. Put differently, current criteria based on conventional deterministic procedures are consistent with a condition in which liquefaction would be expected to occur, on average, every 400 years in Seattle. To obtain a consistent likelihood of liquefaction at other locations, performance-based analyses should be performed for a liquefaction return period of 400 years for the location of interest.

The actual, desired return periods associated with different performance levels will need to be determined by WSDOT personnel; these return periods may vary from one hazard (e.g., initiation, lateral spreading, settlement) to another. This process is usually accomplished by a calibration exercise in which return periods associated with conventional criteria are calculated; the WSliq program was designed to make such analyses as easy as possible to perform.

Chapter 4

Susceptibility to Liquefaction

4.1 INTRODUCTION

The first step in a liquefaction hazard evaluation is to determine whether the site of interest contains soils that are capable of liquefying, i.e., whether or not they are susceptible to liquefaction. Note that, as used in this report, susceptibility and initiation are separate issues. A soil considered susceptible to liquefaction is one that can liquefy under some level of loading, and a non-susceptible soil cannot – no matter how strong the loading may be. Some profiles are not susceptible to liquefaction and others are highly susceptible.

Liquefaction susceptibility can be judged at different levels. The general deposit-level susceptibility can be preliminarily screened by using historical, geological, hydrological, and compositional criteria, as described by Kramer (1996). Youd (1998) developed a useful and practical deposit-level screening procedure that includes liquefaction susceptibility but also elements of initiation and effects. Liquefaction susceptibility can also be evaluated at the layer level, i.e., by distinguishing between the characteristics of the various layers that make up a soil deposit.

For many years, only sands were considered to be susceptible to liquefaction. Gravels were considered to be too permeable for high pore pressures to be maintained, even if the gravel was loose enough to exhibit highly contractive behavior, and fine-grained soils were considered to have sufficient cohesion to prevent the deleterious behavior associated with liquefaction even if high pore pressures were generated. However, the geotechnical engineering profession's understanding of liquefaction susceptibility has improved significantly in the past 10 to 15 years, principally because of knowledge gained from earthquakes in California, Turkey, and Taiwan. These advances have helped to clarify the susceptibility of fine-grained soils, i.e., silts and clays, to liquefaction; they have also pointed out that previously used procedures are not valid. Clays are generally not susceptible to liquefaction, although some may exhibit behavior

that is similar in some respects to liquefiable soils. Silts may or may not be susceptible to liquefaction; silts that are susceptible can be particularly problematic because of their relatively low permeability.

This chapter provides a review of the conditions under which various types of soils are and are not susceptible to liquefaction. It begins by introducing a procedure for deposit-level susceptibility evaluation and then describes a procedure for layer-level evaluation.

4.2 DEPOSIT-LEVEL SUSCEPTIBILITY EVALUATION

A preliminary screening of liquefaction susceptibility can be based on the Susceptibility Rating Factor, *SRF*, which is defined as follows:

$$SRF = F_{\text{hist}} \times F_{\text{geology}} \times F_{\text{comp}} \times F_{\text{gw}} \quad (4.1)$$

where F_{hist} = liquefaction history factor, F_{geology} = geology factor, F_{comp} = composition factor, and F_{gw} = ground water factor. Procedures for determining the values of the various factors are described in the following sections. When the SRF is computed according to these procedures, the susceptibility of the site to liquefaction can be estimated from Table 4.1.

Table 4.1 Characterization of overall site susceptibility to liquefaction hazards.

<i>SRF</i>	Site Susceptibility
0 – 5	Very Low
5 – 10	Low
10 – 25	Moderate
25 – 50	High
> 50	Very High

Note that this scale is not linear, i.e., that a doubling of the *SRF* does not imply a doubling of susceptibility. The scale should also be recognized as being qualitative in nature; the numerical values it produces should not be used in place of sound engineering judgment.

Note also that the various factors listed in this document have been determined through a combination of engineering analysis and engineering judgment. As such, they

should be revisited periodically and revised as necessary as additional data become available and further research is completed.

4.2.1 Liquefaction History Factor

Historical observations can be very useful in determining the susceptibility of sites to future occurrences of liquefaction. The fact that liquefaction has occurred at the site of interest in the past, particularly if it occurred in earthquakes that produced low to moderate levels of shaking, may be a very strong indicator of susceptibility in future events. On the other hand, the fact that liquefaction is known not to have occurred in the past, particularly if the site has been subjected to significant levels of shaking, may be a strong indicator of non-susceptibility. Therefore, the liquefaction history factor is defined in such a way that it takes on high values for sites that have liquefied in the past, and very high values if that liquefaction occurred under modest levels of ground shaking.

The history factor is composed of two historical components that are multiplied together. The first is a component intended to reflect past observations of the occurrence of liquefaction; the second is a component that reflects the past seismic history of the site. Therefore, the liquefaction history factor is defined as

$$F_{\text{hist}} = C_{\text{obs}} \times C_{\text{seis}} \quad (4.2)$$

The two components are determined from tables 4.2 and 4.3:

Table 4.2 Historical observation factors.

Historical Liquefaction Observations	C_{obs}
Widespread liquefaction	10
Limited liquefaction	5
No liquefaction	1
Unknown	2.5

Table 4.3 Past seismicity history factors.

Past Peak Acceleration Index	C_{seis}
0.00 – 0.05 g	5.0
0.05 – 0.1 g	3.0
0.1 – 0.2 g	2.0
0.2 – 0.3 g	1.5
0.3 – 0.4 g	1.2
> 0.4 g	1.0

Note that the value of F_{hist} depends both on observations of behavior in past earthquakes and on the known seismic history of the site of interest. For a site at which widespread liquefaction was observed in an earthquake producing ground motions of 0.15 g, the value of F_{hist} would be $F_{\text{hist}} = 10 \times 2.0 = 20$. For a site at which no liquefaction was observed under earthquake shaking as high as 0.35 g, the value of F_{hist} would be much lower, i.e., $F_{\text{hist}} = 1 \times 1.2 = 1.2$. The extreme difference (i.e., factor of $20/1.2 = 16.7$) in F_{hist} for these cases is intentional; the comparative histories would indicate a much higher level of susceptibility for one site relative to the other. Note also that sites for which liquefaction (or no liquefaction) observations are not available will have an increased C_{obs} value relative to sites for which observations of no liquefaction are available. This is intended to reflect the difference between knowing that liquefaction has not occurred and not having information on whether liquefaction has occurred. In the absence of information on the PGA value for which liquefaction observations were made, the Past Peak Acceleration Index can be taken as the USGS peak acceleration with a return period of 108 years; this value is intended to distinguish between regions of high and low seismicity in areas where evidence of liquefaction may exist.

4.2.2 Geology Factor

Geology is one of the dominant factors influencing liquefaction susceptibility. Soil deposits susceptible to liquefaction generally occur within a limited range of depositional environments; hence susceptibility can be correlated to geologic conditions in a preliminary screening procedure. Determination of the geology factor requires site classification, which is a subjective task best performed by geologists with a good knowledge of local and regional geomorphology. The reliability of the site classification will depend on the nature of the data available to the person making the classification. The geology factor, therefore, is defined as the product of two components.

$$F_{\text{geology}} = C_{\text{class}} \times C_{\text{quality}} \quad (4.3)$$

Youd and Perkins (1987) described liquefaction susceptibility of sedimentary deposits in qualitative terms, accounting for the fact that liquefaction resistance increases with time since deposition. The depositional types identified by Youd and Perkins were

used to develop values of the classification component, C_{class} , for liquefaction susceptibility evaluation. The factors are presented in Table 4.4.

Table 4.4 Geologic classification factors.

Type of Deposit	Nature of Sediments in General Distribution of Cohesionless Deposits	Classification Component, C_{class} (by age of deposit)			
		< 500 yrs	Holocene	Pleistocene	Pre-Pleistocene
Uncompacted fill	Variable	10	-	-	-
River channel	Locally variable	10	6	2	1
Delta (coastal)	Widespread	10	6	2	1
Loess	Variable	6	6	6	-
Flood plain	Locally variable	6	4	2	1
Delta (continental)	Widespread	6	4	2	1
Lacustrine and playa	Variable	6	4	2	1
Colluvium	Variable	6	4	2	1
Dunes	Widespread	6	4	2	1
Estuarine (coastal)	Locally variable	6	4	2	1
Beach (low wave energy)	Widespread	6	4	2	1
Lagoonal	Locally variable	6	4	2	1
Foreshore	Locally variable	6	4	2	1
Alluvial fan and plain	Widespread	4	2	2	1
Beach (high wave energy)	Widespread	4	2	1	1
Talus	Widespread	2	2	1	1
Glacial till	Widespread	2	2	1	1
Tuff	Rare	2	2	1	1
Compacted fill	Variable	2	-	-	-
Rock	Widespread	0	0	0	0

The reliability of this classification may be relatively high or low, depending on who is doing the classification and the quality of information available to that person. To account for the beneficial effects of high-quality information, a quality component, C_{quality} , is determined from Table 4.5.

If a site can be classified by more than one of the above categories, the geology factor may be estimated by interpolation.

Table 4.5 Classification quality factors.

Basis for Classification	C_{quality}
Site reconnaissance by geologist	1.0
Site reconnaissance by engineer	1.1
Review of geologic maps (1:24000 or better)	1.2
Estimation	1.5

4.2.3 Compositional Factor

Soil composition, in addition to depositional environment, plays an important role in the occurrence of liquefaction. Surficial effects of liquefaction are observed most frequently in loose, uniformly graded, rounded, clean to slightly silty sands overlain by thin layers of fine-grained soils. Therefore, factors such as gradation, particle shape, fines content, fines plasticity, and cap presence can affect liquefaction susceptibility.

The composition factor is defined as the product of six different components and defined as

$$F_{\text{comp}} = C_{\text{gradation}} \times C_{\text{shape}} \times C_{\text{fines}} \times C_{\text{plasticity}} \times C_{\text{wc}} \times C_{\text{cap}} \quad (4.4)$$

The values of the components can be obtained from tables 4.6a-f:

Table 4.6 (a) gradation factors, (b) particle shape factors, (c) fines content factors, (d) fines plasticity factors, (e) water content factors, and (f) impermeable cap factors.

Coeff. of Uniformity	$C_{\text{gradation}}$
1-2	1.00
2-3	0.95
3-4	0.90
4-5	0.85
> 5	0.75
Unknown	1.00

(a)

Particle Shape	C_{shape}
Rounded	1.00
Sub-rounded	0.95
Subangular	0.90
Angular	0.80
Unknown	1.00

(b)

Fines Content	C_{fines}
0 – 20%	1.00
20 – 40%	0.95
40 – 60%	0.90
60 – 80%	0.85
80 – 100%	0.80
Unknown	1.00

(c)

Fines PI	$C_{\text{plasticity}}$
0 – 7	1.00
7 – 12	0.80
12 – 20	0.50
20 – 30	0.25
> 30	0.10
Unknown	1.00

(d)

Water Content	C_{wc}
$w_c > 0.85LL$	1.00
$0.80LL \leq w_c \leq 0.85LL$	0.90
$w_c < 0.80LL$	0.80
Unknown	1.00

(e)

Cap Presence	C_{cap}
Yes	1.20
No (sand)	1.00
No (gravel)	0.50
Unknown	1.10

(f)

The plasticity and water content coefficients were developed with consideration of recent liquefaction susceptibility criteria proposed by Idriss and Boulanger (2006) and Bray and Sancio (2006).

4.2.4 Groundwater Factor

The process of liquefaction involves the buildup of excess porewater pressure within a liquefaction-susceptible soil. Consequently, liquefaction-susceptible soils must be saturated (or very nearly saturated).

Because liquefaction loading and resistance typically decrease and increase, respectively, with increasing depth, liquefaction is commonly observed at relatively shallow depths. Earthquake reconnaissance following past earthquakes around the world

has shown that the effects of liquefaction in natural soils are usually observed at sites with groundwater table depths that are lower than about 3 m, that some cases of liquefaction have occurred at sites with groundwater tables at depths of 10 m, and that only a few instances of liquefaction have been observed at sites with water tables deeper than 15 m.

These factors indicate that susceptibility to liquefaction hazards can be assumed to decrease with increasing water table depth. Accordingly, values of the groundwater factor can be estimated from Table 4.7:

Table 4.7 Groundwater factors.

Groundwater Table Depth	Groundwater Factor, F_{gw}
< 3 m	1.0
3 – 6 m	0.9
6 – 10 m	0.8
10 – 15 m	0.7
> 15 m	0.6
Unknown	1.0

The groundwater table depth used to determine F_{gw} should be the lowest depth that can be reasonably anticipated over the lifetime of the structure that is to be constructed at the site of interest. The potential for increased or perched groundwater levels should be evaluated in determining F_{gw} .

4.3 EXAMPLES

The proposed procedure for preliminary deposit-level screening of liquefaction susceptibility can be illustrated by a series of examples. The examples are selected to represent a range of hypothetical site conditions at a series of locations across Washington State. The examples also represent a range of available information on which the screening procedure could be based.

Example 1: Sodo District, Seattle

This hypothetical site is in the area of Seattle south of Safeco Field and near the Duwamish River. The site is underlain by artificial fill placed hydraulically during the early part of the century and by alluvial soils deposited by the river. The sands are

generally relatively clean, poorly graded, and of subangular particle shape. Groundwater in the area is at a depth of approximately 3 m. Localized liquefaction has been observed in the area in the 1949 Olympia, 1965 Seattle-Tacoma, and 2001 Nisqually earthquakes; ground motions of approximately 0.22g were recorded in the area in the Nisqually earthquake. The susceptibility rating factor for the site is calculated below.

Liquefaction History Factor			$F_{hist} = 7.5$
$C_{obs} =$	5	Limited liquefaction PHA = 0.22g	
$C_{seis} =$	1.5		
Geology Factor			$F_{geology} = 10$
$C_{class} =$	10	Fill/River channel Geologist site visit	
$C_{quality} =$	1.0		
Compositional Factor			$F_{comp} = 0.86$
$C_{gradation} =$	0.95	$C_u = 2.2$ Subangular Low fines content Nonplastic fines Unknown No cap	
$C_{shape} =$	0.90		
$C_{fines} =$	1.00		
$C_{plasticity} =$	1.00		
$C_{wc} =$	1.00		
$C_{cap} =$	1.00		
Groundwater Factor			$F_{gw} = 1.0$
Susceptibility Rating Factor			SRF = 64

The *SRF* of 64 means that the liquefaction susceptibility of this site is Very High, a fact that should not be surprising, given that liquefaction has been observed in the area in past earthquakes.

Example 2: Andresen Road Interchange, Vancouver

The Andresen Road interchange lies in a flood plain of the Columbia River. The flood plain deposits resulted from the glacial outburst floods of Glacial Lake Missoula that occurred during the Pleistocene. Some low-lying areas were subsequently filled with shallow deposits of silt and organic silt. Perched groundwater is anticipated at depths of 2 to 3 m. The susceptibility rating factor for the site is calculated below.

The Andreson Road interchange site has an *SRF* of 36, which indicates a High susceptibility to liquefaction. Additional information on the liquefaction and ground shaking history of the site could lead to a significant reduction of the *SRF*; confirmation

of the geologic characterization by a geologist would produce a reduction of nearly 20 percent.

Liquefaction History Factor			$F_{hist} = 7.5$
	$C_{obs} =$	2.5	Unknown > 0.1g
	$C_{seis} =$	3.0	
Geology Factor			$F_{geology} = 4.8$
	$C_{class} =$	4	Pleistocene & Holocene From map
	$C_{quality} =$	1.2	
Compositional Factor			$F_{comp} = 1.0$
	$C_{gradation} =$	1.0	All unknown
	$C_{shape} =$	1.0	
	$C_{fines} =$	1.0	
	$C_{plasticity} =$	1.0	
	$C_{wc} =$	1.00	
	$C_{cap} =$	1.0	
Groundwater Factor			$F_{gw} = 1.0$
Susceptibility Rating Factor			$SRF = 36$

Example 3: Capitol Boulevard Undercrossing, Olympia

The Capitol Boulevard undercrossing of I-5 lies in an area of post-Pleistocene fluvial deposits comprising loose to medium-dense silty fine sands and sandy silts overlying medium-dense to dense advance outwash sands. No liquefaction was observed at the site during the 1949 Olympia and 2001 Nisqually earthquakes, which likely produced shaking with a PHA > 0.2g. Groundwater at the site is expected to be more than 30 m below the ground surface. The susceptibility rating factor for the site is calculated below.

The *SRF* of 7 indicates that the Capitol Boulevard undercrossing site has a Very Low susceptibility to liquefaction, principally because of the very deep groundwater table. If a perched water condition could develop at this site, the *SRF* could be considerably higher.

Liquefaction History Factor			$F_{hist} = 1.5$
	$C_{obs} =$	1.0	No liquefaction observed PHA > 0.2g
	$C_{seis} =$	1.5	
Geology Factor			$F_{geology} = 6.6$
	$C_{class} =$	6	Fluvial deposits Engineer's interpretation
	$C_{quality} =$	1.1	
Compositional Factor			$F_{comp} = 1.14$
	$C_{gradation} =$	1.0	Unknown Unknown > 20% Nonplastic Unknown Silt cap present
	$C_{shape} =$	1.0	
	$C_{fines} =$	0.95	
	$C_{plasticity} =$	1.0	
	$C_{wc} =$	1.00	
	$C_{cap} =$	1.2	
Groundwater Factor			$F_{gw} = 0.6$
Susceptibility Rating Factor			SRF = 7

Example 4: Yakima River Site

A site near the Yakima River contains floodplain deposits from Pleistocene glacial outburst flooding and more recent fluvial sedimentation. The site is underlain by medium dense to dense sandy gravel with occasional cobbles. Groundwater is at a depth of approximately 8 m. The susceptibility rating factor for the site is calculated below.

Liquefaction History Factor			$F_{hist} = 3.0$
	$C_{obs} =$	1.0	No liquefaction observed PHA > 0.05g
	$C_{seis} =$	3.0	
Geology Factor			$F_{geology} = 4.0$
	$C_{class} =$	4.0	Pleistocene/Holocene Geologist site visit
	$C_{quality} =$	1.0	
Compositional Factor			$F_{comp} = 0.5$
	$C_{gradation} =$	1.0	Unknown Unknown Unknown Unknown Uncapped gravel Unknown Gravel cap
	$C_{shape} =$	1.0	
	$C_{fines} =$	1.0	
	$C_{plasticity} =$	1.0	
	$C_{wc} =$	1.00	
	$C_{cap} =$	0.5	
Groundwater Factor			$F_{gw} = 0.8$
Susceptibility Rating Factor			SRF = 3

Liquefaction susceptibility of the Yakima River site would be classified as Very Low, primarily because of the nature of the soil (uncapped gravel) and the relatively deep groundwater table.

Example 5: Bone River Site

A site at Bone River near Willapa Bay on the Washington coast is underlain by fluvial/alluvial deposits consisting of thick sequences of silt and silty sand. The groundwater table varies from 2 to 6 m in depth. The silty sands generally contain at least 40 percent fines that have PIs of 15 to 20. The susceptibility rating factor for the site is calculated below.

Liquefaction History Factor			$F_{hist} = 2.5$
	$C_{obs} =$	2.5	Unknown Strong CSZ motions
	$C_{seis} =$	1.0	
Geology Factor			$F_{geology} = 10$
	$C_{class} =$	10	River channel deposits Geologist site visit
	$C_{quality} =$	1.0	
Compositional Factor			$F_{comp} = 0.43$
	$C_{gradation} =$	0.95	$C_u > 2$ Unknown 40 – 60% fines PI = 15 – 20 No cap (sand) Unknown Unknown
	$C_{shape} =$	1.0	
	$C_{fines} =$	0.9	
	$C_{plasticity} =$	0.5	
	$C_{wc} =$	1.0	
	$C_{cap} =$	1.0	
Groundwater Factor			$F_{gw} = 0.9$
Susceptibility Rating Factor			$SRF = 10$

The Bone River site shows an SRF of 10, which would classify the site as being of Low to Moderate susceptibility.

4.4 LAYER-LEVEL SUSCEPTIBILITY EVALUATION

Liquefaction susceptibility must also be evaluated on a layer-by-layer basis when site-specific liquefaction potential and liquefaction-related hazards are assessed for design purposes. While the deposit-level evaluation procedure described in Section 4.2 makes use of historical, geological, and groundwater data, layer-level evaluations focus more on compositional characteristics.

Soils that would be classified as clean sands must be considered as susceptible to liquefaction; such soils may not liquefy if they are in a very dense state, but that aspect of their behavior should be considered in an evaluation of their potential for liquefaction initiation (Chapter 5). Gravelly soils should be considered to be susceptible to liquefaction if they are bounded by materials of permeability sufficiently low to prevent the dissipation of excess pore pressure during earthquake shaking.

The primary difficulty in evaluating liquefaction susceptibility lies in the susceptibility of fine-grained soils and coarse-grained soils with high fines contents. For many years, such soils were considered to be non-susceptible to liquefaction. Then, after silty soils had been observed to liquefy in a number of earthquakes, the modified Chinese criteria were recommended (Seed and Idriss, 1982; Seed et al., 1985) for evaluation of liquefaction susceptibility of fine-grained soils. Following observations of liquefaction in fine-grained soils for which the Chinese criteria indicated non-susceptibility, extensive research on the liquefaction susceptibility of fine-grained soils was undertaken. At this stage, two major studies have proposed criteria for evaluating the liquefaction susceptibility of fine-grained soils. These criteria are consistent for some conditions and differ for others; both were developed by using the field observations and laboratory testing results of well-respected leaders of the geotechnical engineering profession. At the present time, data sufficient to prove one or the other to be more appropriate do not exist. As a result, both must be considered plausible, and both should be considered in a liquefaction susceptibility evaluation.

4.4.1 Boulanger and Idriss (2005)

Boulanger and Idriss (2005) reviewed case histories and laboratory tests involving the cyclic loading of different fine-grained soils. Boulanger and Idriss identified two types of behavior that they described as “sand-like” and “clay-like” on the basis of stress normalization and stress-strain behavior. Soils exhibiting sand-like behavior can be considered susceptible to liquefaction. Soils exhibiting clay-like behavior are not susceptible to liquefaction, although Boulanger and Idriss were careful to point out that they may be susceptible to other forms of behavior that can lead to earthquake damage.

Boulanger and Idriss found that soil plasticity characteristics determine whether an individual soil is likely to exhibit sand-like or clay-like behavior, and proposed that the distinction can be made on the basis of plasticity index, PI . Figure 4.1 shows the transition between sand-like and clay-like behavior observed by Boulanger and Idriss – the soil is clearly sand-like at $PI < 3$ and clay-like at $PI > 8$. While the transitional nature of the soil behavior was emphasized, a simple (and conservative) guideline of $PI = 7$ was recommended when a distinct indication of susceptibility is required and detailed laboratory testing results are not available.

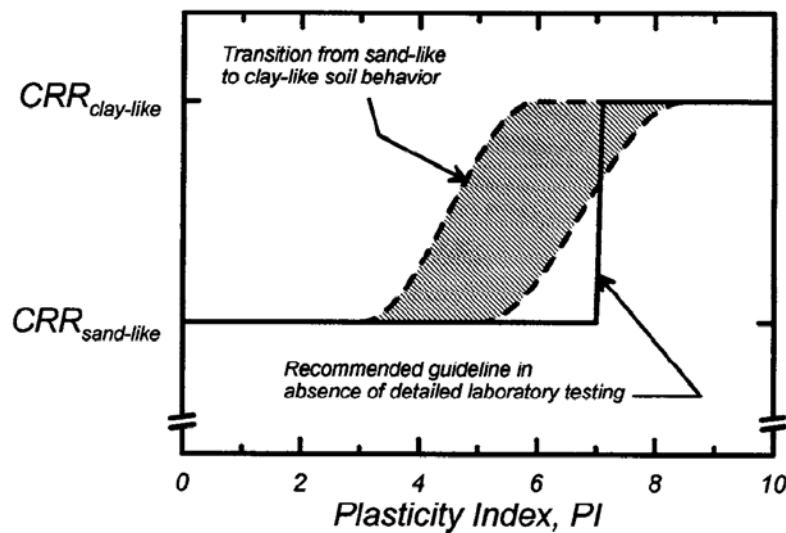


Figure 4.1. Transition from sand-like to clay-like behavior with plasticity index for fine-grained soils (Boulanger and Idriss, 2005).

To quantify the transitional nature of observed sand-like to clay-like behavior, a numerical relationship was established. The PI transition from clay-like to sand-like behavior from Boulanger and Idriss (2005) can be described with a susceptibility index, defined as

$$S_{BI} = \left[1 + \left(\frac{\ln PI}{1.843} \right)^{11.483} \right]^{-2.0} \quad (4.5)$$

which has a value of 0.0 for clay-like behavior and 1.0 for sand-like behavior. The relationship between S_{BI} and the graphical relationship presented by Boulanger and Idriss is shown in Figure 4.2.

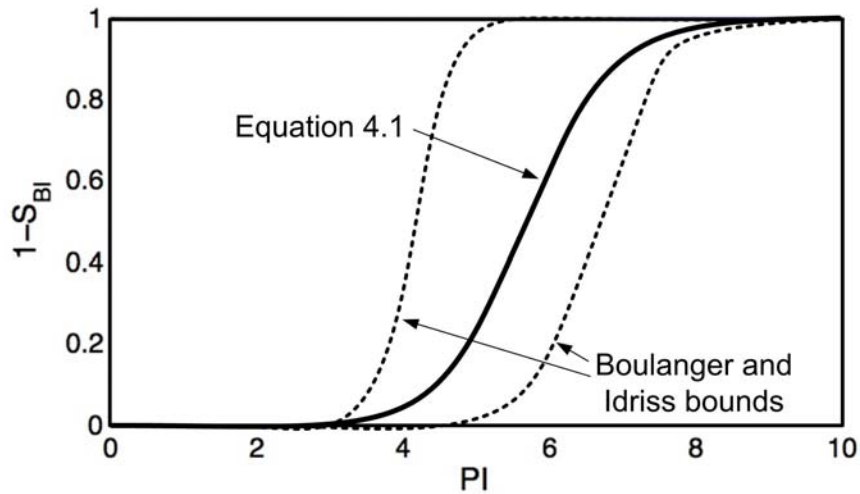


Figure 4.2. Relationship between SBI and Boulanger and Idriss (2005) transition zone boundaries.

4.4.2 Bray and Sancio (2006)

Bray and Sancio (2006) investigated fine-grained soils that liquefied during the 1994 Northridge, 1999 Kocaeli, and 1999 Chi-Chi earthquakes and proposed new compositional criteria for liquefaction susceptibility evaluation. In addition to the plasticity index, Bray and Sancio found the ratio of water content to liquid limit (w_c/LL) to also influence liquefaction susceptibility. Bray and Sancio found soils with $PI < 12$ and $w_c/LL > 0.85$ to be consistently susceptible, and soils with $PI > 18$ or $w_c/LL < 0.80$ to be consistently non-susceptible to liquefaction. Other soils were considered to be moderately susceptible, with testing recommended to further establish their liquefaction susceptibility. Figure 4.3 shows the boundaries of the most-likely, moderately, and unlikely zones of liquefaction susceptibility recommended by Bray and Sancio (2006).

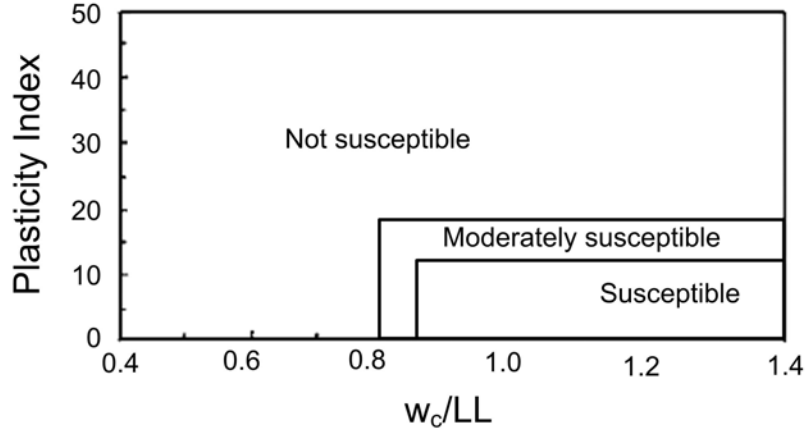


Figure 4.3. Ranges of w_c/LL and plasticity index for various susceptibility categories according to Bray and Sancio (2006).

A function similar to that used to approximate the Boulanger and Idriss criterion can be developed to quantify Bray and Sancio’s susceptibility criteria. The equation is simply the product of two terms that have same general form as Equation 4.5, i.e.,

$$S_{BS} = \left[1 + \left(\frac{\ln PI}{2.778} \right)^{33.077} \right]^{-2.0} \left[1 + \left(\frac{4.401}{\ln(w_c / LL)} \right)^{360.471} \right]^{-2.0} \quad (4.6)$$

These equations were determined by assuming the boundary between susceptibility and non-susceptibility to be uniformly distributed within the ‘moderately susceptible’ zone of Bray and Sancio, and by fitting a function that would have the same mean and variance with respect to both PI and w_c/LL . As in Equation 4.5, a value of 0.0 indicates non-susceptibility and 1.0 indicates susceptibility. A three-dimensional view of S_{BS} is shown in Figure 4.4. Equation 4.6 represents Bray and Sancio’s “moderate susceptibility” zone as a smooth transitional zone in which S_{BS} varies from near 0.0 to near 1.0. The expression for S_{BS} provides a quantitative indication of liquefaction susceptibility according to the procedure of Bray and Sancio (2006).

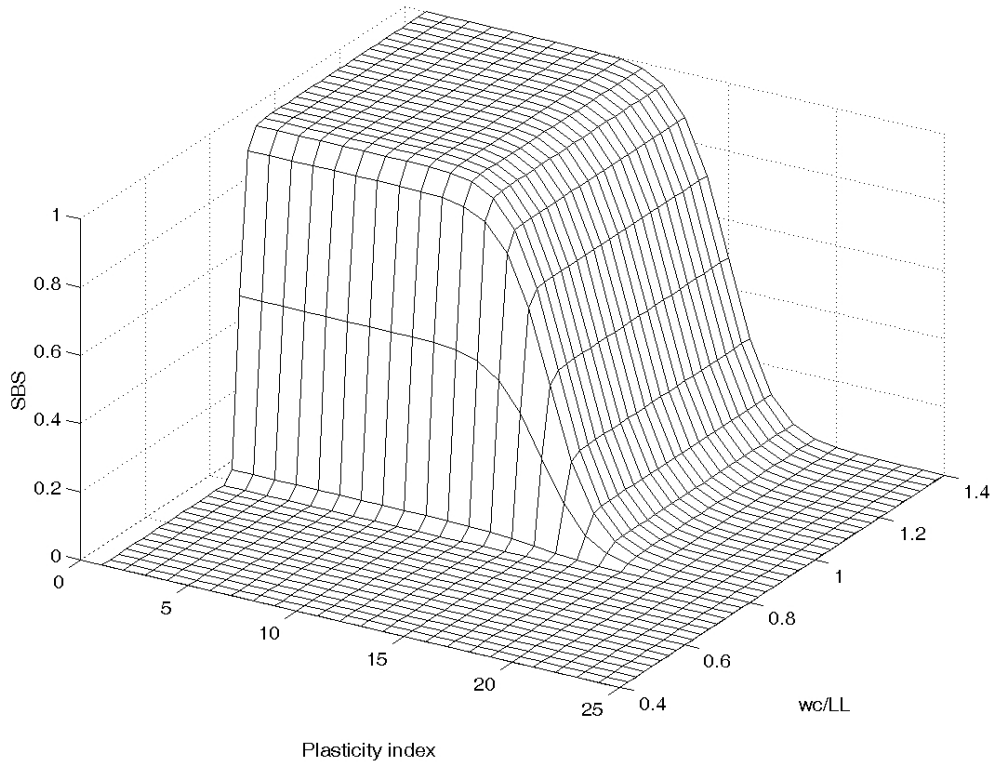


Figure 4.4. Illustration of variation of S_{BS} with plasticity index and w_c/LL ratio based on Equation 4.2.

Note that the Bray and Sancio model strictly predicts non-susceptibility for non-plastic soils ($PI = 0$) at w_c/LL ratios lower than 0.8. This aspect of the model is inconsistent with the definition of liquefaction susceptibility employed in this document because it appears to mix the susceptibility issue with the initiation issue (given that non-plastic soils at low water contents may not liquefy because their high density gives them high resistance to initiation rather than because they are inherently non-liquefiable).

4.4.3 Discussion

The susceptibility models of Boulanger and Idriss (2005) and Bray and Sancio (2006) are consistent for non-plastic fine-grained soils with high water contents (e.g., for $PI < 4$ and $w_c > 0.85LL$) and for plastic fine-grained soils ($PI > 20$). For fine-grained soils of moderate plasticity ($4 < PI < 20$) and lower water contents ($w_c < 0.85LL$), however, they can produce different indications of liquefaction susceptibility. Some of this difference is likely due to semantics, specifically what is considered to constitute

“liquefaction.” Bray and Sancio’s model considers a wider range of soils to be susceptible to liquefaction than does the model of Boulanger and Idriss. However, Boulanger and Idriss provide a more limited definition of liquefaction. In a somewhat simplified sense, Bray and Sancio’s model identifies fine-grained soils that are susceptible to the development of significant strains and potential reduction of strength. Boulanger and Idriss’ model identifies soils that have those characteristics *and* exhibit what they refer to as sand-like behavior. From a practical standpoint, one might wonder whether the difference is significant because the development of significant strain and the reduction of strength can lead to physical damage regardless of the responsible behavioral mechanism(s). The main implications of the difference lie in the applicability of common procedures for evaluating the potential for initiation of liquefaction – these procedures are based on case histories that involve predominantly clean sands and non-plastic silty sands. The question of whether penetration-based liquefaction potential procedures can be reliably applied to moderately plastic fine-grained soils has not been definitively answered.

4.5 SUSCEPTIBILITY INDEX

At the present time, the susceptibility models of Boulanger and Idriss (2005) and Bray and Sancio (2006) offer valid, defensible, yet different approaches to the evaluation of liquefaction susceptibility. While it may be argued that they treat the definition of liquefaction somewhat differently, both are useful in identifying soils that are likely to exhibit liquefaction, or at least liquefaction-like, behavior. Until sufficient evidence becomes available to indicate that one of these approaches, or yet another approach, provides a more reliable indication of liquefaction susceptibility than the other, it is recommended that both approaches be considered in a liquefaction susceptibility evaluation.

4.5.1 Combination of S_{BI} and S_{BS}

Equations 4.5 and 4.6 can be used to provide a quantitative estimate of susceptibility to liquefaction. The definitions of S_{BI} and S_{BS} allow the susceptibility models of Boulanger and Idriss (2005) and Bray and Sancio (2006) to be combined to

provide a single index for liquefaction susceptibility estimation. Given the two susceptibility estimation equations (Equation 5.1 and Equation 5.2) proposed by well-known and widely respected researchers, one can evaluate liquefaction susceptibility by using a weighted average of both methods. Therefore, the final liquefaction susceptibility for a given soil condition can be expressed as a “Susceptibility Index” defined as

$$SI = w_1 S_{BI} + w_2 S_{BS} \quad (4.7)$$

where w_1 and w_2 are user-defined weighting factors subject to the constraint that both are nonnegative and $w_1 + w_2 = 1$. The Susceptibility Index from Equation 4.7, therefore, ranges from 0.0 to 1.0.

4.5.2 Effects of Parametric Uncertainty

The preceding relationships for S_{BI} and S_{BS} assume that the parameters on which the susceptibility evaluations are based, PI and w_c/LL , are known with certainty. As a result, the transitions in S_{BI} and S_{BS} are quite sharp as illustrated, for example, in Figure 4.5. In reality, there is some uncertainty in the measurement of PI , w_c , and LL . This uncertainty can be expected to lead to additional uncertainty in the prediction of S_{BI} and S_{BS} , and, consequently, also in SI .

Phoon and Kulhawy (1999a,b) tabulated data for 33 different soils and found that the average coefficient of variation, C.O.V., of the plasticity index was 0.29. The average coefficients of variation for w_c and LL were both found to be 0.18. Huang (2008) added this parametric uncertainty to the model uncertainty expressed in equations 4.5 and 4.6 to produce revised expressions for S_{BI} and S_{BS} , i.e.,

$$S_{BI} = \left[1 + \left(\frac{\ln PI}{1.938} \right)^{6.676} \right]^{-2.0} \quad (4.8)$$

$$S_{BS} = \left[1 + \left(\frac{\ln PI}{2.778} \right)^{33.077} \right]^{-2.0} \left[1 + \left(\frac{4.401}{\ln(w_c / LL)} \right)^{360.471} \right]^{-2.0} \quad (4.9)$$

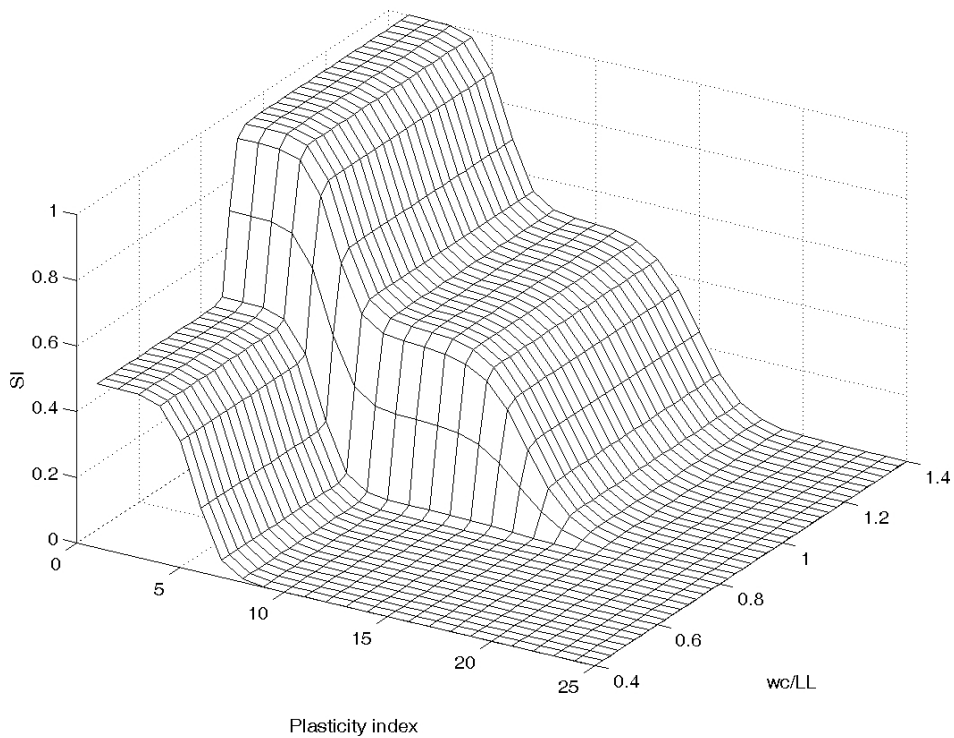


Figure 4.5. Variation of SI based on equal weighting of Boulanger-Idriss and Bray-Sancio susceptibility models. Effects of parametric uncertainty not included.

Substituting these expressions into Equation (4.7) produces an expression for SI that includes the effects of parametric uncertainty, and thereby eliminates the sharp transitions found in the preceding expression. This result, illustrated graphically in Figure 4.6, shows the significant effects of parametric uncertainty and is used in the WSliq code.

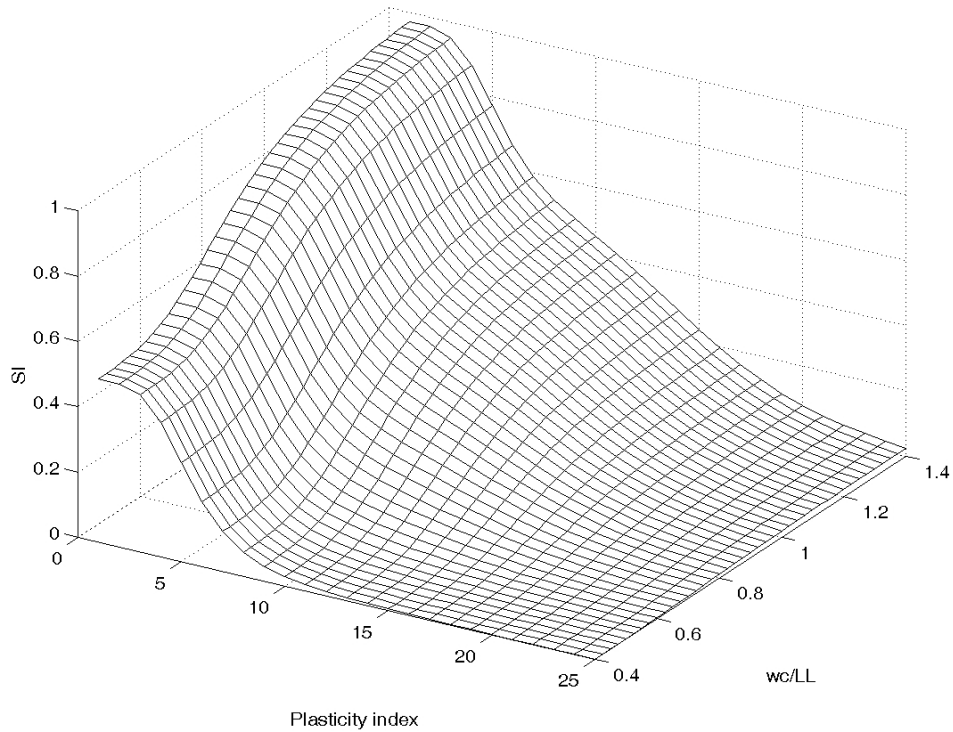


Figure 4.6. Variation of SI based on equal weighting of Boulanger-Idriss and Bray-Sancio susceptibility models. Effects of parametric uncertainty included.

4.6 RECOMMENDATIONS

Liquefaction-susceptible soils, as defined in this document, are those for which liquefaction is possible under some level of earthquake loading. With that definition in mind, all clean sands should be considered susceptible to liquefaction. Gravels should be considered susceptible to liquefaction when drainage is impeded by the presence of less permeable soils. Non-plastic ($PI = 0$) fine-grained soils should also be considered susceptible to liquefaction.

At this point, evaluations of liquefaction susceptibility for fine-grained soils with some plasticity should consider both the Boulanger-Idriss and Bray-Sancio criteria. When both agree and produce low SI values (SI less than about 0.2), the soil may be considered non-susceptible. When both agree and produce high SI values (SI greater than about 0.8), the soil should be considered susceptible. Soils for which S_{BI} and S_{BS} are significantly different may be soils for which available penetration-based liquefaction potential procedures are of questionable applicability; the liquefaction susceptibility of

such soils should be carefully evaluated on a case-by-case basis, and the soil may require cyclic testing for evaluation of their potential behavior.

4.7 EXAMPLES

The proposed procedure for layer-level screening of liquefaction susceptibility can be illustrated by a series of examples. The examples illustrate cases in which soils are clearly susceptible and non-susceptible but focus on conditions for which susceptibility is not as clear.

Case 1: Silty sand with $PI = 1$, $w_c = LL$		
Values	SI value	Comments
$S_{BI} = 1.00$ $S_{BS} = 0.76$	0.88	High likelihood of liquefaction. Would be considered susceptible by both Boulanger-Idriss and Bray-Sancio criteria when applied deterministically; SI value is less than 1.0 because of uncertainty in measured w_c/LL ratio.

Case 2: Silty sand with $PI = 3$, $w_c = 0.9LL$		
Values	SI value	Comments
$S_{BI} = 0.96$ $S_{BS} = 0.63$	0.80	High likelihood of liquefaction. Both Boulanger-Idriss and Bray-Sancio values are greater than 0.5; SI value is less than 1.0 primarily because of uncertainty in measured w_c/LL ratio.

Case 3: Silty sand with $PI = 6$, $w_c = 0.9LL$		
Values	SI value	Comments
$S_{BI} = 0.40$ $S_{BS} = 0.63$	0.51	Moderate likelihood of liquefaction. Boulanger-Idriss value less than 0.5 and Bray-Sancio value greater than 0.5. Deterministically, both Boulanger-Idriss and Bray-Sancio would classify as susceptible, but Boulanger-Idriss would be borderline classification. Treat as susceptible unless proven otherwise (by laboratory testing).

Case 4: Silty sand with $PI = 9$, $w_c = 0.85LL$		
Values	SI value	Comments
$S_{BI} = 0.09$ $S_{BS} = 0.51$	0.30	Mixed likelihood of liquefaction. Would be considered non-susceptible by Boulanger-Idriss and susceptible by Bray-Sancio criteria when applied deterministically. Differences in S_{BI} and S_{BS} are large – laboratory testing recommended.

Case 5: Silty sand with $PI = 5$, $w_c = 0.8LL$		
Values	<i>SI</i> value	Comments
$S_{BI} = 0.62$ $S_{BS} = 0.45$	0.54	Moderate likelihood of liquefaction. Would be considered susceptible by Boulanger-Idriss and non-susceptible by Bray-Sancio criteria when applied deterministically. Low w_c may be indication of sufficiently high density to preclude initiation, but should be considered susceptible.

Case 5: Silty sand with $PI = 15$, $w_c = 0.9LL$		
Values	<i>SI</i> value	Comments
$S_{BI} = 0.01$ $S_{BS} = 0.31$	0.16	Low likelihood of liquefaction. Would be considered strongly non-susceptible by Boulanger-Idriss and moderately susceptible by Bray-Sancio criteria. Candidate for laboratory testing.

Case 5: Silty sand with $PI = 15$, $w_c = 0.75LL$		
Values	<i>SI</i> value	Comments
$S_{BI} = 0.01$ $S_{BS} = 0.17$	0.09	Very low likelihood of liquefaction. Would be considered non-susceptible by both Boulanger-Idriss and Bray-Sancio criteria.

Chapter 5

Initiation of Liquefaction

5.1 INTRODUCTION

Evaluating the potential for initiation of liquefaction is one of the most important parts of a liquefaction hazard evaluation. A soil that is judged to be susceptible to liquefaction (Chapter 4) may not liquefy if the anticipated level of ground shaking is not strong enough to overcome the inherent liquefaction resistance of the soil. Evaluating the potential for initiation of liquefaction, referred to subsequently as liquefaction potential, involves comparing the anticipated level of loading produced by earthquake shaking at a particular site with the liquefaction resistance of the soil at that site.

The initiation of liquefaction depends on the level of anticipated ground shaking and is quite sensitive to the density of the soil. *In situ* soil density, however, is notoriously difficult to measure, particularly for the types of loose, saturated, cohesionless soils that are normally of concern in a liquefaction evaluation; techniques that attempt to measure *in situ* density frequently disturb the soil in a way that changes the density. As a result, measurements of density are usually replaced by measurements of penetration resistance—standard penetration test (SPT) and/or cone penetration test (CPT). Procedures for evaluating liquefaction potential based on both are presented in this chapter.

As described in Chapter 2, seismic environments vary tremendously from highly active areas in western Washington to relatively inactive areas in eastern Washington. Even within western Washington, the seismicities of different areas can vary substantially, particularly with respect to the magnitudes of earthquakes that can occur. Because magnitude is a critical parameter in the characterization of earthquake loading in conventional liquefaction potential analyses, it is important that such analyses properly account for the range of magnitudes that can occur at a particular site. The manner in which magnitude should be represented in liquefaction potential analyses has been a subject of some controversy in geotechnical earthquake engineering. The controversy

has resulted, however, from the desire to minimize the number of calculations required to evaluate liquefaction potential, which requires that the range and distribution of earthquake magnitudes that produce strong ground motion at a particular site be represented by a single magnitude. This issue is resolved by the research described in this report, and the entire distribution of magnitudes can be easily included in the liquefaction potential calculations for any site in Washington State by using the WSliq program.

5.2 BACKGROUND

The state of practice of liquefaction potential evaluation has essentially changed only incrementally over the past 20 years. The cyclic stress approach, in which both loading and resistance are characterized in terms of cyclic shear stress amplitudes, remains the most commonly used in practice. The most commonly used form of the cyclic stress approach is that recommended by participants at a 1996 National Earthquake Hazards Reductions Program (NEHRP) workshop and described by Youd et al. (2001). Since that time, a great deal of research on soil liquefaction has been performed, and many papers have been added to the liquefaction literature. Nearly all of those papers have dealt with detailed investigations of different components of the cyclic stress approach or with its application to case histories in which liquefaction was (or was not) observed. In recent years, two additional cyclic stress-based procedures have been developed: a deterministic procedure by Idriss and Boulanger (2004) and a probabilistic procedure using SPT data (Cetin et al., 2004) and/or CPT data (Moss et al., 2006). The Idriss and Boulanger (2004) procedure is significant because it brings a unifying element of soil mechanics into the procedure in a way that has not previously existed; it is based on a critical state framework that was not sufficiently developed at the time that the NEHRP and earlier procedures were developed. The Cetin et al. (2004) and Moss et al. (2006) procedures are notable not only for their relatively advanced statistical basis but also for the thorough and consistent manner in which their case history databases were assembled and vetted.

Taken together, the NEHRP, Idriss and Boulanger, and Cetin/Moss procedures are considered to provide the best currently available coverage of the problem of

liquefaction initiation. The procedures are based on different data sets, model different components of the cyclic stress approach differently, and produce generally consistent, but somewhat different, results. They have different historical rates of usage and different levels of mechanistic accuracy. Each has advantages and limitations with respect to each other, and none can be considered, on the basis of available evidence, to be clearly superior to the others. As discussed in Section 5.6, the use of all of these methods is recommended to produce a stable and consistent final liquefaction potential evaluation that reflects the strengths of each. The following sections provide a brief description of the salient features of each procedure; the intention is not to describe the details and justification for each – users are expected to read the references to obtain that information – but to illustrate the manner in which they compare and contrast with each other.

5.3 REQUIRED INFORMATION

Evaluation of liquefaction potential requires comparison of the anticipated level of loading imposed on a soil profile with the inherent resistance of the soil profile to liquefaction. Since both loading and resistance can vary with depth, the potential for liquefaction must be evaluated at different depths within the soil profile of interest. The key to the evaluation process is the expression of both loading and resistance in common terms. Usually, both are expressed in terms of normalized cyclic shear stress amplitudes known as the cyclic stress ratio (*CSR*) for loading, and the cyclic resistance ratio (*CRR*) for resistance. The cyclic stress approach defines loading in terms of cyclic shear stress amplitudes, which can be obtained from site response analyses or by correlation to peak ground acceleration. Peak ground acceleration is usually tied to a particular hazard level, as represented by a mean annual rate of exceedance (or a return period). The peak acceleration would be obtained from a seismic hazard curve, which is the result of a probabilistic seismic hazard analysis (PSHA). PSAs may be performed on a site-specific basis for important projects but are more commonly obtained from the USGS National Seismic Hazard Mapping Project (<http://geohazards.cr.usgs.gov/eq/>).

Site response analyses require definition of stiffness and damping characteristics throughout the soil profile (including non-liquefiable layers that may be located above or

below the layers of interest); these characteristics may be measured directly (e.g., shear wave velocity measurements) or correlated to other measured parameters (e.g., SPT resistance). Correlation to peak ground acceleration is frequently accomplished by using amplification factors, which require knowledge of local surficial geology. Ground motion duration effects are accounted for by specification of earthquake magnitude, which is used to adjust the cyclic shear stress amplitude. To account for duration effects that are not reflected in peak acceleration values, the cyclic stress approach also makes use of earthquake magnitude. Because ground motions are typically specified by means of PSHA, a specific ground motion level comprises contributions from many different magnitudes. Therefore, the distribution of magnitude is required for an accurate evaluation of liquefaction potential. Such information can be extracted from a site-specific PSHA or from the deaggregation files available from the USGS National Seismic Hazard Mapping Project (<http://geohazards.cr.usgs.gov/eq/>).

Evaluation of liquefaction potential requires accurate characterization of subsurface conditions by using sufficient sampling to allow definition of soil type and fines content and *in situ* penetration (SPT and/or CPT) tests as indicators of the density of potentially liquefiable soil layers. The subsurface investigation should establish the depths and thicknesses of all liquefaction-susceptible soil layers and should define penetration resistance and fines content profiles in all such layers. Such testing should also establish the plasticity index for soils with significant amounts of fines; as discussed in Chapter 3, liquefaction susceptibility is strongly influenced by fines plasticity. Because liquefaction resistance is evaluated by correlation to penetration resistance, it is imperative that it be determined accurately. SPT testing is notoriously equipment- and operator-dependent, so efforts must be expended to ensure that standard equipment/procedures, or accurate corrections for non-standard equipment/procedures, are used. Appendix A describes standard SPT equipment and procedures and provides procedures for correcting measured penetration resistances for deviations from those standards. CPT testing, due in part to its more recent introduction into practice, is considerably more standardized and less operator-dependent than SPT testing.

5.4 PROCEDURES

The basic procedure for evaluating liquefaction potential involves characterization of loading and resistance, which are described in order in this section. Liquefaction resistance can be determined on the basis of SPT resistance or CPT resistance; procedures for both are presented. As previously discussed, a number of liquefaction evaluation procedures are available in the literature, and it is important to recognize that each represents a specific approach to the problem. Although they frequently share common terms and notation, they are usually developed in such a way that multiple terms are inter-related; therefore, one cannot mix and match terms from different procedures.

5.4.1 Characterization of Loading

Earthquake loading is characterized, for the purposes of liquefaction potential evaluation, by a cyclic stress ratio, *CSR*, that can be defined in two ways: (1) by calculating the maximum shear stress at the depth of interest from the results of a site-specific ground response analysis, or (2) by estimating the maximum shear stress at the depth of interest from peak ground surface acceleration and a depth reduction factor that represents the variation of shear stress amplitude with depth for typical soil profiles.

The procedure for characterization of earthquake loading can be accomplished in the following series of steps:

1. *Determine the governing ground motion criterion.* In conventional liquefaction potential evaluations, ground motions are specified in terms of specific hazard levels, e.g., as a motion with a 10 percent probability of exceedance in a 50-year period, which corresponds to a 475-year return period. The performance-based approach developed in this research takes all hazard levels properly into account; in that case, a governing ground motion criterion is not needed, as discussed in Section 5.6.3.
2. *Determine the peak ground acceleration associated with the governing ground motion criterion.* For special projects, the characteristics of such motions can be obtained from a site-specific probabilistic seismic hazard analysis (PSHA). For most projects, however, these parameters can be obtained from regional PSHAs performed by the USGS National Seismic

Hazard Mapping Project (<http://geohazards.cr.usgs.gov/eq/>). The peak ground accelerations obtained from the USGS website correspond to “firm rock” sites (average shear wave velocity of 760 m/sec, or 2,500 ft/sec, within the upper 30 m). The use of the 2002 USGS data is recommended at this time. A database of USGS hazard data on a grid across Washington State is built into the WSliq program; this eliminates the time and effort required to download and process hazard data from the USGS website. Step-by-step procedures for expanding and/or updating the hazard database are described in the WSliq User’s Manual (Appendix H). The database can be used to interpolate to any return period of interest (between 72 and 4,975 years).

3. *Account for the effects of local site conditions.* Local site conditions are known to strongly affect earthquake ground motions, and it is imperative that they be accounted for in an evaluation of liquefaction potential. The results of a PSHA will generally provide a peak acceleration value at a particular point in a soil profile (typically at the ground surface for a site-specific PSHA, or at a bedrock outcrop for a USGS PSHA). The corresponding motions at the depths of potentially liquefiable soil layers must then be computed. This can be accomplished by rigorous or simplified approaches.
 - a. Rigorous approach. Perform site-specific ground response analyses to compute the cyclic shear stresses for the actual subsurface conditions at the site. These analyses should be performed with a suite of at least seven different input motions all scaled to be consistent with the ground motion hazard obtained from the PSHA. The peak cyclic shear stress amplitudes at the depths of interest should be taken as the averages of the peak values produced by the site-specific analyses. The advantage of this approach is that it considers the actual soil profile and its effects on the transmission of seismic waves from bedrock to the ground surface, thereby providing, at least in theory, a more accurate indication of loading. The disadvantage is that it

requires site-specific ground response analyses with appropriately scaled earthquake ground motions, which can be time-consuming to prepare.

In the rigorous approach, the cyclic shear stress is then normalized by initial vertical effective stress to obtain a cyclic stress ratio defined as

$$CSR = 0.65 \frac{\tau_{\max}}{\sigma'_{vo} \cdot MSF} \quad (5.1)$$

where τ_{\max} is the peak cyclic shear stress, σ'_{vo} is the initial vertical effective stress, MSF is a magnitude scaling factor that accounts for ground motion duration by empirical correlation to magnitude (Table 5.1), and the 0.65 factor is a relic of early liquefaction potential evaluation procedures (which helped relate transient earthquake loading to harmonic laboratory loading) that has been retained in contemporary procedures.

The rigorous approach is recommended when a strong impedance contrast exists within or at the bottom of any potentially liquefiable layer. For liquefaction potential evaluation purposes, a strong impedance contrast is defined as a boundary between materials where the shear wave velocity of the upper material is less than 70 percent of the shear wave velocity of the material immediately beneath it.

Table 5.1. Calculation of magnitude scaling factor by methods of NCEER and Idriss and Boulanger. Cetin/Moss models do not make use of magnitude scaling factor.

NCEER (Youd et al., 2001)	Idriss and Boulanger (2004)
$MSF = \begin{cases} \left(\frac{7.5}{M_w}\right)^{2.95} & M_w \leq 7.5 \\ \left(\frac{7.5}{M_w}\right)^{2.56} & M_w > 7.5 \end{cases}$	$MSF = \min \left\{ \begin{array}{l} 6.9 \exp[-M_w / 4] - 0.058 \\ 1.8 \end{array} \right\}$

Figure 5.4 shows the variation of the magnitude scaling factor (MSF) with magnitude for the two procedures that make use of a magnitude scaling factor. In both cases, the MSF value decreases with increasing magnitude, which causes the CSR to increase with increasing magnitude. The result is a higher level of loading for higher magnitude (hence, longer duration) events, all other things being equal.

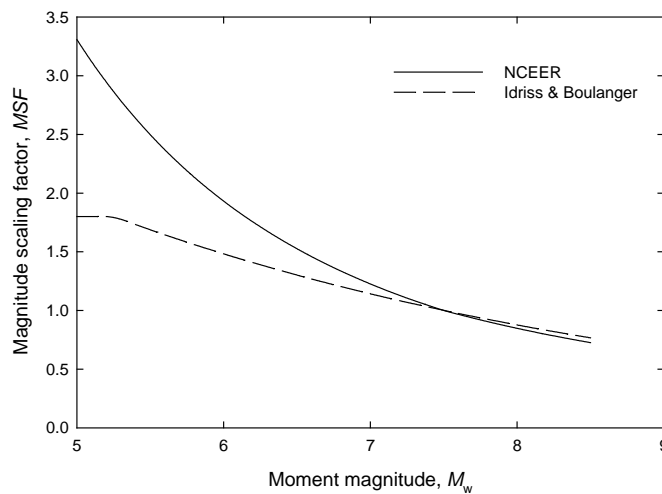


Figure 5.1. Variation of magnitude scaling factor with earthquake magnitude for NCEER and Idriss and Boulanger models.

- b. Simplified approach. The simplified approach estimates cyclic shear stress amplitudes from peak ground surface accelerations by using semi-empirical functions that describe the average behavior of many different soil profiles. The peak ground surface accelerations can be obtained from site-specific ground response analysis, but since those analyses can predict cyclic shear stresses in potentially liquefiable layers directly, they are not used with the simplified approach. Peak ground surface acceleration is usually obtained by multiplying bedrock peak acceleration values by amplification factors expressed as functions of mapped surface geology. The amplification factors,

which account for nonlinear response at higher levels of shaking, can be estimated as

$$\ln F = \alpha + \beta \ln(a_{\max})_{\text{rock}} \quad (5.2)$$

where α and β are as given in Table 5.2.

Table 5.2. Coefficients for estimation of peak ground surface acceleration amplification factor (after Stewart et al. 2003).

Surface Geology Category	α	β
Quaternary alluvium	-0.15	-0.13
Holocene lacustrine/marine	-0.59	-0.39
Holocene coarse	-0.11	-0.10
Holocene fine/mixed	-0.50	-0.33
Pleistocene	0.14	0.02
Tertiary	0.23	-0.02
Mesozoic + Igneous	-0.13	-0.08

4. *Compute the cyclic stress ratio.* For all potentially liquefiable layers, compute *CSR* as

$$CSR = 0.65 \frac{a_{\max}}{g} \cdot \frac{\sigma_{vo}}{\sigma'_{vo}} \cdot \frac{r_d}{MSF} \quad (5.3)$$

where a_{\max} = peak ground surface acceleration (from Step 3), g = acceleration of gravity (in same units as a_{\max}), σ_{vo} = total vertical stress at depth of interest, and r_d = depth reduction factor determined as indicated in Table 5.3.

Table 5.3 Depth correction factor calculation.

NCEER (Youd et al., 2001)	Idriss and Boulanger (2004)
$r_d = \frac{1 - 0.4113z^{0.5} + 0.04052z + 0.001753z^{1.5}}{1 - 0.4117z^{0.5} + 0.05729z - 0.006205z^{1.5} + 0.00121z^2}$ <p>where z is the depth below the ground surface in meters.</p>	$r_d = \exp[\alpha(z) + \beta(z)M_w]$ <p>where</p> $\alpha(z) = -1.012 - 1.126 \sin\left(\frac{z}{11.73} + 5.133\right)$ $\beta(z) = 0.106 + 0.118 \sin\left(\frac{z}{11.28} + 5.142\right)$ <p>with z in meters and limited to a maximum depth of 20 m, below which the use of site-specific response analysis is recommended.</p>

The variation of r_d with depth for the NCEER and Idriss and Boulanger procedures is similar; the Cetin/Moss procedures do not break r_d out as a separate variable, although they both account for depth effects in a different manner. Although they differ slightly, all are consistent in producing a trend of decreasing shear stress amplitude with depth, which is consistent with wave propagation theory.

5.4.2 Characterization of Resistance

Liquefaction resistance is generally characterized by some form of penetration resistance modified to account for a variety of additional variables that can affect liquefaction resistance. Historically, liquefaction resistance has been most commonly correlated to SPT resistance. In recent years, however, additional case histories with CPT data have become available and have been used to develop improved correlations between liquefaction resistance and CPT tip resistance. CPT-based methods can be considered reliable, provided that they are supplemented by information sufficient to confirm the soil types inferred from the CPT test; such information is usually obtained from soil borings.

Procedures for characterizing liquefaction resistance of sands and silty sands based on SPT and CPT testing are presented in the following section. Note that the

reliability of any liquefaction hazard evaluation will be improved by performing both SPT- and CPT-based liquefaction potential analyses; the use of both procedures should be considered for projects with difficult soil conditions and/or severe consequences of liquefaction.

5.4.2.1 SPT-Based Resistance

SPT-based liquefaction evaluation procedures are based on the correlation of liquefaction resistance to the corrected standard penetration resistance of the soil. The correction process involves the application of a number of correction factors to the field-measured SPT resistance. The process can be accomplished in the following steps:

1. *Develop profiles of the measured SPT resistance and fines content within all potentially liquefiable soils.* The SPT equipment and procedures used to obtain the measured SPT resistances should be recorded during the site investigation and considered during the liquefaction potential evaluation process. The importance of accurate SPT measurements on the reliability of a liquefaction hazard evaluation cannot be overemphasized.

Interpolation of SPT resistances and fines contents between the points at which they are measured should be done with due consideration of site geology.

2. *Correct the measured SPT resistances for deviations from standard equipment and procedures.* Corrections for rod length, sampler type, borehole diameter, and energy are described in Appendix A.
3. *Compute clean sand corrected SPT resistance.* The presence of fines is accounted for by a fines correction. The NCEER and Idriss and Boulanger procedures specify fines corrections as indicated in Table 5.4. The Cetin procedure accounts for the effects of fines, along with other parameters, in an equation (Equation 5.5) described subsequently.

Table 5.4 Clean sand SPT value calculation

NCEER (Youd et al., 2001)	Idriss and Boulanger (2004)
$(N_1)_{60,cs} = \alpha + \beta(N_1)_{60}$ where $\alpha = \begin{cases} 0 & FC \leq 5\% \\ \exp[1.76 - 190/FC^2] & 5\% < FC < 35\% \\ 1.0 & FC \geq 35\% \end{cases}$ $\beta = \begin{cases} 1.0 & FC \leq 5\% \\ 0.99 + FC^{1.5}/1000 & 5\% < FC < 35\% \\ 1.2 & FC \geq 35\% \end{cases}$ and FC is in percent.	$(N_1)_{60,cs} = (N_1)_{60} + \Delta(N_1)_{60}$ where $\Delta(N_1)_{60} = \exp \left[1.63 + \frac{9.7}{FC} - \left(\frac{15.7}{FC} \right)^2 \right]$ and FC is in percent.

4. Compute the cyclic resistance ratio at a standard vertical effective stress of 1 atm. Table 5.5 presents equations for calculating $CRR_{\sigma' = 1 \text{ atm}}$ as functions of $(N_1)_{60,cs}$ for the NCEER and Idriss-Boulanger procedures. The Cetin equation includes terms that account for *in situ* vertical effective stress, so this step is not required in that procedure.

Table 5.5 Calculation of cyclic resistance ratio at 1 atm

NCEER (Youd et al., 2001)	Idriss and Boulanger (2004)
$CRR_{\sigma' = 1 \text{ atm}} = \frac{1}{34 - (N_1)_{60,cs}} + \frac{(N_1)_{60,cs}}{135}$ $+ \frac{50}{(10(N_1)_{60,cs} + 45)^2} - \frac{1}{200}$	$CRR_{\sigma' = 1 \text{ atm}} = \exp \left[\frac{(N_1)_{60,cs}}{14.1} + \left(\frac{(N_1)_{60,cs}}{126} \right)^2 \right]$ $- \left[\left(\frac{(N_1)_{60,cs}}{23.6} \right)^3 + \left(\frac{(N_1)_{60,cs}}{25.4} \right)^4 - 2.8 \right]$

5. Compute the cyclic resistance ratio at the *in situ* vertical effective stress. The NCEER and Idriss & Boulanger procedures require that the value of

CRR be adjusted to account for the *in situ* vertical effective stress using the relationships

$$CRR_{\sigma'} = CRR_{\sigma'=1 \text{ atm}} K_{\sigma} \quad (5.4)$$

and the expressions for K_{σ} are shown in Table 5.6.

Table 5.6 Calculation of overburden stress correction factor, K_{σ}

NCEER (Youd et al., 2001)	Idriss and Boulanger (2004)
$K_{\sigma} = \min \left\{ \begin{array}{l} \left(\frac{\sigma'_{vo}}{p_a} \right)^{f-1} \\ 1.0 \end{array} \right\}$ <p>where $f = 0.7 - 0.8$ for $D_r = 40 - 60\%$ and $f = 0.6 - 0.7$ for $D_r = 60 - 80\%$.</p>	$K_{\sigma} = \min \left\{ \begin{array}{l} 1 - C_{\sigma} \ln \left(\frac{\sigma'_{vo}}{p_a} \right) \\ 1.0 \end{array} \right\}$ <p>where</p> $C_{\sigma} = \frac{1}{18.9 - 2.55\sqrt{(N_1)_{60,cs}}}$ <p>and $(N_1)_{60,cs}$ is limited to a maximum value of 37.</p>

The Cetin et al. procedure allows direct computation of CRR at the *in situ* vertical effective stress as

$$CRR_{\sigma'} = \exp \left[\frac{(N_1)_{60}(1 + 0.004FC) - 29.53 \ln M_w - 3.7 \ln(\sigma'_{vo}/p_a) + 0.05FC - 16.85 + 2.70\Phi^{-1}(P_L)}{13.32} \right] \quad (5.5)$$

where p_a is atmospheric pressure (in the same units as σ'_{vo}) and P_L is the probability of liquefaction. P_L values of 0.6 have been found to produce results that are generally consistent with the NCEER procedure, however, Cetin et al. recommend deterministic analyses be performed with $P_L = 0.15$.

5.4.2.2 CPT-Based Resistance

CPT procedures have been developed that are similar to SPT-based procedures. Until relatively recently, however, fewer data have been available with which to calibrate CPT procedures than SPT procedures. Recent studies, however, have developed and

vetted a significant database of case histories for which CPT data are available, thereby allowing development of new CPT-based procedures.

CPT-based procedures are affected by the fact that no sample is obtained in a cone penetration test. Because SPT-based procedures have shown that liquefaction resistance is affected by fines content (which can be measured with the samples obtained from that test), CPT-based procedures must attempt to account for the presence of fines indirectly, i.e., by using parameters measured in the CPT test, typically the friction ratio. The implications of this requirement on recommended procedures are discussed in Section 5.6.

CPT-based liquefaction evaluation procedures are based on correlations between liquefaction resistance and corrected CPT tip resistances. The correction process and the use of corrected tip resistances to compute CRR can be accomplished in the following steps:

1. *Develop profiles of measured CPT tip resistance, q_{cm} , and sleeve resistance, f_{sm} , within all potentially liquefiable soils.* CPT data is usually acquired digitally, so this data is typically contained in an ASCII file.
2. *Develop a profile of friction ratio, computed as*

$$R_f = \frac{f_{sm}}{q_{cm}} \cdot 100\% \quad (5.6)$$

within all potentially liquefiable soils.

3. *Adjust the measured tip resistance for effective overburden pressure as*

$$q_{c1} = C_N q_{cm} \quad (5.7)$$

Expressions for C_N are presented in Table 5.7.

Table 5.7 Calculation of overburden stress adjustment factor, C_N

Idriss and Boulanger (2004)	Moss et al. (2006)
$C_N = \left(\frac{\sigma'_{vo}}{p_a} \right)^{1.338 - 0.249(q_{c1}/p_a)^{0.264}} \leq 1.7$ <p>Note: Since q_{c1} is required to compute C_N (on which q_{c1} depends), iteration is required.</p>	$C_N = \left(\frac{\sigma'_{vo}}{p_a} \right)^{-c}$ <p>where</p> $c = 0.78 q_c^{-0.33} \left(R_f \left \log(10 + q_c) \right ^{-1.21} \right)^{0.32 q_c^{-0.35} - 0.49}$

4. *Normalize the corrected tip resistance as*

$$q_{c1N} = q_{c1}/p_a \quad (5.8)$$

5. *Compute the clean sand corrected CPT resistance.* The effects of fines can be accounted for by a fines correction using the relationship

$$q_{c1N,cs} = K_c q_{c1N} \quad (5.9)$$

where K_c is a fines correction factor (Table 5.8).

Table 5.8 Calculation of fines correction factor, K_c

Idriss and Boulanger (2004)	Moss et al. (2006)
$K_c = \begin{cases} 1.0 & \text{for } FC \leq 5\% \\ \text{undefined} & \text{for } FC > 5\% \end{cases}$ <p>Idriss and Boulanger do not recommend a fines correction for $FC > 5\%$. Therefore, their model is directly applicable only for clean sands; it will produce conservative results when applied to silty sands.</p>	<p>Moss et al. (2006) use friction ratio as a proxy for fines content in the equation shown in Step 8; therefore, no specific fines correction is required for that model.</p>

6. *Consider the potential for “thin layer effects” associated with relatively thin, stiff layers within the profile.* The presence of thin granular layers within softer materials, which is not uncommon in many fluvial deposits, can lead to measured CPT resistances that under-represent the actual density of the thin granular layer. Thin layer correction procedures have been proposed; however, they are based on elastic theory, which is considered to have limited applicability to the liquefaction problem. There is little question those CPT resistances near layer boundaries can be locally influenced by those boundaries, and that individual q_{c1} values within about 1 m of such boundaries can be inaccurate. For the most common case of a granular layer sandwiched between softer layers, the effect of the softer layers will be to reduce the measured tip resistance, which will lead to a conservative estimate of liquefaction potential. If such conditions exist and result in a conclusion of marginal liquefaction potential (e.g., a factor of safety slightly above or below 1.0), the

reasonableness of the result should be re-evaluated with consideration of site stratigraphy, depositional environment, and available soil sample data.

7. Compute the cyclic resistance ratio at a standard vertical effective stress of 1 atm. Table 5.9 presents equations for calculating $CRR_{\sigma=1 \text{ atm}}$ as functions of q_{c1N} .

Table 5.9 Calculation of cyclic resistance ratio at 1 atm vertical effective stress.

<p>Idriss and Boulanger</p> $CRR_{\sigma=1 \text{ atm}} = \exp \left[\frac{q_{c1N}}{540} + \left(\frac{q_{c1N}}{67} \right)^2 - \left(\frac{q_{c1N}}{80} \right)^3 + \left(\frac{q_{c1N}}{114} \right)^4 - 3 \right]$
<p>Moss et al.</p> <p>See Step 8</p>

8. Compute the cyclic resistance ratio at the *in situ* vertical effective stress.

The value of CRR is adjusted to account for the *in situ* vertical effective stress by using the relationships

$$CRR_{\sigma'} = CRR_{\sigma'=1 \text{ atm}} K_{\sigma} \quad (5.10)$$

and the expressions for K_{σ} are shown in Table 5.10.

Table 5.10 Calculation of overburden stress correction factor, K_{σ}

<p>Idriss and Boulanger (2004)</p> $K_{\sigma} = \min \left\{ \begin{array}{l} 1 - C_{\sigma} \ln \left(\frac{\sigma'_{vo}}{P_a} \right) \\ 1.0 \end{array} \right\}$ <p>where</p> $C_{\sigma} = \frac{1}{37.3 - 8.27(q_{c1N})^{0.264}}$ <p>and q_{c1N} is limited to a maximum value of 211.</p>
--

The Moss et al. procedure allows direct computation of CRR at the *in situ* vertical effective stress as (Eq. 5.11)

$$CRR = \exp \left[\frac{q_{cl}^{1.045} + 0.11R_f q_{cl} + 0.001R_f + c(1 + 0.85R_f) - 0.848 \ln M_w - 0.002 \ln \sigma'_{vo} - 20.923 + 1.632\Phi^{-1}(P_L)}{7.177} \right]$$

where c is the exponent calculated in Step 3.

5.4.3 Evaluation of Liquefaction Potential

After loading has been expressed in terms of the cyclic stress ratio and resistance has been expressed in terms of the cyclic resistance ratio, liquefaction potential can be expressed in terms of a factor of safety against liquefaction defined as

$$FS_L(z) = \frac{CRR(z)}{CSR(z)} \quad (5.12)$$

where $CSR(z)$ is the value of the cyclic stress ratio at depth z , which was computed in Step 4 of Section 5.4.1, and $CRR(z)$ is the cyclic resistance ratio at the same depth, which was computed in Step 5 of Section 5.4.2.1 (for SPT-based case) or Step 8 of Section 5.4.2.2 (for CPT-based case).

5.5 DISCUSSION

The deterministic cyclic stress approach to evaluating liquefaction potential has been used for the past 40 years. Its results have been shown to be biased toward conservatism (i.e., to predict “false positives” much more frequently than “false negatives”), which was the intent of its developers. When used for design with factors of safety in the typical range of 1.2 to 1.5, it will only rarely result in the occurrence of liquefaction at a site with an acceptable factor of safety. However, it may very well predict the occurrence of liquefaction at a site that would actually not liquefy under design-level loading.

The cyclic stress approach has one characteristic that complicates its used in the type of more advanced and complete evaluations of liquefaction hazard that the geotechnical engineering profession is moving toward with the development of performance-based earthquake engineering. In the cyclic stress approach, the characterization of loading requires two pieces of earthquake-related information: the

peak ground surface acceleration and the earthquake magnitude. The fact that hazard levels are usually specified solely in terms of peak acceleration (e.g., the peak acceleration at a particular return period) has led to confusion among professionals about how to specify a corresponding magnitude in a single-scenario analysis. Some engineers propose using modal magnitude (i.e., the magnitude that produces the strongest contribution to peak acceleration at the return period of interest) and some propose using mean magnitude. The short answer is that, for Washington State, the use of mean magnitude produces results that are closer to those computed with the entire distribution of possible magnitudes than does use of modal magnitude. The fact that the value of the mean magnitude itself may not contribute strongly to peak acceleration at a particular location should not be any more troubling than the fact that 3.5, the expected value of the numbers returned by multiple tosses of a fair die, does not appear on any of the faces of that die.

5.6 RECOMMENDATIONS

The following sections present recommendations for the evaluation of liquefaction potential in Washington State. It must be recognized that the procedures described in this chapter allow evaluation of the potential for initiation of liquefaction. However, the fact that liquefaction is initiated at a particular site does not, by itself, mean that significant damage will occur. The potential for liquefaction-related damage, which is much more closely related to permanent deformations than to the generation of high porewater pressures (which is all that the initiation of liquefaction implies) depends on the effects of liquefaction – for example, lateral spreading, settlement, and/or instability, which are covered in subsequent chapters. Nevertheless, one strategy, which may be appropriate in cases where very loose soils exist, is to design (or remediate) so that liquefaction will not be initiated.

The use of SPT-based procedures for evaluating liquefaction potential is encouraged at this time for most sites for two primary reasons. First, SPT sampling produces a physical sample that can be used to confirm properties such as fines content and plasticity index, which strongly affect liquefaction susceptibility and resistance. Second, available procedures for predicting the effects of liquefaction are almost all SPT-

based at this time. Because performance is related to these effects, and design/hazard evaluation is related to performance, the availability of SPT data will be required anyway.

5.6.1 Single-Scenario Analyses

Use of the single-scenario approach is not recommended for analysis or design. It requires representation of the entire range and distribution of earthquake magnitudes affecting a site by a single magnitude. Its only advantage over the multiple scenario approach is in speed (i.e., fewer calculations), and that advantage is effectively eliminated by the multiple-scenario option in the WSliq program. The single-scenario option is useful, however, for investigating the sensitivity of liquefaction potential to various combinations of peak acceleration and magnitude or to different soil properties.

5.6.2 Multiple-Scenario Analyses

For analysis and design at this time, the use of weighted multiple-scenario analyses is recommended. Multiple-scenario analyses properly account for the range and distribution of earthquake magnitudes that contribute to ground motion hazard. Those distributions, as obtained from USGS deaggregation files, are built into the WSliq program so that performing a multiple-scenario analysis is no more difficult than performing a single-scenario analysis.

The availability of multiple credible procedures for evaluating liquefaction potential should also be taken advantage of. The use of weighted average factors of safety, based on contributions from the NCEER, Idriss and Boulanger, and Cetin/Moss procedures, is recommended. The weighting factors should be no less than 0.2 and no greater than 0.5, and the three weighting factors should add up to 1.0. The WSliq program allows the entry of weighting factors and computation of individual and weighted average factors of safety.

With the use of weighted average, multiple-scenario analyses, a design factor of safety of 1.3 is recommended.

5.6.3 Performance-Based Analyses

A transition toward the use of performance-based concepts in the evaluation of liquefaction potential is recommended. The performance-based approach, as described in Chapter 3, considers all possible ground motion levels (rather than just a single level, as in the multiple scenario approach) and thereby produces a more complete and consistent evaluation of the potential for initiation of liquefaction. Use of the performance-based approach, however, requires different performance criteria because that approach can predict the actual return period of liquefaction (rather than a factor of safety against liquefaction for a ground motion with a single, specified return period). Since a performance-based procedure requires a probabilistic estimate of response, the Cetin et al. liquefaction potential model was used in the performance-based formulation developed for this project.

A preliminary calibration exercise has been performed to identify an appropriate design-level return period for liquefaction in Washington State. The results of that exercise indicate that conventional deterministic procedures for evaluation of liquefaction hazard (based on 475-year peak acceleration values and mean magnitudes) produce results consistent with liquefaction return periods of approximately 400 years along the I-5 corridor and eastward. The same procedures produce results consistent with longer return periods at sites closer to the Pacific coast. To achieve uniformity of liquefaction hazard for constructed facilities throughout the state, a design-level liquefaction return period of 400 years is preliminarily recommended. It is also recommended that WSDOT engineers record the results of both multiple-scenario and performance-based analyses at locations throughout the state to further evaluate the relationship between liquefaction return period and factor of safety against liquefaction.

5.7 OTHER CONSIDERATIONS

The procedures described in the preceding section can be used for the types of soils for which the great majority of liquefaction hazard evaluations are performed. On occasion, the behavior of other types of soils during earthquakes may require consideration. The following sections provide some basic considerations for such cases.

5.7.1 Behavior of Plastic Silts and Clays

The liquefaction potential of fine-grained soil is influenced by the plasticity of the soil. Non-plastic, cohesionless, fine-grained soils (principally coarse silts), which can liquefy, can be identified with the use of the compositional criteria presented in Section 4.2.3. The potential for liquefaction of non-plastic, cohesionless, fine-grained soils can be evaluated by using the procedures described in the previous section.

Plastic, cohesive, fine-grained soils can soften and weaken during earthquake loading, but these phenomena should not be referred to with the term “liquefaction.” The behavior of clays and plastic silts is different than that exhibited by non-plastic granular soils, and different procedures should be used to evaluate their performance. Boulanger and Idriss (2004, 2005) describe procedures for evaluating the behavior of such soils under earthquake loading conditions.

5.7.2 Liquefaction of Gravelly Soils

Gravelly soils present distinct problems for evaluating liquefaction potential. CPT tests can be invalidated, and the equipment damaged, by the presence of gravel-sized and larger particles. SPT tests can also be influenced by the presence of large particles that impede penetration; the extent to which this occurs is a function of the large-particle content.

There are three primary options for characterizing the liquefaction resistance of gravelly soils: Becker Penetrometer testing (BPT), short-interval SPT, and shear wave velocity.

5.7.2.1 Becker Penetrometer

The most reliable procedure for characterizing the liquefaction resistance of gravelly soils is the Becker Penetrometer Test (BPT). The BPT involves driving a 6-inch-diameter steel casing with a diesel pile driving hammer; cuttings are blown up through the casing pneumatically. The BPT resistance is measured as the number of blows of the hammer required to advance the casing by 12 inches.

Because only a few case histories of liquefaction have been investigated with BPT testing, no direct correlations to liquefaction resistance are available. Instead, the BPT

blowcount is converted to an equivalent SPT blowcount by using data from sites at which both tests have been performed. This correlation is an approximate one, with the greatest data scatter in the region of greatest importance ($N_{60} < 30$ bpf). An important source of variability in BPT measurements is variability of hammer energy. Two primary approaches to energy variability are available:

1. Estimation of hammer energy through correlation to bounce-chamber pressure – Harder and Seed (1986) developed an energy correction procedure based on bounce-chamber pressure measurements.
2. Direct measurement of transmitted energy – Sy and Campanella (1994) instrumented Becker casings with strain gauges and accelerometers and used a pile driving analyzer to measure the transmitted energy.

The direct measurement method has, to date, provided results consistent with that of the bounce-chamber pressure method; since bounce-chamber pressure measurement is considerably less difficult and expensive, its use is recommended.

Another issue in BPT-based measurements is the effect of casing friction. In order for the BPT casing to advance, friction between the casing and the surrounding soil must be overcome, so part of the measured BPT resistance is provided by casing friction and part by tip resistance. Because the tip resistance is of primary interest for SPT correlations, the casing friction must be accounted for, particularly for deep (> 30 m) BPT measurements or measurements in loose soils overlain by thick denser soils. Harder and Seed (1986) did not explicitly separate casing friction resistance from tip resistance, so the effect of casing friction is indirectly accounted for in their BPT-SPT correlation. Sy et al. (1995) used instrumented casings with wave equation analysis to separate casing friction resistance from tip resistance.

5.7.2.2 Short-Interval SPT

In soils in which at least 50 percent pass the #4 sieve (0.25-inch), it can be possible to characterize liquefaction resistance by using short-interval SPT measurements. Short-interval SPT tests are performed by recording SPT penetration resistance in 1-inch increments. Interference with penetration by large particles produces a sudden increase in short-interval penetration resistance. Those portions of the

penetration resistance profile are discarded, and the remaining values are scaled to produce an apparent 12-inch penetration resistance. A degree of judgment is required to identify cases of interference, and a remaining tendency for unconservative bias (toward higher SPT values) due to undetected interference requires consideration (e.g., by using 25th to 40th percentile values).

5.7.2.3 Shear Wave Velocity

Shear wave velocity-based characterization of liquefaction resistance is attractive because of the ability to “sample” large volumes of soil in their *in situ* state by means of various geophysical tests. Spectral analysis of surface waves (SASW) tests are particularly appealing because they allow measurement of shear wave velocity from the ground surface, i.e., without borings, which can be quite difficult to advance in many gravelly soils.

Shear wave velocity-based procedures produce more uncertain results in liquefaction potential evaluations, even for sands. The extension of their use to gravelly soils is possible but not supported by a substantial amount of field case history data. As a result, they should be applied and interpreted with great care. They are potentially useful for identifying sites where liquefaction potential is quite high or quite low, but should not be used by themselves for sites with borderline liquefaction potential.

5.8 EXAMPLES

The procedures for evaluating liquefaction potential described in the preceding sections can be illustrated by a series of examples. The examples show the results of single-scenario, multiple-scenario, and performance-based analyses for a hypothetical soil profile (Figure 5.5) assumed to exist at different locations within Washington State.

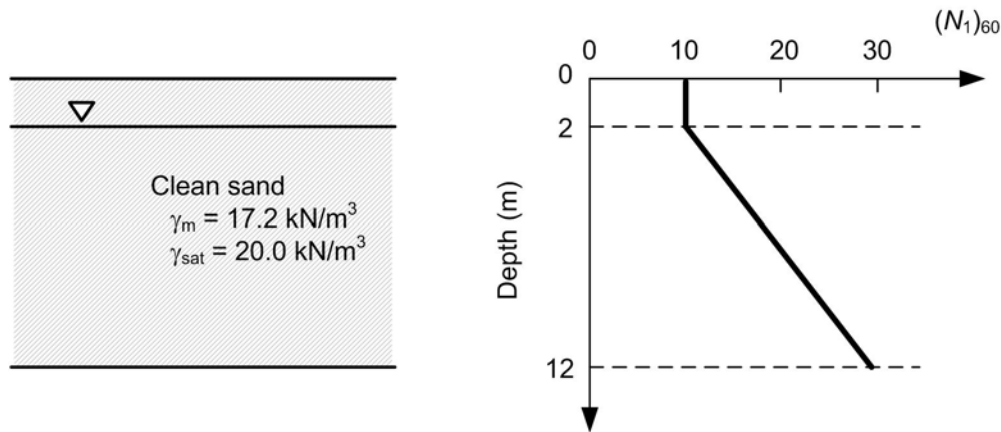


Figure 5.2 Subsurface profile for idealized site.

The following sections present the results of various analyses performed with the WSliq program at different locations in Washington State.

5.8.1 Single-Scenario Analyses

Single-scenario liquefaction potential analyses, as described in Section 5.6.1, are useful for quick examination of liquefaction potential under various assumed scenarios and for evaluating sensitivities to variations in different earthquake and/or site parameters. For example, Figure 5.6 shows the variation of factor of safety against liquefaction with depth for the hypothetical soil profile shown in Figure 5.5 located in Seattle. The loading scenario is that associated with the 475-year *PGA* and either the mean magnitude ($M_w = 6.6$) or modal magnitude ($M_w = 7.0$). The factors of safety obtained by using modal magnitudes are considerably lower than those obtained by using mean magnitudes, since the modal magnitude is significantly larger than the mean magnitude for Seattle.

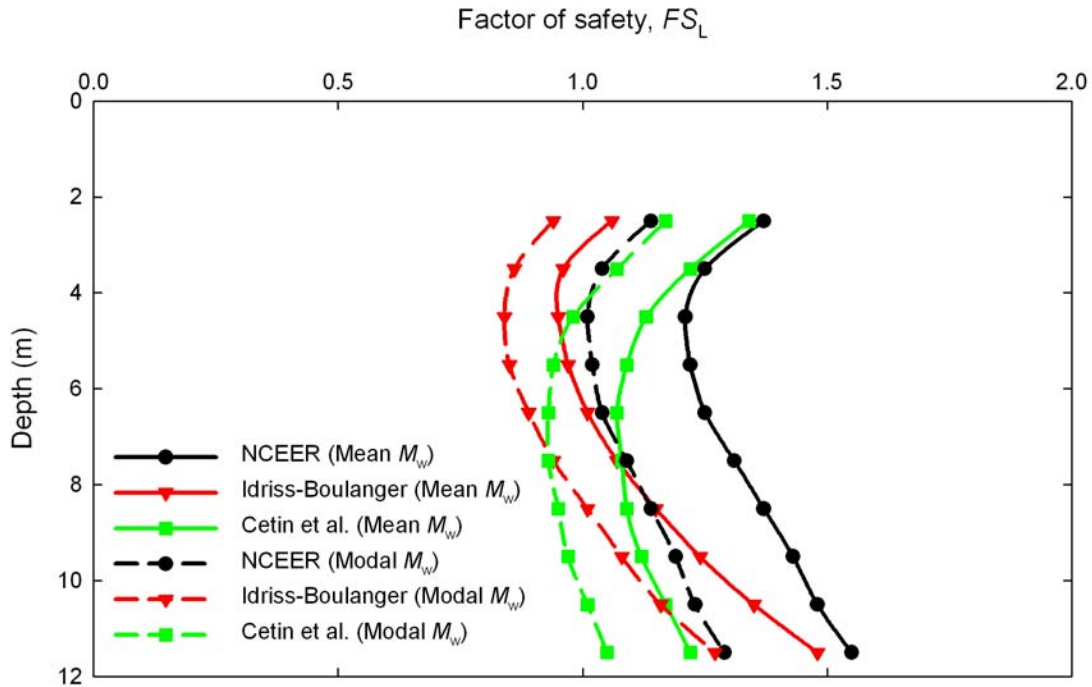


Figure 5.3 Variation of FS_L with depth for NCEER, Idriss-Boulanger, and Cetin et al. procedures, assuming mean and modal magnitudes for 475-year peak ground acceleration.

Single-scenario analyses can also be used to examine differences in liquefaction potential for sites in different locations within the state. Figure 5.7 shows profiles of factor of safety with depth for the hypothetical soil profile at seven locations within Washington State computed with the Idriss-Boulanger procedure. The factor of safety values differ significantly, reflecting the significant differences in seismicity that exist across the state. The sites in central and eastern Washington (Pasco and Spokane) have very high factors of safety, suggesting that liquefaction under the assumed 475-year ground motions is very unlikely. The sites located along I-5 (Vancouver, Olympia, Seattle, and Bellingham) have similar factors of safety, with those of Seattle and Olympia lower than those of Vancouver and Bellingham primarily because of their proximity to the Seattle Fault and potential Cascadia intraplate events (Section 2.2). The hypothetical site has the lowest factors of safety when located in Long Beach, due primarily to the very high mean magnitude (Table 2.1) produced by its close proximity to potential Cascadia interplate events (Section 2.2).

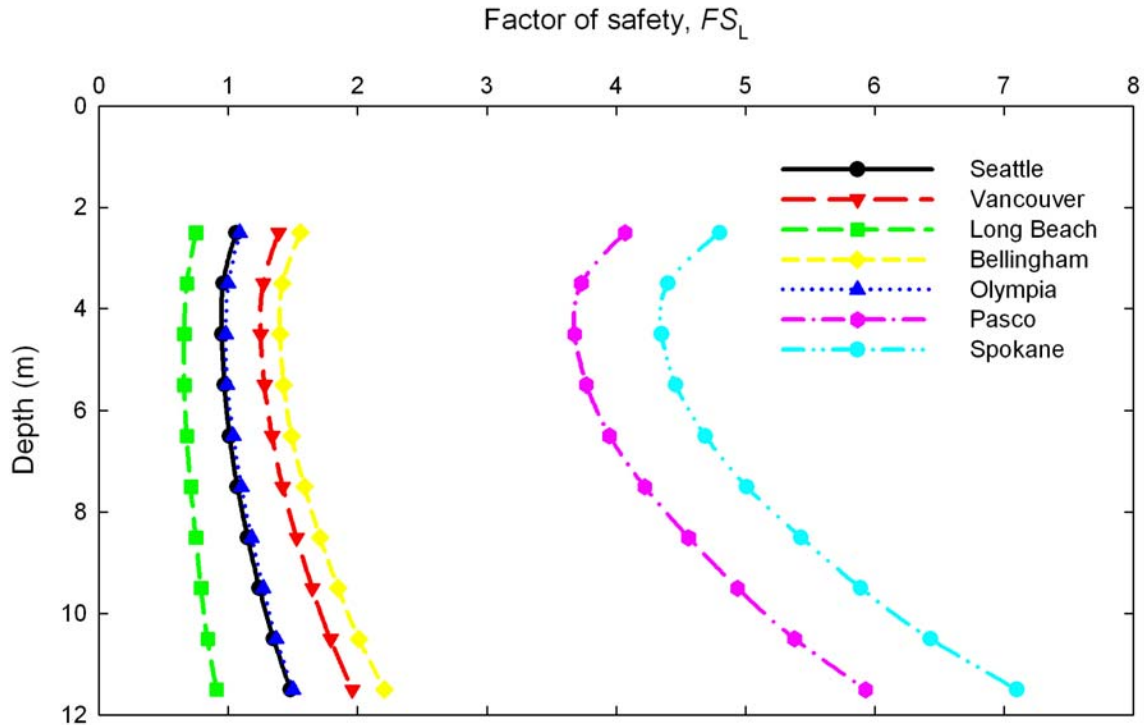


Figure 5.4 Variation of FS_L with depth for Idriss-Boulanger procedure at different locations in Washington State, assuming mean magnitudes for 475-year peak ground acceleration.

5.8.2 Multiple-Scenario Analyses

Multiple-scenario liquefaction potential analyses, as described in Section 5.6.2, allow consideration of all magnitudes contributing to the peak ground acceleration at a particular site. The multiple-scenario analysis eliminates the need to choose between mean, modal, or other magnitudes because all contributing magnitudes are used with weights proportional to their contribution to peak ground acceleration. Figure 5.8 shows the results of multiple-scenario analyses for the hypothetical site located in Seattle. Comparison of the factor of safety values in Figure 5.8 with those in Figures 5.6 and 5.7 shows that the single-scenario analyses conducted with mean magnitudes are more consistent with the multiple-scenario analyses than single-scenario analyses conducted with modal magnitudes; this trend has been found to be consistent across the state.

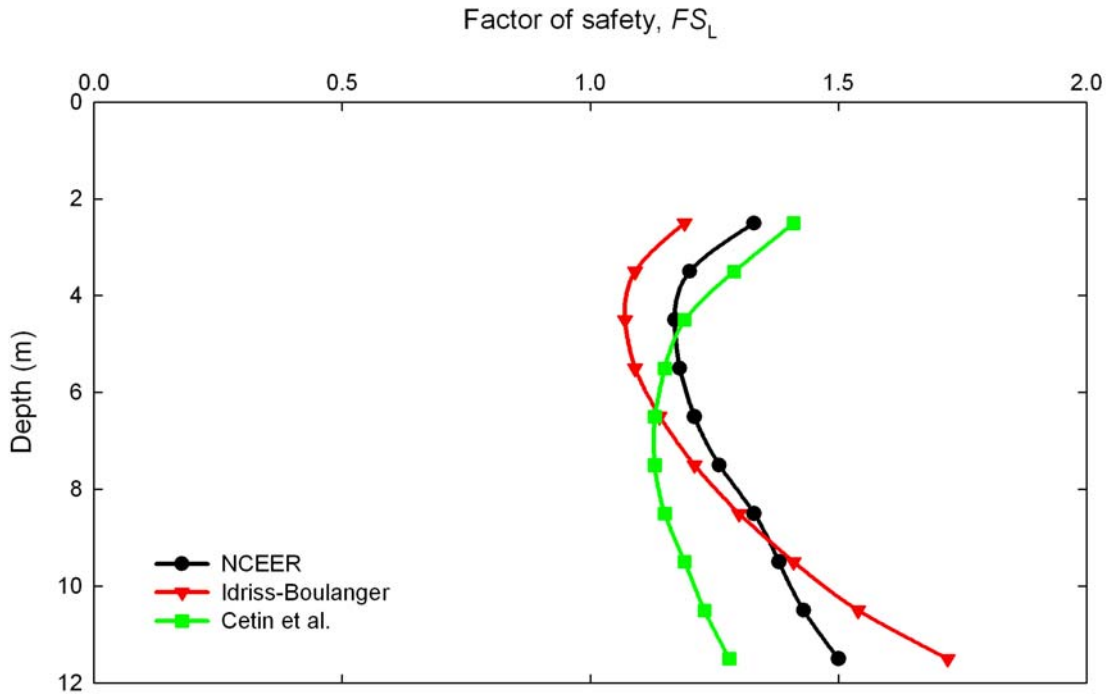


Figure 5.5 Variation of FS_L with depth for NCEER, Idriss-Boulanger, and Cetin et al. procedures using multiple-scenario approach for 475-year peak ground acceleration.

Multiple-scenario analyses can also be used to examine differences in liquefaction potential for sites in different locations within the state. Figure 5.9 shows profiles of factor of safety with depth for the hypothetical soil profile at seven locations within Washington State computed with the Idriss-Boulanger procedure. As with the single-scenario analyses, the multiple-scenario factor of safety values also reflect the significant differences in seismicity that exist across the state.

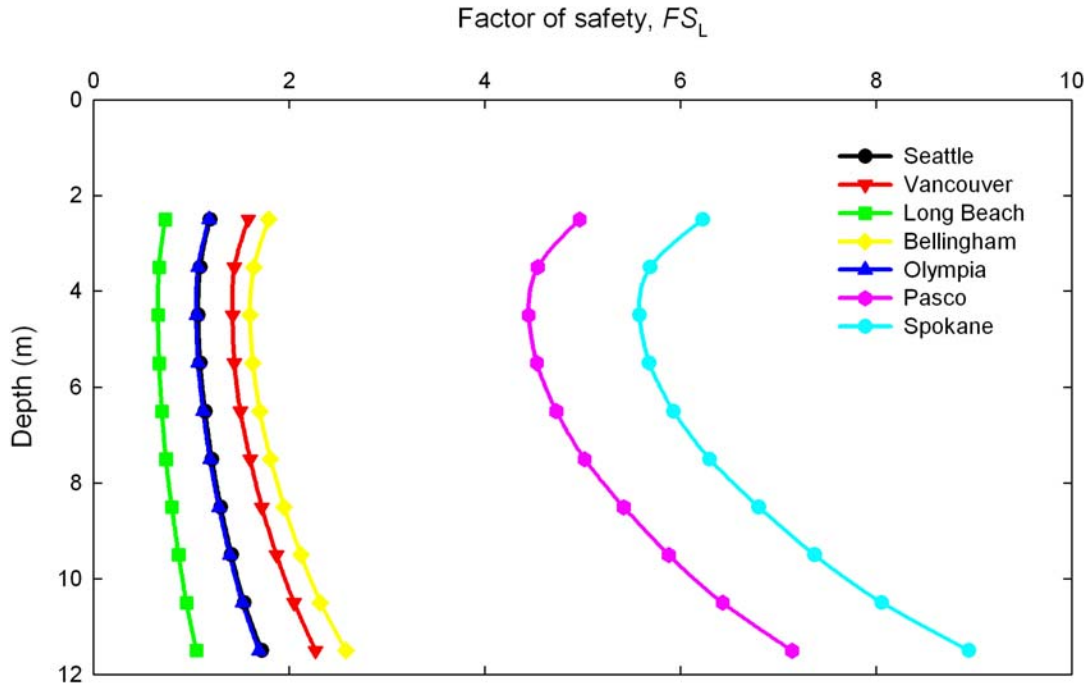


Figure 5.6 Variation of FS_L with depth for Idriss-Boulanger procedure at different locations in Washington State using multiple-scenario approach for 475-year peak ground acceleration.

5.8.3 Performance-Based Analyses

Performance-based liquefaction potential analyses, as described in Section 5.6.3, allow the most complete characterization of liquefaction hazards in that all scenarios, ranging from frequent, relatively weak shaking to rare, strong shaking with explicit consideration of all magnitudes, are accounted for. Performance-based analyses allow calculation of factor of safety hazard curves for each depth in the soil profile, as illustrated for Seattle in Figure 5.10. Note that factor of safety hazard curves are expressed in terms of rates of *non-exceedance*. The value of $\Lambda_{FS_L^*}$ should be interpreted as the mean annual rate (or inverse of the return period) at which the actual factor of safety will be less than FS_L . Note that $\Lambda_{FS_L^*}$ increases with increasing FS_L , since weaker motions producing higher factors of safety occur more frequently than stronger motions that produce lower factors of safety. The mean annual rate of factor of safety non-exceedance is used because non-exceedance of a particular factor of safety represents an undesirable condition, just as exceedance of an intensity measure does in a ground motion hazard analysis; because lower case lambda (λ) is commonly used to represent

mean annual rate of exceedance, an upper case lambda (Λ) is used here to represent mean annual rate of non-exceedance.

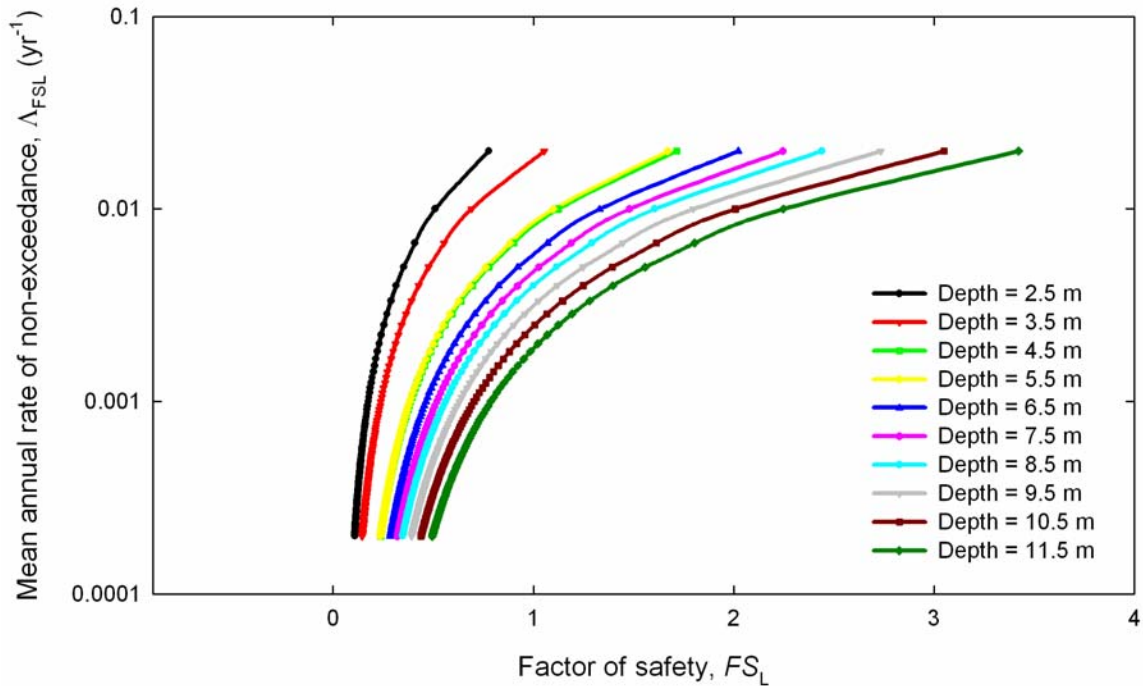


Figure 5.7 Factor of safety hazard curves for various depths in hypothetical soil profile located in Seattle.

The FS_L hazard curves shown in Figure 5.10 can be used to express liquefaction hazards for the hypothetical profile in two ways. First, selection of a particular return period, say 475 years, can be used to compute the corresponding FS_L value at each depth in the profile (Figure 5.11). Second, selection of a particular FS_L value, say $FS_L = 1.0$, can be used to compute the corresponding mean annual rate of non-exceedance of that value. Since liquefaction is expected to occur when $CRR < CSR$ (i.e., when $FS_L < 1.0$), the return period of liquefaction corresponds to the reciprocal of the mean annual rate of non-exceedance of $FS_L = 1.0$, i.e., $T_{R,L} = 1/\Lambda_{FS_L=1.0}$. Figure 5.12 shows the return period of liquefaction at different depths for the hypothetical soil profile when located in Seattle. The return period can be seen to increase with depth in a manner consistent with the increasing SPT resistance with depth.

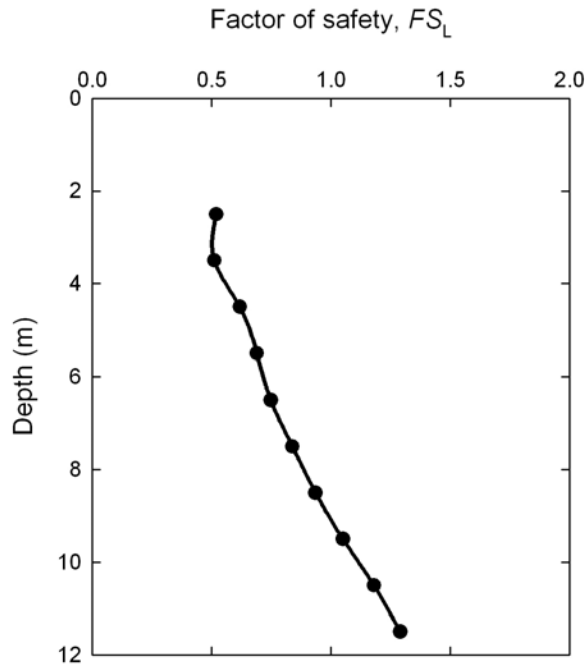


Figure 5.8 Variation of 475-year factor of safety with depth for hypothetical soil profile located in Seattle.

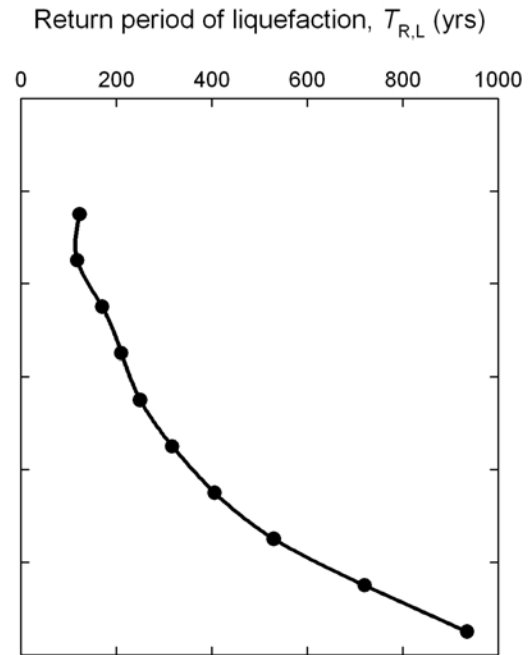


Figure 5.9 Variation of return period of liquefaction with depth for hypothetical soil profile located in Seattle.

Performance-based analyses can also be used to examine differences in liquefaction potential for sites in different locations within the state. Figure 5.13 shows profiles of liquefaction return period with depth for the hypothetical soil profile at five locations within Washington State. As with the single-scenario and multiple-scenario analyses, the performance-based return periods also reflect the significant differences in seismicity that exist across the state. The return periods for Pasco and Spokane are greater than 1,000 years at all depths and are not shown in Figure 5.13.

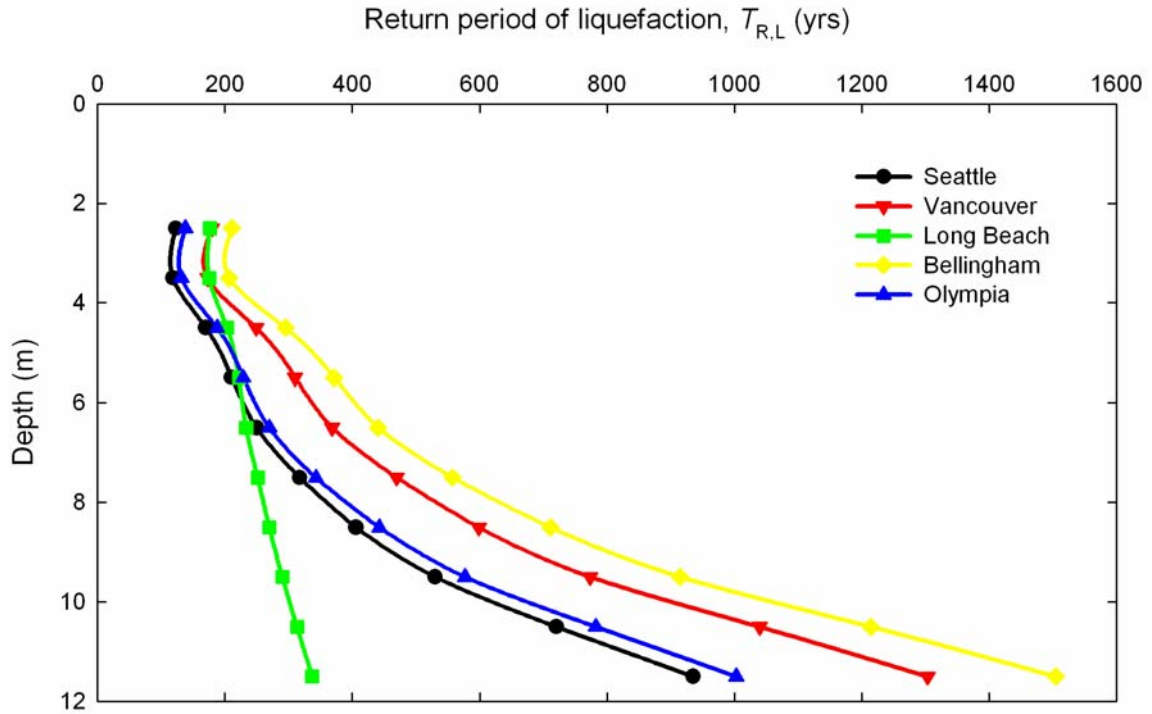


Figure 5.10 Variation of return period of liquefaction with depth for hypothetical soil profile at different locations within Washington State.

Chapter 6

Lateral Spreading

6.1 INTRODUCTION

Lateral spreading can occur in gently sloping ground and in the vicinity of natural and cut slopes. It occurs in situations where the soil is dense enough that flow sliding (Chapter 7) cannot occur, but it can also lead to significant permanent deformations. Lateral spreading is of particular concern in the design of bridge foundations because many bridges cross rivers or other bodies of water at sites frequently underlain by sloping deposits of loose, saturated, cohesionless soil. Also, the subsurface deformations of laterally spreading soils can impose significant bending demands on pile foundations that extend through the deforming soils.

It is important to recognize that lateral spreading does not require very loose soils to occur. It can produce potentially damaging deformations in medium dense soils, particularly when ground motion durations are long, as they are likely to be in high magnitude earthquakes such as those produced by the Cascadia Subduction Zone.

The most commonly used procedures for estimating lateral spreading displacements imply that soils with SPT resistances of greater than 15 do not produce any lateral spreading deformations and that soils with SPT resistances of less than 15 behave identically with respect to lateral spreading deformations. Because soils do not actually behave that way, an improved model was developed and is recommended for estimating lateral spreading displacements.

6.2 BACKGROUND

Because the damage caused by lateral spreading is closely related to the permanent deformations it produces, procedures for evaluating lateral spreading hazards have focused on estimating permanent displacements. It should be recognized that lateral spreading is an effect of liquefaction, i.e., that its occurrence is conditional upon the

initiation of liquefaction. If liquefaction is not triggered, permanent shear strains will be small (though not zero) and, therefore, permanent deformations will be small.

A number of different approaches to the lateral spreading displacement problem have been proposed, ranging from purely empirical statistical correlations to numerical approaches based on nonlinear site response analyses with advanced constitutive models. These approaches adhere to basic principles of soil mechanics to different degrees and are consistent with field observations of lateral spreading behavior to different degrees.

Bartlett and Youd (1992) developed the first widely used empirical procedure for estimating lateral spreading displacement. A subsequent extension of that procedure (Youd et al., 2002) has become a *de facto* standard in geotechnical engineering practice. However, the Youd et al. (2002) procedure, like its predecessor and imitators, is based purely on regression upon a database of observed lateral spread case histories. Youd et al. went to considerable lengths to investigate many different forms of the predictor variables before settling on those that were used in the final model. The variables used in the model reflect slope geometry, material properties, and level of earthquake loading, all of which are known to influence lateral spreading. However, the primary variable used to describe material properties – T_{15} – introduces some potential limitations to the applicability of the Youd et al. model. The T_{15} parameter implies behavioral characteristics that are inconsistent with the known behavior of liquefiable soils. T_{15} is defined as the cumulative thickness of all sublayers with corrected SPT resistances of less than 15. This definition implicitly assumes that liquefiable soils with SPT resistances of greater than 15 provide no contribution to lateral spreading displacement, and that all liquefiable soils with SPT resistances less than 15 contribute equally to lateral spreading displacement. It implies, for example, large and discontinuous differences in behavior between two soils with $(N_1)_{60}$ values of 14 and 16, and no difference in behavior between two soils with, say, $(N_1)_{60}$ values of 4 and 14. These implications clearly conflict with the known behavior of liquefiable soils. Furthermore, the T_{15} parameter makes no distinction between the contribution of a shallow soil layer (with a given $(N_1)_{60} < 15$) and a deeper layer of the same soil. These limitations can combine to produce potentially inaccurate estimates of lateral spreading displacement, particularly for thick deposits of potentially liquefiable soil.

More recently, lateral spreading models based on cumulative strain potential have been developed. The concept of density-related potential strains and their role in estimating liquefaction-related deformations (e.g., Seed et al, 1973; Seed et al., 1975; Seed, 1979) was developed many years ago. In recent years, new models for estimating lateral spreading displacements based on strain potential (e.g., Shamoto et al., 1998; Zhang et al., 2004; Faris et al., 2006) have been proposed. These models are based on the idea that each element of liquefied soil will develop a level of shear strain that is related to its density and the severity of the shaking it is exposed to. Laboratory tests on individual elements of soil have shown that maximum, or “limiting,” shear strains increase continuously with increasing ground shaking intensity and with decreasing penetration resistance. Procedures for estimating lateral spreading displacements involve integrating limiting strains over the thickness of a soil profile. These models use the experimentally measured mechanical behavior of soils to overcome the previously described limitations of T_{15} . However, the link between cyclic shear strains based on laboratory tests with no static shear stress and permanent shear strains in the presence of static shear stress is not well established, nor is the reasonableness of the implicit assumption that the shear strain potential is reached in all potentially liquefiable soil layers. Nevertheless, after calibration, these models appear to predict observed lateral spreading displacements with levels of accuracy similar to those of the BY models.

As part of the research described in this report, a new model for predicting lateral spreading displacement was developed. The model is consistent with the known mechanics of liquefiable soil and with observed case histories of liquefaction in the field. A constitutive model that accounts for the most important characteristics of liquefiable soils was developed and implemented within a nonlinear, one-dimensional site response analysis program. The site response program was then used to develop a “numerical database” of lateral spreads – employing thousands of combinations of slope geometries, material properties, and earthquake loadings – which was then used to determine the basic form of an empirical displacement estimation relationship. That form of the relationship was then calibrated against available field case history data by using standard multiple regression techniques. The result is an empirical predictive model that is consistent with the mechanical behavior of liquefiable soil and with available field data.

The predictive equation also allows estimation of a probability distribution for lateral spreading displacement, which allows the development of performance-based procedures for evaluating lateral spreading hazards. A more detailed description of the development of and basis for this model is presented in Appendix D.

6.3 REQUIRED INFORMATION

Evaluation of lateral spreading hazards requires characterization of subsurface conditions, principally soil density, fines content, and groundwater conditions, to sufficient depth to characterize all potentially liquefiable soils (Chapter 5). Currently, most available procedures for estimating lateral spreading displacement use SPT resistance as a proxy for soil density. When additional case histories with measured CPT resistance become available, CPT-based lateral spreading models will undoubtedly become available. Until that time, however, available CPT data should be transformed to equivalent SPT resistances, with recognition of the uncertainty that exists in the transformation. The Youd et al. (2002) model also requires the mean grain size of the soils with SPT resistances to be less than 15. The new procedures developed in this research account for the effect of fines plasticity on the strength of cyclically loaded soils.

Information on ground surface topography is also required to define the type of potential spreading case that may exist and to provide a quantitative description of the slope geometry. It should be emphasized that characterization of the surface topography beyond the boundaries of a specific project site may be required, since lateral spreads can involve large areas of soil. Historically, the geometries of lateral spreading case histories have been divided into two categories: ground slope geometries and free-face geometries. Ground slope geometries are slopes of constant average inclination, i.e., those that can reasonably be idealized as infinite slopes. Free-face geometries are those with significant slope breaks, i.e., localized areas of steeper inclination such as river banks. Most lateral spreading models require the user to characterize a slope of interest as either a ground slope or a free-face case.

Finally, earthquake loading information is required. Historically, most empirical predictions of lateral spreading displacement have used earthquake magnitude and distance to represent loading. Recent cumulative strain models, however, require

estimation of cyclic stress ratio to account for the effects of earthquake loading on limiting shear strain. The information required for estimation of cyclic stress ratio was described in Chapter 5. In the future, it is likely that actual ground motion parameters will provide improved estimates of lateral spreading displacement, but sufficient field data to validate such predictions are not yet available.

6.4 PROCEDURES

A number of procedures for estimating lateral spreading displacement have been developed and used in practice. Some of those procedures differ in their basic approaches, some differ with respect to the databases they are calibrated against, and some differ in the ways they characterize subsurface conditions, slope geometry, and earthquake loading. At this time, no single procedure has been shown to be consistently superior to the other well-founded procedures across all conditions likely to be encountered in practice. As a result, the most consistent and stable estimates of lateral spreading displacement should be produced by a combination of methods.

The following sections describe four procedures for estimating lateral spreading displacement. The first, the Youd et al. (2002) model, has been widely used in practice but characterizes subsurface conditions in a manner that can produce counter-intuitive sensitivities to important parameters. The second, the Kramer and Baska (2007) model, is similar to the Youd et al. (2002) model but uses an improved approach to characterization of subsurface conditions. The third, the Zhang et al. (2004) model, is a cumulative strain-type model. The fourth is a new procedure that provides an upper bound estimate of lateral spreading displacement (Idriss and Boulanger, 2008). Recommendations for the combined use of these procedures are presented in Section 6.6.

6.4.1 Youd et al. (2002) Model

Bartlett and Youd (1992) compiled a large database of lateral spreading case histories from Japan and the western United States. By investigating a large number of potential parameters, Bartlett and Youd (1992) were able to identify those that were most closely related to lateral spreading displacement and develop a regression-based predictive relationship. Youd et al. (2002) used an expanded and corrected version of the

1992 database to develop the predictive relationship. The Youd et al. (2002) model can be implemented in the following series of steps:

1. Characterize the slope of interest as a ground slope case or a free-face case.
2. Using Figure 6.1, compute the ground slope inclination, S , for ground slope cases, or the free-face ratio, W , for free-face cases.

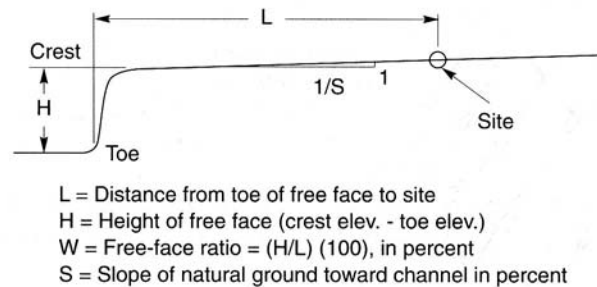


Figure 6.1 Slope geometry notation

3. Identify the moment magnitude, M_w , and the closest horizontal distance to the energy source, R , for the event of interest.
4. Divide the soil profile into sublayers and determine the corrected SPT resistance, fines content, and mean grain size of each sublayer.
5. Compute the cumulative thickness, T_{15} , of soil layers with corrected SPT resistance, $(N_1)_{60}$, less than or equal to 15, in which liquefaction is expected to occur (i.e., layers for which $FS_L \leq 1.0$).
6. Determine the average fines content, F_{15} (in percent), of the soil layers that contribute to T_{15} .
7. Determine the mean grain size, $D_{50_{15}}$ (in mm), of the soil layers that contribute to T_{15} .
8. Check the applicability of the Youd et al. (2002) model to the site of interest by comparing the parameters obtained in the preceding steps against the ranges shown in Table 6.1. The results of any analyses based on parameters that lie outside these ranges should be interpreted very carefully.

Table 6.1 Recommended range of variable values for the Youd et al. (2002) predictive equation.

Variable	Description	Range
T_{15}	Equivalent thickness of saturated cohesionless soils (clay content ≤ 15 percent) in m.	1 to 15 m
M	Moment magnitude of the earthquake.	6.0 to 8.0
Z_T	Depth to top of shallowest layer contributing to T_{15} .	1 to 15 m
W	Free face ratio.	1 to 20 percent
S	Ground slope.	0.1 to 6 percent
$F_{15}, D50_{15}$	Applicable combinations of F_{15} and $D50_{15}$ should be obtained from the figure below.	

9. Compute the expected lateral spreading displacement from the equation

$$\log D_H = b_0 + b_1 M_w + b_2 \log R^* + b_3 R + b_4 \log W + b_5 \log S + b_6 \log T_{15} + b_7 \log(100 - F_{15}) + b_8 \log(D50_{15} + 0.1 \text{ mm}) \quad (6.1)$$

where D_H = horizontal displacement in meters and $R^* = R + 10^{-0.89M_w - 5.64}$.

The values of the coefficients are presented in Table 6.2.

Table 6.2. Coefficients for Youd et al. (2002) model.

Model	b_0	b_1	b_2	b_3	b_4	b_5	b_6	b_7	b_8
Ground slope	-16.213	1.532	-1.406	-0.012	0	0.338	0.540	3.413	-0.795
Free Face	-16.713	1.532	-1.406	-0.012	0.592	0	0.540	3.413	-0.795

6.4.2 Kramer and Baska (2006) Model

Kramer and Baska (2006) used a series of nonlinear analyses with an advanced constitutive model capable of representing the mechanics of liquefiable soil to identify an improved method of characterizing subsurface conditions. By calibrating this improved model against field case histories, they produced a model that is consistent with basic soil mechanics and with observed lateral spreading behavior. The Kramer and Baska (2006) procedure can be implemented in the following series of steps:

1. Characterize the slope of interest as a ground slope case or a free-face case.
2. Using Figure 6.1, compute the ground slope inclination, S , for ground slope cases, or the free-face ratio, W , for free-face cases.
3. Identify the moment magnitude, M_w , and the closest horizontal distance to the energy source, R , for the event of interest.
4. Divide the soil profile into a series of sublayers. A maximum sublayer thickness of 1 m is recommended.
5. Determine the average SPT resistance and fines content, and of each sublayer of liquefiable soil (i.e., sublayers for which $FS_L \leq 1.0$).
6. Determine the clean sand corrected SPT resistance, $(N_1)_{60,cs}$, for each liquefiable sublayer using the relationship

$$(N_1)_{60,cs} = \alpha + \beta(N_1)_{60} \quad (6.2)$$

where α and β are as given in the Table 6.3.

Table 6.3. Fines content correction variables.

Fines content, FC	α	β
$FC \leq 5\%$	0	1.0
$5\% < FC < 35\%$	$\exp[1.76 - 190/FC^2]$	$0.99 + FC^{1.5}/1000$
$FC \geq 35\%$	5.0	1.2

7. Check the applicability of the Kramer and Baska (2006) model to the site of interest by comparing the parameters obtained in the preceding steps against the ranges shown in Table 6.4. The results of any analyses based

on parameters that lie outside these ranges should be interpreted very carefully.

Table 6.4 Recommended range of variable values for the predictive equation.

Variable	Description	Range
T^*	Equivalent thickness of saturated cohesionless soils in m.	0.001 to 20 m
M_w	Moment magnitude of the earthquake.	6.0 to 8.0
R	Distance from the site to the hypocenter of the earthquake in km.	0 to 100 km
W	Free face ratio (height of free face/distance to the free face from the point of displacement) in percent.	≤ 20 percent
S	Ground slope in percent.	0 to 6 percent

8. Compute the equivalent thickness parameter, T_{gs}^* or T_{ff}^* , for ground slope or free-face sites, respectively, from

$$T_{gs}^* = 2.586 \sum_{i=1}^n t_i \exp[-0.05N_i - 0.04z_i] \geq 0.001 \text{ m} \quad (6.3)$$

$$T_{ff}^* = 5.474 \sum_{i=1}^n t_i \exp[-0.08N_i - 0.10z_i] \geq 0.001 \text{ m}$$

9. Compute the median lateral spreading displacement using the equation

$$\hat{D}_H = \begin{cases} 0 & \text{for } \sqrt{D_H} \leq 0 \\ \left(\sqrt{D_H}\right)^2 & \text{for } \sqrt{D_H} > 0 \end{cases} \quad (6.4)$$

where

$$\sqrt{D_H} = \frac{\beta_1 + \beta_2 T_{gs}^* + \beta_3 T_{ff}^* + 1.231M - 1.151 \log R^* - 0.01R + \beta_4 \sqrt{S} + \beta_5 \log W}{1 + 0.0223(\beta_2 / T_{gs}^*)^2 + 0.0135(\beta_3 / T_{ff}^*)^2}$$

where $R^* = R + 10^{0.89M_w - 5.64}$

$N_i = (N_1)_{60,cs}$ (as calculated using the fines correction of Youd et al. (2002)) for the i^{th} sublayer

t_i = sublayer thickness (limited to a maximum value of 1 m)

PI_i = plasticity index (in percent) of the i^{th} sublayer

the model-specific β coefficients are as indicated in Table 6.5.

Table 6.5. Coefficients for Kramer and Baska (2006) model.

Model	β_1	β_2	β_3	β_4	β_5
Ground slope	-7.207	0.067	0.0	0.544	0.0
Free face	-7.518	0.0	0.086	0.0	1.007

Note that the Kramer-Baska model can be used to predict the probability distribution of lateral spreading displacement. The regression analyses performed to identify the β coefficients in Step 9 also reveal that the residuals are approximately normally distributed with constant variance, $\sigma_{\sqrt{D_H}}^2 = 0.0784$. The probability of exceeding some non-negative lateral spreading displacement, d , can therefore be estimated as

$$P[D_H > d] = 1 - \Phi \left[\frac{\sqrt{d} - \sqrt{D_H}}{\sigma_{\sqrt{D_H}}} \right] = 1 - \Phi \left[3.571 (\sqrt{d} - \sqrt{D_H}) \right] \quad (6.5)$$

where Φ is the standard normal cumulative distribution. Note that negative values of $\sqrt{D_H}$ can be used in equation 6.5.

6.4.3 Zhang et al. (2004) Model

Zhang et al. (2004) made use of a laboratory test-based relationship among “maximum cyclic shear strain,” relative density, and factor of safety against liquefaction (Ishihara and Yoshimine, 1992) to develop a cumulative shear strain model for predicting lateral spreading displacement. Maximum cyclic shear strains were defined by Ishihara and Yoshimine (1992) as the maximum shear strain (in any direction) under transient loading conditions. Zhang et al. (2004) capped the maximum cyclic shear strains by the limiting shear strains proposed by Seed (1979) and used empirical relationships between relative density and penetration resistance (SPT or CPT) to allow lateral spreading displacement to be predicted in the following series of steps:

1. Characterize the slope of interest as a ground slope case or a free-face case.
2. Using Figure 6.1, compute the ground slope inclination, S , for ground slope cases, or the free-face ratio, W , for free-face cases.

3. Divide the soil profile into a series of sublayers and determine the average SPT or CPT resistance for each sublayer.
4. Compute the factor of safety against liquefaction for each sublayer.
5. Using the penetration resistance and factor of safety against liquefaction, use Figure 6.2 to determine the maximum shear strain, γ_{\max} . Zhang et al. recommend the use of a modified form of Meyerhof's relationship to estimate relative density as $D_r = 14\sqrt{(N_1)_{60}}$ for $(N_1)_{60} < 42$.

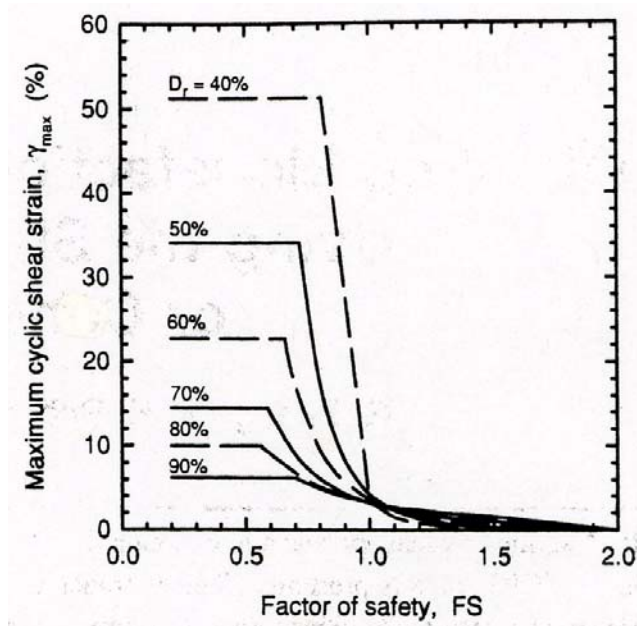


Figure 6.2. Variation of maximum cyclic shear strain with factor of safety and relative density (after Zhang et al., 2004).

6. Compute the lateral displacement index, LDI by integrating maximum shear strains with depth over all potentially liquefiable layers, i.e.,

$$LDI = \int_0^{z_{\max}} \gamma_{\max} dz \quad (6.6)$$

7. Compute the expected lateral spreading displacement as

$$D_H = \begin{cases} (S + 0.2) \cdot LDI & \text{ground slope case} \\ 6W^{-0.8} \cdot LDI & \text{free - face case} \end{cases} \quad (6.7)$$

6.4.4 Idriss and Boulanger (2008) Model

Idriss and Boulanger (2008) described an alternative cumulative strain model. Idriss and Boulanger considered slopes in loose, saturated soils to move toward a relative density-dependent limiting shear strain upon initiation of liquefaction. Using the curves shown in Figure 6.3, Idriss and Boulanger recommended that a limiting shear strain (upper portion of Figure 6.3) be computed as

$$\gamma_{\text{lim}} = 1.859 \left(1.1 - \sqrt{\frac{(N_1)_{60cs}}{46}} \right)^3 \quad (6.8)$$

Then, the maximum expected shear strain for a given level of loading could be related to the density of the soil and the factor of safety against liquefaction using

$$\gamma_{\text{max}} = \begin{cases} 0 & \text{if } FS_L \geq 2 \\ \gamma_{\text{lim}} & \text{if } FS_L \leq A \\ \min(B, \gamma_{\text{lim}}) & \text{if } A \leq FS_L \leq 2 \end{cases} \quad (6.9)$$

where

$$A = 0.535 + 0.398 \sqrt{\max(5.6, (N_1)_{60cs})} - 0.0924 \max(5.6, (N_1)_{60cs})$$

$$B = 0.035(1 - A) \left(\frac{2 - FS_L}{FS_L - A} \right)$$

With the maximum strain values computed for potentially liquefiable layers in a soil profile, the lateral displacement index, taken as a measure of the potential maximum displacement, can be computed by integrating the maximum strains over the thickness of the profile, i.e.,

$$LDI = \int_0^{z_{\text{max}}} \gamma_{\text{max}} dz \quad (6.10)$$

The LDI produces a displacement value that implicitly assumes that all potentially liquefiable layers reach their respective maximum strain values, and that all of those values are acting in the same direction. As such, users should be careful to interpret the value as its developers intended – as a measure of potential maximum displacement.

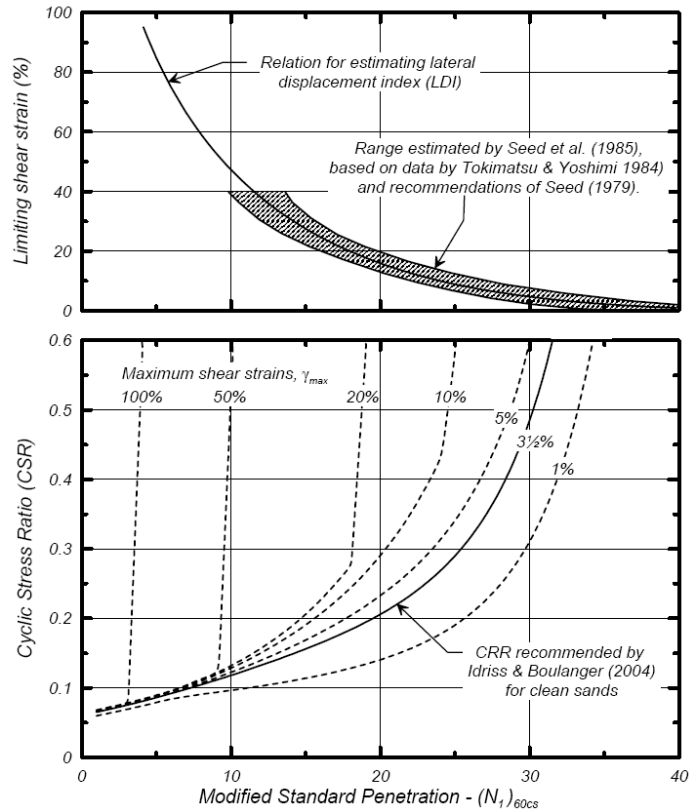


Figure 6.3 Variation of limiting strain with SPT resistance and variation of maximum shear strain with SPT resistance and cyclic stress ratio.

6.5 DISCUSSION

The four procedures described in the preceding section have a number of similarities but also are distinctly different. The Youd et al. (2002) model is familiar to nearly all geotechnical earthquake engineers as it (and its predecessor) has been the workhorse of lateral spreading hazard evaluation for many years. By virtue of its basic formulation, however, it is susceptible to inaccuracy for very loose ($(N_1)_{60} < 5$) soils, medium dense ($15 < (N_1)_{60} < 30$) soils, and cases in which liquefiable soils exist at large depths.

There are several significant differences between the Kramer and Baska (2006) model and the model of Youd et al. First, the Kramer and Baska (2006) model is based on a square root transformation of displacement rather than the logarithmic transformation used by Youd et al. The square root transformation is a desirably milder transformation than the logarithmic transformation and gives more consistent differences

between observed and predicted displacements. Second, Baska's thickness parameter, T^* , is a continuous function of corrected SPT resistance. It varies smoothly with changes in $(N_1)_{60}$ rather than changing abruptly at $N = 15$ and not changing at all above and below that value. Third, Baska's T^* also varies with sublayer depth. A deep sublayer of soil at a particular SPT resistance contributes less to lateral spreading displacement than a shallow sublayer of identical soil in Baska's model, particularly for free-face conditions. Finally, Baska's relationship does not require grain size information. With these modifications, Baska's model produces displacement predictions that are slightly better than those of Youd et al. (2002) with respect to the empirical database it is calibrated against. The Baska model recognizes that liquefaction can be initiated at large depths without necessarily producing large surface effects. This aspect of its behavior helps reconcile the fact that there is no physical reason for defining a limiting depth below which liquefaction cannot occur with the observation that liquefaction at depths greater than 15 to 20 m has not been observed to cause significant surface effects. The more realistic physical basis for the Baska model makes it more likely to produce reliable predictions of future events than procedures based purely on statistical regression.

The Zhang et al. (2004) and Idriss and Boulanger (2008) models, with their basis derived from laboratory test results, bring soil mechanics into the prediction in a different way than the Kramer-Baska model. They provide for a smooth variation of lateral spreading displacement with changes in penetration resistance and depth, and also account for the potential of medium dense soils to contribute to lateral spreading displacement. It should be recognized, however, that these models predict potential maximum displacements rather than expected displacements, which are the product of the Youd et al. (2002) and Baska models.

6.6 RECOMMENDATIONS

The following sections present recommendations for evaluating lateral spreading displacements in potentially liquefiable soils. Such analyses should be performed following an evaluation of liquefaction potential, and contributions to lateral spreading displacement should only be considered for soils in which liquefaction is initiated.

6.6.1 Single-Scenario Analyses

Use of the single-scenario approach is not recommended for analysis or design. It requires representation of the entire ranges and distributions of magnitude and distance affecting a site by a single magnitude-distance pair. Its only advantage over the multiple scenario approach is in speed (i.e., fewer calculations), and that advantage is effectively eliminated by the multiple-scenario option in the WSLIQ program. The single-scenario option is useful, however, for investigating the sensitivity of liquefaction potential to various combinations of magnitude and distance.

6.6.2 Multiple-Scenario Analyses

For analysis and design at this time, the use of weighted multiple-scenario analyses is recommended. Multiple-scenario analyses properly account for the ranges and distributions of earthquake magnitude and source-to-site distance that contribute to lateral spreading displacements. Those distributions, as obtained from USGS deaggregation files, are built into the WSliq program so that performing a multiple-scenario analysis is no more difficult than performing a single-scenario analysis.

The availability of multiple credible procedures for evaluating liquefaction potential should also be taken advantage of. The use of weighted average lateral spreading displacements, based on contributions from the Youd et al. (2002), Kramer and Baska (2006), and Zhang et al. (2004) procedures, is recommended. The weighting factors should be no less than 0.1 and should add up to 1.0. The WSliq program allows the entry of weighting factors and the computation of individual and weighted average factors of safety. Although they can be changed manually, the default weighting factors in WSliq are given in Table 6.6.

Table 6.6. Default weighting factors for lateral spreading models in WSliq.

Model	Weighting factor
Youd et al. (2002)	0.35
Kramer and Baska (2006)	0.65

6.6.3 Performance-Based Analyses

As part of the research described in this report, a performance-based procedure for estimating lateral spreading displacement was developed (Franke, 2005). Since a performance-based procedure requires a probabilistic estimate of response, the Kramer-Baska model was used. A brief description of the performance-based model is given in Appendix E.

A transition toward the use of performance-based concepts in the evaluation of lateral spreading hazards is recommended. The performance-based approach, as described in Chapter 3, considers all possible ground motion levels (rather than just a single level, as in the multiple scenario approach) and thereby produces a more complete and consistent evaluation of the lateral spreading hazard. Use of the performance-based approach, however, requires different performance criteria because that approach can predict the actual return period of different lateral spreading displacements (rather than a lateral spreading displacement for an event with a single specified return period).

6.7 OTHER CONSIDERATIONS

Lateral spreading can cause significant damage to bridges, bridge approaches, and other structures. Bridges that cross rivers, lakes, and other bodies of water are frequently underlain by naturally deposited liquefiable soils. Other bridges may be supported on or in fill materials placed with little or no compaction.

The permanent ground surface displacements associated with lateral spreading are generally the best indicators of potential damage. However, damage to pile foundations, which has been observed in many earthquakes, also depends on the distribution of displacement with depth.

6.7.1 Subsurface Deformations

The permanent displacements predicted by the three recommended lateral spreading models described in Section 6.4 are ground surface displacements that include contributions from various soil layers beneath the ground surface. Cumulative strain models, such as that of Zhang et al. (2004) and Idriss and Boulanger (2008), provide the most direct means of estimating subsurface displacement patterns. Assuming that non-

zero maximum shear strains occur in each of N sublayers, the fraction of total lateral displacement of the n^{th} sublayer can be estimated as

$$\frac{d_n}{D_H} = \frac{(\gamma_{\max})_n h_n}{LDI} \quad (6.11)$$

where $(\gamma_{\max})_n$ is the maximum shear strain of the n^{th} sublayer, h_n is the thickness of the n^{th} sublayer, and D_H is the total computed lateral spreading displacement (not restricted to the method of Zhang et al. (2004)).

6.7.2 Pore Pressure Redistribution

At some sites, soil layers in which high porewater pressures are likely to be generated are overlain by low-permeability soils. It is possible for porewater pressures to redistribute within such layers during and after the strongest part of earthquake shaking. When this occurs, the density of the soil will change as the effective stress changes. Of particular concern is the case in which porewater pressures migrate upward, thereby decreasing the effective stress, and consequently the density, of the soil just below the low-permeability layer.

In extreme cases, the reduction in density can cause the available (residual) strength of the soil to drop below the shear stress required for static equilibrium and lead to the type of flow slide deformations described in Chapter 8. In less extreme cases, however, the reduced density can cause a reduction in stiffness that can lead to larger lateral spreading deformations than would occur without the low-permeability layer.

Although the effect of low-permeability layers likely exists to some degree in the databases against which the lateral spreading estimation procedures described in this chapter are calibrated, it is likely that these procedures will somewhat underestimate the permanent strains in soil layers affected by this phenomenon. Quantitative procedures for determining the magnitude and effects of such density changes are not currently available. Until they are, it is recommended that measured SPT resistances in soil layers within 2 m of overlying low-permeability layers be reduced by 20 percent for the purpose of lateral spreading displacement calculation.

6.8 EXAMPLES

The procedures for evaluating lateral spreading displacement described in the preceding sections can be illustrated by a series of examples. The examples show the results of single-scenario, multiple-scenario, and performance-based analyses for a hypothetical soil profile (Figure 6.4) assumed to exist at different locations within Washington State. The hypothetical soil profile used for lateral spreading examples is identical to that used for the liquefaction initiation examples (Figure 5.4) except that the profile is inclined at a 2 percent slope and the SPT values are 5 blows/ft lower at all depths.

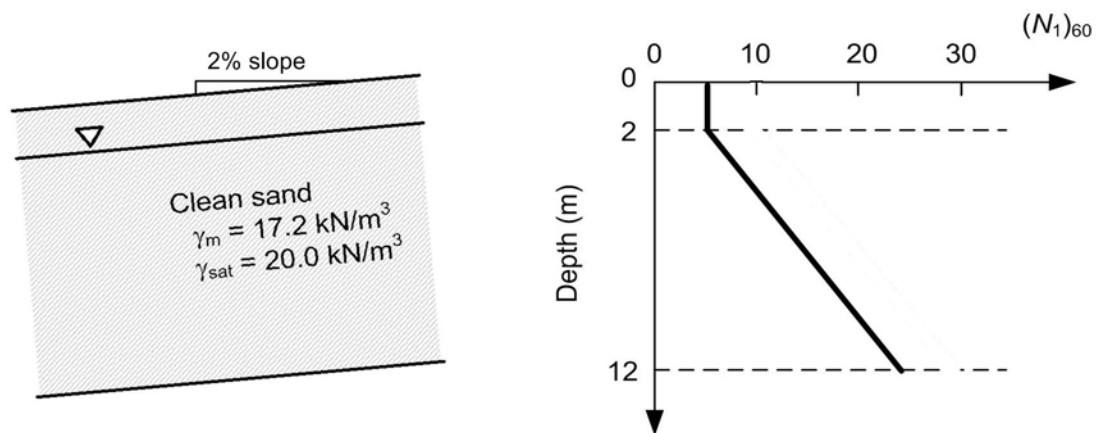


Figure 6.4. Subsurface profile for idealized site.

The following sections present the results of various analyses performed with the WSliq program at different locations in Washington State.

6.8.1 Single-Scenario Analyses

Single-scenario lateral spreading analyses, as described in Section 6.6.1, are useful for quick examination of lateral spreading displacements under various assumed scenarios and for evaluating sensitivities to variations in different earthquake and/or site parameters. For example, Table 6.7 shows the computed lateral spreading displacements for the hypothetical soil profile at seven locations in Washington state. The potential maximum displacements predicted by the Idriss and Boulanger (2008) model can also be

seen to be significantly greater, as expected, than those predicted by the Baska-Kramer and Youd et al. models.

Table 6.7 Computed lateral spreading displacements for various scenarios, assuming mean magnitudes and distances associated with 475-year Seattle PGA values.

Location	Post-Liquefaction Settlement (m)		
	Youd et al.	Baska-Kramer	Idriss-Boulanger
Seattle	0.24	0.16	6.73
Vancouver	0.31	0.13	5.52
Long Beach	37.4	4.63	7.33
Bellingham	0.05	0	4.97
Olympia	0.11	0	5.79
Pasco	0	0	0
Spokane	0	0	0

6.8.2 Multiple-Scenario Analyses

Multiple-scenario lateral spreading analyses, as described in Section 6.6.2, allow consideration of all magnitudes and distances contributing to the ground motion hazard at a particular site. The multiple-scenario analysis eliminates the need to choose between mean, modal, or other magnitudes and distances because all contributing magnitudes and distances are used with weights proportional to their contribution to peak ground acceleration. The 975-year displacements from the multiple-scenario analyses shown in Table 6.8 are more consistent than those obtained from the various single-scenario options described in the preceding sections.

Table 6.8 Computed lateral spreading displacements for multiple-scenario magnitudes and distances associated with 975-year Seattle PGA values.

Location	Post-Liquefaction Settlement (m)		
	Youd et al.	Baska-Kramer	Idriss-Boulanger
Seattle	2.64	1.01	6.46
Vancouver	2.14	0.77	4.33
Long Beach	42.7*	4.62	7.30
Bellingham	0.69	0.29	4.18
Olympia	1.77	0.52	5.14
Pasco	0.09	0.04	0.21
Spokane	0	0.02	0.03

*magnitude values above recommended maxima used in calculations

6.8.3 Performance-Based Analyses

Performance-based liquefaction potential analyses, as described in Section 6.6.3, allow the most complete characterization of lateral spreading hazards in that all scenarios—ranging from frequent, relatively weak shaking to rare, strong shaking with explicit consideration of all contributing magnitudes and distances—are accounted for. Performance-based analyses allow calculation of lateral spreading hazard curves for various locations. Figure 6.5 shows the lateral spreading hazard curve for the hypothetical profile of Figure 6.4 when located in the seven previously described cities.

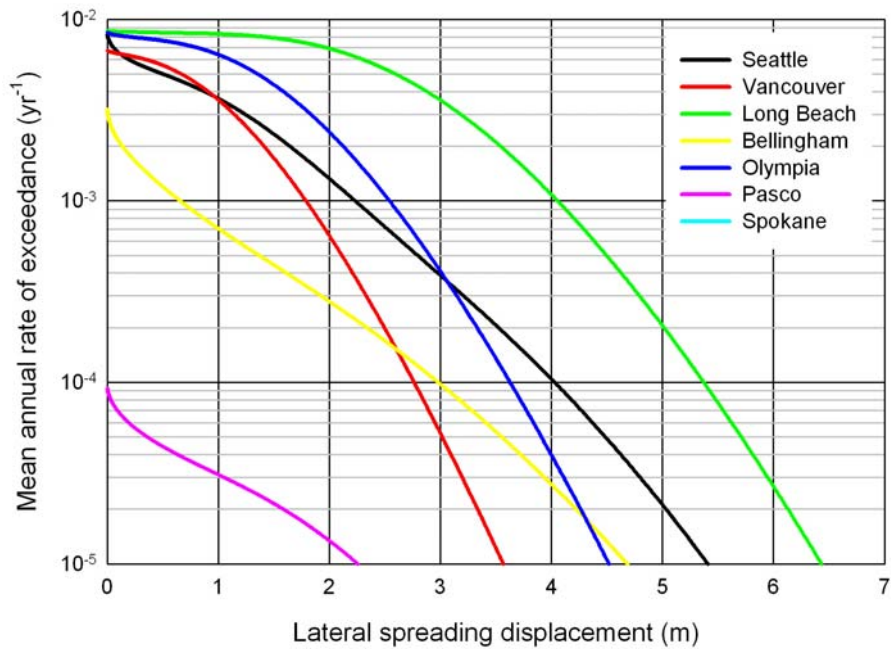


Figure 6.5 Lateral spreading hazard curve for hypothetical soil profile located in Seattle.

Table 6.9 Computed lateral spreading displacements at 475-yr and 975-yr hazard levels from performance-based lateral spreading analysis.

Location	475-yr Lateral Spreading Displacement (m)	975-yr Lateral Spreading Displacement (m)
Seattle	1.55	2.21
Vancouver	1.38	1.78
Long Beach	3.50	4.04
Bellingham	0.11	0.63
Olympia	2.10	2.53
Pasco	0	0
Spokane	0	0

Chapter 7

Post-Liquefaction Settlement

7.1 INTRODUCTION

Vertical movement of the ground surface following earthquake shaking is commonly referred to as earthquake-induced settlement. When liquefiable soils are involved, these displacements can result from several different mechanisms. In some cases, vertical ground displacements result from shear-induced ground deformations such as those associated with lateral spreading or other forms of instability at sloping-ground sites. In other cases, ground surface settlements may be associated with ground loss due to sand boil ejection. Settlement of shallow foundations and the structures they support may be caused by full or partial bearing failure, or by accumulated strains associated with rocking behavior. Finally, settlement on level-ground sites may result from the dissipation of excess porewater pressure following earthquake shaking. Such settlements, which are the subject of this chapter, can occur in moderately dense as well as loose soils, but the amount of settlement decreases with increasing soil density. Liquefaction-induced settlement can produce damage to bridge approaches, abutments, and shallow foundations. It can also cause downdrag loading on deep foundations.

Available procedures for estimating liquefaction-induced settlement are based on observed soil behavior in laboratory tests and on observed field behavior from earthquake case histories. Because relatively few well-documented case histories of post-liquefaction settlement are available, the uncertainty in predicted settlement is significant. This chapter describes a series of procedures that can be used to estimate post-liquefaction settlement for different earthquake scenarios, different ground motion hazard levels, and different settlement hazard levels.

7.2 BACKGROUND

The most common form of liquefaction-induced settlement is that which results from the volumetric compression that occurs when excess porewater pressures dissipate

under level-ground conditions (i.e., when shearing deformations are insignificant). The contractive nature of sands subjected to vibratory loading has been recognized for many years. Silver and Seed (1971) showed experimentally that the densification of dry sands subjected to cyclic loading depended on the density of the sand, the number of cycles of loading applied to the sand, and the amplitude of the cyclic shear strain induced in the sand. Over the years, several procedures for estimating the post-liquefaction settlement of sands have been proposed.

Tokimatsu and Seed (1987) reviewed previous laboratory test data, which showed post-liquefaction volumetric strain to be related to relative density and peak shear strain. They then related relative density to SPT resistance and peak shear strain to cyclic stress ratio to develop curves relating volumetric strain to $(N_1)_{60}$ and CSR (Figure 7.1). The curves in Figure 7.1 show that post-liquefaction volumetric strain increases with increasing loading and decreasing SPT resistance and suggest that volumetric strains can be as large as 10 percent in extremely loose sands. They also show that, for strong levels of shaking, the soil reaches a limiting volumetric strain. The Tokimatsu and Seed procedure computes ground surface settlement by integrating volumetric strain over the depth of the liquefiable layer, i.e., as

$$\Delta H = \int \varepsilon_v dz \quad (7.1)$$

This integral is usually evaluated numerically by dividing the soil profile into a series of sublayers of constant SPT resistance, and then summing the computed settlements of the individual sublayers.

Ishihara and Yoshimine (1992) used a similar approach to the estimation of post-earthquake settlement. Ishihara and Yoshimine developed a procedure that allows soil density to be expressed in terms of relative density, SPT resistance, or CPT tip resistance; peak shear strain is then correlated to density and factor of safety against liquefaction, as shown in Figure 7.2. The resulting curves extend to FS_L values of up to 2.0, which provides the ability to estimate settlements associated with dissipation of pore pressures lower than those required to trigger liquefaction; the curves indicate that no settlement should be expected for $FS_L \geq 2.0$. Ishihara and Yoshimine's curves can be used to estimate the volumetric strain in each of a series of sublayers, after which settlement can be computed by using Equation 7.1.

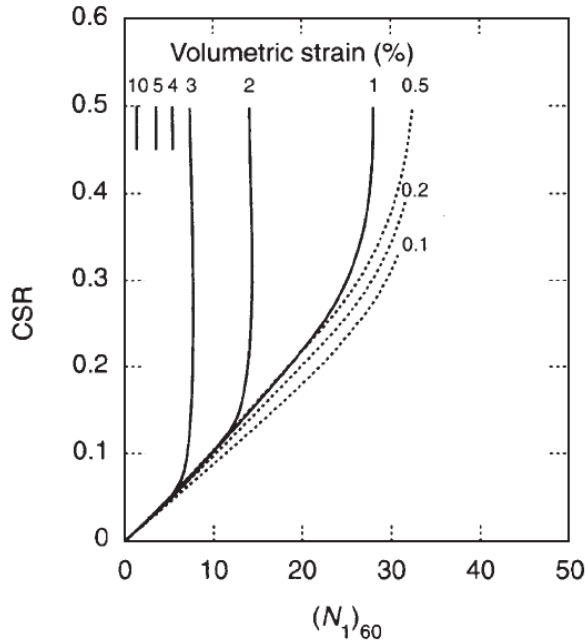


Figure 7.1. Variation of volumetric strain with corrected SPT resistance and cyclic stress ratio (after Tokimatsu and Seed, 1987).

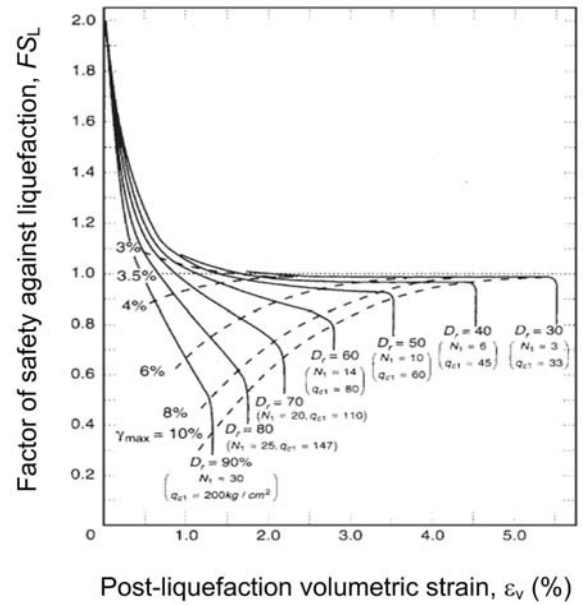


Figure 7.2. Variation of volumetric strain with relative density, SPT and CPT resistance, and factor of safety against liquefaction (after Ishihara and Yoshimine, 1992).

Shamoto et al. (1998) used basic principles of soil mechanics along with laboratory test results to define an expression for maximum residual volumetric strain, $(\varepsilon_{vr})_{\max}$, as a function of initial density (expressed in terms of a fines-adjusted SPT value) and cyclic stress ratio. This strain is used to define a ground settlement potential

$$(D_s)_{\max} = \int (\varepsilon_{vr})_{\max} dz \quad (7.2)$$

which is interpreted as a conservative estimate of the expected settlement. By comparing predicted values of the settlement index with actual values for a series of case histories, the expected settlement value was found to be approximately 84 percent of the value computed by using Equation (7.2). Therefore, the Shamoto et al. (1998) settlement can be computed as

$$D_s = 0.84 \int (\varepsilon_{vr})_{\max} dz \quad (7.3)$$

Wu and Seed (2004) performed cyclic simple shear tests on a single sand and developed a relationship between $(N_1)_{60,cs}$, CSR , and volumetric strain (Figure 7.4). These curves are of the same form as those of Tokimatsu and Seed (Figure 7.1) and Shamoto et al. (Figure 7.3). The Wu and Seed curves generally plot below those of Tokimatsu and Seed (1987) and show a much weaker tendency for limiting strain development (i.e., the curves do not become vertical at moderate CSR levels). In the Wu and Seed model, settlements are computed by integrating volumetric strain over the thickness of the soil profile, as described in Equation 7.1.

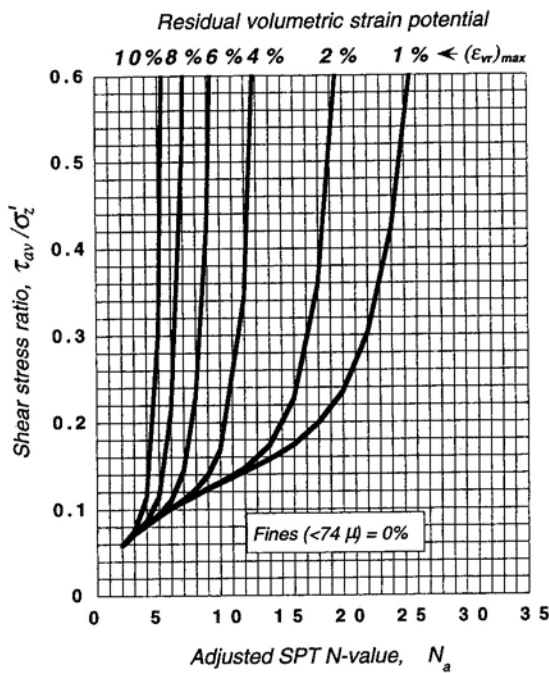


Figure 7.3. Variation of maximum residual volumetric strain with corrected SPT resistance and cyclic stress ratio for clean sands (after Shamoto et al., 1998).

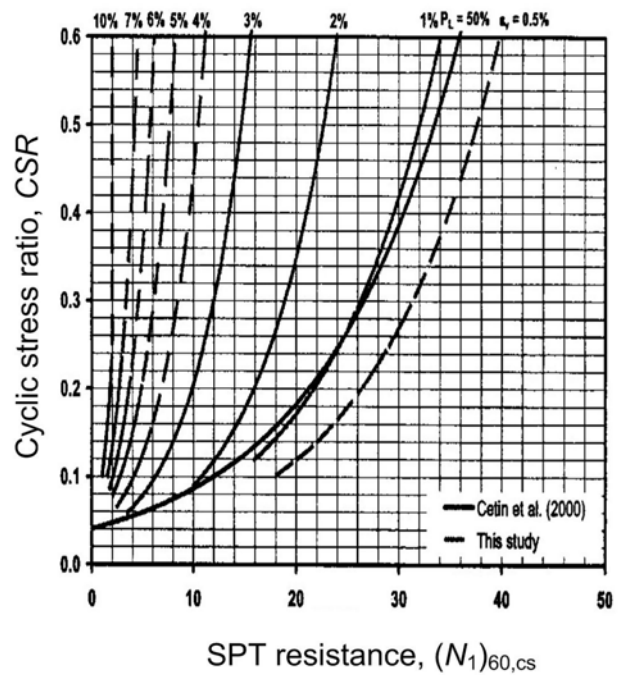


Figure 7.4. Variation of volumetric strain with corrected SPT resistance and cyclic stress ratio (after Wu and Seed, 2006).

7.3 REQUIRED INFORMATION

Evaluation of settlement hazards requires characterization of subsurface conditions, principally soil density, fines content, and groundwater conditions, to sufficient depth to characterize all potentially liquefiable soils (Chapter 4). Currently, most available procedures for estimating post-liquefaction settlement use SPT resistance

as a proxy for soil density. When additional case histories with measured CPT resistance become available, CPT-based settlement procedures will undoubtedly become available. Until that time, however, available CPT data should be transformed to equivalent SPT resistances, with recognition of the uncertainty that exists in the transformation.

The post-liquefaction settlement procedures described in this chapter apply to level ground conditions. It should be recognized that vertical movements of the ground surface can also be caused by shearing mechanisms, e.g., lateral spreading, flow failure, and bearing failure. Evaluation of those hazards requires information described in the chapters on lateral spreading (Chapter 5) and residual strength (Chapter 7).

Finally, earthquake loading information is required. Most empirical predictions of settlement require estimation of cyclic stress ratio to account for the effects of earthquake loading on volumetric strain; one requires estimation of the factor of safety against the initiation of liquefaction. The information required for estimating cyclic stress ratio and factor of safety is described in Chapter 4. In the future, it is likely that actual ground motion parameters will provide improved estimates of settlement, but sufficient field data to validate such predictions are not yet available.

7.4 PROCEDURE

A number of procedures for estimating post-liquefaction settlement have been developed and used in practice. The procedures are generally similar in that they all provide an estimate of volumetric strain, which is then integrated one-dimensionally over the thickness of the soil deposit to obtain a settlement index. The settlement index may then be adjusted by a factor obtained by calibration against case histories of actual post-liquefaction settlement.

The volumetric strain relationships used in the settlement calculations are based on laboratory test results, generally for a small number of different sands. At this time, the different procedures appear to predict average post-liquefaction settlements in case history databases with about equal levels of accuracy; however, the predicted settlements for individual case histories within the database can vary significantly. As a result, more consistent and stable estimates of post-liquefaction settlement should be produced by a combination of methods.

The following sections describe four procedures for estimating post-liquefaction settlement. The first two, Tokimatsu and Seed (1984) and Ishihara and Yoshimine (1992), are the approaches most commonly used in contemporary geotechnical engineering practice. The other two, Shamoto et al. (1998) and Wu and Seed (2004), are more recent approaches based on extensive laboratory testing programs and field calibration efforts. Recommendations for the combined use of these procedures are presented in Section 7.6.

7.4.1. Determination of Cyclic Stress Ratio

All of the post-liquefaction settlement models share a common measure of earthquake loading – the cyclic stress ratio. The cyclic stress ratio can be estimated in the series of steps described in Section 5.4.1.

7.4.2 Tokimatsu and Seed Model

Tokimatsu and Seed (1984) used a correlation between $(N_1)_{60}$ and relative density and an estimate of the shear strain potential of liquefied soil from $(N_1)_{60}$ and cyclic stress ratio to produce the chart shown in Figure 7.1. The shear strain potential relationship was based, in part, on engineering judgment. The Tokimatsu and Seed model can be implemented in the following series of steps:

1. *Develop profiles of measured SPT resistance and fines content within all potentially liquefiable soils.* The SPT equipment and procedures used to obtain the measured SPT resistances should be recorded during the site investigation and considered during the liquefaction potential evaluation process. Interpolation of SPT resistances and fines contents between points at which they are measured should be done with due consideration of site geology.
2. *Correct the measured SPT resistances for deviations from standard equipment and procedures.* Corrections for rod length, sampler type, borehole diameter, and energy are described in Appendix A.
3. *Compute clean sand corrected SPT resistance.* The original Tokimatsu and Seed paper is based on clean sand data and does not explicitly provide

for a fines content correction. However, the reduction in measured SPT resistance that results from the presence of fines is likely to lead to overestimated volumetric strain when uncorrected SPT resistances are used for very silty sands. As a result, the use of corrected SPT resistance as obtained from the NCEER procedure (Table 5.4) is recommended.

4. *Compute the volumetric strain for each sublayer.* Using the curves in Figure 7.1 and the previously determined CSR and $(N_1)_{60}$ values, determine the corresponding values of volumetric strain.
5. *Compute the expected settlement.* The expected settlement is obtained as the sum of all sublayer settlements, which are approximated assuming constant volumetric strain within each sublayer, i.e.,

$$\Delta H = \sum_{i=1}^n t_i \varepsilon_{v,i} \quad (7.4)$$

where n is the number of sublayers.

7.4.3 Ishihara and Yoshimine Model

The Ishihara and Yoshimine (1992) model parameterizes the loading differently than the Tokimatsu and Seed (1984) model. Ishihara and Yoshimine (1984) use the factor of safety against liquefaction, FS_L , and various indicators of soil density (relative density, SPT resistance, CPT resistance) to predict volumetric strain. The graphical relationship (Figure 7.2) shows that volumetric strains increase when the factor of safety drops below 1.0 – sharply for looser sands and gradually for denser ones. The Ishihara and Yoshimine model can be implemented in the following series of steps:

1. *Develop profiles of measured SPT resistance and fines content within all potentially liquefiable soils.* The SPT equipment and procedures used to obtain the measured SPT resistances should be recorded during the site investigation and considered during the liquefaction potential evaluation process. Interpolation of SPT resistances and fines contents between points at which they are measured should be done with due consideration of site geology.

2. *Correct the measured SPT resistances for deviations from standard equipment and procedures.* Corrections for rod length, sampler type, borehole diameter, and energy are described in Appendix A. The Japanese SPT value, N_1 , used in Figure 7.2, however, is based on an energy ratio of 72 percent (i.e., $(N_1 = 0.833(N_1)_{60})$).
3. *Compute the factor of safety against liquefaction.* Using one of the procedures described in Chapter 5, compute the factor of safety against liquefaction for each sublayer.
4. *Compute the volumetric strain for each sublayer.* Using the curves in Figure 7.2 and the previously determined FS_L and density parameters, determine the corresponding values of volumetric strain.
5. *Compute the expected settlement.* The expected settlement is obtained as the sum of all sublayer settlements, which are approximated assuming constant volumetric strain within each sublayer, i.e.,

$$\Delta H = \sum_{i=1}^n t_i \varepsilon_{v,i}$$

where n is the number of sublayers.

7.4.4 Shamoto et al. Model

The Shamoto et al. (1998) model is similar in form to the Tokimatsu and Seed (1984) model, but the form of the volumetric strain model is based on a constitutive model and laboratory test results. Volumetric strains were found to be related to maximum shear strains in samples subjected to uniform amplitude cyclic loading. By using a correction factor to account for transient loading effects, the chart shown in Figure 7.3 was obtained for clear sands. Similar charts were produced for fines contents of 10 percent and 20 percent. The settlement values obtained by directly integrating volumetric strains were then compared with case history observations and a calibration factor developed to optimize predictive accuracy in an average sense. The Shamoto et al. model can be implemented in the following series of steps:

1. *Develop profiles of measured SPT resistance and fines content within all potentially liquefiable soils.* The SPT equipment and procedures used to

obtain the measured SPT resistances should be recorded during the site investigation and considered during the liquefaction potential evaluation process. Interpolation of SPT resistances and fines contents between points at which they are measured should be done with due consideration of site geology.

2. *Correct the measured SPT resistances for deviations from standard equipment and procedures.* Corrections for rod length, sampler type, borehole diameter, and energy are described in Appendix A. The Japanese SPT value, N_1 , however, is based on an energy ratio of 72 percent (i.e., $(N_1) = 0.833(N_1)_{60}$).
3. *Compute the clean sand corrected SPT resistance.* The presence of fines is accounted for by a fines correction to produce the fines-adjusted SPT resistance, N_a , used in Figure 7.3. The fines-adjusted SPT resistance is calculated as

$$N_a = N_1 + \Delta N_f \quad (7.5)$$

where ΔN_f is computed as

$$\Delta N_f = \begin{cases} 0 & FC \leq 5 \\ FC - 5 & 5 < FC < 10 \\ 0.1FC + 4 & FC \geq 10 \end{cases} \quad (7.6)$$

4. *Compute the volumetric strain for each sublayer.* Using the curves in figures 7.3 (clean sand), 7.5 (10 percent fines), 7.6 (20 percent fines) and the previously determined CSR and $(N_1)_{60}$ values, determine the corresponding values of maximum residual volumetric strain, $(\epsilon_{vr})_{\max}$. The shear stress ratios shown on the ordinates of those plots are equivalent to CSR .
5. *Compute the expected settlement.* The expected settlement is obtained as the sum of all sublayer settlements, which are approximated assuming constant volumetric strain within each sublayer, i.e.,

$$\Delta H = 0.84 \sum_{i=1}^n t_i (\epsilon_{vr})_{\max} \quad (7.7)$$

where n is the number of sublayers.

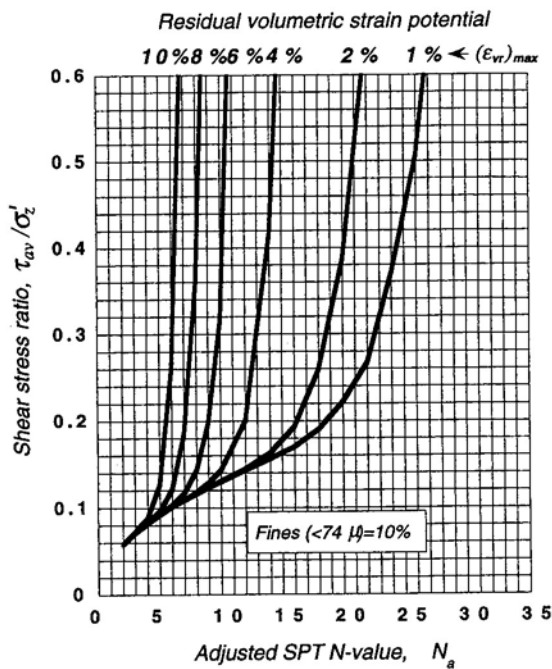


Figure 7.5. Variation of maximum residual volumetric strain with corrected SPT resistance and cyclic stress ratio for sands with 10 percent fines (after Shamoto et al., 1998).

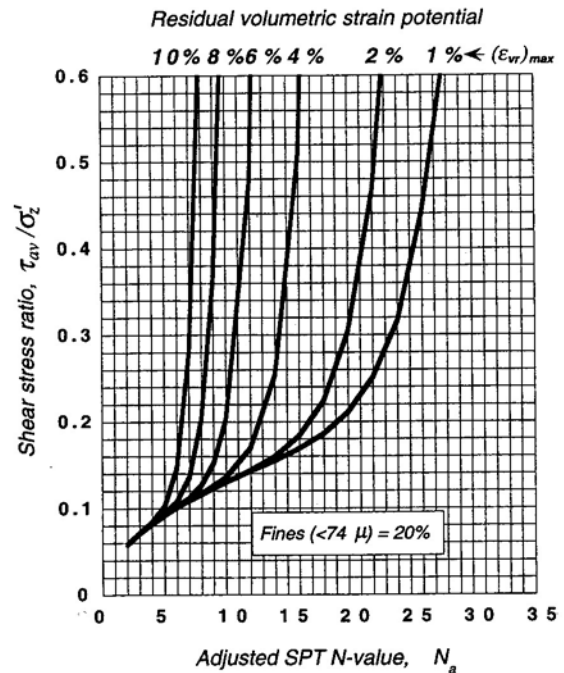


Figure 7.6. Variation of maximum residual volumetric strain with corrected SPT resistance and cyclic stress ratio for sands with 20 percent fines (after Shamoto et al., 1998).

7.4.5 Wu and Seed Model

The Wu and Seed (2004) model is also similar to the Tokimatsu and Seed (1984) model, but the volumetric strain curves are based upon the results of cyclic simple shear tests on a single sand. The model has been calibrated against field case history data, however, and found to predict observed settlements about as accurately as the other models described here. The Wu and Seed model can be implemented in the following series of steps:

1. *Develop profiles of measured SPT resistance and fines content within all potentially liquefiable soils.* The SPT equipment and procedures used to obtain the measured SPT resistances should be recorded during the site investigation and considered during the liquefaction potential evaluation process. Interpolation of SPT resistances and fines contents between

points at which they are measured should be done with due consideration of site geology.

2. *Correct the measured SPT resistances for deviations from standard equipment and procedures.* Corrections for rod length, sampler type, borehole diameter, and energy are described in Appendix A.
3. *Compute the clean sand corrected SPT resistance.* The presence of fines is accounted for by a fines correction. The fines content correction provides a clean sand SPT value given by

$$(N_1)_{60,cs} = \begin{cases} (N_1)_{60} & FC \leq 5 \\ (N_1)_{60} \cdot \left[1 + 0.004FC + 0.05 \frac{FC}{(N_1)_{60}} \right] & 5 < FC < 35 \\ (N_1)_{60} \cdot \left[1.14 + \frac{1.4}{(N_1)_{60}} \right] & FC \geq 35 \end{cases} \quad (7.8)$$

where FC = fines content in percent.

4. *Compute the volumetric strain for each sublayer.* Using the curves in Figure 7.4 and the previously determined CSR and $(N_1)_{60}$ values, determine the corresponding values of volumetric strain.
5. *Compute the expected settlement.* The expected settlement is obtained as the sum of all sublayer settlements, which are approximated assuming constant volumetric strain within each sublayer, i.e.,

$$\Delta H = \sum_{i=1}^n t_i \varepsilon_{v,i}$$

where n is the number of sublayers.

7.5 DISCUSSION

The four post-liquefaction settlement procedures described in this chapter are all quite similar, and they all predict the average settlements of a group of case histories with about equal accuracy. All of the procedures compute settlement by integrating

volumetric strain over the thickness of a soil profile, generally with an adjustment that increases their overall consistencies with observed case history settlements.

The cyclic stress ratio for a typical liquefiable soil deposit with shallow groundwater tends to decrease with depth. This fact, combined with the fact that cohesionless soil compressibility decreases with increasing depth, helps explain why liquefaction at depths greater than 15 to 20 m has not been observed to cause significant surface effects.

The Tokimatsu and Seed (1984) procedure has likely been the most commonly used in U.S. geotechnical engineering practice, followed by the Ishihara and Yoshimine (1992) procedure. The two newer procedures bring the results of more detailed laboratory investigations to the problem. Although all four procedures predict settlement with about equal overall accuracy, they predict settlements of some individual case histories differently. For some case histories, the observed settlements are underpredicted by some procedures and overpredicted by others. Using the average of all four procedures, therefore, has the potential to improve prediction accuracy. It also allows realization of the benefits of all four procedures and the laboratory testing, case history databases, and volumetric strain models they incorporate. The average should also produce more consistent estimates of post-liquefaction settlement.

7.6 RECOMMENDATIONS

The following sections present recommendations for evaluating post-liquefaction settlements in potentially liquefiable soils. Such analyses should be performed following an evaluation of liquefaction potential, and contributions to post-liquefaction settlement should only be considered for soils in which liquefaction is initiated.

7.6.1 Single-Scenario Analyses

Use of the single-scenario approach is not recommended for analysis or design. It requires representation of the entire ranges and distributions of magnitude and PGA affecting a site by a single magnitude-PGA pair. Its only advantage over the multiple scenario approach is in speed (i.e., fewer calculations), and that advantage is effectively eliminated by the multiple-scenario option in the WSliq program. The single-scenario

option is useful, however, for investigating the sensitivity of liquefaction potential to various combinations of magnitude and distance.

7.6.2 Multiple-Scenario Analyses

For analysis and design at this time, the use of weighted multiple-scenario analyses is recommended. Multiple-scenario analyses properly account for the range and distribution of earthquake magnitudes that contribute to ground motion hazard. Those distributions, as obtained from USGS deaggregation files, are built into the WSliq program so that performing a multiple-scenario analysis is no more difficult than performing a single-scenario analysis.

The availability of multiple credible procedures for evaluating post-liquefaction settlement should also be taken advantage of. The use of weighted average settlements, based on contributions from the Tokimatsu and Seed, Ishihara and Yoshimine, Shamoto et al., and Wu and Seed procedures, is recommended. The weighting factor for any procedure should be not be less than 0.1, and the four weighting factors should add up to 1.0. The WSliq program allows the entry of weighting factors and the computation of individual and weighted average factors of safety. Although they can be changed manually, the default weighting factors in WSliq are given in Table 7.1.

Table 7.1. Default weighting factors for post-liquefaction settlement models in WSliq.

Model	Weighting factor
Tokimatsu and Seed (1984)	0.25
Ishihara and Yoshimine (1992)	0.25
Shamoto et al. (1998)	0.25
Wu and Seed (2004)	0.25

7.6.3 Performance-Based Analyses

As part of the research described in this report, a performance-based procedure for estimating post-liquefaction settlement was developed. Since a performance-based procedure requires a probabilistic estimate of response, the predictions of the Wu and Seed model were analyzed and used to develop the performance-based model. A detailed description of the performance-based model is given in Appendix F.

A transition toward the use of performance-based concepts in the evaluation of settlement hazards is recommended. The performance-based approach, as described in Chapter 3, considers all possible ground motion levels (rather than just a single level, as in the multiple scenario approach) and thereby produces a more complete and consistent evaluation of the settlement hazard. Use of the performance-based approach, however, requires different performance criteria because that approach can predict the actual return period of different settlements (rather than the settlement for an event with a single, specified return period).

7.7 OTHER CONSIDERATIONS

The procedures described in this chapter apply to the settlements caused by volume change associated with the dissipation of excess porewater pressure in liquefiable soils. It should be recognized that apparent settlement of liquefiable soils can also be associated with shearing deformations that occur with no volume change. In soil deposits subject to lateral spreading, vertical deformations may occur as a result of both porewater pressure dissipation and shearing.

Post-earthquake settlements can also occur in soils not susceptible to liquefaction, such as dry sands and even compacted fills. Procedures for estimating settlements under such conditions are described by Whang et al. (2004; 2005).

7.8 EXAMPLES

The procedures for evaluating settlement described in the preceding sections can be illustrated by a series of examples. The examples show the results of single-scenario, multiple-scenario, and performance-based analyses for a hypothetical soil profile (Figure 7.7) assumed to exist at different locations within Washington State. The hypothetical soil profile used for the settlement examples is identical to that used for the liquefaction initiation examples (Figure 5.4) except that the SPT values are 5 blows/ft lower at all depths.

The following sections present the results of various analyses performed with the WSliq program at different locations in Washington State.

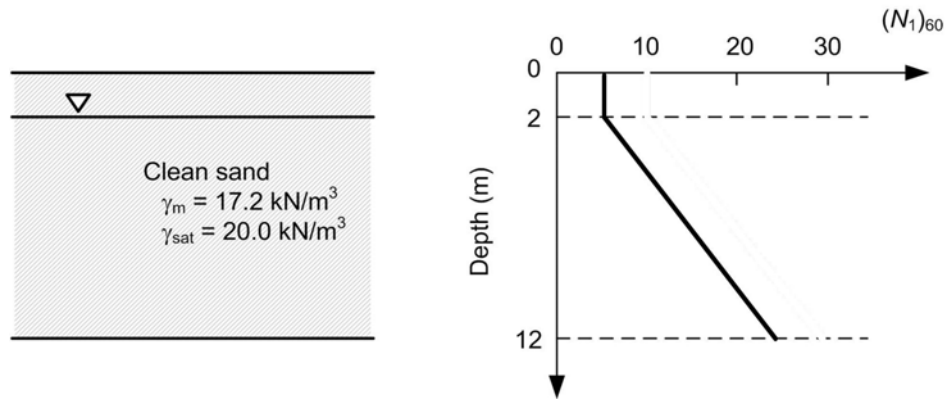


Figure 7.7. Subsurface profile for idealized site.

7.8.1 Single-Scenario Analyses

Single-scenario post-liquefaction settlement analyses, as described in Section 7.6.1, are useful for quickly estimating settlements under various assumed scenarios and for evaluating sensitivities to variations in different earthquake and/or site parameters. For example, Table 7.2 shows the computed post-liquefaction settlements for the hypothetical soil profile shown in Figure 7.7 located in seven cities across Washington state. Three of the four settlement values are reasonably consistent, but the Shamoto et al. values tend to be somewhat higher, particularly in Long Beach, which is affected by longer duration, larger magnitude events.

Table 7.2 Computed post-liquefaction settlements for various scenarios assuming mean and modal magnitudes and distances associated with 975-year ground motion hazard level.

Location	Post-Liquefaction Settlement (m)			
	Tokimatsu-Seed	Ishihara-Yoshimine	Shamoto et al.	Wu-Seed
Seattle	0.20	0.30	0.62	0.26
Vancouver	0.16	0.23	0.34	0.18
Long Beach	0.21	0.32	0.96	0.33
Bellingham	0.13	0.20	0.27	0.14
Olympia	0.17	0.24	0.37	0.19
Pasco	0	0	0	0
Spokane	0	0	0	0

7.8.2 Multiple-Scenario Analyses

Multiple-scenario settlement analyses, as described in Section 7.6.2, allow consideration of all magnitudes contributing to the ground motion hazard at a particular site. The multiple-scenario analysis eliminates the need to choose between mean, modal, or other magnitudes because all contributing magnitudes are used with weights proportional to their contribution to peak ground acceleration. The 475-year settlements from the multiple-scenario analyses shown in Table 7.3 are more consistent than those obtained from the various single-scenario options described in the preceding section.

Table 7.3 Computed post-liquefaction settlements for multiple-scenario magnitudes associated with 975-year ground motions.

Location	Post-Liquefaction Settlement (m)			
	Tokimatsu-Seed	Ishihara-Yoshimine	Shamoto et al.	Wu-Seed
Seattle	0.19	0.28	0.60	0.25
Vancouver	0.13	0.18	0.38	0.15
Long Beach	0.21	0.32	0.98	0.33
Bellingham	0.12	0.18	0.28	0.14
Olympia	0.15	0.22	0.40	0.18
Pasco	0.01	0.01	0.01	0.01
Spokane	0	0	0	0

7.8.3 Performance-Based Analyses

Performance-based settlement analyses, as described in Section 7.6.3, allow the most complete characterization of post-liquefaction settlement hazards in that all scenarios, ranging from frequent, relatively weak shaking to rare, strong shaking with explicit consideration of all contributing magnitudes and distances, are accounted for. Performance-based analyses allow calculation of post-liquefaction settlement hazard curves. Figure 7.8 shows the settlement hazard curves for the hypothetical profile of Figure 7.7 when located in each of the seven previously considered cities. Table 7.4 presents the 975-yr settlement values for each of these locations.

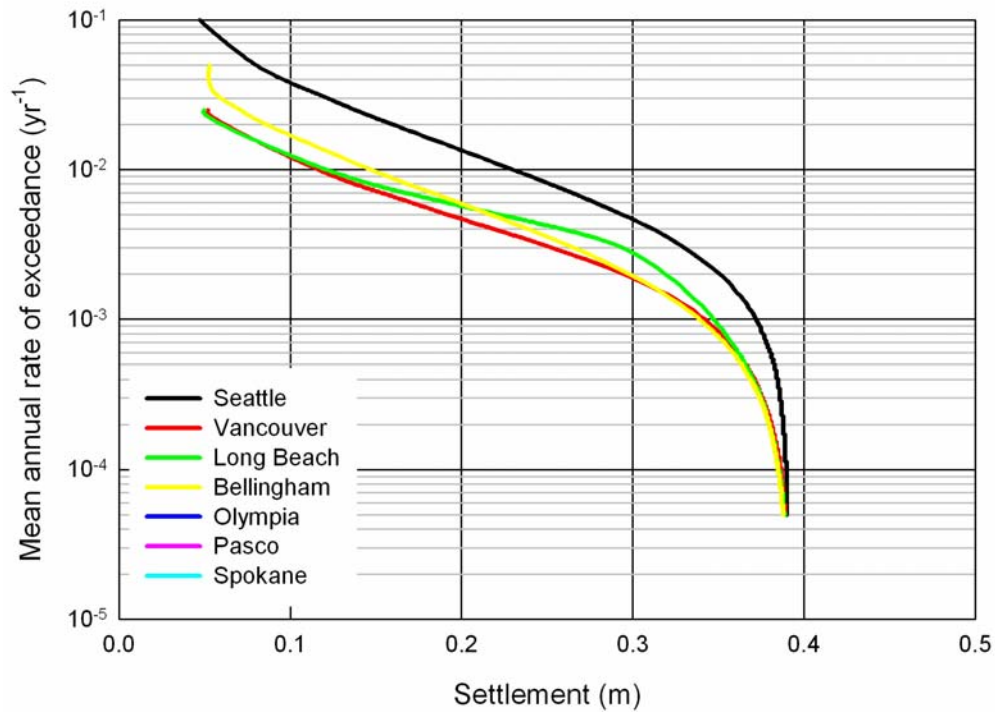


Figure 7.8. Seismic hazard curve for post-liquefaction settlement.

Table 7.4 Computed post-liquefaction settlements for various scenarios associated with 475-year and 975-year ground motions.

Location	475-year Post-Liquefaction Settlement (m)	975-year Post-Liquefaction Settlement (m)
Seattle	0.35	0.37
Vancouver	0.29	0.34
Long Beach	0.32	0.35
Bellingham	0.30	0.34
Olympia		
Pasco		
Spokane		

Chapter 8

Residual Strength of Liquefied Soil

8.1 INTRODUCTION

Once a soil has been determined to be susceptible to liquefaction and the anticipated loading sufficient to initiate liquefaction, the potential for gross instability must be considered. The most dangerous form of instability is the development of a flow slide, which can involve a tremendous volume of soil and produce very large soil deformations. Structures supported on soils involved in flow slides are almost invariably destroyed or damaged beyond repair. Furthermore, structures located on stable ground below flow slides can be damaged by the impact of flowing soil. Flow slides usually occur adjacent to bodies of water (lakes, rivers, bays) where the combination of sloping ground and loose, saturated soil promotes their occurrence; thus, their potential for damaging bridges, bridge approaches, and roadways must be considered. Evaluation of the potential for flow slide development requires evaluation of the residual strength of a liquefied soil.

Estimation of the residual strength of liquefied soil has proven to be one of the most difficult problems in geotechnical earthquake engineering practice. Several procedures have been proposed, but all produce highly uncertain estimates of residual strength. Complicating their use is the fact that the uncertainty has not been quantified. As a result, residual strength estimates are frequently made on an inconsistent, *ad hoc* basis in practice. This chapter provides a brief review of past work in the area of residual strength prediction, and recommended procedures for estimating residual strength. Examples of residual strength estimation are also included.

8.2 BACKGROUND

It is important to recognize that flow slide failures are driven by static stresses; the role of an earthquake is to produce sufficient porewater pressure to cause the available shear strength of the soil to drop from its original value to its residual value. In many

cases, the original (pre-earthquake) shear strength is sufficient to support structures such as bridges, approach embankments, and retaining walls, but the residual strength is not. When liquefaction occurs in such cases, the static driving stresses, i.e., the shear stresses required to maintain static equilibrium, exceed the available strength of the soil. As in any case in which static stresses exceed static strengths, failure will occur. What makes liquefaction-related flow slides particularly troublesome, however, is the degree to which (and speed with which) the available strength can be reduced. In some soils, the residual strength can be a very small fraction of the original strength, in which case the unbalanced forces (driving minus resisting) are quite large; these unbalanced forces accelerate the soil above a failure surface and cause large and rapid movements in the downslope direction. Flow slide failures are characterized by the sudden nature of their origin, the speed with which they develop, and the large distance over which the liquefied materials often move.

Several mechanisms can lead to flow failures, and the existence of these different mechanisms complicates the process of residual strength estimation. In some cases, liquefaction can be triggered under truly undrained conditions during earthquake shaking; the residual strength will therefore be the residual strength of the soil at its *in situ* (and pre-earthquake) density. In other cases, high excess porewater pressures generated in one area of a soil deposit may migrate into another area following the earthquake; if the latter area is one that is more critical than the former from a stability standpoint, flow failure may occur at some time following earthquake shaking. Similar behavior can occur when the redistribution of porewater pressure is impeded by silt lenses or other low-permeability materials; in such cases, rebound of the soil skeleton under the lower effective stresses produced by the migrating porewater pressures can lead to a reduced residual strength, and eventually to flow failure following ground shaking. Finally, flow failures can occur on interfaces, such as the interface between a pile and the adjacent soil, when porewater pressures become high; because no dilation may be required (for smooth foundation elements), such failures can occur in both loose and dense soils, although the effects are likely to be much more severe in loose soils than in dense.

A number of different approaches to the problem of residual strength estimation are available; in order to put the different methods into perspective, they are briefly

reviewed here. The different methods have advantages and limitations, and the available data with which to compare their relative validities are not as extensive as is desired.

Early work on the shear strength of liquefied soil concentrated on measurement of that strength in the laboratory. Castro (1969) used undrained triaxial tests on samples of very loose to medium dense clean sands to develop a framework for understanding the behavior of liquefiable sands that remains helpful to this day. Poulos et al. (1985) extended observations from laboratory tests to develop the concept of a steady state of deformation for liquefiable soils. A soil shearing at constant volume and strain rate with constant shear stress and normal effective stress was considered to be at the steady state of deformation; the shearing resistance of the soil under those conditions was termed the steady state strength. According to steady state concepts, the steady state strength is only a function of the density of the soil. Tests have shown that the steady state strength measured in the laboratory is quite sensitive to the density of the soil, hence small uncertainties and/or variability in soil density can lead to substantial differences in residual strength. Furthermore, the *in situ* density of a loose, saturated sand (the type of soil that geotechnical engineers are most concerned about with respect to flow slides) is very difficult to measure accurately. As a result of these difficulties, the steady state approach has become more useful as a general framework for understanding soil behavior than as a practical method for evaluating the shear strength of liquefied soil.

Recognizing the difficulties inherent in the laboratory-based steady state approach, Seed (1986) developed a correlation between SPT resistance and the apparent shear strength back-calculated from observed flow slide case histories. The back-calculation procedure required identification of appropriate case histories, compilation of data describing the geometry and material properties of those case histories, determination of the spatial extent of liquefaction in each case history, characterization of a “representative” SPT resistance for each case history, and back-calculation of the apparent residual strength of the liquefied zone. By applying a consistent methodology to a number of case histories, a relationship between the apparent residual strength and the representative SPT resistance could be obtained. Seed and Harder (1990) provided an update of Seed’s original procedure by using additional case history data and improved procedures to account for the inertial effects in the back-calculation process; this update,

which has been commonly used in practice since its publication, is shown in Figure 8.1. The figure presents the data obtained from the back-calculation analyses with a range of residual strength values for most of the case histories, and upper and lower bound curves that envelope the individual data points. While this represents a reasonable presentation and interpretation of the available data, the range between the upper and lower bound curves is quite wide. A soil with $(N_1)_{60,cs} = 10$, for example, would have a residual strength ranging from about 100 psf to 500 psf. Seed and Harder (1990) recommended that “the lower-bound, or near lower-bound relationship between S_r and $(N_1)_{60,cs}$... be used for residual strength analyses ...” because of the high degree of scatter and uncertainty and the limited number of available case histories. The procedure does not, however, provide detailed information on how the representative SPT resistances were obtained for the different case histories, nor on how they should be obtained for a particular site.

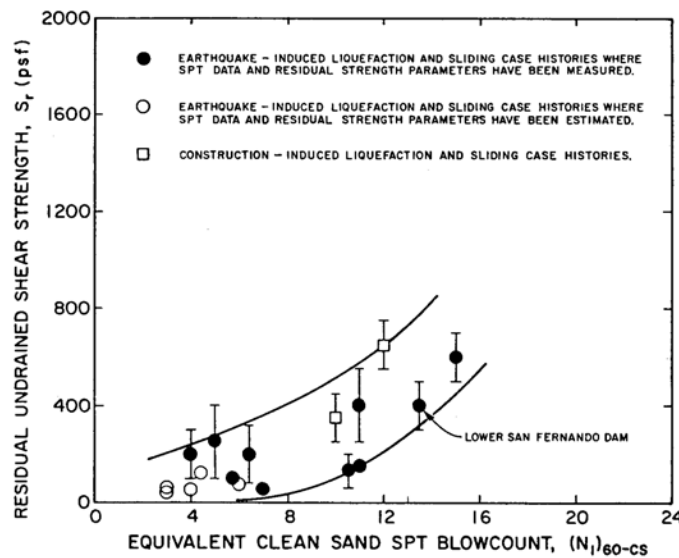


Figure 8.1 Estimation of residual strength from SPT resistance (Seed and Harder, 1990).

Idriss (1999) re-evaluated the case histories of Seed and Harder (1990), adding some and eliminating others, and developed a relationship between residual strength and corrected SPT resistance. Idriss produced a single curve that represents residual strength by a best-fit exponential function of median corrected SPT resistance (Figure 8.2); error bars indicating uncertainty in the back-calculated residual strengths are also shown. The

curve produced by Idriss passes through the lower portion of the range of Seed and Harder. The Idriss curve is attractive in that it can be interpreted as a single recommended residual strength value for a particular SPT resistance, and the SPT resistance from which residual strength is to be estimated is defined in clear, unambiguous terms.

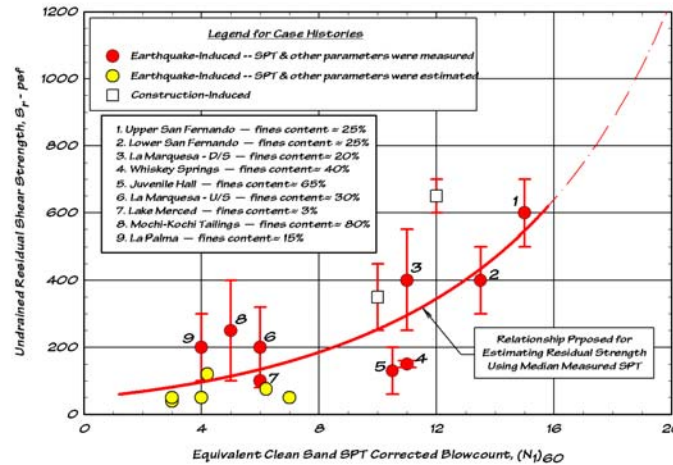


Figure 8.2 Estimation of residual strength from SPT resistance (Idriss, 1998).

Within the past 10 to 15 years, a different approach to estimating residual strength has been developed. This approach is expressed in the form of a normalized residual strength, i.e., a ratio of residual strength to initial effective overburden pressure. By using the logic that soil density increases with effective overburden pressure and that residual strength increases with increasing density, residual strength can be expected to increase with increasing effective overburden pressure. Extending this argument to the case in which the density and residual strength increase at exactly the same rate (in which case the steady state line and the consolidation curve are parallel), the ratio of residual strength to initial effective overburden pressure would be expected to be constant. This concept has been applied to a number of soils with ratios of S_r/σ'_{v0} reported as being in the range of about 0.07 to 0.20. Stark and Mesri (1992) reasoned that the factors that would influence the value of S_r/σ'_{v0} for a particular soil would also affect penetration resistance, and they developed a procedure to predict S_r/σ'_{v0} as a function of SPT

resistance. Olson and Stark (2002) revised the work of Stark and Mesri (1992) to produce the updated relationship shown in Figure 8.3. Olson and Stark's relationship is based on a larger set of case history data (from which lateral spreading cases used in the work of Seed and Harder were removed) and makes use of the mean $(N_1)_{60}$ value within the liquefied zone. Olson and Stark did not find a systematic variation of normalized residual strength with fines content and therefore recommended no fines content correction.

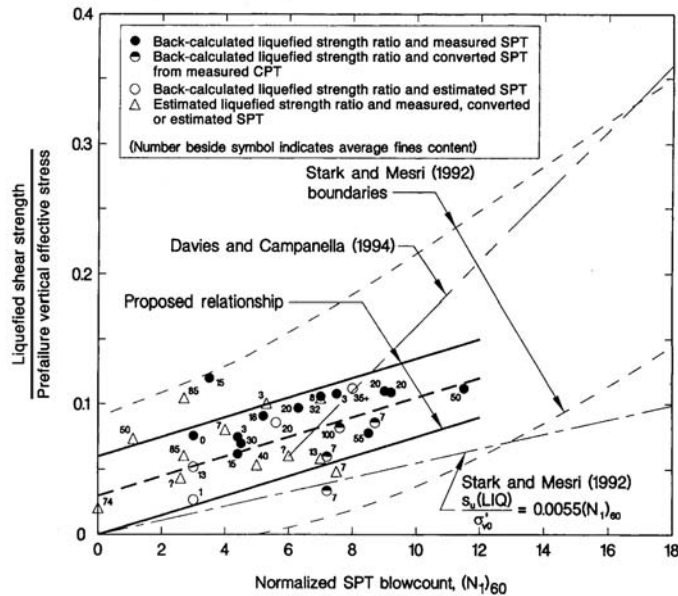


Figure 8.3 Estimation of residual strength ratio from SPT resistance (Olson and Stark, 2002).

Idriss and Boulanger (2007) re-examined the case history database of Olson and Stark (2002) and eliminated case histories they considered unreliable or insufficiently documented. They used these data to develop predictive relationships for normalized residual strength ratio as a function of corrected SPT resistance. Figure 8.4 shows the residual strength ratio curves developed by Idriss and Boulanger for two conditions: conditions in which significant void redistribution is not expected (upper curve) and conditions in which void redistribution is expected to be significant (lower curve).

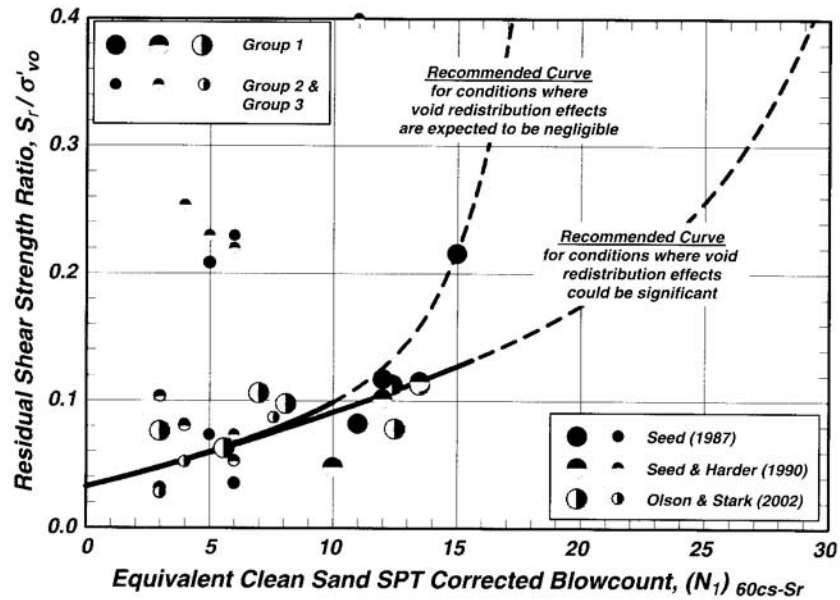


Figure 8.4 Estimation of residual strength ratio from SPT resistance (Idriss and Boulanger, 2007).

Kramer and Wang (2007) developed a hybrid procedure that combines elements of the classical and normalized strength approaches. The hybrid model considers residual strength to be a function of both corrected SPT resistance and effective stress, but without the restriction of proportionality inherent in the normalized strength approach. The hybrid model is of a general form derived from basic principles of soil mechanics and is calibrated against a database of flow slide case histories with consideration of uncertainty and quality. It considers the conditions under which flow slides are observed not to occur in order to avoid underpredicting residual strength at low effective stress levels. The hybrid model is formulated in both deterministic and probabilistic form; examples of the residual strengths predicted by the deterministic model are shown in Figure 8.5. Kramer and Wang did not find a systematic variation of residual strength with fines content in the flow slide case history database and therefore recommended no fines content correction.

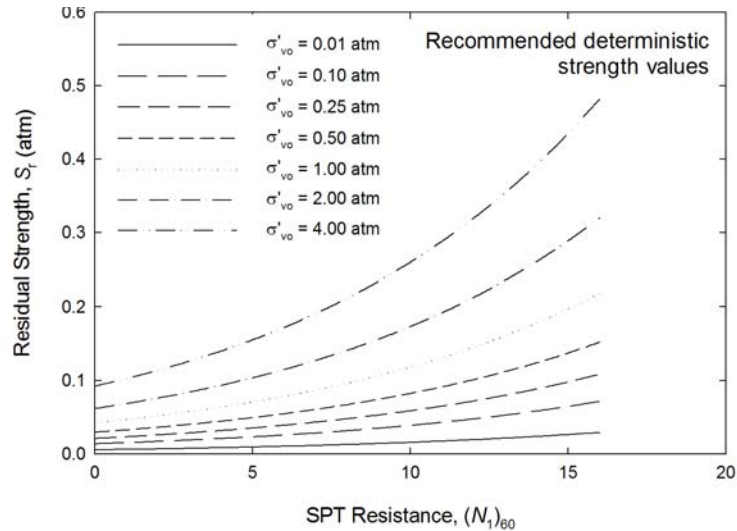


Figure 8.5 Variation of residual strength ratio with SPT resistance and initial vertical effective stress using Kramer-Wang model.

8.3 REQUIRED INFORMATION

Estimation of flow slide potential requires accurate characterization of the geometry and properties of all soils, not just those for which liquefaction is expected. The potential for flow sliding is evaluated by means of limit equilibrium slope stability analyses, so all of the information needed to perform such analyses is required. This includes the geometry, unit weight, and shear strength parameters for all non-liquefiable soil units.

The pertinent soil properties for the liquefiable soils are density, penetration resistance, and fines content; as in the case of evaluating liquefaction potential (Chapter 3), efforts must be expended to ensure that standard equipment/procedures, or accurate corrections for non-standard equipment/procedures, are used in SPT testing. Some models also require initial vertical effective stress for estimation of residual strength. Calculation of vertical effective stress requires accurate determination of the thicknesses and unit weights of all liquefiable and overlying layers; knowledge of the position of the groundwater table is also important.

In addition, other factors beyond the standard factors considered in most stability analyses can influence flow slide stability. Many potential flow slides involve masses of soil sliding into bodies of water. This is the potential for hydroplaning, in which water trapped beneath a portion of the rapidly sliding soil greatly reduces the apparent sliding

resistance of those soils. While hydroplaning would not typically affect the results of an analysis of the potential for flow sliding, it could significantly affect the runout distance and, therefore, the potential effects of a flow slide. The potential for delayed failure associated with pore pressure redistribution should also be evaluated; such failures occur most frequently where liquefiable layers are “capped” by low permeability soil layers. The subsurface investigation program should look carefully for the presence of silt or clay lenses beneath which porewater could be trapped. Continuous lenses that are unfavorably oriented could lead to impeded drainage and local reductions of soil density that could significantly reduce the residual strength of the soil.

8.4 PROCEDURE

As mentioned previously, several approaches for estimating residual strength have been developed and used in practice. These approaches are based on similar databases of flow slide case histories but make different assumptions about the mechanisms of soil behavior at large strain. The classical approach is commonly used in practice but implicitly assumes that residual strength is related only to corrected SPT resistance, i.e., that the effects of effective stress are completely reflected in $(N_1)_{60}$. The normalized approach assumes direct proportionality of residual strength to effective stress and thereby predicts unrealistically low residual strengths for soils at shallow depths. A hybrid model, in which residual strength depends on both corrected SPT resistance and effective stress, was developed as part of this research.

The following sections describe the three procedures for estimating residual strength. Recommendations for the combined use of these procedures are presented in Section 8.6.

8.4.1 Idriss Model

The Idriss model is of the classical form, in which residual strength is taken as a unique function of corrected SPT resistance. It is similar to the procedure of Seed and Harder (1990) but produces a single estimate rather than a wide band (Figure 8.1) of residual strength values; the Idriss model corresponds to the lower portion of the Seed and Harder band. The Idriss model is also based on an unambiguous measure of SPT

resistance (i.e., median rather than “representative” SPT resistance). Estimation of residual strength with the Idriss method can be accomplished in the following series of steps:

1. *Identify the spatial extent of soil expected to liquefy.* This can be accomplished by using the liquefaction initiation procedures described in Chapter 5.
2. *Divide the liquefied region into zones of approximately constant SPT resistance.* For many sites, the liquefied zone may be treated as having a single SPT resistance, but sites subjected to very strong shaking may have liquefied soils with a range of SPT values.
3. *Determine the average fines content for each zone of liquefied soil.* This may be done using statistical methods when sufficient data are available, augmented by engineering and geological judgment when data are sparse.
4. *Correct the SPT resistances for fines content.* Using the results of the two preceding steps for each zone of liquefied soil, compute

$$(N_1)_{60,cs} = (N_1)_{60} + \Delta N \quad (8.1)$$

where ΔN is a fines correction obtained from Table 8.1.

Table 8.1. Variation of fines content correction with fines content (Seed and Harder, 1990).

FC (%)	0	10	25	50	75
ΔN	0	1	2	4	5

5. *Determine the median $(N_1)_{60}$ value for each zone of liquefied soil.* This may be done using statistical methods when sufficient data are available, augmented by engineering and geological judgment when data are sparse.
6. *Compute the residual strength using the median SPT values from Step 5.* The residual strength (in atm) from the Idriss model (Figure 8.2) is very closely approximated by

$$S_r = 0.0239 \exp[0.16(N_1)_{60,cs}] \leq 0.5 \quad (8.2)$$

7. *Evaluate the potential for pore pressure redistribution effects.* At present, procedures for accurate, quantitative prediction of pore pressure redistribution effects are not available. Experience has shown, however,

that pore pressure redistribution can occur when liquefiable soil layers are "capped" by impermeable layers of silt and/or clay. In such cases, residual strengths may be lower than estimated on the basis of *in situ* SPT resistances, so additional conservatism may be in order.

8.4.2 Normalized Strength Model – Olson and Stark

The normalized strength model of Olson and Stark (2002) accounts for the effects of effective stress on the rate of increase of residual strength with SPT resistance. The residual strength can be estimated by using the Olson and Stark model in the following series of steps:

1. *Identify the spatial extent of the soil expected to liquefy.* This can be accomplished by using the procedures described in Chapter 5.
2. *Divide the liquefied region into zones of approximately constant SPT resistance and depth.* Because the Olson-Stark model treats residual strength as a function of both SPT resistance and effective stress, depth must also be considered in representing the residual strength of a liquefied zone.
3. *Determine the average $(N_1)_{60}$ value for each zone of liquefied soil.* This may be done using statistical methods when sufficient data are available, and augmented by engineering and geological judgment when data are sparse.
4. *Determine the average initial vertical effective stress in each zone of liquefied soil.* Initial vertical effective stresses for each zone of liquefiable soil are required. In general, calculation of initial vertical effective stress based on a one-dimensional column of soil above the point at which residual strength is being estimated will be sufficient.
5. *Compute the residual strength.* The residual strength (in atm) from the Olson-Stark model (Figure 8.3) can be computed as

$$S_r = \sigma'_{vo} [0.03 + 0.0075(N_1)_{60}] \quad (8.3)$$

where σ'_{vo} is the vertical effective stress (in atm).

6. *Evaluate the potential for pore pressure redistribution effects.* At present, procedures for accurate, quantitative prediction of pore pressure redistribution effects are not available. Experience has shown, however, that pore pressure redistribution can occur when liquefiable soil layers are "capped" by impermeable layers of silt and/or clay. In such cases, residual strengths may be lower than estimated on the basis of *in situ* SPT resistances, so additional conservatism may be in order.

8.4.3 Normalized Strength Model – Idriss and Boulanger

The normalized strength model of Idriss and Boulanger (2007) accounts for the effects of effective stress on the rate of increase of residual strength with SPT resistance. The residual strength can be estimated by using the Idriss and Boulanger model in the following series of steps:

1. *Identify the spatial extent of the soil expected to liquefy.* This can be accomplished by using the procedures described in Chapter 5.
2. *Divide the liquefied region into zones of approximately constant SPT resistance and depth.* Because the Idriss-Boulanger model treats residual strength as a function of both SPT resistance and effective stress, depth must also be considered in representing the residual strength of a liquefied zone.
3. *Determine the average corrected $(N_1)_{60,cs}$ value for each zone of liquefied soil.* This may be done using statistical methods when sufficient data are available, and augmented by engineering and geological judgment when data are sparse. The same fines content correction used in the Idriss (1998) model (Equation 8.1 and table 8.1) should be used.
4. *Determine the average initial vertical effective stress in each zone of liquefied soil.* Initial vertical effective stresses for each zone of liquefiable soil are required. In general, calculation of initial vertical effective stress based on a one-dimensional column of soil above the point at which residual strength is being estimated will be sufficient.

5. *Compute the residual strength.* The residual strength (in atm) from the Idriss-Boulanger model (Figure 8.4) can be computed as

$$\frac{S_r}{\sigma'_{vo}} = \exp \left[\frac{(N_1)_{60,cs}}{16} + \left(\frac{(N_1)_{60,cs} - 16}{21.2} \right)^3 - 3.0 \right] \cdot \left[1 + \exp \left(\frac{(N_1)_{60,cs}}{2.4} - 6.6 \right) \right] \leq \tan \phi' \quad (8.3a)$$

for cases in which the effects of void redistribution are not expected to be significant (i.e., upper curve in figure 8.4), or as

$$\frac{S_r}{\sigma'_{vo}} = \exp \left[\frac{(N_1)_{60,cs}}{16} + \left(\frac{(N_1)_{60,cs} - 16}{21.2} \right)^3 - 3.0 \right] \leq \tan \phi' \quad (8.3b)$$

for cases in which void redistribution is expected to be significant (i.e., lower curve in figure 8.4).

8.4.4 Kramer-Wang Hybrid Model

As part of the current research project, a hybrid model for residual strength was developed. The hybrid model combines elements of both the classical and normalized strength approaches but is not as restricted as either method. Residual strengths can be estimated using the hybrid model in the following series of steps:

1. *Identify the spatial extent of the soil expected to liquefy.* This can be accomplished using the procedures described in Chapter 5.
2. *Divide the liquefied region into zones of approximately constant SPT resistance and constant depth.* Because the Kramer-Wang model treats residual strength as a function of both SPT resistance and effective stress, depth must also be considered in representing the residual strength of a liquefied zone.
3. *Determine the average $(N_1)_{60}$ value for each zone of liquefied soil.* This may be done using statistical methods when sufficient data are available, augmented by engineering and geological judgment when data are sparse.
4. *Determine the average initial vertical effective stress in each zone of liquefied soil.* Initial vertical effective stresses for each zone of liquefiable soil are required. In general, calculation of initial vertical effective stress

based on a one-dimensional column of soil above the point at which residual strength is being estimated will be sufficient.

5. *Compute the residual strength.* The residual strength (in atm) from the hybrid model can be computed as

$$S_r = \exp[-8.444 + 0.109\bar{N} + 5.379\bar{S}^{0.1} - 0.253\sigma_m] \quad (8.4)$$

where \bar{N} = average value of $(N_1)_{60}$, \bar{S} = mean vertical effective stress (in atm), and

$$\sigma_m = \sqrt{1.627 + 0.000796\bar{N}^2 + 0.0194\bar{N} - 0.027\bar{N}\bar{S}^{0.1} - 3.099\bar{S}^{0.1} + 1.635\bar{S}^{0.2}}$$

The hybrid model predicts residual strengths that vary with SPT resistance and vertical effective stress as shown in Figure 8.4.

6. *Evaluate the potential for pore pressure redistribution effects.* At present, procedures for accurate, quantitative prediction of pore pressure redistribution effects are not available. Experience has shown, however, that pore pressure redistribution can occur when liquefiable soil layers are "capped" by impermeable layers of silt and/or clay. In such cases, residual strengths may be lower than estimated on the basis of *in situ* SPT resistances, so additional conservatism may be in order.

8.5 DISCUSSION

Figure 8.5 shows how the Idriss, Olson-Stark, and hybrid models predict back-calculated residual strengths from observed flow slide case histories. The plots indicate that the uncertainty in predicted residual strength is significant. The level of scatter in Figure 8.5 can be seen to be lowest for the hybrid model. For some projects, it may be advisable to perform probabilistic stability analyses when the potential for flow sliding exists, particularly given the high degree of uncertainty in residual strength estimation. A probabilistic version of the Kramer-Wang hybrid model can be expressed as

$$S_r(P) = \exp[\overline{\ln S_r} + \Phi^{-1}(P)\sigma_{\ln S_r}] \quad (8.5)$$

where P is the probability of non-exceedance (i.e., the percentile value), and

$$\overline{\ln S_r} = -8.444 + 0.109\overline{N} + 5.379(\overline{\sigma'_{vo}})^{0.1}$$

$$\sigma_{\ln S_r} = \sqrt{\sigma_m^2 + 0.00073\overline{N}^2 COV_N^2 + 4.935(\overline{S})^{0.2} COV_{\sigma'_{vo}}^2}$$

$$\sigma_m^2 = 1.627 + 0.00073\overline{N}^2 + 0.0194\overline{N} - 0.027\overline{N}\overline{S}^{0.1} - 3.099\overline{S}^{0.1} + 1.621\overline{S}^{0.2}$$

While the median predicted residual strength of a loose $((N_1)_{60} = 10)$ sand at shallow depth $(\sigma'_{vo} = 1 \text{ atm})$ is about 0.11 atm, for example, there is a 10 percent chance that the residual strength is below 0.042 atm and above 0.27 atm.

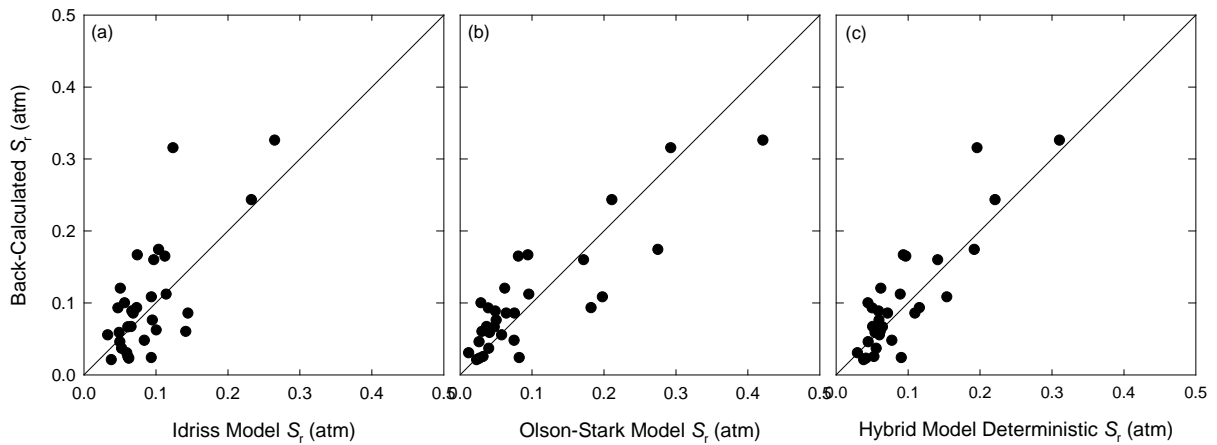


Figure 8.6 Comparison of back-calculated residual strengths with residual strength values predicted by (a) Idriss model, (b) Olson-Stark model, and (c) deterministic hybrid model.

Note that the deterministic model of Equation 8.4 is equivalent to the probabilistic model of Equation 8.5 with $P = 0.4$, $COV_N = 0.3$, and $COV_{\sigma'} = 0.05$; the $P = 0.4$ curve was found to provide a lower boundary to the back-calculated residual strengths for all available, well-documented flow slide case histories. As shown in Figure 8.6, the effects of different levels of uncertainty in SPT resistance and initial vertical effective stress are relatively small in comparison to the substantial uncertainty in available case history data.

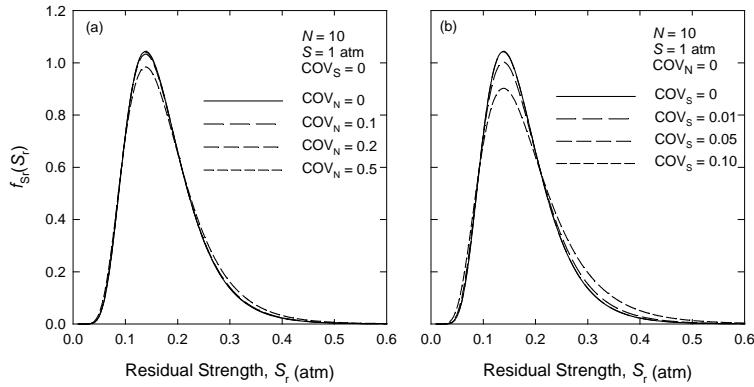


Figure 8.7 Probability density functions for residual strength: (a) different uncertainties in SPT resistance, and (b) different uncertainties in initial vertical effective stress.

8.6 RECOMMENDATIONS

As previously discussed, prediction of residual strength is a very difficult problem. The classical and normalized strength approaches can produce substantially different results under certain conditions, and available data with which to confirm the potential superiority of either are not available. The hybrid model, which predicts observed case history behavior more accurately than either, produces residual strength estimates that fall between those of the classical and normalized strength models.

For design and evaluation purposes, the use of a weighted average of the residual strengths produced by the three models described in Section 8.4 is recommended. The recommended weighting factors are given in Table 8.2.

Table 8.2 Weighting factors for residual strength estimation

Model	Weighting Factor
Idriss	0.2
Olson-Stark	0.2
Idriss-Boulanger	0.2
Hybrid	0.4

8.7 OTHER CONSIDERATIONS

Because the residual strength of liquefied soil is a relatively poorly understood topic, there are a number of factors that are not included in most quantitative residual strength models but that still merit consideration in the evaluation of an appropriate residual strength value for design and hazard evaluation.

8.7.1 Pore Pressure Redistribution

The development of excess porewater pressure in liquefiable soils typically produces hydraulic gradients that drive porewater flow both during and after earthquake shaking. Such flow is accompanied by redistribution of porewater pressures and, hence, changes in effective stress. When this occurs, the density of the soil will change as the effective stress changes. At some sites, soil layers in which high porewater pressures are likely to be generated are overlain by low-permeability soils. Of particular concern is the case in which porewater pressures migrate upward, thereby decreasing the effective stress, and consequently the density, of the soil just below the low-permeability layer.

Because residual strength is sensitive to soil density, the reduction in density can cause the available residual strength of the soil to drop below the shear stress required for static equilibrium and lead to flow slide deformations. The degree to which this phenomenon can occur depends on the density, thickness, and permeability of the zone of high porewater pressure, as well as on its geometric relationship to zones that are critical from a static stability standpoint; relatively thick zones of loose soil with high porewater pressures can generate substantial volumes of flow that are more likely to produce density changes.

Formal procedures for evaluating reductions in residual strength due to pore pressure redistribution are not available at this time. As a result, an element of engineering judgment is required to account for the potential effects of pore pressure redistribution. It is recommended that such judgment should consider the potential for significant density change, estimate the effects of that density change on the apparent SPT resistance of soil in stability-critical regions, and use a modified SPT resistance with the procedures presented in this chapter to estimate the available residual strength.

8.7.2 High SPT Values

Available case history data contain no observations of flow slides in soils with corrected clean sand SPT resistances of greater than about 14 to 16. Furthermore, laboratory test data suggest that undrained residual strength increases rapidly with increasing density beyond levels corresponding to that range of SPT resistance. The Idriss, Idriss-Boulanger, and hybrid models all predict increasing rates of residual

strength with increasing SPT resistance; the Olson-Stark model does not. The extent to which any of the residual strength models can be reliably extrapolated to high SPT resistances is not established; however, it appears that the recommended weighted average of the four models can be used to provide guidance for residual strength estimation for corrected SPT values of up to 20 blows/ft. Residual strength values greater than those predicted by these models for SPT values of 20 blows/ft may be unconservative, so it is recommended that residual strengths be capped at the levels corresponding to corrected SPT values of 20 blows/foot unless special investigations provide justification for the use of higher strengths.

8.7.3 Consideration of Uncertainty

Although the Idriss, Olson-Stark, and Idriss-Boulanger models provide deterministic equations for estimating residual strength, they should be recognized as approximations to sets of scattered data. The hybrid model quantifies the uncertainty in residual strength and allows estimation of a probability distribution for residual strength. A specific probability level for design or evaluation must be selected by the designer with due consideration of the risk and consequences of a flow slide failure. Rather than selecting a particular probability level for design, however, it would be preferable to perform a probabilistic slope stability analysis in which a mean factor of safety is computed as a weighted average for a range of residual strengths each weighted by its respective probabilities; in this way, the mean factor of safety reflects the entire range of residual strengths expected for the soil in question.

Another factor that should be considered in flow slide stability analyses is the spatial variability of *in situ* soil density. If spatial variability is not random and/or isotropic, there may be some potential for looser (hence, lower residual strength) zones to be oriented in an unfavorable configuration with respect to slope stability. While spatial variability and the presence of loose or weak seams is a consideration in all stability analyses, it is particularly important in flow slide stability evaluations because of the high sensitivity of residual strength to soil density.

8.8 EXAMPLES

The residual strength calculations are easily illustrated for a hypothetical soil profile such as that shown in Figure 8.7. In this profile, the residual strength increases linearly with depth from a value of 5 blows/ft at 2-m depth to a value of 25 blows/ft at 12-m depth.

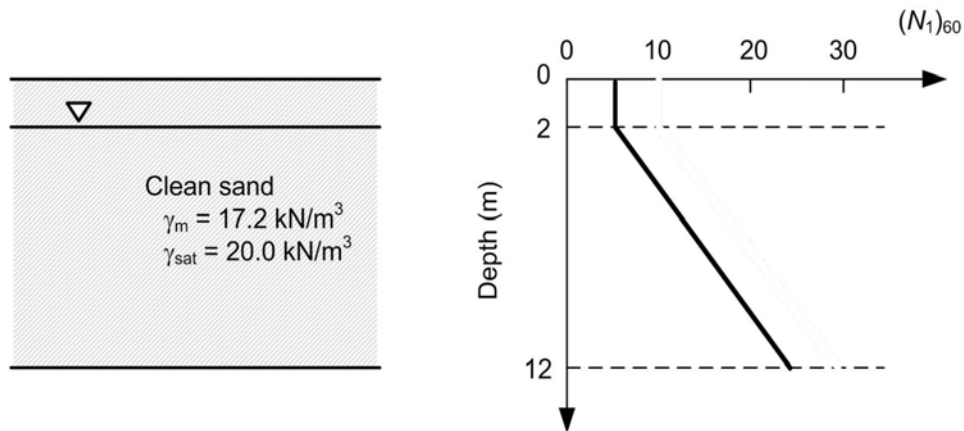


Figure 8.8 Hypothetical soil profile for residual strength calculation.

In WSliq, the residual strength calculations are easily performed for any of a series of residual strength models. Using the WSDOT recommended option, WSliq computes the variation of residual strength with depth for the Kramer-Wang hybrid, Idriss, and Olson-Stark models, and then uses the weighting factors in Table 8.2 to compute a recommended residual strength profile (Figure 8.8).

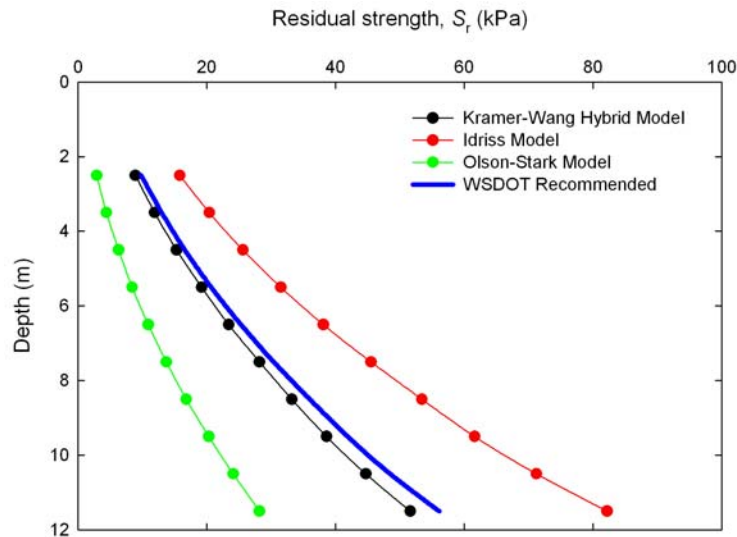


Figure 8.9 Variation of computed residual strength with depth for hypothetical soil profile.

Chapter 9

Discussion

9.1 INTRODUCTION

This report has described the results of an extensive research investigation conducted over a period of three biennia at the University of Washington. The intent of the project was to provide WSDOT with improved procedures and tools for evaluation of liquefaction hazards in Washington State. This goal has remained constant over the past six years, even as individual elements of the work has changed in scope and direction in response to various developments.

One development that strongly influenced the direction of the investigation was the intention of AASHTO to move toward basing design requirements upon ground motions with a 2% probability of exceedance in a 50-yr period, which is equivalent to a 2,475-yr return period. This effort was intended to raise design requirements in areas of the central and eastern United States where existing design requirements were perceived as being too low. The effects of this change, however, would have been considerably greater in Washington than in California, and greater yet in other parts of the country such as Memphis and Charleston. The implications of the change were also significantly greater for geotechnical hazards, particularly liquefaction problems, than for structural hazards.

Because of the magnitude-dependence of common liquefaction hazard evaluation procedures, 2,475-yr based procedures would have caused liquefaction hazards to be based on very large ($M_w > 8$) magnitude earthquakes in significant portions of western Washington, and magnitudes of nearly 9 along the Pacific coast. Criteria based on such high magnitude events, when combined with the high peak accelerations expected for 2,475-yr events, combined to require high levels of expensive soil improvement at many sites with liquefiable soils – levels much higher than required in much more seismically active areas such as California.

In response to the consequences of this potential change in policy, a portion of the University of Washington research was shifted toward development of methods that could ensure consistent and predictable levels of performance, i.e., methods that would consider the entire range of ground motions that could occur at any location in Washington State instead of just one, rarely occurring level. This shift occurred as the Pacific Earthquake Engineering Research (PEER) Center, with which the Principal Investigator for the UW project was closely associated, was developing a framework for performance-based earthquake engineering.

The PEER framework was capable, conceptually, of probabilistically considering all ranges of ground motions and all ranges of response to develop a performance-based model for liquefaction hazards. The research supported by WSDOT and described in this report brought this conceptual capability to reality for the first time for three separate problems – liquefaction potential, lateral spreading, and post-liquefaction settlement. The WSliq computer program that accompanies this report allows these advanced, performance-based evaluations, which involve millions of technical analyses at a given location, to be performed by practicing engineers.

The results of the analyses can be used to design for specified performance levels with performance based on the quantities that most strongly influence performance with respect to liquefaction – typically, permanent deformations. They account for all possible earthquake locations, all possible earthquake magnitudes, all possible levels of ground shaking for all of the locations and magnitudes, and all possible responses given all of the levels of ground motions. They recognize the uncertainties that exist in each of these quantities, and in the models used to predict performance, and characterize those uncertainties to the greatest degree possible in contemporary earthquake engineering practice. They then integrate the various measures of performance over all of the uncertain variables and models to produce an objective, probabilistic estimate of anticipated performance.

9.2 BENEFITS

It is anticipated that the results of this research will be implemented in two stages. The first, which can be done immediately, is to use the multiple-scenario options

presented for each of the response analyses – liquefaction potential, lateral spreading, and post-liquefaction settlement – described in this report. By using the multiple-scenario analyses, users will eliminate the issue of which magnitude to select that is inherent in the single-scenario analyses commonly used in contemporary practice. The multiple-scenario analyses use all magnitudes, weighted according to their contribution to the peak acceleration at the return period of interest, to make a more stable, accurate prediction of response. The WSliq program makes these analyses very easy to perform – easier, in fact, than performing conventional single-scenario analyses.

The second stage of implementation, which should begin hand-in-hand with the first stage, is to gain experience with performance-based hazard analyses, and to develop a sense of what actual return periods are associated with various performance levels in current analyses. By completing performance-based analyses for all cases in which multiple-scenario analyses are completed, the return periods for various performance levels can be computed at locations across the state. A database of these return periods should form the basis for determination of improved, return period-based, design criteria. The use of such criteria will provide more uniform and consistent levels of safety in structures across the entire state, and will allow WSDOT to optimize the use of its resources to achieve the greatest overall improvements in seismic safety.

9.3 FINAL COMMENTS

The WSliq program that accompanies this report is a new and unique tool for evaluation of liquefaction hazards. It automates procedures that engineers have historically performed by hand or using spreadsheet calculations. It was designed to perform the millions of individual liquefaction hazard analyses that are required to estimate the return periods of response parameters such as factor of safety, required penetration resistance, lateral spreading displacement, or post-liquefaction settlement, and it makes those analyses very easy for the engineer to perform.

The program has been designed to be modular in architecture. As new information about fault location and activity is developed, and as new attenuation relationships for the estimation of ground shaking are developed, ground motion hazard analyses such as those performed by the U.S. Geological Survey (USGS), will need to be

repeated – the USGS updates its hazard analyses on a regular basis. When this occurs, the hazard database that WSliq uses will also need to be updated, but the program itself will not require modification; as new response models (i.e., models for estimation of liquefaction potential, lateral spreading displacement, and post-liquefaction settlement) become available, updating of the WSliq code itself should be considered. WSliq provides a utility (Appendix I) for expanding or updating the current ground motion hazard database.

The ease of use of the WSliq program should not be taken to imply that liquefaction hazard analyses are simple or easy, or that they should be performed by engineers who are not familiar with liquefaction and its effects. The evaluation of liquefaction hazards requires geologic interpretation, the acquisition and examination of subsurface soil samples, careful attention to penetration resistance and other field testing procedures, and understanding of the effects of liquefied soil behavior on structures and foundations. The program is intended to simplify the computational parts of liquefaction hazard evaluation for experienced engineers, not to turn liquefaction hazard analysis into a “black box” whose handle can be reliably turned by inexperienced, unsupervised staff.

The developers of the WSliq program look forward to working with WSDOT engineers to maintain, update, and expand the scope of the program, and to assist in the implementation of performance-based design and evaluation procedures into WSDOT practice.

ACKNOWLEDGMENTS

The research described in this report and implemented in the accompanying computer program was supported over an extended period of time by the Washington State Department of Transportation. The author would like to thank the Department, particularly Tony Allen of the Materials Laboratory and Keith Anderson and Kim Willoughby of the Research Office, for their years of support of this research.

Many University of Washington graduate students, some of whom were funded directly by the project and others who worked on unfunded or related projects, contributed to the research described in this report. These students include Ph.D. students Allen Jones, David Baska, C.H. Wang, Roy Mayfield, and Yi-Min Huang, and Masters students Fujen Ho, Brian Bennetts, Kevin Franke, and Aaron Hartvigsen.

Some aspects of the work described in this report benefited from related research supported by the Pacific Earthquake Engineering Research (PEER) Center, the U.S. Geological Survey, and the John R. Kiely Professorship at the University of Washington. The author also developed a number of the concepts that underpin this work during a 2003 sabbatical stay in the International Centre for Geohazards at the Norwegian Geotechnical Institute where he was supported as a senior research scientist. All of this support is gratefully acknowledged.

REFERENCES

- AASHTO, 2004, *LRFD Bridge Design Specifications*, American Association of State Highway and Transportation Officials, Third Edition, Washington, D.C., USA.
- Allen, T. M., 2005, Development of Geotechnical Resistance Factors and Downdrag Load Factors for LRFD Foundation Strength Limit State Design, *Publication No. FHWA-NHI-05-052*, Federal Highway Administration, Washington, DC, 41 pp.
- Arango, I., Ostadan, F., Cameron, J., Wu, C.L., and Chang, C.Y. (2004). "Liquefaction probability of the BART Transbay Tube backfill," Proceedings of the 11th International Conference on Soil Dynamics and Earthquake Engineering and 3rd International Conference on Earthquake Geotechnical Engineering, Vol. I, pp. 456-462.
- Baecher, G.B. and Christian, J.T. (2003). *Reliability and Statistics in Geotechnical Engineering*, John Wiley and Sons, New York, 620 pp.
- Bartlett, S.F. and Youd, T.L. (1992). "Empirical analysis of horizontal ground displacement generated by liquefaction-induced lateral spread," *Technical Report NCEER-92-0021*, National Center for Earthquake Engineering Research, Buffalo, New York.
- Baska, D.A. (2002). "An analytical/empirical model for prediction of lateral spreading displacements," *Ph.D. Dissertation*, University of Washington, Seattle, Washington, 539 pp.
- Boulanger, R. W., and Idriss, I. M. (2004). Evaluating the potential for liquefaction or cyclic failure of silts and clays. *Report UCD/CGM-04/01*, Center for Geotechnical Modeling, University of California, Davis, CA, 130 pp.
- Boulanger, R. W., and Idriss, I. M. (2004). Evaluating the potential for liquefaction or cyclic failure of silts and clays. *Report UCD/CGM-04/01*, Center for Geotechnical Modeling, University of California, Davis, CA, 130 pp.
- Boulanger, R. W., and Idriss, I. M. (2005). "Evaluating cyclic failure in silts and clays." Proceedings, *Geotechnical Earthquake Engineering Satellite Conference on Performance Based Design in Earthquake Geotechnical Engineering: Concepts and Research*. Prepared by TC4 Committee of ICSMGE, Japanese Geotechnical Society, Tokyo, 78-86.
- Bray, J.D. and Sancio, R.B. (2006). "Assessment of the Liquefaction Susceptibility of Fine-Grained Soils," *Journal of Geotechnical and Geoenvironmental Engineering*, Vol. 132, No. 9, pp. 1165-1177.
- Castro, G. (1969). "Liquefaction of sands," *Harvard Soil Mechanics Series 87*, Harvard University, Cambridge, MA.
- Cetin, K.O. (2000). "Reliability-based assessment of seismic soil liquefaction initiation hazard," *Ph.D. Dissertation*, University of California, Berkeley, 602 pp.

- Cetin, K.O., Der Kiureghian, A., and Seed, R.B. (2002). "Probabilistic models for the initiation of soil liquefaction," *Structural Safety*, Vol. 24, 67-82.
- Cetin, K.O., Seed, R.B., Der Kiureghian, A., Tokimatsu, K., Harder, L.F., Kayen, R.E., and Moss, R.E.S. (2004). "Standard penetration test-based probabilistic and deterministic assessment of seismic soil liquefaction potential," *Journal of Geotechnical and Geoenvironmental Engineering*, ASCE, 130(12), 1314-1340.
- Cornell, C.A. (1968). "Engineering seismic risk analysis," *Bulletin of the Seismological Society of America*, 58(5), 1583-1606.
- Cornell, C.A. and Krawinkler, H. (2000). "Progress and challenges in seismic performance assessment," *PEER News*, April, 1-3.
- Deierlein, G.G., Krawinkler, H., and Cornell, C.A. (2003). "A framework for performance-based earthquake engineering," *Proceedings, 2003 Pacific Conference on Earthquake Engineering*.
- Faris, A., Seed, R.B., Kayen, R.E., and Wu, J. (2006). "A semi-empirical model for the estimation of maximum horizontal displacement due to liquefaction-induced lateral spreading," *Proceedings, 8th U.S. National Conference on Earthquake Engineering*, in press.
- Franke, K.W. (2005). "Development of a Performance-Based Model for Prediction of Lateral Spreading Displacements," *Masters Thesis*, University of Washington, Seattle, Washington, 250 pp.
- Harder, L. F., Jr., and Seed, H. B. (1986). "Determination of Penetration Resistance for Coarse-Grained Soils Using the Becker Hammer Drill," *Report No. UCB/EERC-86/06*, Earthquake Engineering Research Center, College of Engineering, University of California, Berkeley.
- Huang, Y.-M. (2008). "Performance-Based Design and Evaluation for Liquefaction-Related Seismic Hazards," Ph.D. Dissertation, University of Washington, 376 pp.
- Hwang, J.H., Chen, C.H., and Juang, C.H. (2005). "Liquefaction hazard: a fully probabilistic method," in *Proceedings of the Sessions of the Geo-Frontiers 2005 Congress*, Earthquake Engineering and Soil Dynamics, R.W. Boulanger et al. eds, ASCE, Paper no. 22.
- Idriss, I. M. (1999). "An update to the Seed-Idriss simplified procedure for evaluating liquefaction potential." *Proceedings*, TRB Workshop on New Approaches to Liquefaction, January, Publication No. FHWA-RD-99-165, Federal Highway Administration.
- Idriss, I.M. and Boulanger, R.W. (2004). "Semi empirical procedures for evaluating liquefaction potential during earthquakes," *Proceedings of the 11th International Conference on Soil Dynamics and Earthquake Engineering and 3rd International Conference on Earthquake Geotechnical Engineering*, Vol. I, 32-56.
- Idriss, I.M. and Boulanger, R.W. (2007). "SPT and CPT-based relationships for the residual shear strength of liquefied soils," *Proceedings, 4th International Conference*

- on Earthquake Geotechnical Engineering, K.D. Pitilakis, ed., Springer, Dordrecht, The Netherlands, 1-22.
- Idriss, I.M. and Boulanger, R.W. (2008). *Soil liquefaction during earthquakes*, EERI Monograph 12, Earthquake Engineering Research Institute, Oakland, California, 262 pp
- Ishihara, K. and Yoshimine, M. (1992). "Evaluation of settlements in sand deposits following liquefaction during earthquakes," *Soils and Foundations*, Vol. 32, No. 1, pp. 173-188.
- Kramer, S.L. (1996). *Geotechnical Earthquake Engineering*, Prentice-Hall, Englewood Cliffs, New Jersey, 653 pp.
- Kramer, S.L., Franke, K.W., Huang, Y.-M., and Baska, D.A. (2007). "Performance-Based Evaluation of Lateral Spreading Displacement," Proceedings, 4th International Conference on Earthquake Geotechnical Engineering, International Society for Soil Mechanics and Geotechnical Engineering, Thessaloniki, Greece.
- Kramer, S.L. and Baska, D.A. (2007). "Estimation of permanent displacements due to lateral spreading," *Journal of Geotechnical and Geoenvironmental Engineering*, ASCE, in review.
- Kramer, S.L. and Wang, C.-H. (2007). "Estimation of the residual strength of liquefied soil, in preparation.
- Krawinkler, H. (2002). "A general approach to seismic performance assessment," *Proceedings*, International Conference on Advances and New Challenges in Earthquake Engineering Research, ICANCEER, 2002, Hong Kong.
- Liao, S.S.C., Veneziano, D., and Whitman, R.V. (1988). "Regression models for evaluating liquefaction probability," *Journal of Geotechnical Engineering*, ASCE, 114(4), 389-409.
- Lidke, D.J., Johnson, S.Y., McCrory, P.A., Personius, S.F., Nelson, A.R., Dart, R.L., Bradley, L., Haller, K.M., and Machette, M.N. (2003). "Map and data for Quaternary faults and folds in Washington State," Open File Report 03-428, U.S. Geological Survey, 16 pp.
- Marrone, J., Ostadan, F., Youngs, R., and Litehiser, J. (2003). "Probabilistic liquefaction hazard evaluation: method and application," in *Transactions of the 17th International Conference on Structural Mechanics in Reactor Technology (SMiRT 17)*, Prague, Czech Republic, Paper no. M02-1.
- Martin, G.R. and Lew, M. eds. (1999). "Recommended Procedures for Implementation of DMG Special Publication 117 – Guidelines for Analyzing and Mitigating Liquefaction Hazards in California," Southern California Earthquake Center, Los Angeles, 63 pp.
- McGuire, R.K. (1995). "Probabilistic seismic hazard analysis and design earthquakes: Closing the loop," *Bulletin of the Seismological Society of America*, 85(5), 1275-1284.

- McGuire, R.K. (2004). *Seismic Hazard and Risk Analysis*, Earthquake Engineering Research Institute, Oakland, California, 120 pp.
- Moss, R.E.S., Seed, R.B., Kayen, R.E., Stewart, J.P., der Kiureghian, A., and Cetin, K.O. (2006). "CPT-Based Probabilistic and Deterministic Assessment of in Situ Seismic Soil Liquefaction Potential," *Journal of Geotechnical and Geoenvironmental Engineering*, Vol. 132, No. 8, pp. 1032-1051
- National Center for Earthquake Engineering Research (1997). *Proceedings of the NCEER workshop on evaluation of liquefaction resistance of soils*, T.L. Youd and I.M. Idriss, editors, Technical Report NCEER, 97-022.
- Olson, S. M., and Stark, T. D. (2002). "Liquefied strength ratio from liquefaction flow case histories." *Canadian Geotechnical Journal*, Vol. 39, pp. 629-647. [Olsen spelled Olson on pages 118, 122, and elsewhere]
- Phoon, K and Kulhawy, F. H. (1999a). Characterization of geotechnical variability. *Canadian Geotechnical Journal*, 36(4):612–624.
- Phoon, K and Kulhawy, F. H. (1999b). Evaluation of geotechnical property variability. *Canadian Geotechnical Journal*, 36(4):625–639.
- Poulos, S.J., Castro G., and France, J.W. (1985). "Liquefaction evaluation procedure," *Journal of Geotechnical Engineering*, ASCE, Vol. 111, No. 6, pp. 772-792.
- Seed, H.B. (1979). "Soil liquefaction and cyclic mobility evaluation for level ground during earthquakes," *Journal of Geotechnical Engineering*, ASCE, 105(2), 201-255.
- Seed, H.B. (1986). "Design problems in soil liquefaction," *Journal of Geotechnical Engineering*, ASCE, Vol. 113, No. 8, pp. 827-845.
- Seed, H.B. and Idriss, I.M. (1971). "Simplified procedure for evaluating soil liquefaction potential," *Journal of the Soil Mechanics and Foundations Division* , ASCE, 107(SM9), 1249-1274.
- Seed, H.B. and Idris, I.M, (1982). *Ground Motions and Soil Liquefaction During Earthquakes*," Earthquake Engineering Research Institute Monograph .
- Seed, H.B., Lee, K.L., Idriss, I.M., and Makdisi, F. (1973). "Analysis of the slides in the San Fernando dams during the earthquake of Feb. 9, 1971," *Report No. EERC 73-2*, Earthquake Engineering Research Center, University of California, Berkeley, 150 pp.
- Seed, H.B., Lee, K.L., Idriss, I.M., and Makdisi, F. (1975). "The slides in the San Fernando dams during the earthquake of Feb. 9, 1971," *Journal of the Geotechnical Engineering Division*, ASCE, 101(7), 651-688.
- Seed, R. B., Cetin, K. O., Moss, R. E. S., Kammerer, A., Wu, J., Pestana, J., Riemer, M., Sancio, R. B., Bray, J. D., Kayen, R. E., and Faris, A. (2003). "Recent advances in soil liquefaction engineering: A unified and consistent framework." Keynote presentation, 26th Annual ASCE Los Angeles Geotechnical Spring Seminar, Long Beach, CA.
- Seed, R.B. and Harder, L.F. (1990). "SPT-based analysis of cyclic pore pressure generation and undrained residual strength," *Proceedings*, H. Bolton Seed Memorial

- Symposium, University of California, Berkeley, Vol. 2, J.M. Duncan ed., pp. 351-376.
- Seed, H.B., Tokimatsu, K., Harder, L.F., and Chung, R. M., 1985, "Influence of SPT Procedures in Soil Liquefaction Resistance Evaluations," *Journal of the Geotechnical Engineering Division*, ASCE, Vol. 111, No. 12.
- Shamoto, Y., Zhang, J.-M., and Tokimatsu, K. (1998). "Methods for evaluating residual post-liquefaction ground settlement and horizontal displacement," *Soils and Foundations*, Special Issue No. 2, 69-83.
- Silver, N.L. and Seed, H.B. (1971). "Volume changes in sands during cyclic loading," *Journal of the Soil Mechanics and Foundations Division*, ASCE, Vol 97, No. SM9, pp. 1171-1180.
- Stark, T.D. and Mesri, G. (1992). "Undrained shear strength of sands for stability analysis," *Journal of Geotechnical Engineering*, ASCE, Vol. 118, No. 11, pp. 1727-1747.
- Stewart, J.P. and Whang, D.H. (2003). "Simplified procedure to estimate ground settlement from seismic compression in compacted soils," *Proc. 2003 Pacific Conference on Earthquake Engineering*, Christchurch, New Zealand, Paper 46.
- Stewart, J.P., Liu, A.H., and Choi, Y. (2003). Amplification factors for spectral acceleration in tectonically active regions," *Bulletin of the Seismological Society of America*, 93(1), 332-352.
- Sy, A. and Campanella, R.G. (1994). "Becker and standard penetration tests (BPT-SPT) correlations with consideration of casing friction," *Canadian Geotechnical Journal*, Vol. 31, No. 3, pp. 343-356.
- Sy, A., Campanella, R.G. and Stewart, R.A. (1995). "BPT-SPT correlations for evaluations of liquefaction resistance in gravelly soils," in Evans, M.D. and Fragaszy, R.J., editors, *Static and Dynamic Properties of Gravelly Soils: American Society of Civil Engineers Geotechnical Special Publication no. 56*, p. 1-19.
- Tokimatsu, K. and Seed, H.B. (1987). "Evaluation of settlements in sand due to earthquake shaking," *Journal of Geotechnical Engineering*, ASCE, Vol. 113, No. 8, pp. 861-878.
- Tokimatsu, K. and Seed, H.B. (1987). "Evaluation of settlements in sand due to earthquake shaking," *Journal of Geotechnical Engineering*, ASCE, Vol. 113, No. 8, pp. 861-878. [9]
- Toprak, S., Holzer, T.L., Bennett, M.J., and Tinsley, J.C. III. (1999). "CPT- and SPT-based probabilistic assessment of liquefaction," *Proc., 7th U.S.-Japan Workshop on Earthquake Resistant Design of Lifeline Facilities and Countermeasures Against Liquefaction*, Seattle, Multidisciplinary Center for Earthquake Engineering Research, Buffalo, NY, 69-86.
- Whang, D.H., Moyneur, M.S., Duku, P., and Stewart, J.P. (2005). "Seismic compression behavior of nonplastic silty sands," in *Proceedings of an International Symposium on Advanced Experimental Unsaturated Soil Mechanics*, A. Tarantino, E. Romero, and Y.J. Cui (eds.), Trento, Italy, June 27-29, A.A. Balkema Publishers, pp 257-263.

- Whang, D.H., Stewart, J.P., and Bray, J.D. (2004). "Effect of compaction conditions on the seismic compression of compacted fill soils," *Geotechnical Testing Journal*, ASTM, 27 (4), 371-379.
- Wu, J. and Seed, R.B. (2004). "Estimation of liquefaction-induced ground settlement (case studies)," *Proceedings, Fifth International Conference on Case Histories in Geotechnical Engineering*, New York, pp. 1-8.
- Yegian, M.Y. and Whitman, R.V. (1978). "Risk analysis for ground failure by liquefaction," *Journal of the Geotechnical Engineering Division*, ASCE, 104(GT7), 907-905.
- Youd, T.L., (1998). *Screening Guide for Rapid Assessment of Liquefaction Hazard at Highway Bridge Sites*, Technical Report MCEER-98-0005, Multidisciplinary Center for Earthquake Engineering Research, Buffalo New York.
- Youd, T.L. and Noble, S.K. (1997). "Liquefaction criteria based on statistical and probabilistic analyses," *Proceedings of the NCEER Workshop on Evaluation of Liquefaction Resistance of Soils*, National Center for Earthquake Engineering Research, Buffalo, NY, 201-205.
- Youd, T.L. and Perkins, D.M. (1987). "Mapping of Liquefaction Severity Index," *Journal of Geotechnical Engineering*, ASCE, Vol. 113, No. 11, pp. 1374-1392.
- Youd, T.L. et al. (2001). "Liquefaction resistance of soils: Summary report from the 1996 NCEER and 1998 NCEER/NSF workshops on evaluation of liquefaction resistance of soils," *Journal of Geotechnical and Geoenvironmental Engineering*, ASCE, 127(10), 817-833.
- Youd, T.L., Hansen, C.M., and Bartlett, S.F. (2002). "Revised multilinear regression equations for prediction of lateral spread displacement", *Journal of Geotechnical and Geoenvironmental Engineering*, ASCE, 128(12), 1007-1017.
- Zhang, G., Robertson, P.K., and Brachman, R.W.I. (2004). "Estimating liquefaction-induced lateral displacements using the standard penetration test or cone penetration test," *Journal of Geotechnical and Geoenvironmental Engineering*, ASCE, 130(8), 861-871.

Appendix A

SPT Corrections

The standard penetration test, which is described by ASTM Standard D1586-99, is very commonly used for evaluation of liquefaction resistance. The need to compare standard penetration test (SPT) resistances from investigations of field case histories in different countries, where SPT equipment and procedures differ, has led to the development of a series of SPT corrections. By applying these corrections to measured SPT data, corrected SPT values that correspond to the values inferred in liquefaction case history interpretations can be obtained. The use of properly corrected SPT values will maximize the reliability of liquefaction resistance estimates.

The SPT corrections account for deviations from standard values of effective vertical stress, drilling rod length, the presence or absence of spacers, borehole diameter, and energy ratio. When sampling takes place with standard values for these parameters, no corrections are required. Of these, the energy ratio is frequently influential; it is recommended that drill rigs be calibrated for energy periodically so that the actual delivered energy is known with confidence.

Assuming that the measured SPT resistance, N_m , is available, the corrected SPT resistance can be computed as the product of the measured resistance and a series of correction factors, i.e., as

$$(N_1)_{60} = N_m \cdot C_N \cdot C_R \cdot C_S \cdot C_B \cdot C_E \quad (\text{A.1})$$

where the correction factors are as described in Table A.1.

Table A.1. SPT equipment/procedure correction factors

Factor	Correction	Comments								
C_N	$C_N = \sqrt{1/\sigma'_{vo}}$ where σ'_{vo} is the vertical effective stress at depth of SPT test in atm	Liao and Whitman (1988)								
C_R	<p>The graph shows the correction factor C_R as a function of rod length in meters. The x-axis represents C_R with values 0.7, 0.8, 0.9, and 1.0. The y-axis represents Rod Length (m) with values from 0 to 30 in increments of 5. A solid curve starts at approximately (0.75, 3) and increases towards $C_R = 1.0$ as rod length increases, reaching a value of 1.0 at approximately 15 meters and remaining constant thereafter. A vertical dashed line is drawn at $C_R = 1.0$.</p>	Rod length is measured from point of hammer impact to tip of sampler. NCEER (1997) Youd et al. (2001) Seed et al. (2003)								
C_S	$C_S = 1 + (N_1)_{60}/100$ with limits of $1.10 \leq C_S \leq 1.30$	For samplers with space for interior liners used without the liners in place Youd et al. (2001) Seed et al. (2003)								
C_B	<table border="0" style="width: 100%;"> <tr> <td style="text-align: center;"><u>Borehole diameter</u></td> <td style="text-align: center;"><u>C_B</u></td> </tr> <tr> <td style="text-align: center;">65-115 mm (2.7-4.5 in)</td> <td style="text-align: center;">1.00</td> </tr> <tr> <td style="text-align: center;">150 mm (6 in)</td> <td style="text-align: center;">1.05</td> </tr> <tr> <td style="text-align: center;">200 mm (8 in)</td> <td style="text-align: center;">1.15</td> </tr> </table>	<u>Borehole diameter</u>	<u>C_B</u>	65-115 mm (2.7-4.5 in)	1.00	150 mm (6 in)	1.05	200 mm (8 in)	1.15	Youd et al. (2001) Seed et al. (2003)
<u>Borehole diameter</u>	<u>C_B</u>									
65-115 mm (2.7-4.5 in)	1.00									
150 mm (6 in)	1.05									
200 mm (8 in)	1.15									
C_E	$C_E = E_R/60$ where E_R = fraction of theoretical impact energy expressed in percent	Best approach is to use direct energy measurements during sampling, otherwise use calibrated hammer (preferably with mechanical release system). If necessary, E_R can be approximately estimated from Table A.2.								

Table A.2. Procedures for Estimating SPT Energy Correction Factor

Equipment	Approximate E_R	Approximate C_E	Comments
Safety hammer	40 – 75%	0.7 to 1.2	Rope and cathead – rope not wet or excessively worn, two turns of rope around cathead, normal release
Donut hammer	30 – 60%	0.5 to 1.0	Rope and cathead – rope not wet or excessively worn, two turns of rope around cathead, normal release
Donut hammer	70 – 85%	0.5 to 1.0	Rope and cathead – with Japanese “throw” release
Automatic trip hammer (safety or donut)	50 – 80%	0.8 to 1.4	
All	-	-	For poor quality equipment and/or workmanship, further adjustments may be required

REFERENCES

- Liao, S.S.C., Veneziano, D., and Whitman, R.V. (1988). “Regression models for evaluating liquefaction probability,” *Journal of Geotechnical Engineering*, ASCE, 114(4), 389-409.
- National Center for Earthquake Engineering Research (1997). *Proceedings of the NCEER workshop on evaluation of liquefaction resistance of soils*, T.L. Youd and I.M. Idriss, editors, Technical Report NCEER, 97-022.
- Seed, R. B., Cetin, K. O., Moss, R. E. S., Kammerer, A., Wu, J., Pestana, J., Riemer, M., Sancio, R. B., Bray, J. D., Kayen, R. E., and Faris, A. (2003). "Recent advances in soil liquefaction engineering: A unified and consistent framework." Keynote presentation, 26th Annual ASCE Los Angeles Geotechnical Spring Seminar, Long Beach, CA.
- Youd, T.L. et al. (2001). “Liquefaction resistance of soils: Summary report from the 1996 NCEER and 1998 NCEER/NSF workshops on evaluation of liquefaction resistance of soils,” *Journal of Geotechnical and Geoenvironmental Engineering*, ASCE, 127(10), 817-833.

Appendix B

Performance-Based Earthquake Engineering

Performance-based earthquake engineering (PBEE) refers to an emerging paradigm in which the “performance” of a system of interest can be quantified and predicted on a discrete or continuous basis. The notion of performance means different things to different stakeholders, and an important goal of PBEE is to allow performance to be expressed using terms and quantities that are of interest and meaning to a wide range of stakeholders.

Implicit in the development of PBEE is the idea that performance can be quantified and predicted with accuracy sufficient to allow decisions regarding design, repair, and replacement to be made with confidence. Continuing developments in the field of earthquake engineering are providing engineers with the tools necessary to make such predictions. The full development of PBEE will allow performance to be expressed in terms of “risk” i.e., in terms that reflect both the direct and indirect losses associated with the occurrence of earthquakes. Such losses can be expressed in terms of casualties, economic losses, and lost time.

PEER FRAMEWORK

PBEE is generally formulated in a probabilistic framework to evaluate the risk associated with earthquake hazards at a particular site. The term “risk” is used to denote loss, which can be expressed in terms of cost, fatalities, or other measures. The term “hazard” is used to describe levels of ground shaking, system response, and/or physical damage, but has no specific connotation of loss. Minimizing the uncertainty in hazard and risk estimates requires minimizing the uncertainties in the variables and the relationships between the variables that go into the calculation of hazard and risk. If we limit ourselves to hazards associated with liquefaction, we can consider uncertainties in the level of shaking and uncertainties in the response of the soil deposit given various levels of shaking. Obviously, we would like to be able to accurately predict (a) the level of shaking accurately and (b) the response of a liquefiable soil deposit, given that level of shaking.

The PBEE framework being developed by the Pacific Earthquake Engineering Research Center (PEER) computes risk as a function of ground shaking through the use of several intermediate variables. The ground motion is characterized by an *Intensity Measure*, IM , which could be any one of a number of ground motion parameters (e.g., PGA , Arias intensity, I_a , etc.). The effects of the IM on a system of interest are expressed in terms that make sense to engineers in the form of *Engineering Demand Parameters*, or $EDPs$ (e.g., excess pore pressure, settlement, etc.). The physical effects associated with the $EDPs$ are expressed in terms of *Damage Measures*, or DMs (e.g., settlement-induced crack width). Finally, the risk associated with the DM is expressed in a form that is useful to decision-makers by means of *Decision Variables*, DV (e.g., repair cost). The mean annual rate of exceedance of various DV levels, λ_{DV} , can be expressed in terms of the other variables as

$$\lambda_{DV} = \sum_{k=1}^{N_{DM}} \sum_{j=1}^{N_{EDP}} \sum_{i=1}^{N_{IM}} P[DV | DM_k] P[DM_k | EDP_j] P[EDP_j | IM_i] \Delta \lambda_{IMi} \quad (B.1)$$

where $P[a|b]$ describes the probability of exceeding a given b , and where N_{DM} , N_{EDP} , and N_{IM} are the number of increments of DM , EDP , and IM , respectively; accuracy increases with increasing number of increments.

The PEER framework has the important benefit of being modular. The framing equation (Equation B.1) can be broken down into a series of components, e.g.,

$$\lambda_{EDP}(edp) = \sum_{i=1}^{N_{IM}} P[EDP > edp | IM = im_i] \Delta \lambda_{IMi} \quad (B.2a)$$

$$\lambda_{DM}(dm) = \sum_{j=1}^{N_{EDP}} P[DM > dm | EDP = edp_j] \Delta \lambda_{EDPj} \quad (B.2b)$$

$$\lambda_{DV}(dv) = \sum_{k=1}^{N_{DM}} P[DV > dv | DM = dm_k] \Delta \lambda_{DMk} \quad (B.2c)$$

The problem of performance evaluation can therefore be broken into four basic components – evaluation of ground motion hazard, evaluation of system response to the ground motions, evaluation of physical damage resulting from the system response, and evaluation of losses associated with the physical damage. The problem requires identification of appropriate metrics of ground motion, system response, physical damage, and losses, which are denoted by

the previously described *IM*, *EDP*, *DM*, and *DV* terms; in view of the desire to account for uncertainty, these terms are treated as random variables. It also requires, however, the ability to predict *EDP* in response to *IM*, *DM* in response to *EDP*, and *DV* in response to *DM*; these are accomplished by response models, damage models, and loss models, respectively. In the PEER framework, these models are all formulated probabilistically – for example, the response model must be able to predict the probability distribution of *EDP* for a given *IM* value.

RESPONSE PREDICTION

Currently, the geotechnical engineer's primary contribution to the PBEE process comes primarily in the evaluation of $P[EDP|IM]$ as indicated in Equation (B.2a). This process involves establishing an appropriate *IM*, which should be one that the *EDP*(s) of interest are closely related to (furthermore, the *EDP*(s) of interest should be ones that the *DM*(s) of interest are closely related to, and the *DM*(s) of interest should be ones that the *DV*(s) of interest are closely related to). Luco and Cornell (2001) defined *efficient* intensity measures as those that produced little dispersion in *EDP*; put differently, an efficient *IM* is one for which the uncertainty in $EDP|IM$ is low. The efficiency of *IMs* varies from one type of problem to another, and can also vary from one *EDP* to another. Selection of efficient *IMs* is critical to the reliable and economical implementation of PBEE procedures. Luco and Cornell (2001) also described sufficient *IMs* as those for which the use of additional ground motion information does not reduce uncertainty in $EDP|IM$. A perfectly sufficient *IM* would be one that tells an engineer all he/she needs to know about the motion's potential for producing response in a system of interest.

The notions of efficiency and sufficiency are important for the performance-based evaluation of liquefaction hazards because conventional procedures for evaluating liquefaction potential are based on an *IM* that is moderately efficient but distinctly insufficient. The moderate efficiency comes from the fact that liquefaction potential is evaluated using peak ground acceleration, which is a measure of the high-frequency content of a ground motion. The generation of excess porewater pressure, however, is clearly related to shear strain amplitude, which basic wave propagation concepts (in a linear system) indicate is proportional to particle velocity. Because of the smoothing effects of integration (from acceleration to velocity), strain amplitude is more closely related to intermediate frequencies (often in the range of 1-2 Hz). The insufficiency comes from the fact that excess pore pressures increase incrementally during an

earthquake, hence the duration of a ground motion, which is not reflected in peak acceleration alone, affects excess porewater pressure generation. In the earliest modern procedures for liquefaction potential evaluation, the effects of duration were accounted for by the introduction of a magnitude scaling factor. The need for the magnitude scaling factor is, in and of itself, evidence that peak acceleration is insufficient for prediction of liquefaction potential. Therefore, the basic PEER framework, which assumes sufficiency, had to be modified for the liquefaction problem; the details of the required modifications are described in the following appendices.

PERFORMANCE PREDICTION

Performance can be described in a number of different ways depending on the perspective of the stakeholder. The current state of geotechnical engineering practice with respect to liquefaction problems is to express liquefaction potential in terms of a factor of safety against liquefaction for a specific level of ground motion (i.e., that associated with a particular return period). If the indicated factor of safety is less than 1.0 – 1.2, the potential effects of liquefaction are investigated.

Liquefaction effects are commonly expressed in terms of response parameters – *EDPs*, to use the PEER notation adopted in this report. In conventional practice, the computed *EDPs* correspond to some level of ground motion and are therefore conditional upon that ground motion. The actual likelihood of those *EDPs* being reached is not determined. The performance-based approach allows evaluation of the actual likelihood of a given *EDP* level being reached or exceeded, and therefore represents a much more complete, rational, and consistent measure of the anticipated response. This level of response, however, does not provide a direct indication of the damage that it would produce – such a prediction requires knowledge of the capacity of the system to tolerate the predicted response.

The next step in the development of performance-based procedures to levels beyond those included in the current work is to extend the framework to the prediction of damage. If the level of response, expressed in terms of an *EDP*, exceeds the capacity of the system of interest to resist that level of response, some level of damage is likely to occur. If the response is expressed in terms of a demand, *D*, and the capacity as *C*, a limit state, *LS*, will be reached when the demand exceeds the capacity, so

$$P_{LS} = P[D > C] \quad (B.3)$$

It should be noted that multiple limit states, which would have different capacities associated with them, can be defined for a given system of interest. Then, recognizing that the capacity (for example, the allowable displacement) is uncertain, the probability of reaching the limit state can be expressed as

$$P_{LS} = \sum_{allc} P[D > c | C = c]P[C = c] \quad (B.4)$$

The mean annual rate of exceeding the limit state, therefore, can be expressed as the product of the seismicity rate and the probability of exceeding the limit state, i.e., as

$$\lambda_{LS} = \nu \sum_{allc} P[D > c | C = c]P[C = c] \quad (B.5)$$

In this manner, the uncertainty in capacity, frequently referred to by geotechnical engineers as the allowable level of response, can be properly accounted for in the performance-based procedure. It has been shown (Jalayer, 2003) that this procedure can be expressed in terms of an LRFD-type framework; development of such a framework for liquefaction-related hazards would allow the benefits of performance-based design and evaluation to be realized in a format that is familiar to and convenient for geotechnical engineers.

Jalayer, F. (2003). "Direct probabilistic seismic analysis: Implementing nonlinear dynamic assessments," Ph.D. dissertation, Stanford University, Stanford, California, 238 pp.

Luco, N., and Cornell, C. A., (2001). "Structure-specific scalar intensity measures for near-source and ordinary earthquake ground motions," *Earthquake Spectra*, submitted.

Appendix C

Performance-Based Procedure for Initiation of Liquefaction

This appendix describes a procedure in which the entire range of potential ground shaking can be considered in a fully probabilistic liquefaction potential evaluation using a performance-based earthquake engineering (PBEE) framework. The result is a direct estimate of the return period for liquefaction, rather than a factor of safety or probability of liquefaction conditional upon ground shaking with some specified return period. As such, the performance-based approach can be considered to produce a more complete and consistent indication of the likelihood of liquefaction at a given location than conventional procedures. In this paper, the performance-based procedure is introduced and then used to compare the actual likelihoods of liquefaction at identical sites located in areas of different seismicity; the results show that the consistent use of conventional procedures for evaluating liquefaction potential produces inconsistent actual likelihoods of liquefaction.

LIQUEFACTION POTENTIAL

Liquefaction potential is generally evaluated by comparing consistent measures of earthquake loading and liquefaction resistance. It has become common to base the comparison on cyclic shear stress amplitude, usually normalized by initial vertical effective stress and expressed in the form of a cyclic stress ratio, *CSR*, for loading and a cyclic resistance ratio, *CRR*, for resistance. The potential for liquefaction is then described in terms of a factor of safety against liquefaction, $FS_L = CRR/CSR$.

Characterization of Earthquake Loading

The cyclic stress ratio is most commonly evaluated by using the “simplified method” first described by Seed and Idriss (1971), which can be expressed as

$$CSR = 0.65 \frac{a_{\max}}{g} \cdot \frac{\sigma_{vo}}{\sigma'_{vo}} \cdot \frac{r_d}{MSF} \quad (C.1)$$

where a_{\max} = peak ground surface acceleration, g = acceleration of gravity (in same units as a_{\max}), σ_{vo} = initial vertical total stress, σ'_{vo} = initial vertical effective stress, r_d = depth reduction factor, and MSF = magnitude scaling factor, which is a function of earthquake magnitude. The depth reduction factor accounts for compliance of a typical soil profile, and the magnitude scaling factor acts as a proxy for the number of significant cycles, which is related to the ground motion duration. Note that two pieces of loading information – a_{\max} and earthquake magnitude – are required for estimating the cyclic stress ratio.

Characterization of Liquefaction Resistance

The cyclic resistance ratio is generally obtained by correlation to *in situ* test results, usually standard penetration (SPT), cone penetration (CPT), or shear wave velocity (V_s) tests. Of these, the SPT has been most commonly used and will be used in the remainder of this paper. A number of SPT-based procedures for deterministic (Seed and Idriss, 1971; Seed et al., 1985; Youd et al., 2001, Idriss and Boulanger, 2004) and probabilistic (Liao et al., 1988; Toprak et al., 1999; Youd and Noble, 1997; Juang and Jiang, 2000; Cetin et al., 2004) estimation of liquefaction resistance have been proposed.

Deterministic Approach

Figure C1(a) illustrates the widely used liquefaction resistance curves recommended by Youd et al. (2001), which are based on discussions at an NCEER Workshop (National Center for Earthquake Engineering Research, 1997). The liquefaction evaluation procedure described by Youd et al. (2001) will be referred to hereafter as the NCEER procedure. The NCEER procedure has been shown to produce reasonable predictions of liquefaction potential (i.e., few cases of non-prediction for sites at which liquefaction was observed) in past earthquakes and is widely used in contemporary geotechnical engineering practice. For the purposes of this paper, a conventionally liquefaction-resistant site will be considered to be one for which $FS_L \geq 1.2$ for a 475-year ground motion using the NCEER procedure. This standard is consistent with that

recommended by Martin and Lew (1999), for example, and is considered representative of those commonly used in current practice.

Probabilistic Approach

Recently, a detailed review and careful re-interpretation of liquefaction case histories (Cetin, 2000; Cetin et al., 2004) was used to develop new probabilistic procedures for evaluating liquefaction potential. The probabilistic implementation of the Cetin et al. (2004) procedure produces a probability of liquefaction, P_L that can be expressed as

$$P_L = \Phi \left[-\frac{(N_1)_{60}(1+\theta_1 FC) - \theta_2 \ln CSR_{eq} - \theta_3 \ln M_w - \theta_4 \ln(\sigma'_{vo}/p_a) + \theta_5 FC + \theta_6}{\sigma_\varepsilon} \right] \quad (C.2)$$

where Φ is the standard normal cumulative distribution function, $(N_1)_{60}$ = corrected SPT resistance, FC = fines content (in percent), CSR_{eq} = cyclic stress ratio (Equation B.1) without MSF , M_w = moment magnitude, σ'_{vo} = initial vertical effective stress, p_a is atmospheric pressure (in same units as σ'_{vo}), σ_ε is a measure of the estimated model and parameter uncertainty, and θ_1 - θ_6 are model coefficients obtained by regression. As Equation (C.2) shows, the probability of liquefaction includes both loading terms (again, peak acceleration, as reflected in the cyclic stress ratio, and magnitude) and resistance terms (SPT resistance, fines content, and vertical effective stress). Mean values of the model coefficients are presented for two conditions in Table C.1 – a case in which the uncertainty includes parameter measurement/estimation errors and a case in which the effects of measurement/estimation errors have been removed. The former would correspond to uncertainties that exist for a site investigated with a normal level of detail and the latter to a “perfect” investigation (i.e., no uncertainty in any of the variables on the right side of Equation C.2). Figure C.1(b) shows contours of equal P_L for conditions in which measurement/estimation errors are included; the measurement/estimation errors have only a slight influence on the model coefficients but a significant effect on the uncertainty term, σ_ε .

Table C1. Cetin et al. (2004) model coefficients with and without measurement/estimation errors (after Cetin et al., 2002).

Case	Meas./est. errors	θ_1	θ_2	θ_3	θ_4	θ_5	θ_6	σ_ε
I	Included	0.004	13.79	29.06	3.82	0.06	15.25	4.21
II	Removed	0.004	13.32	29.53	3.70	0.05	16.85	2.70

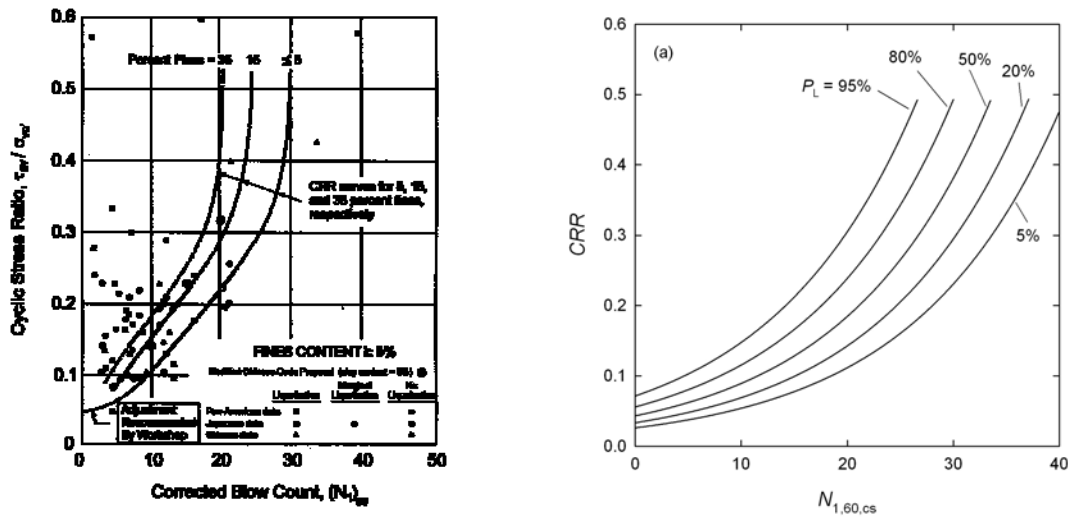


Figure C.1. (a) Deterministic cyclic resistance curves proposed by Youd et al. (2001), and (b) cyclic resistance curves of constant probability of liquefaction with measurement/estimation errors by Cetin et al., (2004).

Direct comparison of the procedures described by Youd et al. (2001) and Cetin et al. (2004) is difficult because various aspects of the procedures are different. For example, Cetin et al (2004) found that the average effective stress for their critical layers were at lower effective stresses (~ 0.65 atm) instead of the standard 1 atm and made allowances for those differences. Also, the basic shapes of the cyclic resistance curves are different – the Cetin et al. (2004) curves (Figure C.3) have a smoothly changing curvature, whereas the Youd et al. (2001) curve (Figure C.1) is nearly linear at intermediate SPT resistances ($(N_1)_{60} \approx 10-22$), with higher curvatures at lower and higher SPT resistances. An approximate comparison of the two methods can be made by substituting CRR for CSR_{eq} in Equation (C.2) and then rearranging the equation in the form

$$CRR = \exp \left[\frac{(N_1)_{60} (1 + \theta_1 FC) - \theta_3 \ln M_w - \theta_4 \ln(\sigma'_{vo}/p_a) + \theta_5 FC + \theta_6 + \sigma_\varepsilon \Phi^{-1}(P_L)}{\theta_2} \right] \quad (C.3)$$

where Φ^{-1} is the inverse standard normal cumulative distribution function. The resulting value of CRR can then be used in the common expression for FS_L . Arango et al. (2004) used this formulation without measurement/estimation errors (Case II in Table C.1) and found that the Cetin et al. (2004) and NCEER procedures yielded similar values of FS_L for a site in San Francisco when a value of $P_L \approx 0.65$ was used in Equation (C.3). A similar exercise for a site in Seattle with measurement/estimation errors (Case I in Table C.1) shows equivalence of FS_L when a value of $P_L \approx 0.6$ is used. Cetin et al. (2001) suggest the use of a deterministic curve equivalent to that given by Equation (C.3) with $P_L = 0.15$, which would produce a more conservative result than the NCEER procedure. The differences between the two procedures are most pronounced at high CRR values; the NCEER procedure contains an implicit assumption of $(N_1)_{60} = 30$ as an upper bound to liquefaction susceptibility, while Cetin et al. (2004), whose database contained considerably more cases at high CSR levels, indicate that liquefaction is possible (albeit with limited potential effects) at $(N_1)_{60}$ values above 30.

SEISMIC HAZARD ANALYSIS

Ground shaking levels used in seismic design and hazard evaluations are generally determined by means of seismic hazard analyses. Deterministic seismic hazard analyses are used most often for special structures or for estimating upper bound ground shaking levels. In the majority of cases, however, ground shaking levels are determined by probabilistic seismic hazard analyses.

Probabilistic seismic hazard analyses consider the potential levels of ground shaking from all combinations of magnitude and distance for all known sources capable of producing significant shaking at a site of interest. The distributions of magnitude and distance, and of ground shaking level conditional upon magnitude and distance, are combined in a way that allows estimation of the mean annual rate at which a particular level of ground shaking will be exceeded. The mean annual rate of exceeding a ground motion parameter value, y^* , is usually expressed as λ_{y^*} ; the reciprocal of the mean annual rate of exceedance is commonly referred to

as the return period. The results of a probabilistic seismic hazards assessment (PSHA) are typically presented in the form of a seismic hazard curve, which graphically illustrates the relationship between λ_{y^*} and y^* .

The ground motion level associated with a particular return period is therefore influenced by contributions from a number of different magnitudes, distances, and conditional exceedance probability levels (usually expressed in terms of a parameter, ε , defined as the number of standard deviations by which $\ln y^*$ exceeds the natural logarithm of the median value of y for a given M and R). The relative contributions of each $M - R$ pair to λ_{y^*} can be quantified by means of a deaggregation analysis (McGuire, 1995); the deaggregated contributions of magnitude and distance are frequently illustrated in diagrams such as that shown in Figure 2.5. Because both peak acceleration and magnitude are required for cyclic stress-based evaluations of liquefaction potential, the marginal distribution of magnitude can be obtained by summing the contributions of each distance and ε value for each magnitude; magnitude distributions for six return periods at a site in Seattle analyzed by the U.S. Geological Survey (<http://eqhazmaps.usgs.gov>) are shown in Figure 2.6. The decreasing significance of lower magnitude earthquakes for longer return periods, evident in Figure 2.6, is a characteristic shared by many other locations.

PERFORMANCE-BASED LIQUEFACTION POTENTIAL EVALUATION

In practice, liquefaction potential is usually evaluated by using deterministic *CRR* curves, a single ground motion hazard level, for example, for ground motions with a 475-yr return period, and a single earthquake magnitude, usually the mean or mode. In contrast, the performance-based approach incorporates probabilistic *CRR* curves and contributions from *all* hazard levels and *all* earthquake magnitudes.

The roots of performance-based liquefaction assessment are in the method of seismic risk analysis introduced by Cornell (1968). The first known application of this approach to liquefaction assessment was presented by Yegian and Whitman (1978), although earthquake loading was described as a combination of earthquake magnitude and source-to-site distance rather than peak acceleration and magnitude. Atkinson et al. (1984) developed a procedure for estimating the annual probability of liquefaction by using linearized approximations of the *CRR*

curves of Seed and Idriss (1983) in a deterministic manner. Marrone et al. (2003) described liquefaction assessment methods that incorporate probabilistic *CRR* curves and the full range of magnitudes and peak accelerations in a manner similar to the PBEE framework described herein. Hwang et al. (2005) described a Monte Carlo simulation-based approach that produces similar results.

PBEE is generally formulated in a probabilistic framework to evaluate the risk associated with earthquake shaking at a particular site. The risk can be expressed in terms of economic loss, fatalities, or other measures. The Pacific Earthquake Engineering Research Center (PEER) has developed a probabilistic framework for PBEE (Cornell and Krawinkler, 2000; Krawinkler, 2002; Deierlein et al., 2003) that computes risk as a function of ground shaking through the use of several intermediate variables. The ground motion is characterized by an *Intensity Measure*, *IM*, which could be any one of a number of ground motion parameters (e.g., a_{\max} , Arias intensity, etc.). The effects of the *IM* on a system of interest are expressed in terms used primarily by engineers in the form of *Engineering Demand Parameters*, or *EDPs* (e.g., excess pore pressure, FS_L , etc.). The physical effects associated with the *EDPs* (e.g., settlement, lateral displacement, etc.) are expressed in terms of *Damage Measures*, or *DMs*. Finally, the risk associated with the *DM* is expressed in a form that is useful to decision-makers by means of *Decision Variables*, *DV* (e.g., repair cost, downtime, etc.). The mean annual rate of exceedance of various *DV* levels, λ_{DV} , can be expressed in terms of the other variables as

$$\lambda_{dv} = \sum_{k=1}^{N_{DM}} \sum_{j=1}^{N_{EDP}} \sum_{i=1}^{N_{IM}} P[DV > dv | DM = dm_k] P[DM = dm_k | EDP = edp_j] P[EDP = edp_j | IM = im_i] \Delta \lambda_{im_i} \quad (C.4)$$

where $P[a|b]$ describes the conditional probability of a given b , and N_{DM} , N_{EDP} , and N_{IM} are the number of increments of *DM*, *EDP*, and *IM*, respectively. Extending this approach to consider epistemic uncertainty in *IM*, although not pursued in this paper, is straightforward. By integrating over the entire hazard curve (approximated by the summation over $i = 1, N_{IM}$), the performance-based approach includes contributions from all return periods, not just the return periods mandated by various codes or regulations.

For a liquefiable site, the geotechnical engineer's initial contribution to this process for evaluating liquefaction hazards comes primarily in the evaluation of $P[EDP|IM]$. Representing the *EDP* by FS_L and combining the probabilistic evaluation of FS_L with the results of a seismic

hazard analysis allows the mean annual rate of *non-exceedance* of a selected factor of safety, FS_L^* , to be computed as

$$\Lambda_{FS_L^*} = \sum_{i=1}^{N_{IM}} P[FS_L < FS_L^* | IM_i] \Delta \lambda_{IM_i} \quad (C.5)$$

The value of $\Lambda_{FS_L^*}$ should be interpreted as the mean annual rate (or inverse of the return period) at which the actual factor of safety will be less than FS_L^* . Note that $\Lambda_{FS_L^*}$ increases with increasing FS_L^* , since weaker motions producing higher factors of safety occur more frequently than stronger motions that produce lower factors of safety. The mean annual rate of factor of safety non-exceedance is used because non-exceedance of a particular factor of safety represents an undesirable condition, just as exceedance of an intensity measure does; because lower case lambda (λ) is commonly used to represent mean annual rate of exceedance, an upper case lambda (Λ) is used here to represent mean annual rate of non-exceedance. Since liquefaction is expected to occur when $CRR < CSR$ (i.e., when $FS_L^* < 1.0$), the return period of liquefaction corresponds to the reciprocal of the mean annual rate of non-exceedance of $FS_L^* = 1.0$, i.e., $T_{R,L} = 1 / \Lambda_{FS_L^*=1.0}$.

The PEER framework assumes *IM* sufficiency, i.e., that the intensity measure is a scalar that provides all of the information required to predict the *EDP*. This sufficiency, however, does not exist for cyclic stress-based liquefaction potential evaluation procedures, as evidenced by the long-recognized need for a magnitude scaling factor. Therefore, FS_L depends on more than just peak acceleration as an intensity measure, and calculation of the mean annual rate of exceeding some factor of safety against liquefaction, FS_L^* , can be modified as

$$\Lambda_{FS_L^*} = \sum_{j=1}^{N_M} \sum_{i=1}^{N_{a_{max}}} P[FS_L < FS_L^* | a_{max_i}, m_j] \Delta \lambda_{a_{max_i}, m_j} \quad (C.6)$$

where N_M and $N_{a_{max}}$ are the number of magnitude and peak acceleration increments into which “hazard space” is subdivided, and $\Delta \lambda_{a_{max_i}, m_j}$ is the incremental mean annual rate of exceedance for intensity measure, a_{max_i} , and magnitude, m_j . The values of $\lambda_{a_{max}, m}$ can be visualized as a series of seismic hazard curves distributed with respect to magnitude according to the results of a deaggregation analysis (Figure 2.6); therefore, their summation (over magnitude) yields the total

seismic hazard curve for the site (Figure 2.7). The conditional probability term in Equation (C.6) can be calculated by using the probabilistic model of Cetin et al. (2004), as described in Equation (C.2), with $CSR = CSR_{eq,i} FS_L^*$ (with $CSR_{eq,i}$ computed from $a_{max,i}$) and $M_w = m_j$, i.e.,

$$P[FS_L < FS_L^* | a_{max,i}, m_j] = \Phi \left[-\frac{(N_1)_{60} (1 + \theta_1 FC) - \theta_2 \ln(CSR_{eq,i} FS_L^*) - \theta_3 \ln m_j - \theta_4 \ln(\sigma'_{vo}/p_a) + \theta_5 FC + \theta_6}{\sigma_\varepsilon} \right] \quad (C.7)$$

Another way of characterizing liquefaction potential is in terms of the liquefaction resistance required to produce a desired level of performance. For example, the SPT value required to resist liquefaction, N_{req} , can be determined at each depth of interest. The difference between the actual SPT resistance and the required SPT resistance would provide an indication of how much soil improvement might be required to bring a particular site to an acceptable factor of safety against liquefaction. Given that liquefaction would occur when $N < N_{req}$, or when $FS_L < 1.0$, then $P[N < N_{req}] = P[FS_L < 1.0]$. The PBEE approach can then be applied to produce a mean annual rate of exceedance for N_{req}^*

$$\lambda_{N_{req}^*} = \sum_{j=1}^{N_M} \sum_{i=1}^{N_{a_{max}}} P[N_{req} > N_{req}^* | a_{max,i}, m_j] \Delta \lambda_{a_{max,i}, m_j} \quad (C.8)$$

where

$$P[N_{req} > N_{req}^* | a_{max,i}, m_j] = \Phi \left[-\frac{N_{req}^* (1 + \theta_1 FC) - \theta_2 \ln CSR_{eq,i} - \theta_3 \ln m_j - \theta_4 \ln(\sigma'_{vo}/p_a) + \theta_5 FC + \theta_6}{\sigma_\varepsilon} \right] \quad (C.9)$$

The value of N_{req}^* can be interpreted as the SPT resistance required to produce the desired performance level for shaking with a return period of $1/\lambda_{N_{req}^*}$.

COMPARISON OF CONVENTIONAL AND PERFORMANCE-BASED APPROACHES

Conventional procedures provide a means for evaluating the liquefaction potential of a soil deposit for a given level of loading. When applied consistently to different sites in the same seismic environment, they provide a consistent indication of the likelihood of liquefaction (expressed in terms of FS_L or P_L) at those sites. The degree to which they provide a consistent

indication of liquefaction likelihood when applied to sites in *different* seismic environments, however, has not been established. That issue is addressed in the remainder of this paper.

Idealized Site

Potentially liquefiable sites around the world have different likelihoods of liquefaction because of differences in site conditions (which strongly affect liquefaction resistance) and local seismic environments (which strongly affect loading). The effects of seismic environment can be isolated by considering the liquefaction potential of a single soil profile placed at different locations.

Figure C.2 shows the subsurface conditions for an idealized, hypothetical site with corrected SPT resistances that range from relatively low ($(N_1)_{60} = 10$) to moderately high ($(N_1)_{60} = 30$). Using the cyclic stress-based approach, the upper portion of the saturated sand would be expected to liquefy under moderately strong shaking. The wide range of smoothly increasing SPT resistance, while perhaps unlikely to be realized in a natural depositional environment, is useful for illustrating the main points of this paper.

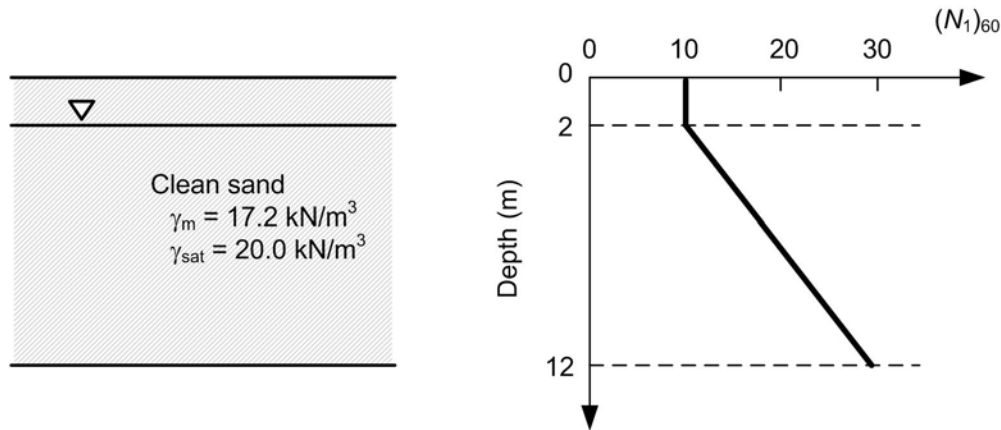


Figure C.2. Subsurface profile for idealized site.

Locations

In order to illustrate the effects of different seismic environments on liquefaction potential, the hypothetical site was assumed to be located in each of the 10 U.S. cities listed in Table C.2. For each location, the local seismicity was characterized by the probabilistic seismic hazard analyses available from the U.S. Geological Survey (using the 2002 interactive deaggregation link with listed latitudes and longitudes). In addition to being spread across the United States, these locations represent a wide range of seismic environments; the total seismic hazard curves for each of the locations are shown in Figure C.3. The seismicity levels vary widely – 475-year peak acceleration values range from 0.12g (Butte) to 0.66g (Eureka). Two of the locations (Charleston and Memphis) are in areas of low recent seismicity with very large historical earthquakes; three (Seattle, Portland, and Eureka) are in areas subject to large-magnitude subduction earthquakes; and two (San Francisco and San Jose) are in close proximity (~ 60 km) in a very active environment.

Table C.2. Peak ground surface (quaternary alluvium) acceleration hazard information for 10 U.S. cities.

Location	Lat. (N)	Long. (W)	475-yr a_{\max}	2,475-yr a_{\max}
Butte, MT	46.003	112.533	0.120	0.225
Charleston, SC	32.776	79.931	0.189	0.734
Eureka, CA	40.802	124.162	0.658	1.023
Memphis, TN	35.149	90.048	0.214	0.655
Portland, OR	45.523	122.675	0.204	0.398
Salt Lake City, UT	40.755	111.898	0.298	0.679
San Francisco, CA	37.775	122.418	0.468	0.675
San Jose, CA	37.339	121.893	0.449	0.618
Santa Monica, CA	34.015	118.492	0.432	0.710
Seattle, WA	47.530	122.300	0.332	0.620

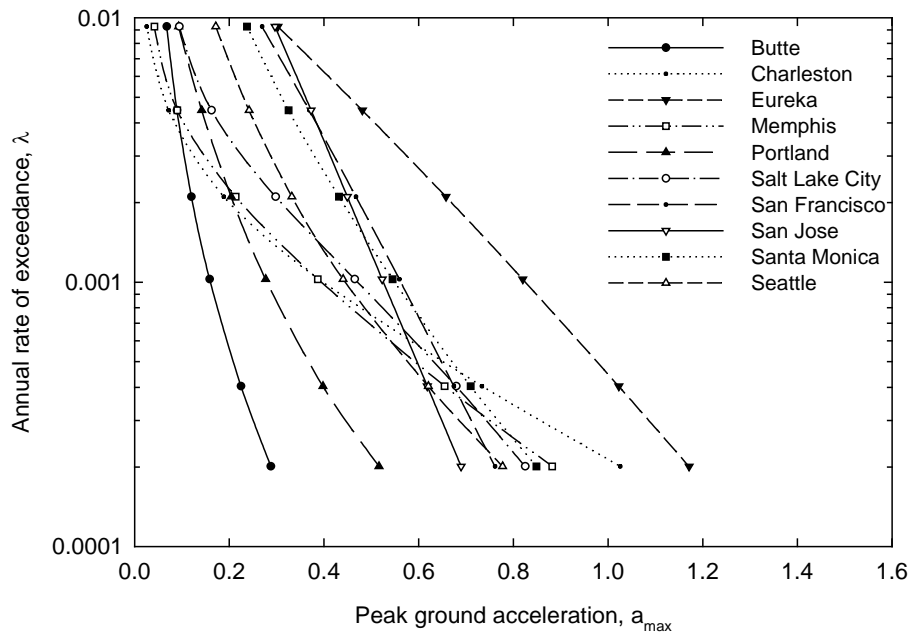


Figure C.3. USGS total seismic hazard curves for quaternary alluvium conditions at different site locations.

Conventional Liquefaction Potential Analyses

Two sets of conventional deterministic analyses were performed to illustrate the different degrees of liquefaction potential of the hypothetical soil profile at the different site locations. The first set of analyses was performed using the NCEER procedure with 475-year peak ground accelerations and magnitude scaling factors computed with the mean magnitude from the 475-year deaggregation of peak ground acceleration. The second set of analyses was performed using Equation (C.2) with $P_L = 0.6$ to produce a deterministic approximation to the NCEER procedure; these analyses will be referred to hereafter as NCEER-C analyses (note that, although applied deterministically in this paper, the NCEER-C approximation to the NCEER procedure used here is *not* equivalent to the deterministic procedure recommended by Cetin et al. (2004)). In all analyses, the peak ground surface accelerations were computed from the peak rock outcrop accelerations obtained from the USGS 2002 interactive deaggregations with a Quaternary alluvium amplification factor (Stewart et al., 2003),

$$F_a = \frac{a_{\max, \text{surface}}}{a_{\max, \text{rock}}} = \exp[-0.15 - 0.13 \ln a_{\max, \text{rock}}] \quad (\text{C.10})$$

The amplification factor was applied deterministically so the uncertainty in peak ground surface acceleration was controlled by the uncertainties in the attenuation relationships used in the USGS PSHAs. The uncertainties in peak ground surface accelerations for soil sites are usually equal to or somewhat lower than those for rock sites (e.g., Toro et al., 1997; Stewart et al., 2003).

The results of the first set of analyses are shown in Figure C.4. Figure C.4(a) shows the variation of FS_L with depth for the hypothetical soil profile at each location. The results are, as expected, consistent with the seismic hazard curves – the locations with the highest 475-year a_{\max} values have the lowest factors of safety against liquefaction. Figure C.4(b) expresses the results of the conventional analyses in a different way – in terms of N_{req}^{det} , the SPT resistance required to produce a performance level of $FS_L = 1.2$ with the 475-year ground motion parameters for each location. The $(N_1)_{60}$ values for the hypothetical soil profile are also shown in Figure C.4(b) and can be seen to exceed the N_{req}^{det} values at all locations/depths for which $FS_L > 1.2$. Note that $N_{req}^{\text{det}} \leq 30$ for all cases, since the NCEER procedure implies zero liquefaction potential (infinite FS_L) for $(N_1)_{60} > 30$.

The results of the second set of analyses are shown in Figure B5, both in terms of FS_L and N_{req}^{det} . The FS_L and N_{req}^{det} values are generally quite similar to those from the first set of analyses, except that required SPT resistances are slightly in excess of 30 (as allowed by the NCEER-C procedure) for the most seismically active locations in the second set. The similarity of these values confirms the approximation of the NCEER procedure to the NCEER-C procedure.

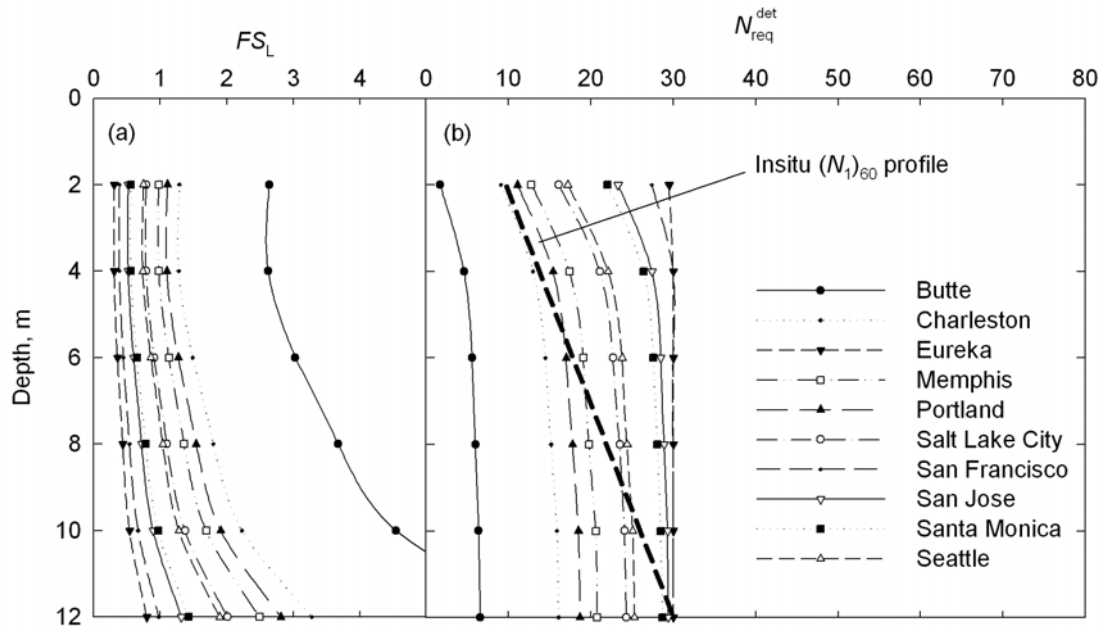


Figure C.4. Profiles of (a) factor of safety against liquefaction and (b) required SPT resistance obtained by using the NCEER deterministic procedure with 475-year ground motions.

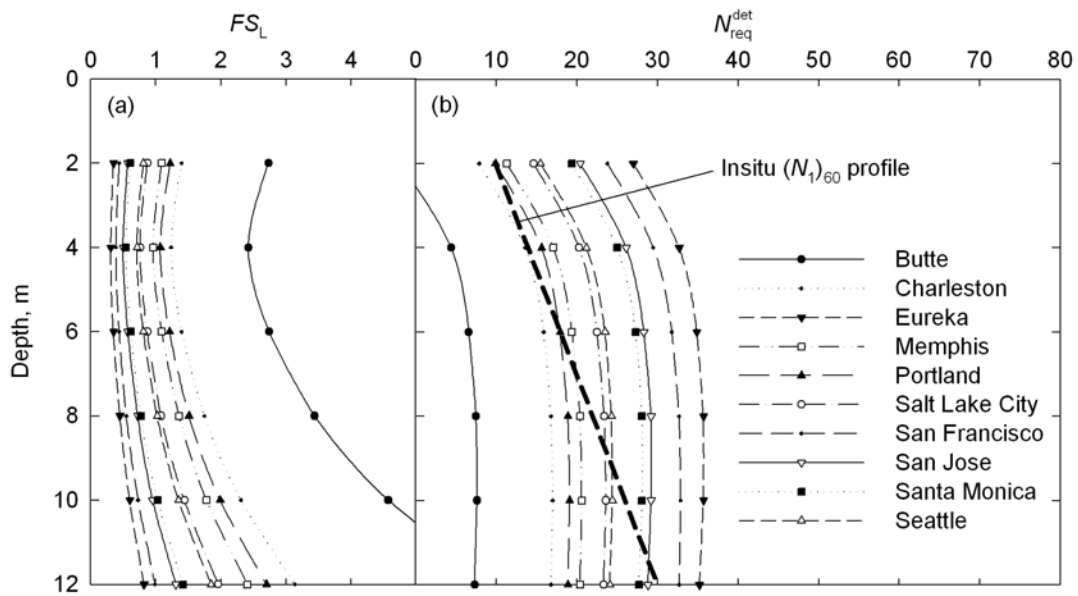


Figure C.5. Profiles of (a) factor of safety against liquefaction and (b) required SPT resistance obtained by using the NCEER-C deterministic procedure for 475-year ground motions.

Performance-Based Liquefaction Potential Analyses

The performance-based approach, which allows consideration of all ground motion levels and fully probabilistic computation of liquefaction hazard curves, was applied to each of the site locations. Figure C.6 illustrates the results of the performance-based analyses for an element of soil near the center of the saturated zone (at a depth of 6 m, at which $(N_1)_{60} = 18$ for the hypothetical soil profile). Figure C.6(a) shows factor of safety hazard curves, and Figure C.6(b) shows hazard curves for N_{req}^{PB} , the SPT resistance required to resist liquefaction. Note that the SPT resistances shown in Figure C.6(b) are those at which liquefaction would actually be expected to occur, rather than the values at which FS_L would be as low as 1.2 (corresponding to a conventionally liquefaction resistant soil, as defined previously), which were plotted in Figures C.4 and C.5. Therefore, the mean annual rates of exceedance in Figure C.6 are equal at each site location for $FS_L = 1.0$ and $N_{req}^{PB} = 18$.

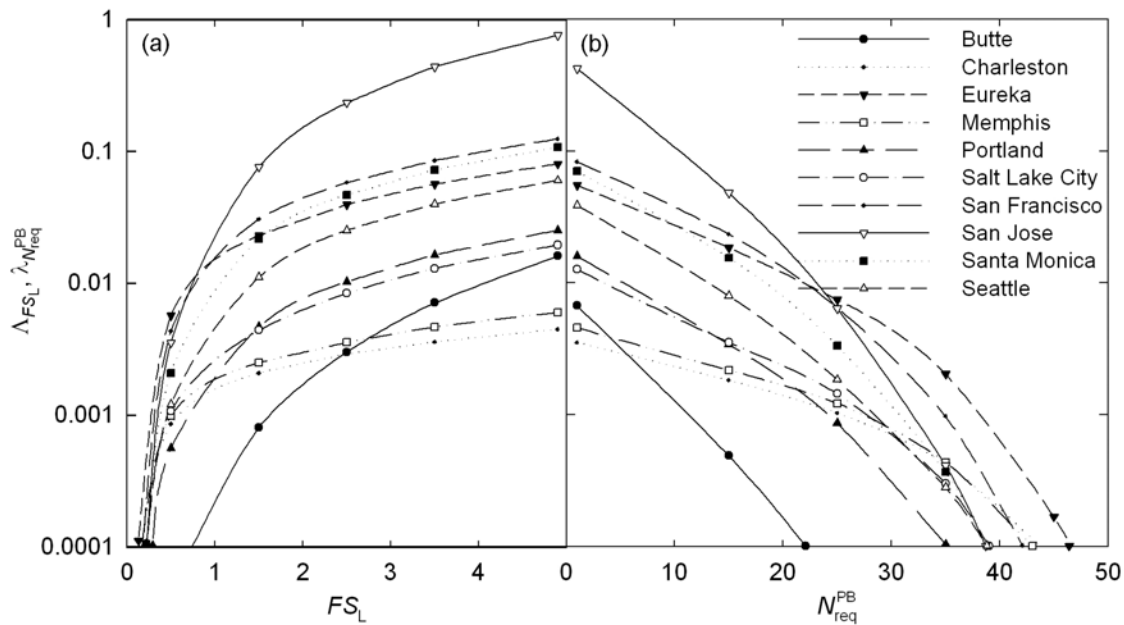


Figure C.6. Seismic hazard curves for 6-m depth: (a) factor of safety against liquefaction, FS_L for $(N_1)_{60} = 18$, and (b) required SPT resistance, N_{req}^{PB} , for $FS_L = 1.0$.

Equivalent Return Periods

The results of the conventional deterministic analyses shown in Figures C.4 and C.5 can be combined with the results of the performance-based analyses shown in Figure C.6 to evaluate the return periods of liquefaction produced in different areas by consistent application of conventional procedures for evaluation of liquefaction potential. For each site location, the process is as follows:

1. At the depth of interest, determine the SPT resistance required to produce a factor of safety of 1.2 by using the conventional approach (from either Figure C.4(b) or C.5(b)). At that SPT resistance, the soils at that depth would have an equal liquefaction potential (i.e., $FS_L = 1.2$ with a 475-year ground motion) at all site locations as evaluated with the conventional approach.
2. Determine the mean annual rate of exceedance for the SPT resistance from Step 1 by using results of the type shown in Figure C.6(b) for each depth of interest. Since Figure C.6(b) shows the SPT resistance for $FS_L = 1.0$, this is the mean annual rate of liquefaction for soils with this SPT resistance at the depth of interest.
3. Compute the return period as the reciprocal of the mean annual rate of exceedance.
4. Repeat steps 1-3 for each depth of interest.

This process was applied to all site locations in Table C.2 to evaluate the return period for liquefaction as a function of depth for each location; the calculations were performed with 475-year ground motions and again with 2,475-year ground motions.

Figure C.7 shows the results of this process for both sets of conventional analyses. It is obvious from Figure C.7 that consistent application of the conventional procedure produces inconsistent return periods and, therefore, different actual likelihoods of liquefaction at the different site locations. Examination of the return period curves shows that they are nearly vertical at depths greater than about 4 m, indicating that the deterministic procedures are relatively unbiased with respect to SPT resistance. The greater verticality of the curves based on the NCEER-C analyses results from the consistency of the shapes of those curves and the constant P_L curves given by Equation (C.2), which were used in the performance-based analyses. Differences between the shapes of the NCEER curve (Figure C.1a) and the curves (Figure C.1b),

particularly for sites subjected to very strong shaking (hence, very high CSRs) such as San Francisco and Eureka, contribute to depth-dependent return periods for the NCEER results.

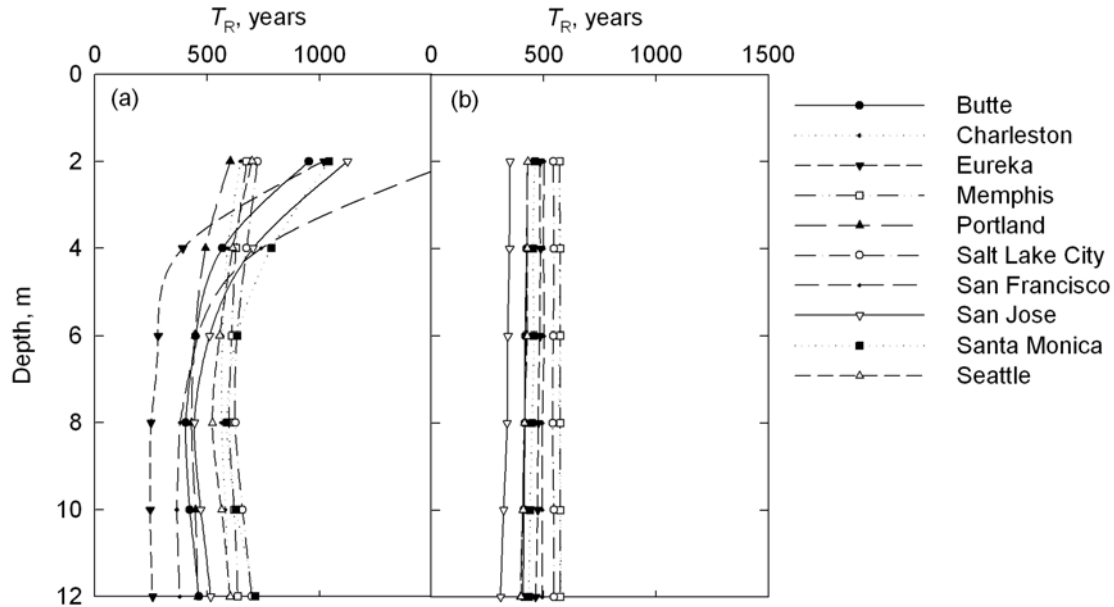


Figure C.7. Profiles of return period of liquefaction for sites with equal liquefaction potential as evaluated by (a) NCEER procedure and (b) NCEER-C procedure with 475-year ground motion parameters.

REFERENCES

- Arango, I., Ostadan, F, Cameron, J., Wu, C.L., and Chang, C.Y. (2004). "Liquefaction probability of the BART Transbay Tube backfill," Proceedings of the 11th International Conference on Soil Dynamics and Earthquake Engineering and 3rd International Conference on Earthquake Geotechnical Engineering, Vol. I, pp. 456-462.
- Atkinson, G.M., Finn, W.D.L., and Charlwood, R.G. (1984). "Simple computation of liquefaction probability for seismic hazard applications," *Earthquake Spectra*, 1(1), 107-123.
- Cetin, K.O. (2000). "Reliability-based assessment of seismic soil liquefaction initiation hazard," Ph.D. Dissertation, University of California, Berkeley, 602 pp.
- Cetin, K.O., Der Kiureghian, A., and Seed, R.B. (2002). "Probabilistic models for the initiation of soil liquefaction," *Structural Safety*, Vol. 24, 67-82.

- Cetin, K.O., Seed, R.B., Der Kiureghian, A., Tokimatsu, K., Harder, L.F., Kayen, R.E., and Moss, R.E.S. (2004). "Standard penetration test-based probabilistic and deterministic assessment of seismic soil liquefaction potential," *Journal of Geotechnical and Geoenvironmental Engineering*, ASCE, 130(12), 1314-1340.
- Cornell, C.A. (1968). "Engineering seismic risk analysis," *Bulletin of the Seismological Society of America*, 58(5), 1583-1606.
- Cornell, C.A. and Krawinkler, H. (2000). "Progress and challenges in seismic performance assessment," *PEER News*, April, 1-3.
- Deierlein, G.G., Krawinkler, H., and Cornell, C.A. (2003). "A framework for performance-based earthquake engineering," Proceedings, 2003 Pacific Conference on Earthquake Engineering.
- Hwang, J.H., Chen, C.H., and Juang, C.H. (2005). "Liquefaction hazard: a fully probabilistic method," in *Proceedings of the Sessions of the Geo-Frontiers 2005 Congress*, Earthquake Engineering and Soil Dynamics, R.W. Boulanger et al. eds, ASCE, Paper no. 22.
- Idriss, I.M. and Boulanger, R.W. (2004). "Semi empirical procedures for evaluating liquefaction potential during earthquakes," Proceedings of the 11th International Conference on Soil Dynamics and Earthquake Engineering and 3rd International Conference on Earthquake Geotechnical Engineering, Vol. I, 32-56.
- Juang, C.H. and Jiang, T. (2000). "Assessing probabilistic methods for liquefaction potential evaluation," *Soil Dynamics and Liquefaction 2000*, R.Y.S. Pak and J. Yamamuro, eds., Geotechnical Special Publication 107, ASCE, New York, 148-162.
- Krawinkler, H. (2002). "A general approach to seismic performance assessment," *Proceedings*, International Conference on Advances and New Challenges in Earthquake Engineering Research, ICANCEER, 2002, Hong Kong.
- Liao, S.S.C., Veneziano, D., and Whitman, R.V. (1988). "Regression models for evaluating liquefaction probability," *Journal of Geotechnical Engineering*, ASCE, 114(4), 389-409.
- Marrone, J., Ostadan, F., Youngs, R., and Litehiser, J. (2003). "Probabilistic liquefaction hazard evaluation: method and application," in *Transactions of the 17th International Conference on Structural Mechanics in Reactor Technology (SMiRT 17)*, Prague, Czech Republic, Paper no. M02-1.
- Martin, G.R. and Lew, M. eds. (1999). "Recommended Procedures for Implementation of DMG Special Publication 117 – Guidelines for Analyzing and Mitigating Liquefaction Hazards in California," Southern California Earthquake Center, Los Angeles, 63 pp.
- McGuire, R.K. (1995). "Probabilistic seismic hazard analysis and design earthquakes: Closing the loop," *Bulletin of the Seismological Society of America*, 85(5), 1275-1284.
- National Center for Earthquake Engineering Research (1997). *Proceedings of the NCEER workshop on evaluation of liquefaction resistance of soils*, T.L. Youd and I.M. Idriss, editors, Technical Report NCEER, 97-022.
- Seed, H.B. and Idriss, I.M. (1971). "Simplified procedure for evaluating soil liquefaction potential," *Journal of the Soil Mechanics and Foundations Division*, ASCE, 107(SM9), 1249-1274.

- Seed, H.B., Tokimatsu, K., Harder, L.F., and Chung, R.M. (1985). "Influence of SPT procedures in soil liquefaction resistance evaluations," *Journal of Geotechnical Engineering*, 111(12), 1425-1445.
- Stewart, J.P. and Whang, D.H. (2003). "Simplified procedure to estimate ground settlement from seismic compression in compacted soils," *Proc. 2003 Pacific Conference on Earthquake Engineering*, Christchurch, New Zealand, Paper 46.
- Toprak, S., Holzer, T.L., Bennett, M.J., and Tinsley, J.C. III. (1999). "CPT- and SPT-based probabilistic assessment of liquefaction," *Proc., 7th U.S.-Japan Workshop on Earthquake Resistant Design of Lifeline Facilities and Countermeasures Against Liquefaction*, Seattle, Multidisciplinary Center for Earthquake Engineering Research, Buffalo, NY, 69-86.
- Toro, G.R., Abrahamson, N.A., and Schneider, J.F. (1997). "Model of strong ground motions from earthquakes in central and eastern North America: Best estimates and uncertainties," *Seismological Research Letters*, 68(1), 41-57.
- Yegian, M.Y. and Whitman, R.V. (1978). "Risk analysis for ground failure by liquefaction," *Journal of the Geotechnical Engineering Division, ASCE*, 104(GT7), 907-905.
- Youd, T.L. and Noble, S.K. (1997). "Liquefaction criteria based on statistical and probabilistic analyses," *Proceedings of the NCEER Workshop on Evaluation of Liquefaction Resistance of Soils*, National Center for Earthquake Engineering Research, Buffalo, NY, 201-205.
- Youd, T.L. et al. (2001). "Liquefaction resistance of soils: Summary report from the 1996 NCEER and 1998 NCEER/NSF workshops on evaluation of liquefaction resistance of soils," *Journal of Geotechnical and Geoenvironmental Engineering, ASCE*, 127(10), 817-833.

Appendix D

Probabilistic Model for Estimation of Lateral Spreading Displacement

Liquefaction has been known to cause significant damage to buildings, bridges, dams, pipelines, and other constructed facilities during earthquakes. This damage frequently results from the liquefaction-related phenomenon of lateral spreading, in which the cyclic stresses induced by earthquake shaking lead to the accumulation of permanent lateral displacement of the soil. These lateral displacements may be accompanied by cracking, settlement, and tilting of the ground surface. Because the displacements can vary in the horizontal and vertical directions, they often impose large demands on structures supported on shallow foundations, and on structural elements such as piles, shafts, and pipelines that extend through the liquefied soil.

Several empirical procedures for estimation of lateral spreading displacements have been reported in the literature and integrated into geotechnical engineering practice. The most commonly used of these procedures are based on regression of lateral spreading case history data and therefore have the important advantage of being based on actual, observed lateral spreading behavior. It can be shown, however, that these methods are not consistent with the basic mechanics of liquefiable soil. This paper presents an alternative formulation of a predictive equation for lateral spreading displacement that is consistent with the mechanics of lateral spreading and calibrated against field observations of lateral spreading. The predictive equation also allows estimation of a probability distribution of lateral spreading displacement.

LATERAL SPREADING

Lateral spreading refers to the accumulation of permanent lateral displacement in soils subjected to earthquake shaking in the presence of static driving stresses. These driving stresses, which can exist under sloping ground surfaces or in the vicinity of localized slopes, are those required to maintain static equilibrium of the slope (shear stresses associated with K_0 conditions are not driving stresses). Depending on the size and steepness of the slope, and on the depth of interest, the static driving stresses may be small or large. The interaction of these static driving stresses with the cyclic stresses produced by earthquake shaking influences the magnitude and pattern of lateral spreading displacement.

Lateral spreading has been observed in numerous earthquakes. Among the best-known examples are those in Niigata, Japan and Anchorage, Alaska. More recently, significant lateral spreads have been observed in California (Boulanger et al., 1997), Japan (Hamada and Wakamatsu, 1998), and Turkey (Cetin et al., 2004). Field evidence of lateral spreading generally includes ground cracking (with and without sand boils) with permanent displacement in the downslope direction or toward nearby free slopes. The ground surface displacements caused by lateral spreading can be measured by surveying methods (given that a pre-earthquake survey exists) or by air photo interpretation. Case histories with measured subsurface displacements are very few; Boulanger et al. (1997) described lateral spreading failures at a Moss Landing, California site where several inclinometers had been installed prior to the 1989 Loma Prieta earthquake. The measured lateral displacement of one of these is shown in Figure D.1(a) – note that the shear strains are largest in the loose, saturated sandy soils and small in the silt and dense sand below 6 m. Lateral spreading has also been produced under controlled, well-instrumented conditions in laboratory model tests. The free-field displacements in four centrifuge tests on models inclined at 2° from horizontal (Figure D.1b) show a similar displacement pattern.

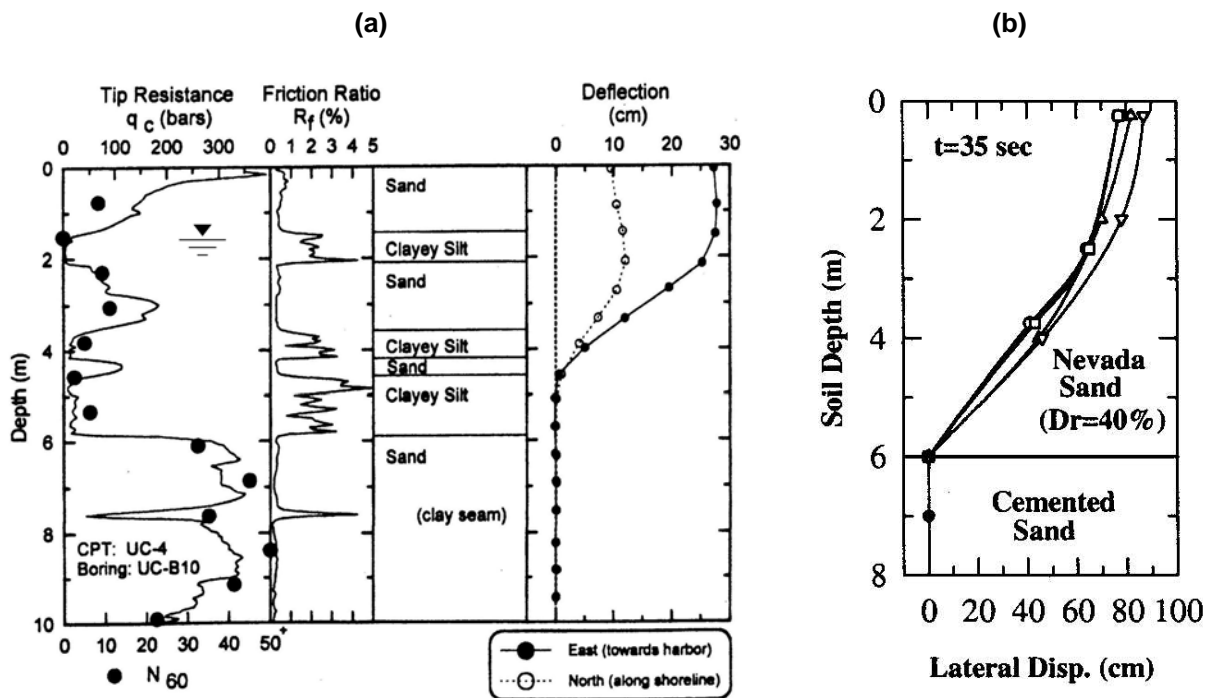


Figure D.1. Typical patterns of lateral spreading displacement: (a) subsurface conditions and permanent lateral displacements at Moss Landing slope inclinometer SI-2 (Boulanger et al., 1997), and (b) permanent lateral displacements at end of shaking in four centrifuge models (Abdoun et al., 2003).

PAST WORK

Lateral spreading is a complicated phenomenon and the mechanics by which it occurs are also complicated. A number of recent studies have helped illuminate the physical processes that control the development of lateral spreading deformations. Other studies have focused on practical, empirical procedures for estimation of lateral spreading displacements.

Mechanics of Liquefaction and Lateral Spreading

The conditions in an element of soil under a sloping ground surface can be simulated in a cyclic simple shear test performed with an initial static shear stress; Figure D.2 shows the results of such a test. Note that the sample is subjected to a positive shear stress at the beginning of the test (Point A). At the end of the first cycle (Point B), the contractive behavior of the soil has caused the effective stress to decrease by more than 40%, and the stiffness of the sample is lower than in the first cycle. When the ratio of shear to normal stress reaches a value of about 0.26 in the second cycle (Point C), the soil begins to dilate and the effective stress increases as the shear stress increases. This “phase transformation” behavior (Ishihara et al., 1975; Ishihara, 1985) continues in subsequent loading cycles and the variation of stiffness becomes more pronounced as the minimum normal stress ratio decreases from cycle to cycle. In the latter cycles, the stiffness is very low when the shear stress is low (Point D) but increases as the soil dilates and the effective stress increases (Point E). The increase in cyclic strain amplitude during the test is accompanied by an increase in permanent strain that is caused by the initial static shear stress, and most of the permanent strain develops after initial liquefaction. Integrated over the stack of soil elements that make up a soil deposit in the field, such permanent strains are manifested in the field as the permanent displacements referred to as lateral spreading.

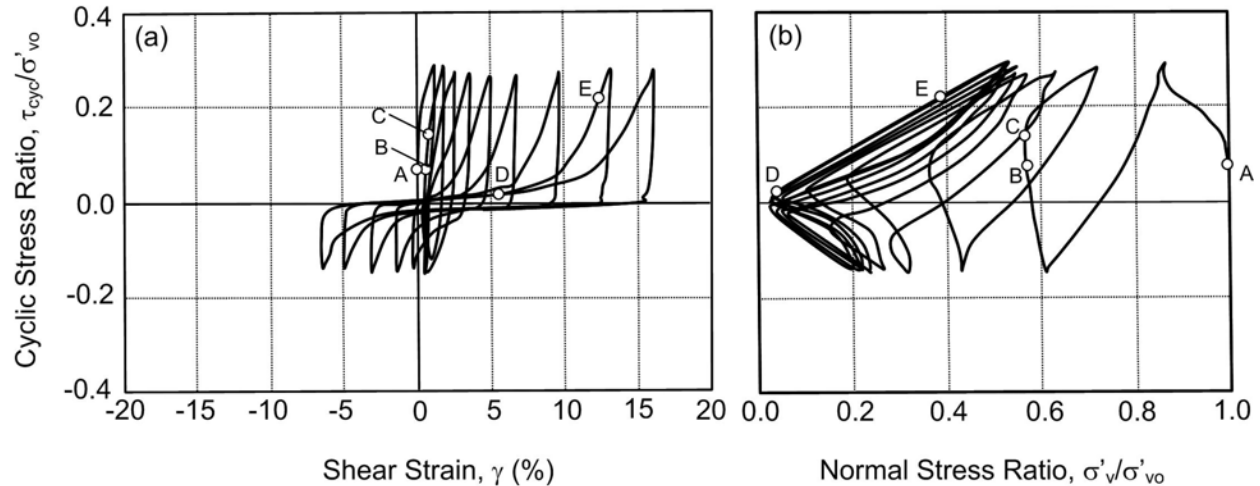


Figure D.2. Laboratory simple shear behavior of saturated sand: (a) stress-strain and (b) stress path behavior with non-zero initial shear stress (after Wu, 2002).

Under such conditions, the accumulation of permanent strain is controlled by the stiffening behavior of the soil as it dilates above the phase transformation line. However, relatively little hard data on this aspect of soil behavior is available. Shamoto et al. (1998) developed a procedure for estimating the potential permanent strain induced in liquefiable soil; the procedure, based on soil behavior measured in laboratory tests (Tokimatsu and Yoshimi, 1983) suggests that shear strain depends on soil density and cyclic stress ratio. As indicated in Figure D.3(a), the potential shear strain decreases with increasing SPT resistance and decreasing CSR. Wu (2002) observed similar behavior in cyclic simple shear tests and produced curves (Figure D.3b) similar to those of Shamoto et al. (1998). Laboratory results of the type observed by Shamoto et al. (1998), Wu (2002) and others indicate that potential shear strains should decrease smoothly with increasing SPT resistance to SPT resistances in excess of 30 blows/ft. Centrifuge tests (e.g., Sharp et al, 2003; Kutter et al., 2004) also show that lateral spreading displacements decrease with increasing relative density, and can be substantial at relative densities of 75% or more. When combined with the common observation of decreasing CSR with depth (all other things being equal), they also suggest that shear strains in the field should decrease with depth for soil of a given SPT resistance.

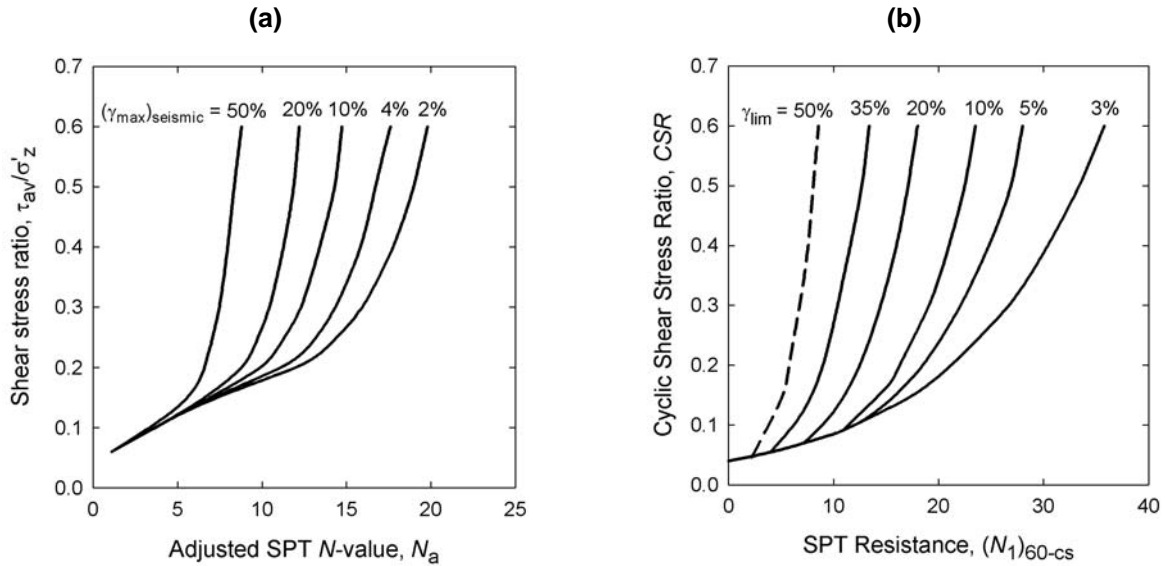


Figure D.3. Variation of potential shear strain with SPT resistance and cyclic stress ratio: (a) after Shamoto et al. (1998), and (b) Wu (2002).

Permanent lateral displacements can occur by another mechanism in the field. In some soil profiles, particularly those in which liquefiable soils are overlain by impermeable soils, pore pressure redistribution may lead to increased void ratios beneath the impermeable soil (Fiegel and Kutter, 1994; Boulanger and Truman, 1996; Kokusho, 1999; Kulasingham et al., 2004). The increased void ratio can cause the residual strength of the soil (which is very sensitive to void ratio) to drop below the static driving stress, thereby resulting in a flow failure that may actually take place after earthquake shaking has ended. Because it is virtually impossible to identify the mechanism producing small to moderate movements in the field, it is possible that some of the scatter in existing databases of lateral spreading case histories result from this mechanism.

Predictive Models

Several investigators have developed predictive relationships for the permanent displacement produced by lateral spreading. Early models (e.g., Hamada et al., 1987; Youd and Perkins, 1987) and some later models (e.g., Rauch and Martin, 2000) considered some of the variables known to influence lateral spreading displacements. More recent models commonly used in practice, however, consider the influence of soil properties, slope geometry, and level of ground motion, though they represent them in different ways. For the purposes of this paper,

these models are divided into two categories – purely empirical “BY-type” models and semi-empirical “strain potential” models, both of which are described in the following sections.

BY-Type Models

Bartlett and Youd (1992) compiled a large database of lateral spreading case histories from Japan and the western United States. By investigating a large number of potential parameters, Bartlett and Youd (1992) were able to identify those that were most closely related to lateral spreading displacement and develop a regression-based predictive relationship. Bardet et al. (1999a) updated and reinterpreted many of the case histories in the Bartlett and Youd database and extended it to include more recent case histories. Bardet et al. developed a six-parameter model of similar form to that of Bartlett and Youd (1992), and a four-parameter model that did not include fines content and grain size terms that are often unavailable in practice. Bardet et al. (1999b) also presented procedures for estimating the probability of exceeding a particular level of permanent displacement. Youd et al. (2002) used an expanded and corrected version of the 1992 database to develop the predictive relationship

$$\log D_H = b_0 + b_1 M_w + b_2 \log R^* + b_3 R + b_4 \log W + b_5 \log S + b_6 \log T_{15} + b_7 \log(100-F_{15}) + b_8 \log(D50_{15} + 0.1 \text{ mm}) \quad (\text{D.1})$$

where D_H = horizontal displacement in meters, M_w = moment magnitude, $R^* = R + 10^{-0.89M_w - 5.64}$, R = closest horizontal distance to the energy source, W = free-face ratio (Figure D.4) in percent, S = ground slope in percent, T_{15} = cumulative thickness (in upper 20 m) of saturated cohesionless soil with $(N_1)_{60} < 15$ (subject to the restriction that the top of the layer is at a depth of 1 to 10 m), F_{15} = average fines content of the soil comprising T_{15} , and $D50_{15}$ = average mean grain size (mm) of the soil comprising T_{15} . The values of the coefficients are presented in Table D1.

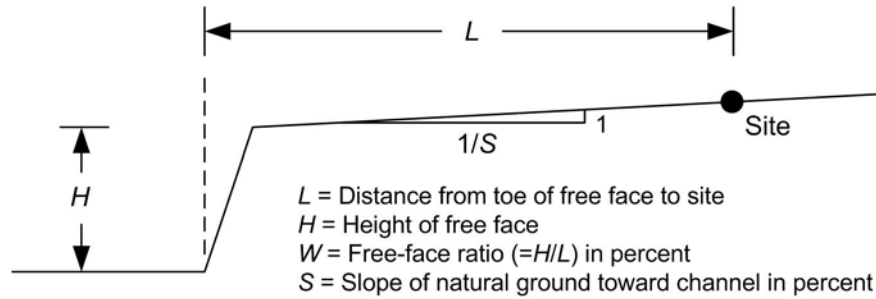


Figure D.4. Illustration of slope geometry terms for empirical lateral spreading models.

Table D.1. Coefficients for Youd et al. (2002) model.

Model	b_0	b_1	b_2	b_3	b_4	b_5	b_6	b_7	b_8
Ground slope	-16.213	1.532	-1.406	-0.012	0	0.338	0.540	3.413	-0.795
Free Face	-16.713	1.532	-1.406	-0.012	0.592	0	0.540	3.413	-0.795

The BY-type models account for soil properties, slope geometry, and level of earthquake shaking. The implications of the manner in which they represent soil properties are discussed subsequently.

Cumulative Strain Potential Models

The concept of density-related potential strain and its role in estimating liquefaction-related deformations (e.g., Seed et al., 1973; Seed et al., 1975; Seed, 1979) was developed many years ago. In recent years, new models for estimating lateral spreading displacements based on strain potential (e.g., Shamoto et al., 1998; Zhang et al., 2004; Faris et al., 2006) have been proposed.

Zhang et al. (2004) capped the laboratory test-based maximum cyclic shear strains predicted as a function of relative density and factor of safety against liquefaction by Ishihara and Yoshimine (1992) with the limiting shear strains proposed by Seed (1979) to develop a cumulative shear strain-based model for lateral spreading displacement. Using empirical relationships between penetration resistance and relative density, either SPT or CPT data can be used to predict permanent displacements as

$$D_H = \begin{cases} (S + 0.2) \cdot LDI & \text{ground slope case} \\ 6W^{-0.8} \cdot LDI & \text{free - face case} \end{cases} \quad (D.2)$$

both with the lateral displacement index, LDI , computed by integrating maximum cyclic shear strain, γ_{\max} , over depth, i.e.

$$LDI = \int_0^{Z_{\max}} \gamma_{\max} dz \quad (D.3)$$

where Z_{\max} = maximum depth below all potentially liquefiable layers with $FS < 2.0$.

Faris et al. (2006) developed a cumulative strain-based model similar to that of Zhang et al. (2004) but based on laboratory-based shear strain potential curves (Figure D.3b) developed by Wu (2002); the Wu (2002) curves indicate that significant shear strain potential exists for soils with SPT resistances of 30 blows/ft or more under strong shaking. The Faris et al. (2006) model predicts the maximum displacement on a particular lateral spread, $D_{H,\max}$, as

$$D_{H,\max} = \exp[1.0443 \ln DPI_{\max} + 0.0046 \ln \alpha + 0.0029 M_w] \quad (D.4)$$

where the maximum displacement potential index, DPI_{\max} , is computed in a manner similar to the lateral displacement index of Zhang et al. (2004), i.e., by integrating the shear strain potential index of Wu (2002) over depth for all potentially liquefiable layers, and α is the ratio of average static horizontal shear stress to initial vertical effective stress.

Discussion

Any relationship that attempts to predict the permanent displacement produced by lateral spreading must account for the properties of the soil in the profile of interest, the geometry of the slope, and the level of ground motion induced by earthquake shaking.

In BY-type relationships, soil properties are accounted for by the T_{15} , F_{15} , and $(D_{50})_{15}$ terms, each of which were identified and used on the basis of their ability to improve the statistical fit to the empirical database of lateral spreading case histories. The T_{15} parameter,

however, can produce permanent displacement estimates with counterintuitive sensitivities to soil properties; for example, the definition of T_{15} implies:

1. *A rapid change in behavior at $(N_1)_{60} = 15$:* The predicted lateral spreading displacement at a site with $(N_1)_{60} = 14$ would be much greater than that at an otherwise identical site with $(N_1)_{60} = 16$. Experimental evidence does not support such an abrupt change in soil behavior with changes in density.
2. *No difference in behavior for $(N_1)_{60} < 15$:* The predicted lateral spreading displacement at a site with $(N_1)_{60} = 5$ would be equal to that at an otherwise identical site with $(N_1)_{60} = 14$. Experimental evidence suggests that the soil characteristics that affect lateral spreading behavior do vary significantly over the range of densities associated with $(N_1)_{60} < 15$.
3. *No contribution from soils with $(N_1)_{60} > 15$:* The predicted lateral spreading displacement is unaffected by layers with $(N_1)_{60} > 15$. Experimental evidence (element and centrifuge tests) shows that soils at relative densities corresponding to $(N_1)_{60} > 15$ do develop permanent strain and can contribute to lateral spreading.
4. *No effect of depth on lateral spreading displacement:* The predicted lateral spreading displacement would be the same for a given layer of loose sand if it was located near the ground surface or located at a depth of, say, 10 m. Experimental evidence shows that the liquefaction behavior of soil is affected by initial effective confining pressure; furthermore, ground motion amplitudes are known to vary with depth.

Cumulative strain-based models such as those of Zhang et al. (2004) and Faris et al. (2006) use estimates of the cyclic strain induced in laboratory specimens of different density under cyclic loading conditions; these strains show smooth and continuous reductions in strain amplitude with increasing density from very loose to moderately dense conditions. The soil profile is treated as a stack of elements over which the potential shear strains, which are all assumed to fully develop in the field, are integrated to produce an estimated displacement index. The displacement index is then used with other variables to estimate actual surface displacement. These models use the experimentally measured mechanical behavior of soils to overcome the previously described limitations of T_{15} . However, the link between cyclic shear strains based on laboratory tests with no static shear stress and permanent shear strains in the presence of static shear stress is not well established, nor is the reasonableness of the implicit assumption that the shear strain potential is reached in all potentially liquefiable soil layers. Nevertheless, after

calibration, these models appear to predict observed lateral spreading displacements with similar levels of accuracy as the BY models.

DEVELOPMENT OF PREDICTIVE EQUATION

The goal of this research was to use recent improvements in understanding of the mechanics of liquefaction and lateral spreading and their effects on nonlinear site response to guide the development of improved predictive relationships for permanent displacement associated with lateral spreading. The investigation involved the following sequence of activities:

1. Use of a numerical model capable of describing the mechanical response of liquefiable soils under sloping ground conditions to develop a database of numerical lateral spreads that reflects the effects of the mechanics of liquefaction and nonlinear site response on lateral spreading.
2. Use of the numerical database to identify the basic form of a predictive relationship that is consistent with the mechanics of liquefaction and lateral spreading and that reflects their effects on nonlinear site response.
3. Calibration of the basic form of the predictive relationship using actual field case history data.

This procedure was intended to produce a predictive relationship that is consistent with the known mechanics of liquefaction, lateral spreading, and nonlinear site response, and also with actual field observations of lateral spreading.

Numerical Modeling of Lateral Spreading

While it is extremely difficult to make accurate *a priori* numerical predictions of phenomena as complicated as lateral spreading, valuable insight into the mechanics of the process can be obtained through numerical modeling. Numerical simulation can allow identification and evaluation of the relative importance of the parameters that influence lateral spreading displacements. In this investigation, numerical modeling was used to better understand the mechanics of lateral spreading and to guide the formulation of a predictive equation for lateral spreading displacement.

In modeling the development of permanent displacements due to lateral spreading, two important aspects of the mechanical behavior of liquefiable soils must be addressed. First, the fact that most of the permanent strain in an element of liquefiable soil loaded with an initial static shear stress occurs after initial liquefaction means that the soil model must accurately predict the onset of initial liquefaction. Second, the soil model must be capable of representing phase transformation behavior and its effects on the accumulation of permanent strain in the presence of an initial static shear stress.

Lateral spreading simulations were performed using one-dimensional, nonlinear, effective stress-based site response analyses as implemented in the computer program WAVE (Horne, 1996). WAVE uses a second-order accurate explicit finite difference scheme to compute the response of a layered soil deposit to vertically propagating shear waves.

The behavior of liquefiable soils is described in WAVE using the UWsand constitutive model (Kramer and Arduino, 1999). The UWsand model is capable of representing the nonlinear, inelastic behavior of “typical” liquefiable sands, i.e., sands that behave in accordance with empirical observations of field liquefaction behavior. The UWsand model uses a Mohr-Coulomb yield function, a hardening rule that constrains nonlinearity to match that described by a particular modulus reduction curve (in this case, the Seed-Idriss upper bound curve (Seed and Idriss, 1970)), the Cundall-Pyke hypothesis (Pyke, 1979) for determination of the plastic shear modulus upon stress reversal, and a non-associative flow rule that captures phase transformation behavior. UWsand was developed in a manner that would allow calibration so that pore pressure generation behavior consistent with that exhibited by typical sands in past earthquakes can be characterized as a function of $(N_1)_{60}$. The predicted response of UWsand for cyclic loading conditions with an initial, static shear stress are shown in Figure D.5; note the general similarity to the experimentally observed behavior in Figure D.2, which indicates UWsand’s ability to represent phase transformation behavior and the accumulation of permanent shear strain in the presence of an initial static shear stress. Without an initial static shear stress, UWsand predicts cyclic shear strains that vary with density and cyclic shear stress amplitude in a manner consistent with experimental results such as those shown in Figure D.3.

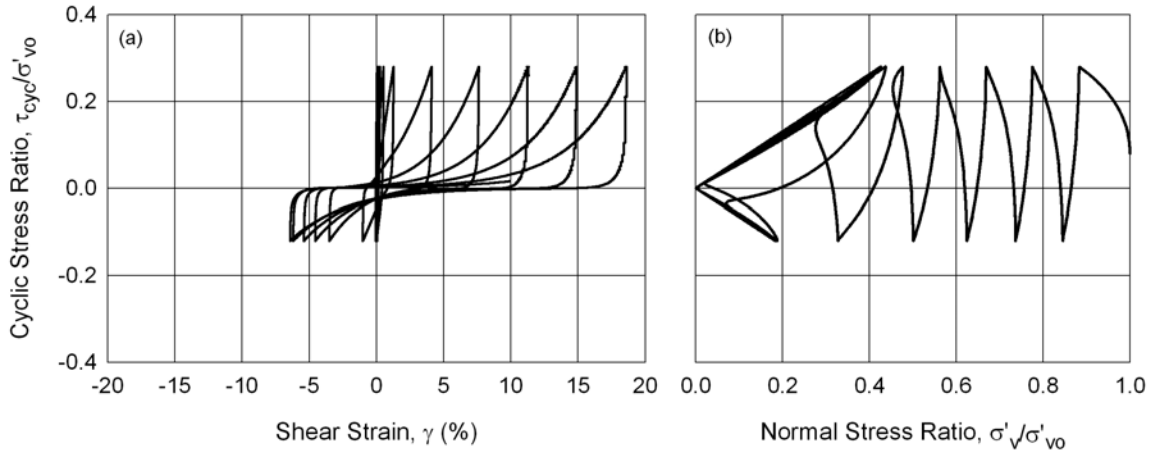


Figure D.5. Simple shear behavior of saturated sand predicted by UWsand model with non-zero initial shear stress: (a) stress-strain and (b) stress path behavior.

Numerical Database of Lateral Spreads

In order to identify the factors that most strongly influence lateral spreading behavior, a series of idealized soil profiles were subjected to a series of earthquake ground motions to produce a database of numerically-generated lateral spreads. Since the analyses were based on a model that represents the mechanical behavior of liquefiable soil, the permanent displacements in the numerical database are considered to reflect the effects of soil mechanics and nonlinear site response on lateral spreading displacements. The database was oriented toward determining the effects of soil density and its distribution with depth on lateral spreading displacement.

Idealized Soil Profiles

A series of idealized soil profiles were analyzed for this research; the profiles were intended to encompass the range of soil profile geometries and properties commonly encountered in areas underlain by liquefiable soils. The profiles used in these simulations are shown in Figure D.6. Certain groups of soil profiles were used to investigate the effects of different geometric or material characteristics; the *blowcount* group included profiles that were identical except for the $(N_1)_{60}$ value(s) of the liquefiable layer, the *depth* group had a liquefiable layer of constant thickness placed at different depths, the *thickness* group had liquefiable layers of different thickness placed at the same depth, and the *variability* group had soil profiles with equal mean $(N_1)_{60}$ but different degrees of spatial variability about the mean.

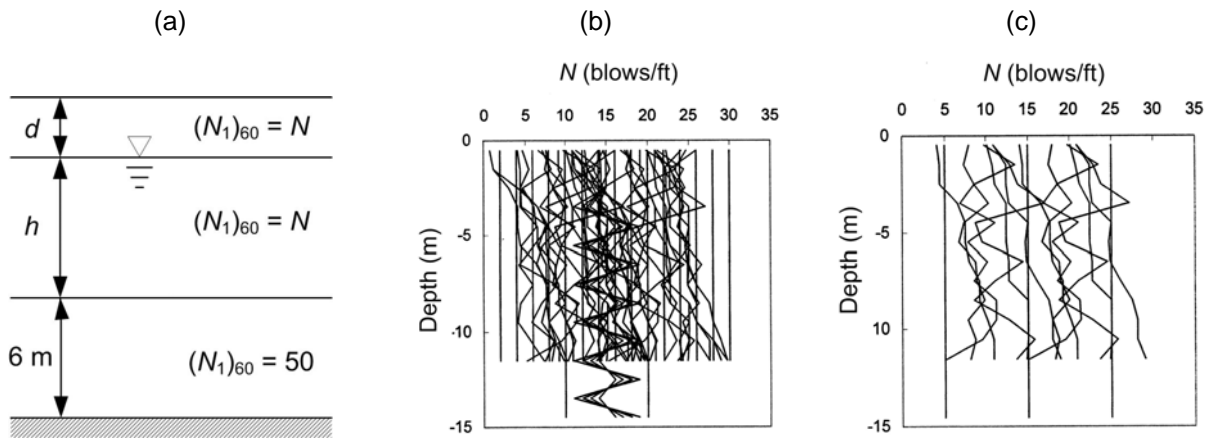


Figure D.6. Soil profiles used in development of numerical database: (a) nomenclature, (b) SPT resistances at depths shallower than $d+h$ for ground slope geometries, and (c) SPT resistances at depths shallower than $d+h$ for free-face geometries.

The above conditions were used for infinite slope inclinations of 1%, 2%, 3%, 4%, 5%, and 6% for the ground slope case, and for free-face ratios of 10, 20, and 30 for the free-face case. The variation of initial shear stress with depth was computed by finite element analysis for the free-face profiles. A total of 91 hypothetical soil profiles were analyzed for the ground slope case; after examination of the results of those analyses, a smaller set of 24 profiles was used for the free-face case.

Input Motions

The primary purpose of the numerical database was to gain insight into the effects of soil profile characteristics on lateral spreading displacements. Therefore, the ground slope soil profiles were subjected to three input motions scaled to peak accelerations of 0.1g, 0.2g, and 0.3g, and the free-face profiles to the same motions scaled only to 0.3g.

Results

The various combinations of soil profiles and input motions produced a total of 5,130 numerical simulations of lateral spreading. Interpretation of the results of the *blowcount* and *depth* groups offered particularly useful insight into their relationship to lateral spreading displacement.

The variation of permanent displacement with $(N_1)_{60}$ for a single motion from the *blowcount* group analyses is shown in Figure D.7(a). As would be expected, permanent

displacement was observed to decrease with increasing $(N_1)_{60}$. Note that the decrease is relatively smooth and continuous, and that significant displacements occur for $(N_1)_{60} > 15$. These results suggest that a cumulative thickness parameter based on a blowcount-weighted summation scheme, in contrast to the simple summation upon which T_{15} is based, could be more consistent with actual soil behavior and therefore more suitable for lateral spreading displacement prediction.

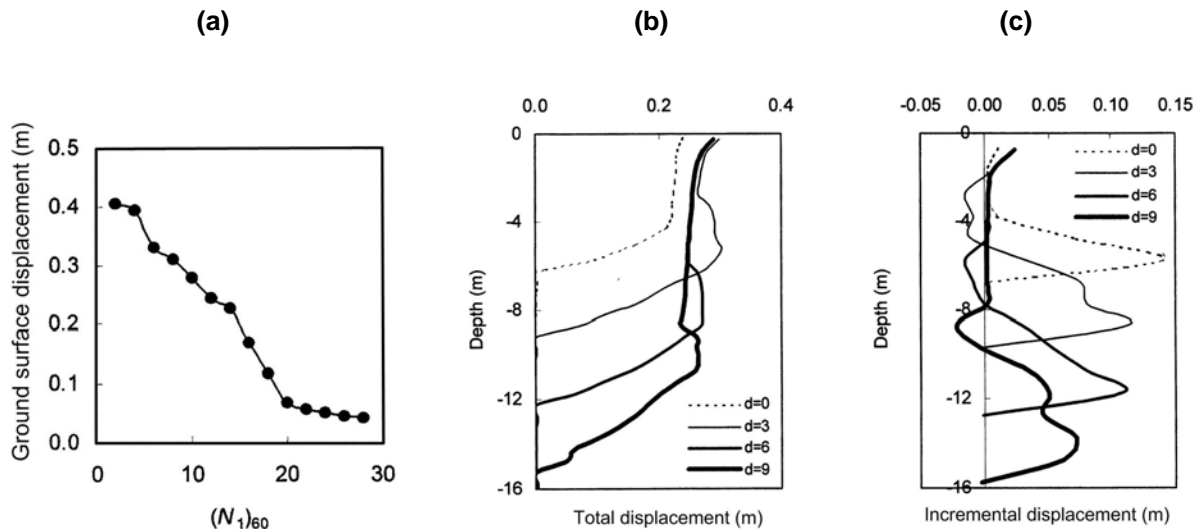


Figure D7. (a) Variation of computed permanent ground surface displacement with $(N_1)_{60}$ for ground slope case (3% slope) with $FC = 20\%$, $d = 3\text{m}$, and $h = 6\text{m}$, (b) variation of computed total permanent displacement with depth for $(N_1)_{60} = 10$, $h = 6\text{m}$, $FC = 20\%$, and 3% ground slope, and (c) variation of incremental permanent displacements with depth.

The *depth* group consisted of a 6-m-thick liquefiable layer placed at different depths within the soil profile. Figures D.7(b) and D.7(c) shows the variation of total and incremental permanent displacement with layer depth; the incremental displacement is the permanent displacement of each 1-m-thick sublayer within the soil profile. The variation of computed displacement with depth is similar to that measured in the field and in model tests, as shown in Figure D.1. The results of the depth group analyses show that the contribution of a particular soil layer to permanent displacement decreases as the depth of that soil layer increases, and suggest that a cumulative thickness parameter for lateral spreading displacement prediction could also be depth-weighted.

Other soil profile groups helped illustrate different aspects of lateral spreading behavior. The *thickness* group showed that the incremental displacements were spread over a greater range of depths for thick profiles than for thin profiles, which suggests that a cumulative parameter

would be appropriate. The *variability* group indicated that permanent displacement increased only slightly with increasing variability of blowcounts about constant or linearly varying trends.

IDENTIFICATION OF FORM OF PREDICTIVE RELATIONSHIP

The basic form of the predictive relationship was arrived at by starting with the Bartlett and Youd form and determining whether or not improvements could be made to any or all of the terms. For purposes of discussion, the terms will be divided into those associated with material properties, slope geometry, and earthquake loading. Additional details are available in Baska (2002).

Material Property Terms

The results of the numerical database of lateral spreads were used to develop an improved representation of material properties. In the BY relationship, material properties are characterized by T_{15} , F_{15} , and $D50_{15}$. Based on the results of the numerical simulations, which reflect current understanding of the mechanics of liquefaction and lateral spreading, a new “equivalent thickness” parameter was developed. The equivalent thickness parameter was intended to reflect (a) the trend of increasing permanent displacement with increasing thickness of loose soil, (b) the smoothly decreasing trend of permanent displacement with increasing SPT blowcount, and (c) the smoothly decreasing trend of permanent displacement with increasing depth.

More than 30 expressions for definition of equivalent thickness were investigated; in the end, an expression of the following form was found to provide good agreement with the numerical lateral spread database

$$T^*(m) = \sum_{i=1}^n t_i e^{-m_1 N_i - m_2 z_i} \quad (D.5)$$

where n = number of sublayers of saturated cohesionless soil with $FS_L \leq 1.0$, t_i = thickness (in meters) of the i^{th} sublayer, $N_i = (N_1)_{60\text{-cs}}$ for the i^{th} sublayer, z_i = depth to the center of the i^{th} sublayer, and m_1 and m_2 are parameters whose values are determined by regression. This

expression considers T^* to be comprised of contributions from a number of sublayers, each of which is weighted by clean sand blowcount and depth. It therefore allows T^* to increase with increasing liquefiable soil thickness and to decrease with increasing blowcount and depth, and to do so in a manner that varies smoothly with each of those parameters.

Slope Geometry Terms

For a given slope, the BY-type models characterize the geometry of the ground surface using the terms S (for the ground slope model) and W (free-face model). Several alternative parameters for describing the ground surface geometry were investigated, but none were found to be appreciably better than S and W .

Ground Motion Terms

As previously discussed, BY-type relationships characterize earthquake loading through the source parameters, M and R , because measured ground motions were not available for the case histories on which BY-type relationships are based. Although permanent displacements are undoubtedly influenced by ground motion amplitude, frequency content, and duration, there remain insufficient data with which to accurately parameterize these characteristics at the locations of observed lateral spreads. Based on these considerations, the earthquake loading terms of the BY-type relationships were retained.

Basic Form

After a thorough investigation of numerous potential expressions for characterization of material, geometric, and earthquake loading effects, the basic predictive relationship initially evaluated with respect to the actual case history database was of the form

$$f_D(D_H) = c_1 + m_3 f_{T^*}(T^*) + m_4 f_F(F) + m_5 f_D(D_{50}) + g_1 f_S(S) + g_2 f_W(W) \quad (D.6)$$

$$+ e_1 f_M(M) + e_2 f_R(R) + e_3 f_{M,R}(M, R)$$

where c_1 is a general coefficient and the coefficients m_i , g_i , and e_i are those associated with material, geometry, and earthquake loading terms, respectively. In this form, g_1 would be zero for free-face cases and g_2 would be zero for ground slope cases.

CALIBRATION OF PREDICTIVE RELATIONSHIP AGAINST EMPIRICAL DATABASE

The final form of the predictive equation was obtained by calibrating the basic form against the empirical (case history) database, evaluating the contribution of each term to the equation, and adjusting the form of the equation as required to produce the best possible fit to the data with the simplest possible form of the equation.

Empirical Database

An empirical database with which to calibrate an equation of the form of Equation D.6 must contain sufficient information to identify all of the variables used in that equation. In particular, the term T^* requires borehole logs with SPT data extending to the bottom of all potentially liquefiable soils at each lateral spreading case history site.

The database used in this investigation was a modified version of the database of Bartlett and Youd (1992), which contained 448 horizontal displacement measurements from 29 lateral spreading sites in seven earthquakes. It should be noted that the case history database includes multiple points from the same lateral spread; these points correspond to different geometric or material conditions at different locations across the spread. The eight cases in which "... lateral spread displacements were clearly impeded by shear or compression forces along the margins or at the toe of the lateral spread ..." (Youd et al., 2002) were removed.

The database required further modification to account for the fact that many boreholes were terminated at depths below which soils that could contribute to lateral spreading displacement still existed. Boreholes at lateral spreading sites in Niigata and Noshiro following the Niigata and Nihonkai-Chubu earthquakes were commonly terminated at depths of 20 m and 10 m, respectively, regardless of the soil type or penetration resistance at those depths. In many cases, borings were terminated in saturated sands with SPT resistances not much greater than 15. The use of prematurely terminated SPT logs would be expected to underestimate T^* and

therefore systematically underpredict lateral spreading displacement. This behavior was confirmed by analyzing the entire database and three subsets of that database obtained by removing cases in which the deepest SPT resistance did not exceed limiting values of $(N_1)_{60,cs} = 20, 25,$ and 30 blows/ft. The results of those analyses showed that displacement predictions were systematically biased toward underprediction and highly dispersed when the entire database (equivalent to a limiting $(N_1)_{60,cs}$ value of zero) was used and also, though to a lesser degree, when limiting values of 20 and 25 blows/ft were used; with the limiting value of $(N_1)_{60,cs} = 30$, displacement predictions were unbiased and less dispersed. For this reason, the database was further modified to include only cases for which corresponding boreholes extended to a depth sufficient to include all saturated cohesionless soils with $(N_1)_{60,cs} \leq 30$. This modification reduced the size of the database to 151 case histories.

Finally, the database was augmented in the same manner as Bartlett and Youd (1992) using 19 case histories from large source-site distance (Ambraseys, 1988). These case histories helped constrain the prediction of lateral spreading displacement at large distances, a situation for which data were sparse in the original Bartlett & Youd database.

Regression Analyses

Model calibration was accomplished by regression analysis using the commercial statistical software package S-Plus. An extensive series of analyses were performed on a variety of different forms of Equation D.6 – the forms differed in the transformations (i.e., linear, logarithmic, square root) applied to the different variables and in the number of predictive variables used. The quality of each model's predictive capability was evaluated in terms of the coefficient of determination (R^2) and the distribution of residuals. Each variable on the right side of Equation D.6 was considered in its unaltered state (i.e., for a variable, $X, f_X = X$) and in transformed states (e.g., $f_X = \log X$). The dependent variable D_H was also considered in its unaltered state and after logarithmic and square root transformations.

Results

The regression analyses indicated that the observed permanent displacements in the case history database were best predicted by a model in which the mean value of the square root of lateral spreading displacement is given by

$$\sqrt{D_H} = \frac{\beta_1 + \beta_2 T_{gs}^* + \beta_3 T_{ff}^* + 1.231M_w - 1.151 \log R^* - 0.01R + \beta_4 \sqrt{S} + \beta_5 \log W}{1 + 0.0223(\beta_2 / T_{gs}^*)^2 + 0.0135(\beta_3 / T_{ff}^*)^2} \quad (D.7)$$

where $T_{gs}^* = 2.586 \sum_{i=1}^n t_i \exp[-0.05N_i - 0.04z_i] \geq 0.001$ m

$T_{ff}^* = 5.474 \sum_{i=1}^n t_i \exp[-0.08N_i - 0.10z_i] \geq 0.001$ m

n = number of liquefied sublayers, $R^* = R + 10^{0.89M - 5.64}$ in km, $N_i = (N_1)_{60,cs}$ (as calculated using the fines correction of Youd et al. (2002)) for the i^{th} sublayer, t_i = sublayer thickness in meters (limited to a maximum value of 1 m), and the model-specific β coefficients are as indicated in Table D2. The expressions for T_{gs}^* and T_{ff}^* are scaled so that a one-meter-thick layer of soil at a depth of 5 m with $(N_1)_{60,cs} = 15$ would have a T^* value of 1.0 m. The denominator on the right side of Equation 10 was added following regression to force the predicted displacements to approach zero as the T^* terms approach zero (which would have occurred “automatically” if a logarithmic, rather than square root, transformation of D_H had been used). The median lateral spreading displacement, \hat{D}_H , can be obtained from the results of Equation (D.7) as

$$\hat{D}_H = \begin{cases} 0 & \text{for } \sqrt{D_H} \leq 0 \\ \left(\sqrt{D_H}\right)^2 & \text{for } \sqrt{D_H} > 0 \end{cases} \quad (D.8)$$

Table D2. Coefficients for proposed model.

Model	β_1	β_2	β_3	β_4	β_5
Ground slope	-7.207	0.067	0.0	0.544	0.0
Free face	-7.518	0.0	0.086	0.0	1.007

BY-type models have used a logarithmic transformation of D_H , which has the desirable characteristic of eliminating negative displacements. However, it also eliminates the possibility of zero lateral spreading displacement for small and/or distant earthquakes. The use of the square root transformation in the proposed model indicates that there are conditions under which

zero lateral spreading displacements are expected since some combinations of variables in Equation (D.7) (e.g., low magnitudes and large distances) can lead to negative values of $\sqrt{D_H}$. Since these combinations represent weaker loading and/or greater resistance than those that produce zero displacement, Equation (D.8) assigns zero median displacement to them.

The level of agreement between observed and median predicted displacements is shown in Figure D.8; the R^2 value of 0.849 is only slightly higher than that (0.836) reported by Youd et al. (2002). The square root transformation of D_H was found to produce residuals that were approximately normally distributed with constant variance, $\sigma_{\sqrt{D_H}}^2 = 0.0784$. The probability of exceeding some non-negative lateral spreading displacement, d , can therefore be estimated as

$$P[D_H > d] = 1 - \Phi \left[\frac{\sqrt{d} - \sqrt{D_H}}{\sigma_{\sqrt{D_H}}} \right] = 1 - \Phi \left[3.571 (\sqrt{d} - \sqrt{D_H}) \right] \quad (\text{D.9})$$

where Φ is the standard normal cumulative distribution. For example, the probabilities of exceeding different lateral spreading displacement levels for a ground-slope site with $T_{gs}^* = 3$ m at $R = 20$ km are shown for different ground slopes and earthquake magnitudes in Figure D.9. It should be noted that negative values of $\sqrt{D_H}$, which can occur for some combinations of input parameters, can be used to compute exceedance probabilities.

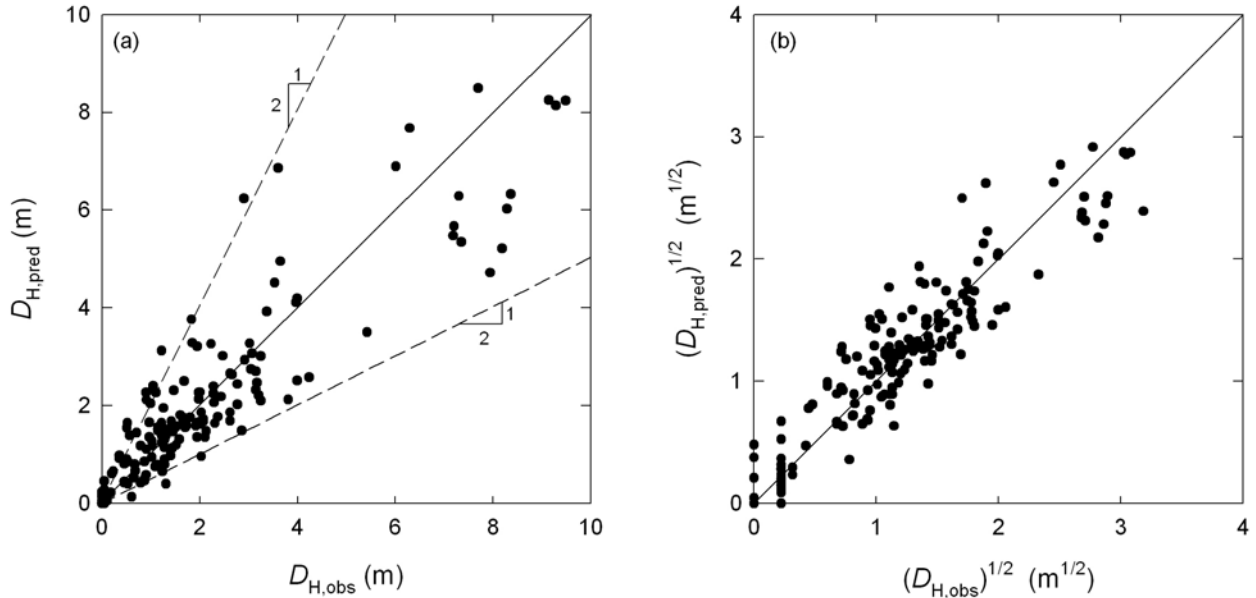


Figure D.8. Relationship between predicted and observed lateral spreading displacements: (a) natural scale, and (b) transformed scale.

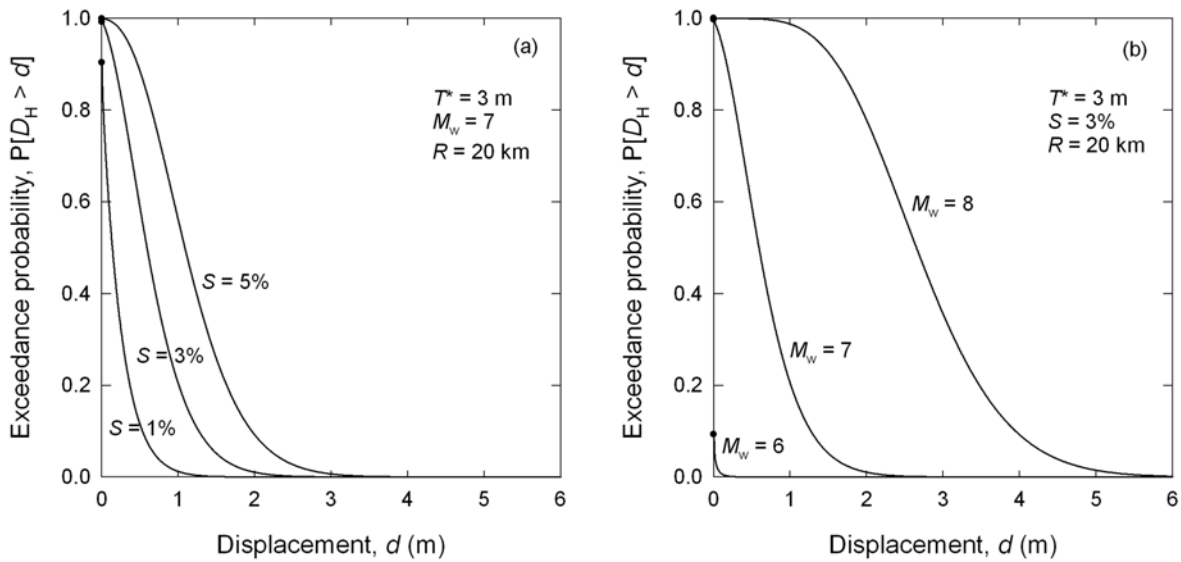


Figure D.9. Displacement exceedance probabilities for (a) three ground slopes, and (b) three magnitudes.

The D_{50} term in Equation D.9 was found not to improve displacement predictions and therefore does not appear in Equation D.10. The database was also parsed into cases in which liquefiable layers were and were not overlain by less permeable layers; the addition of a term

accounting for the presence of an impermeable cap was found not to improve displacement predictions with the available case history database.

Example Application

San Fernando Juvenile Hall suffered extensive damage from lateral spreading in the 1971 San Fernando ($M = 6.4$) earthquake (Thompson, 1973; Bennett, 1989). The lateral spread was approximately 1200 m long and 270 m wide with an average slope of 1.5 percent (Youd, 1973). The maximum displacement has been reported as 1.5 m (Youd, 1973; Bennett, 1989), but photogrammetric measurements indicate a maximum displacement of 2.3 m (O'Rourke et al., 1992). The zone of permanent deformation coincided with zones of loose, saturated sandy silt located at depths of 4 m to 15 m below the ground surface.

Bennett (1989) investigated the site with a series of borings and CPT soundings; data used to compute T_{gs}^* from a boring located in the central portion of the spread is summarized in Table D3. Table D3 also includes fines content, mean grain size, and factor of safety values computed by Bartlett and Youd (1992); the very high factors of safety are for layers either above the water table or with clay contents so high that the layers were judged non-susceptible to liquefaction. The analyses show that liquefaction is expected to have been triggered ($FS_L \leq 1.0$) at two depths in this boring, the lower of which contributes to T_{gs}^* but not to T_{15} (since $(N_1)_{60} > 15$). Considering similar data from four other borings within the Juvenile Hall spread, values of T_{gs}^* range from 1.41 m to 2.83 m (average = 2.21 m). Using those values, along with $M = 6.4$, $R = 0.2$ km, and $S = 1.5\%$, Equation (10) predicts median displacements ranging from 1.65 m to 1.90 m (with an average of 1.79 m). Corresponding values of T_{15} range from 0.91 m to 3.81 m; using the same data, plus the appropriate F_{15} and $D50_{15}$ values for each boring, the Youd et al. (2001) model (Equation D.1) predicts median displacements ranging from 0.09 m to 1.24 m (with an average of 0.60 m). The Zhang et al. (2004) model predicts displacements ranging from 0.81 m to 1.79 m (with an average of 1.26 m). The Faris et al. (2006) model predicts displacements ranging from 0.71 m to 1.28 m (with an average of 1.14 m). The permanent displacements predicted by the various models are illustrated in Figure D.10; the median permanent displacements predicted by the proposed model appear to be closer to the observed permanent displacements than those of the other empirical models for this case history.

Table D.3. Data from Juvenile Hall lateral spreading case history (after Bennett, 1989; Bartlett and Youd, 1992).

Description	Unit	t_i (m)	$(N_1)_{60}$	FC (%)	$(N_1)_{60-cs}$	D_{50} (mm)	FS_L	z_i (m)	$T_{15,i}$ (m)	$T_{gs,i}^*$ (m)
Silt with sand	A1	0.61	6.8	77	13.2	0.03	99.99	0.31	0	0
Silt	A1	0.91	9.5	89	16.4	0.032	99.99	1.07	0	0
Silt	A1	1.13	6.2	83	12.4	0.042	99.99	2.09	0	0
Sandy silt	B1	0.92	2.8	64	8.4	0.037	99.99	3.11	0	0
Sandy silt	B1	0.70	3.9	74	9.7	0.042	99.99	3.92	0	0
Silt with sand	B1	0.81	3.7	74	9.4	0.042	0.29	4.68	0.81	1.08
Silt with sand	B1	0.10	6.1	65	12.3	0.041	0.26	5.13	0.10	0.11
Sandy silt	B2	0.16	6.1	65	12.3	0.041	99.99	5.26	0	0
Silt with sand	B2	0.67	8.2	72	14.8	0.033	99.99	5.68	0	0
Sandy silt	B2	1.31	4.4	66	10.3	0.037	99.99	6.67	0	0
Sandy silt	B2	0.45	18.1	61	26.7	0.050	99.99	7.55	0	0
Sandy silt	C	1.07	17.3	61	25.8	0.050	1.02	8.31	0	0
Sandy silt	C	0.41	17.0	61	25.4	0.050	1.00	9.05	0	0.20
Sandy silt	C	0.05	17.0	61	25.4	0.050	1.00	9.28	0	0.02
Silty sand	C	1.07	19.3	46	28.2	0.095	99.99	9.84	0	0
Sandy silt	C	0.91	18.6	52	27.3	0.069	99.99	10.80	0	0
									$T_{15} = 0.91$ m	$T_{gs}^* = 1.41$ m

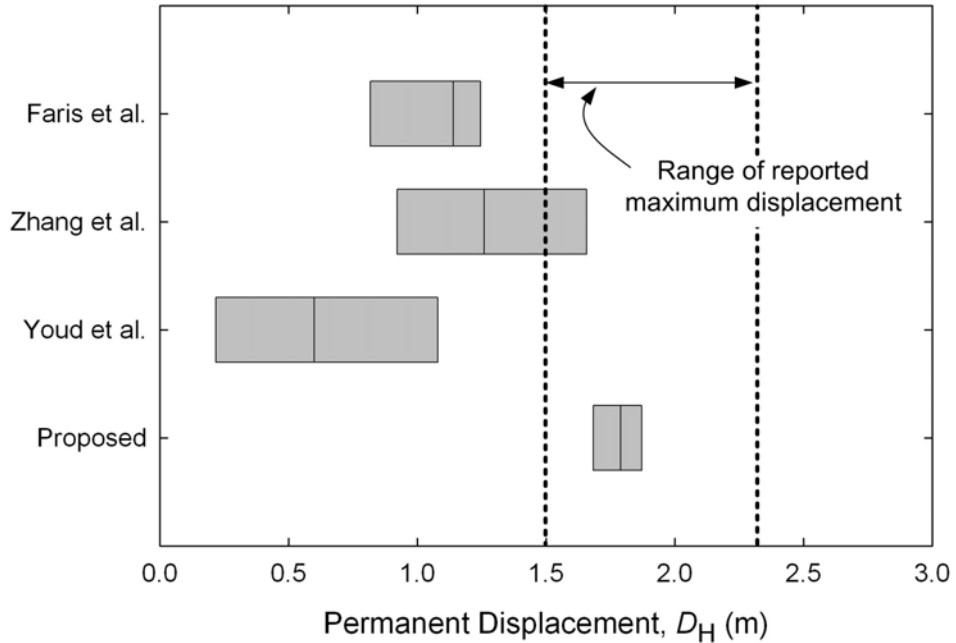


Figure D.10. Illustration of lateral spreading displacements predicted by previous and proposed models for Juvenile Hall case history.

Limitations

Like any empirical model, the proposed model is most applicable to conditions that are consistent with the field observation database against which it was calibrated. The recommended ranges of variable values are presented in Table D.4. Also, as in nearly all preceding lateral spreading models, the individual data points within the case history database were treated as independent, although one would expect a degree of correlation between multiple displacement measurements from some individual lateral spreads.

Table D.4. Recommended ranges of input variables for proposed lateral spreading model.

Variable	Description	Range
T^*	Equivalent sublayer thickness (m)	0.001 to 20 m
M_w	Moment magnitude	6.0 to 8.0
R	Hypocentral distance (km)	1 to 100 km
S	Ground slope (%)	0 to 6%
W	Free-face ratio (%)	0 to 20%

REFERENCES

- Abdoun, T., Dobry, R., O'Rourke, T.D., and Goh, S.H. (2003). "Pile response to lateral spreads: Centrifuge modeling," *J. Geotech. Geoenviron. Eng.*, ASCE, 129(10), 869-878.
- Ambraseys, N.N. (1988). "Engineering seismology," *Earthquake Engineering and Structural Dynamics*, 17, 1-105.
- Bardet, J.P., Tobita, T., Mace, N., and Hu, J. (1999a). "Large-scale modeling of liquefaction-induced ground deformation; Part I: A four-parameter MLR model," *Proceedings of the Seventh U.S. – Japan Workshop on Earthquake Resistant Design of Lifeline Facilities and Countermeasures Against Soil Liquefaction*, Technical Report MCEER-99-0019, Multidisciplinary Center for Earthquake Engineering Research, 155-174.
- Bardet, J.P., Mace, N., Tobita, T., and Hu, J. (1999b). "Large-scale modeling of liquefaction-induced ground deformation; Part II: MLR model applications and probabilistic model," *Proceedings of the Seventh U.S. – Japan Workshop on Earthquake Resistant Design of Lifeline Facilities and Countermeasures Against Soil Liquefaction*, Technical Report MCEER-99-0019, Multidisciplinary Center for Earthquake Engineering Research, 175-190.
- Bartlett, S.F. and Youd, T.L. (1992). "Empirical analysis of horizontal ground displacement generated by liquefaction-induced lateral spread," *Technical Report NCEER-92-0021*, National Center for Earthquake Engineering Research, Buffalo, New York.

- Baska, D.A. (2002). "An analytical/empirical model for prediction of lateral spreading displacements," *Ph.D. Dissertation*, University of Washington, Seattle, Washington, 539 pp.
- Bennett, M. J. (1989). "Liquefaction analysis of the 1971 ground failure at the San Fernando Valley Juvenile Hall, California." *Bull. Assoc. Eng. Geologists*, 26(2), 209–226.
- Boulanger, R. W., and Truman, S. P. (1996). "Void redistribution in sand under post-earthquake loading." *Canadian Geotech. J.*, 33, 829-834.
- Boulanger, R.W., Mejia, L.H., and Idriss, I.M. (1997). "Liquefaction at Moss Landing during Loma Prieta earthquake," *J. Geotech. Geoenviron. Eng.*, ASCE, 123(5), 453-467.
- Cetin, K.O., Youd, T.L., Seed, R.B., Bray, J.D., Stewart, J.P., Durgunoglu, H.T., Lettis, W., and Yilmaz, M.T. (2004). "Liquefaction-induced lateral spreading at Izmit Bay during the Kocaeli (Izmit)-Turkey earthquake," *J. Geotech. Geoenviron. Eng.*, ASCE, 130(12), 1300-1313.
- Faris, A.T., Seed, R.B., Kayen, R.E., and Wu, J. (2006). "A semi-empirical model for the estimation of maximum horizontal displacement due to liquefaction-induced lateral spreading," *Proceedings*, 8th U.S. National Conference on Earthquake Engineering, in press.
- Fiegel, G. L., and Kutter, B. L. (1994a). "Liquefaction mechanism for layered soils." *J. Geotech. Eng.*, ASCE, 120(4), 737–755.
- Hamada, M., Towhata, I., Yasuda, S., and Isoyama, R. (1987). "Study of permanent ground displacement induced by seismic liquefaction," *Computers and Geotechnics*, Elsevier Applied Science Publishers, 4, 197-220.
- Hamada, M. and Wakamatsu, K. (1998). "Liquefaction-induced ground displacement triggered by quaywall movement," *Soils and Foundations*, Special Issue, 2, 85-95.
- Horne, J.C. (1996). "Effects of liquefaction-induced lateral spreading on pile foundations," *Ph.D. dissertation*, University of Washington, Seattle, Washington, 371 pp.
- Ishihara, K., Tatsuoka, F., and Yasuda, S. (1975). "Undrained deformation and liquefaction of sand under cyclic stresses," *Soils and Foundations*, 15(1), 29-44.
- Ishihara, K. and Yoshimine, M. (1992). "Evaluation of settlements in sand deposits following liquefaction during earthquakes," *Soils and Foundations*, 32(1), 173-188.
- Kramer, S.L. and Arduino, P. (1999). "Constitutive modeling of cyclic mobility and implications for site response," *Proceedings, Second International Conference on Earthquake Geotechnical Engineering*, Lisbon, Portugal, 3, 1029-1034.
- Kokusho, T. (1999). "Water film in liquefied sand and its effect on lateral spread." *J. Geotech. Geoenviron. Eng.* 125(10), 817–826.
- Kulasingam, R., Malvick, E. J., Boulanger, R. W., and Kutter, B. L. (2004). "Strength loss and localization at silt interlayers in slopes of liquefied sand." *J. Geotech. Geoenviron. Eng.*, ASCE, 130(11), 1192-1202.
- Kutter, B.L., Gajan, S., Manda, K.K., and Balakrishnan, A. (2004). "Effects of layer thickness and density on settlement and lateral spreading," *J. Geotech. Geoenviron. Eng.*, ASCE, 130(6), 603-614.

- Pyke, R.M. (1979). "Nonlinear soil models for irregular cyclic loadings," *J. Geotech. Engineering Division*, ASCE, 105(GT6), 715-726.
- Rauch, A.F. and Martin, J.R. (2000). "EPOLLS model for predicting average displacements on lateral spreads," *J. Geotech. Geoenviron. Eng.*, ASCE, 126(4), 360-371.
- Seed, H.B. and Idriss, I.M. (1970). "Soil moduli and damping factors for dynamic response analyses," *Report No. EERC 70-10*, Earthquake Engineering Research Center, University of California, Berkeley.
- Seed, H.B., Lee, K.L., Idriss, I.M., and Makdisi, F. (1973). "Analysis of the slides in the San Fernando dams during the earthquake of Feb. 9, 1971," *Report No. EERC 73-2*, Earthquake Engineering Research Center, University of California, Berkeley, 150 pp.
- Seed, H.B., Lee, K.L., Idriss, I.M., and Makdisi, F. (1975). "The slides in the San Fernando dams during the earthquake of Feb. 9, 1971," *J. Geotech. Geoenviron. Eng.*, ASCE, 101(7), 651-688.
- Seed, H.B. (1979). "Soil liquefaction and cyclic mobility evaluation for level ground during earthquakes," *J. Geotech. Eng.*, ASCE, 105(2), 201-255.
- Shamoto, Y., Zhang, J.-M., and Tokimatsu, K. (1998). "Methods for evaluating residual post-liquefaction ground settlement and horizontal displacement," *Soils and Foundations*, Special Issue No. 2, 69-83.
- Sharp, M.K., Dobry, R., and Abdoun, T. (2003). "Liquefaction centrifuge modeling of sands of different permeability," *J. Geotech. Geoenviron. Eng.*, ASCE, 129(12), 1083-1091.
- Tokimatsu, K. and Yoshimi, Y. (1983). "Empirical correlation of soil liquefaction based on N-value and fines content," *Soils and Foundations*, 23(4), 56-74.
- Wu, J., (2002). "Liquefaction triggering and post liquefaction deformations of Monterey 0/30 Sand under uni-directional cyclic simple shear loading," *Ph. D. Dissertation*, University of California, Berkeley, 509 pp.
- Youd, T.L. and Perkins, D.M. (1987). "Mapping of Liquefaction Severity Index," *J. Geotech. Eng.*, ASCE, 113(11), 1374-1392.
- Youd, T.L. et al. (2001). "Liquefaction resistance of soils: Summary report from the 1996 NCEER and 1998 NCEER/NSF workshops on evaluation of liquefaction resistance of soils," *J. Geotech. Geoenviron. Eng.*, ASCE, 127(10), 817-833.
- Youd, T.L., Hansen, C.M., and Bartlett, S.F. (2002). "Revised multilinear regression equations for prediction of lateral spread displacement," *J. Geotech. Geoenviron. Eng.*, ASCE, 128(12), 1007-1017.
- Zhang, G., Robertson, P.K., and Brachman, R.W.I. (2004). "Estimating liquefaction-induced lateral displacements using the standard penetration test or cone penetration test," *J. Geotech. Geoenviron. Eng.*, ASCE, 130(8), 861-871.

Appendix E

Performance-Based Procedure for Lateral Spreading Displacement

In practice, lateral spreading displacements are usually evaluated using a deterministic lateral spreading model and a single scenario corresponding to a single ground motion hazard level, for example, for ground motions with a 475-year return period. In contrast, a performance-based approach incorporates a probabilistic lateral spreading model and contributions from *all* possible earthquake scenarios.

Performance-based earthquake engineering (PBEE) is generally formulated in a probabilistic framework to evaluate the risk associated with earthquake shaking at a particular site. The risk can be expressed in terms of economic loss, fatalities, or other measures. The Pacific Earthquake Engineering Research Center (PEER) has developed a probabilistic framework for PBEE (Cornell and Krawinkler, 2000; Krawinkler, 2002; Deierlein et al., 2003) that computes risk as a function of ground shaking through the use of several intermediate variables. The ground motion is characterized by an *Intensity Measure*, *IM*, which could be any one of a number of ground motion parameters (e.g., a_{\max} , Arias intensity, etc.). The effects of the *IM* on a system of interest are expressed in terms used primarily by engineers in the form of *Engineering Demand Parameters*, or *EDPs* (e.g., excess pore pressure, permanent displacement, etc.). The physical effects associated with the *EDPs* (e.g., settlement, cracking, etc.) are expressed in terms of *Damage Measures*, or *DMs*. Finally, the risk associated with the *DM* is expressed in a form that is useful to decision-makers by means of *Decision Variables*, *DV* (e.g., repair cost, downtime, etc.). The mean annual rate of exceedance of various *DV* levels, λ_{DV} , can be expressed in terms of the other variables as

$$\lambda_{dv} = \sum_{k=1}^{N_{DM}} \sum_{j=1}^{N_{EDP}} \sum_{i=1}^{N_{IM}} P[DV > dv | DM = dm_k] P[DM = dm_k | EDP = edp_j] P[EDP = edp_j | IM = im_i] \Delta \lambda_{im_i} \quad (\text{E.1})$$

where $P[a|b]$ describes the conditional probability of a given b , and N_{DM} , N_{EDP} , and N_{IM} are the number of increments of *DM*, *EDP*, and *IM*, respectively. Extending this approach to consider epistemic uncertainty in *IM*, although not pursued in this paper, is straightforward. By integrating over the entire hazard curve (approximated by the summation over $i = 1, N_{IM}$), the

performance-based approach includes contributions from all return periods, not just the return periods mandated by various codes or regulations.

The portion of the performance-based process that geotechnical engineers are most commonly involved with is the estimation of response expressed by the *EDP*. This process can be extracted from Equation (E.1) and formulated in terms of the mean annual rate of *EDP* exceedance, i.e., as

$$\lambda_{edp} = \sum_{i=1}^{N_M} P[EDP > edp | IM = im_i] \Delta \lambda_{im_i} \quad (E.2)$$

ALTERNATIVE FORM OF BASKA MODEL

As indicated above, development of a performance-based lateral spreading procedure requires a lateral spreading model capable of predicting the probability distribution of lateral spreading displacement. As a result, deterministic models, such as the previously described Youd et al. (2002) and Zhang et al. (2004) models, are not suitable for performance-based analyses. The form of the Baska (2002) lateral spreading model, however, is well suited for development of a performance-based lateral spreading procedure.

Consider the Baska (2002) lateral spreading model for ground slope cases, as described in Appendix D. The terms on the right side of Equation D.7 can be grouped into those associated with loading, site conditions, and uncertainty, thereby allowing the relationship to be written as

$$\sqrt{D_H} = \mathbf{L} + \mathbf{S} + \boldsymbol{\varepsilon} \quad (E.3)$$

where the loading, site, and uncertainty terms are respectively defined as

$$\mathbf{L} = 1.231M - 1.151 \log R^* - 0.01R$$

$$\mathbf{S} = \beta_1 + \beta_2 T_{gs}^* + \beta_3 T_{ff}^* + \beta_4 \sqrt{S} + \beta_5 \log W$$

$$\boldsymbol{\varepsilon} = \sigma_{\sqrt{D_H}} \Phi^{-1}[P]$$

and P is the probability of exceeding the lateral spreading displacement, D_H . The loading term is a function of magnitude and distance, as are typical attenuation relationships. In fact, the

expression for the loading term can be interpreted as an attenuation relationship for Baska's loading parameter, \mathbf{L} . The relationship is shown graphically in Figure E.1.

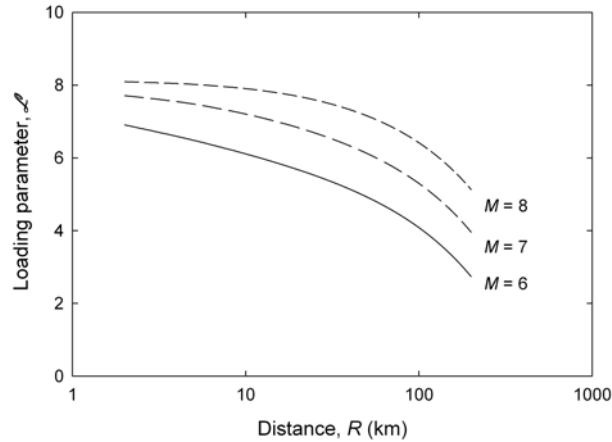


Figure E.1. Variation of loading parameter, \mathbf{L} , with magnitude and distance.

The probability of exceeding some lateral spreading displacement level, d , is illustrated schematically in Figure E.2. From Equation 10, lateral spreading displacement increases linearly with \mathbf{L} , so the relationship between median displacement and \mathbf{L} has unit slope and an intercept that depends on the site parameter, \mathbf{S} , i.e., on material properties (standard penetration test (SPT) resistance) and geometry (depth of liquefiable soils and ground slope). However, the square root transformation can lead, as illustrated by the probability distribution shown in Figure E.2, to some finite probability of negative values of $\sqrt{D_H}$, which represent the probabilities of zero displacement. Given Baska's constant value of $\sigma_{\sqrt{D_H}} = 0.28$, the probability of zero displacement depends on the size of the intercept and the value of \mathbf{L} . If the intercept is small (thin/dense liquefiable layers and/or flat slope) and the loading is low (low M and/or high R), the probability of zero displacement will be high. The combination of M and R values at which the Baska (2002) model predicts zero displacement corresponds well to the bounding conditions for field observations of liquefaction reported by Ambraseys (1988).

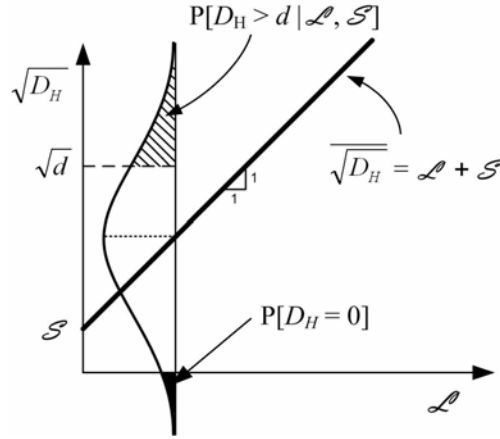


Figure E.2. Schematic illustration of variation of $\sqrt{D_H}$ with L and S for Baska model.

PERFORMANCE-BASED IMPLEMENTATION OF THE BASKA MODEL

By using the alternative formulation of the Baska (2002) model, a performance-based lateral spreading model can be expressed (assuming a single source for simplicity) in terms of lateral spreading displacement conditional upon the site term, i.e., as

$$\lambda_{d|s} = \sum_{i=1}^{N_L} P[D_H > d | \mathbf{s}, \mathbf{L}_i] \Delta \lambda_{L_i} \quad (\text{E.4})$$

which, introducing the mean annual rate of exceedance of a minimum event of interest, ν , can also be written as

$$\lambda_{d|s} = \nu \sum_{i=1}^{N_L} P[D_H > d | \mathbf{s}, \mathbf{L}_i] P[\mathbf{L}_i] \quad (\text{E.5})$$

Recognizing that $\mathbf{L} = f(M, R)$ and making the usual assumption of independence of M and R , then

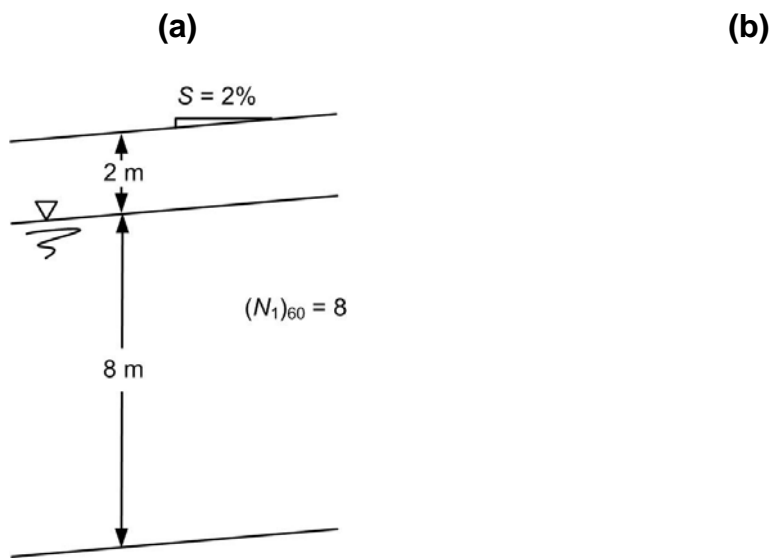
$$\lambda_{d|s} = \nu \sum_{j=1}^{N_M} \sum_{k=1}^{N_R} P[D_H > d | \mathbf{s}, M = m_j, R = r_k] P[M = m_j] P[R = r_k] \quad (\text{E.6})$$

which is of the same form as the equation for a probabilistic seismic hazard analysis (PSHA). Thus, a performance-based analysis using a lateral spreading model in which loading is a function of M and R is computationally equivalent to a PSHA for lateral spreading displacement.

The conditional probability term is evaluated by using Equation (E.6) with $\sqrt{D_H}$ evaluated by using the appropriate values of M , R , and \mathbf{s} . In this manner, the uncertainty in lateral spreading displacement is effectively attributed to the earthquake loading, which is justifiable in light of the common observation of record-to-record variability of ground motions being much higher than uncertainties in terms such as those used to compute \mathbf{s} . Extension of the procedure to integrate over uncertainties in \mathbf{s} , although not pursued in this paper, is straightforward.

Example – Site-Specific Displacement Evaluation

The performance-based lateral spreading model was implemented into the computer program, EZ-FRISK (Risk Engineering, Inc., Boulder, Colorado) by using the attenuation table feature of that program to allow prediction of the variation of $d | \mathbf{s}$ with M and R . In this form, EZ-FRISK was able to compute hazard curves for $d | \mathbf{s}$ at a particular site. Figure E.3 shows a lateral spreading displacement hazard curve for a hypothetical site in Seattle, Washington, USA; the ground slope and SPT profile for this site combine to produce a site parameter value, $\mathbf{s} = -5.7$. For this particular site and location, the 72-year, 224-year, and 475-year lateral spreading displacements (corresponding, respectively, to 50 percent, 20 percent, and 10 percent probabilities of exceedance in a 50-year period) are 0.002 m, 0.64 m, and 1.58 m, respectively.



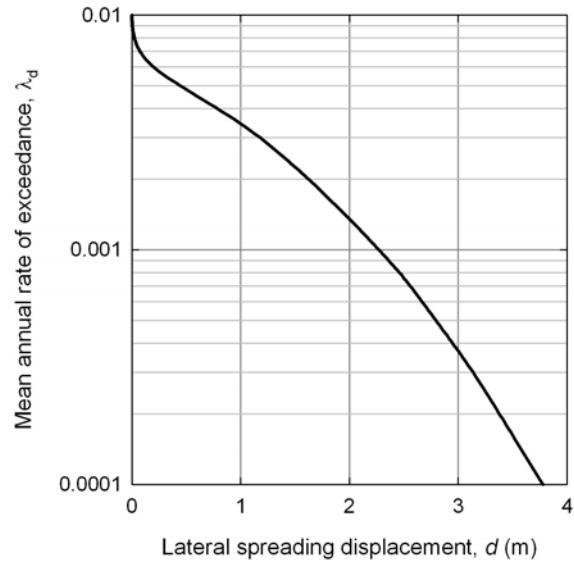


Figure E.3. (a) Hypothetical site in Seattle, Washington (47.53N, 122.30W), and (b) corresponding lateral spreading displacement hazard curve.

Knowing the mean annual rate of exceedance for a given displacement level, the probability of exceeding that displacement level in a given exposure period, T_E , can easily be computed as

$$P = 1 - \exp[-\lambda_d T_E] \quad (E.7)$$

Example – Conditional Displacement Evaluation

Figure E.4 shows a series of conditional hazard curves for different values of \mathbf{s} at the same Seattle location used to develop Figure C3(b). Note that a given value of \mathbf{s} could correspond to many different combinations of T_{gs}^* and S or T_{ff}^* and W . As previously indicated, the site profile shown in Figure E.3(a) corresponds to $\mathbf{s} = -5.7$; increasing the slope of that site to $S = 4.65$ percent would increase \mathbf{s} to -5.3 ; the resulting increase in lateral spreading displacement can be read directly from Figure E.4. Once the performance-based lateral spreading displacement curves have been computed for a given location, the user is only required to evaluate \mathbf{s} for the site of interest in order to determine a lateral spreading displacement value with a known mean annual rate of exceedance.

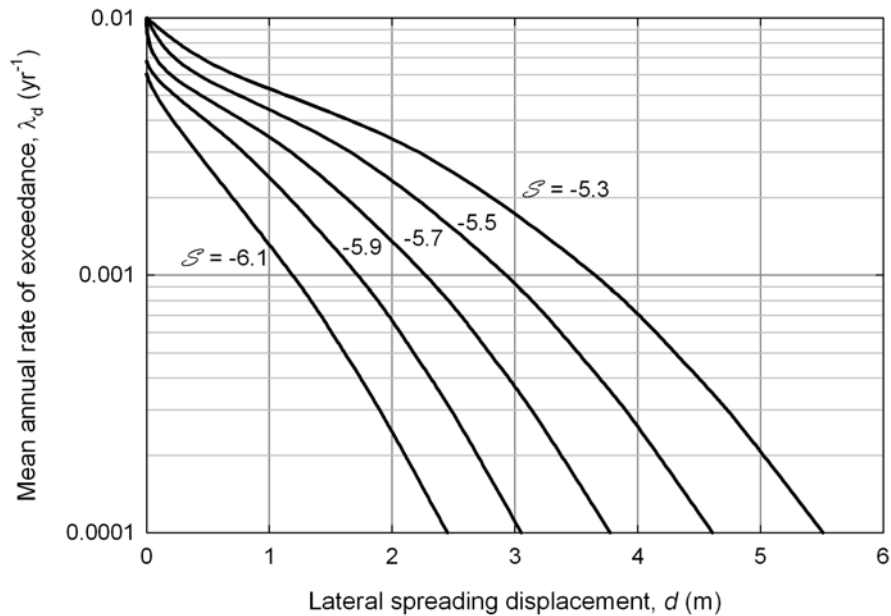


Figure E.4. Hazard curves for conditional lateral spreading displacement for different site term values in Seattle, Washington (47.53N, 122.30W).

COMPARISON OF CONVENTIONAL AND PERFORMANCE-BASED EVALUATIONS

In a conventional lateral spreading displacement evaluation, the results of a PSHA are typically used to identify a single scenario on which the evaluation is based. The scenario is defined by deaggregated magnitude-distance pairs – some engineers use mean values of M and R , and others prefer to use modal values.

USGS deaggregation analyses for 475-year peak acceleration values give mean magnitude and distance values of 6.57 and 36.0 km, respectively, for the Seattle site. Corresponding modal magnitude and distance values are 6.64 and 4.0 km, respectively; the large difference in mean and modal distances results from the contributions of the Seattle fault, which runs through Seattle just south of the downtown area.

The median displacement predicted by the Baska (2002) model using the 475-year mean magnitude and distance values for the site in Figure E.3(a) is 1.91 m; using the computed lateral spreading displacement hazard curve for that site, the actual return period for that level of displacement would be 664 years. The median displacement using the 475-year modal

magnitude and distance values for the same site is 3.23 m; the lateral spreading displacement hazard curve shows an actual return period of 3867 years for that level of displacement. These results indicate the sensitivity of inferred lateral spreading hazard to decisions about how deaggregation results are used; the lateral spreading displacement obtained by using modal values is nearly six times less likely to occur than that obtained by using mean values.

REFERENCES

- Ambraseys, N.N. (1988). "Engineering seismology," *Earthquake Engineering and Structural Dynamics*, 17, 1-105.
- Baska, D.A. (2002). "An analytical/empirical model for prediction of lateral spreading displacements," *Ph.D. Dissertation*, University of Washington, Seattle, Washington, 539 pp.
- Cornell, C.A. and Krawinkler, H. (2000). "Progress and challenges in seismic performance assessment," *PEER News*, April, 1-3.
- Deierlein, G.G., Krawinkler, H., and Cornell, C.A. (2003). "A framework for performance-based earthquake engineering," *Proceedings, 2003 Pacific Conference on Earthquake Engineering*.
- Krawinkler, H. (2002). "A general approach to seismic performance assessment," *Proceedings, International Conference on Advances and New Challenges in Earthquake Engineering Research, ICANCEER, 2002, Hong Kong*.
- Youd, T.L., Hansen, C.M., and Bartlett, S.F. (2002). "Revised multilinear regression equations for prediction of lateral spread displacement", *Journal of Geotechnical and Geoenvironmental Engineering*, ASCE, 128(12), 1007-1017.
- Zhang, G., Robertson, P.K., and Brachman, R.W.I. (2004). "Estimating liquefaction-induced lateral displacements using the standard penetration test or cone penetration test," *Journal of Geotechnical and Geoenvironmental Engineering*, ASCE, 130(8), 861-871.

Appendix F

Performance-Based Settlement Analysis

This appendix describes the development of the performance-based procedure for estimating post-liquefaction settlement introduced in Chapter 7. This procedure was created by developing a probabilistic settlement model, and then combining it with a probabilistic liquefaction initiation model and the results of a probabilistic seismic hazards assessment (PSHA). The procedure also required development of a model for estimating the maximum volumetric strain in order to avoid producing excessively high settlement hazards as a result of potentially unrealistic vertical strain estimates.

PROBABILISTIC ANALYSIS OF GROUND SURFACE SETTLEMENT

In order to allow performance-based evaluation of post-liquefaction settlement, a probabilistic settlement relationship must first be established. Four existing deterministic methods, those proposed by Tokimatsu and Seed (1987), Ishihara and Yoshimine (1992), Shamoto et al. (1998), and Wu and Seed (2004), were investigated through a series of parametric analyses. The four methods were generally consistent, but the Shamoto et al. model tended to predict significantly greater vertical strain than the others for loose conditions ($(N_1)_{60} < 10$). The Ishihara and Yoshimine and Wu and Seed models predicted quite similar values for similar conditions. Tokimatsu and Seed's model predicted pronounced limiting volumetric strains for given $(N_1)_{60}$ values at high loading levels.

Development of the probabilistic model required statistical characterization and comparison of the accuracy of the predictions of all four deterministic models. This was accomplished by carefully comparing published data of observed settlements from case histories with those predicted by the four models.

Evaluation of Settlement Models

Figure F.1 shows the comparisons between predicted (S_p) and observed (S_o) ground surface settlements for a set of case histories compiled by Wu and Seed (2004). All of the models can be seen to make predictions with a significant amount of scatter, which indicates that uncertainty is associated with each of them.

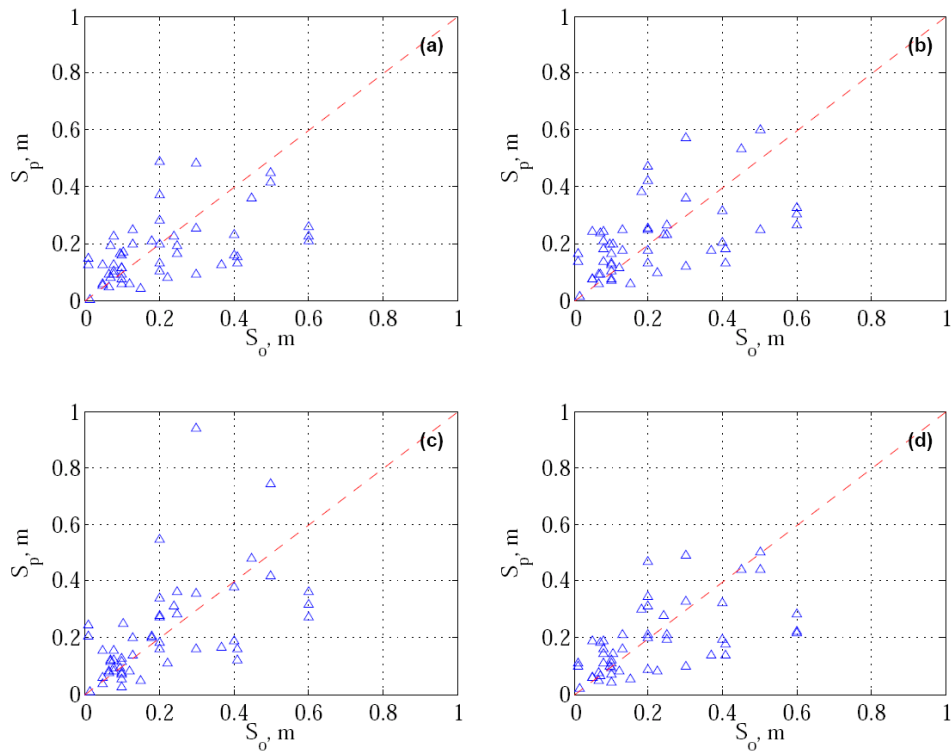


Figure F.1 Predicted and observed settlements for (a) Tokimatsu-Seed, (b) Ishihara-Yoshimine, (c) Shamoto et al., and (d) Wu-Seed models (after Wu and Seed, 2004).

Plots of the residuals of the data seen in Figure F.1 showed a trend of decreasing residuals with increasing observed settlement in each model – all tended to underestimate large ground surface settlements. To produce an appropriate probabilistic settlement model, this bias had to be corrected.

Using the predicted and observed settlement values themselves, power law models were found to be capable of removing bias but produced residuals that varied strongly with settlement magnitude. To produce residuals with constant variance (i.e., homoscedastic residuals), the predicted and observed settlements were subjected to a

logarithmic transformation. Figure F.2 shows log-log plots of the case histories for the four models.

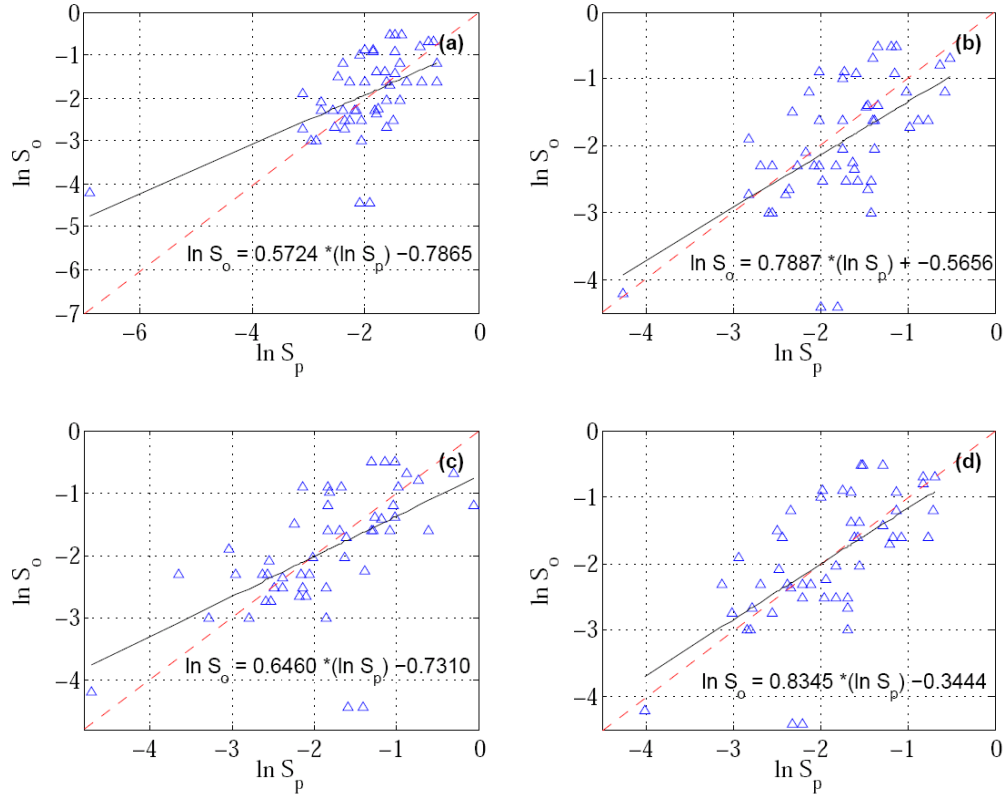


Figure F.2 Predicted and observed logarithmically transformed settlements for (a) Tokimatsu-Seed, (b) Ishihara-Yoshimine, (c) Shamoto et al., and (d) Wu-Seed models.

The model bias was then minimized by fitting linear functions to the logarithmically transformed data points. The results of this exercise suggested that Wu and Seed’s model was less biased than the others (i.e., it required the smallest correction to remove bias) and had the lowest level of dispersion of the bias-corrected logarithmic residuals, which are shown in Figure F.3.

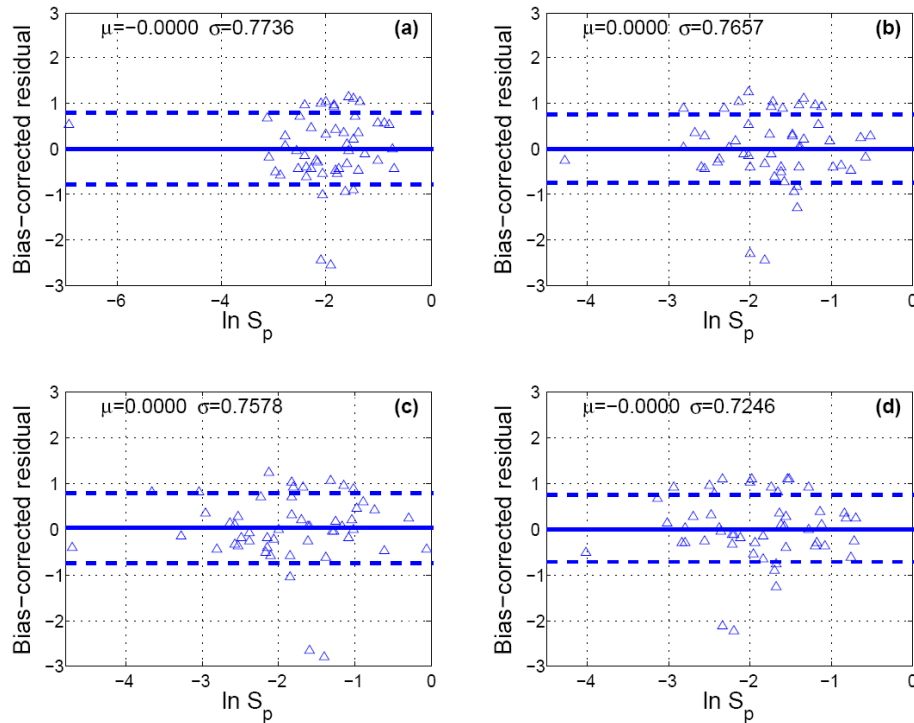


Figure F.3. Residuals from bias-corrected models: (a) Tokimatsu-Seed, (b) Ishihara-Yoshimine, (c) Shamoto et al., and (d) Wu-Seed.

The means of the residuals in Figure F.3 are very close to zero for all of the models, and the variance appears to be relatively constant. The standard deviation of the logarithmic residuals for each model is presented in the figure. The method proposed by Wu and Seed (2004) had the smallest standard deviation ($\sigma_{\ln S} = 0.725$) among all of the models. Examination of the logarithmic residuals showed that they could be represented as lognormally distributed (by the Kolmogorov-Smirnov test at a 95 percent confidence level). On the basis of the results of this evaluation, the bias-corrected Wu and Seed (2004) model was selected for development of a performance-based analysis for post-liquefaction settlement.

Proposed Probabilistic Settlement Model

The preceding analyses were used to identify the bias-corrected Wu and Seed model as the most appropriate probabilistic settlement model. The Wu and Seed (2004) model is expressed graphically (Figure 7.4) in terms of ε_v curves plotted as a function of

SPT resistance and *CSR*. Given that settlements result from the integration of vertical strains and, when divided by initial soil layer thickness, are proportional to average vertical strain, the uncertainty in logarithmic vertical strain was assumed to be the same as that determined for logarithmic settlement, i.e., $\sigma_{\ln \varepsilon_v} = 0.725$. It was then necessary to develop an analytical expression that would predict the vertical strain from $(N_1)_{60}$ and *CSR*. The strains associated with the graphical curves presented by Wu and Seed were interpreted as median strains. After a series of alternative functional forms were tested, the expression selected to describe the relationship between SPT resistance, cyclic stress ratio, and vertical strain predicted by Wu and Seed's graphical model was

$$(N_1)_{60,cs} = \frac{CSR + D}{A + B(CSR + D)} \quad (F.1)$$

where

$$A = 0.002152\hat{\varepsilon}_v + 0.003322$$

$$B = b_1\hat{\varepsilon}_v^2 + b_2\hat{\varepsilon}_v + b_3$$

$$b_1 = -0.00003725\hat{\varepsilon}_v^2 - 0.0001581\hat{\varepsilon}_v + 0.004152$$

$$b_2 = 0.0007936\hat{\varepsilon}_v^2 - 0.002052\hat{\varepsilon}_v + 0.002547$$

$$b_3 = -0.001089\hat{\varepsilon}_v^2 - 0.0006875\hat{\varepsilon}_v + 0.01696$$

$$D = -0.0123652\hat{\varepsilon}_v + 0.02709$$

The quality of the fit given by this expression is illustrated in Figure F.4. Equation F.1 requires an iterative solution for $\hat{\varepsilon}_v$ as a function of SPT resistance and cyclic stress ratio.

The mean value of $\ln \varepsilon_v$ can then be computed as

$$\mu_{\ln \varepsilon_v} = \ln(\hat{\varepsilon}_v) \quad (F.2)$$

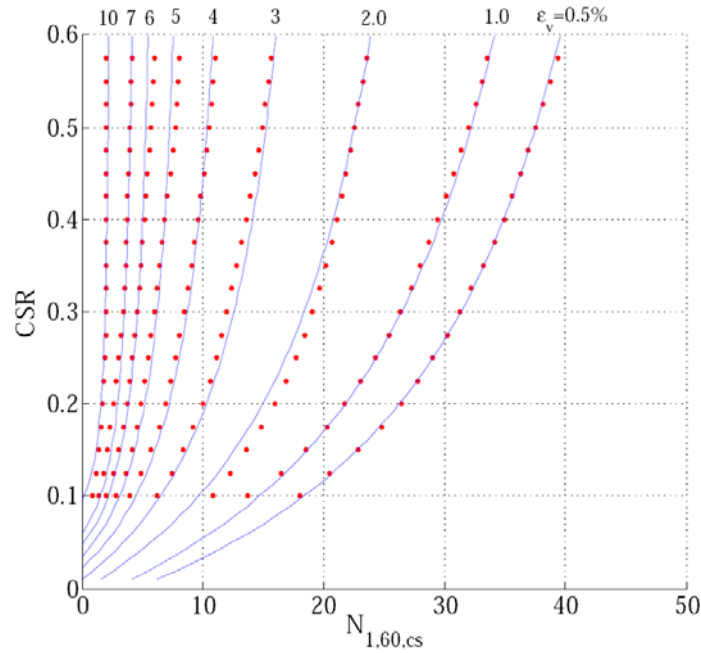


Figure F.4 Representation of Wu and Seed graphical curves (data points) by Equation F.1 (solid curves).

which allows the vertical strain fragility relationship for a given CSR and $(N_1)_{60}$ to be described by

$$P[\varepsilon_v > \varepsilon_v^* | CSR, N] = \Phi \left[\frac{\mu_{\ln \varepsilon_v} - \ln \varepsilon_v^*}{\sigma_{\ln \varepsilon_v}} \right] \quad (F.3)$$

where $\Phi(\cdot)$ is the standard normal cumulative distribution function.

Characterization of Maximum Vertical Strain

Direct computation of vertical strain distributions from the preceding relationship was found to produce significant probabilities of extremely large strain values. This result was found to be caused by the assumption of lognormally distributed vertical strains (given SPT resistance and CSR). At long return periods, the heavy upper tail of the ε_v distribution assigns a significant probability of exceeding strain values that are unrealistically large. Huang (2008) carried out a study of the limiting (maximum) value of vertical strain and found it to be a decreasing function of initial density. Huang

inferred limiting vertical strain from the four deterministic soil models described earlier and developed a relationship for mean limiting strain from a weighted average of the four relationships as shown in Figure F.5; the weighting factors were varied in a manner consistent with the range of vertical strains reached in the laboratory tests upon which the various vertical strain models were developed.

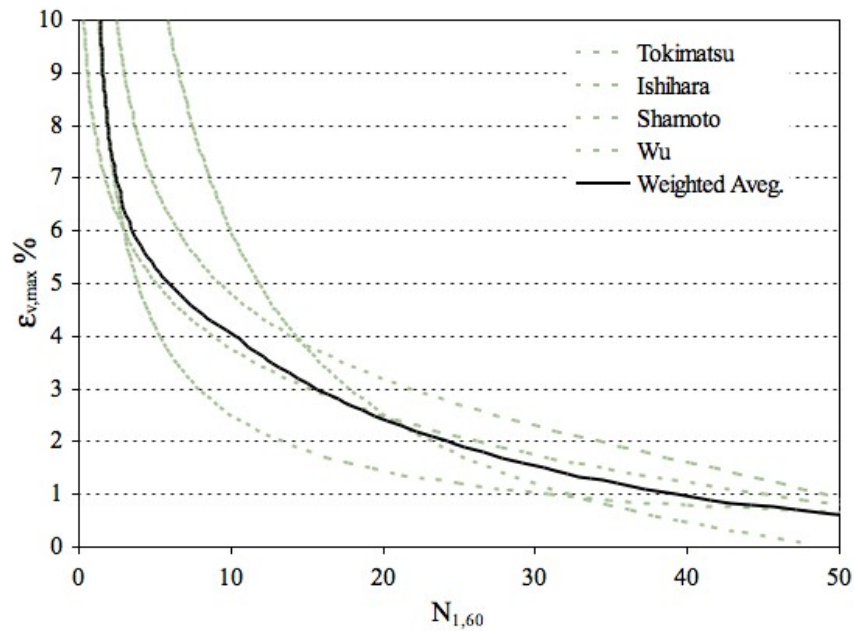


Figure F.5 Maximum vertical strain levels inferred by deterministic vertical strain models, and weighted average used to define mean value (after Huang, 2008).

Because of the approximate nature of the procedure used to develop the limiting strain relationship, its value is also expected to be uncertain. In order to be effective, the distribution of limiting strain must be bounded, so a uniform distribution from $0.5 \bar{\epsilon}_{v,max}$ to $1.5 \bar{\epsilon}_{v,max}$, where $\bar{\epsilon}_{v,max}$ is the weighted average limiting strain illustrated in Figure F.5, was assumed. The nature of this distribution may be revisited as additional experimental data on limiting strain become available.

The existence of a maximum vertical strain affects the fragility curves used to characterize the distribution of vertical strain. Figure F.6 shows a family of fragility curves, illustrating that the conditional probability of exceeding vertical strains greater than the maximum vertical strain is zero.

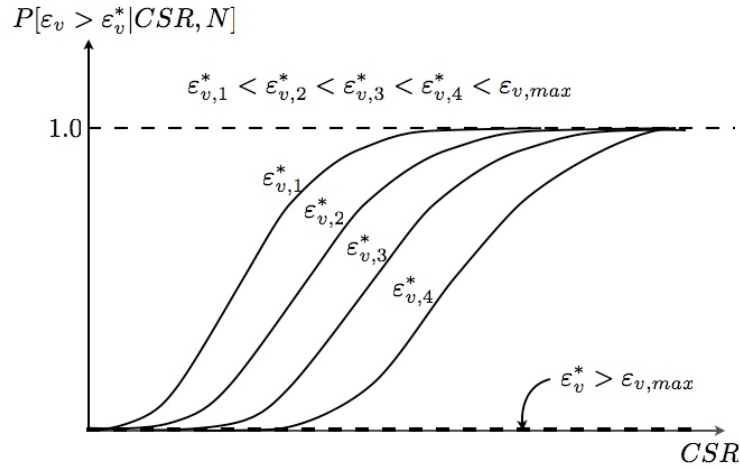


Figure F.6 Schematic illustration of fragility curves with consideration of maximum volumetric strain (Huang, 2008).

CALCULATION OF VERTICAL STRAIN HAZARD CURVE

The vertical strain used to compute post-liquefaction settlement depends on the density of the soil, as reflected by the penetration resistance, and on the level of loading that the soil is subjected to, as reflected in the cyclic stress ratio. The density of the soil is a measured quantity, and the accuracy with which it is known depends on the quality of the subsurface investigation and the skill of the persons making the measurements. Because these can vary significantly from one project to another, and because some of the uncertainty in the probabilistic settlement model is due to uncertainty in the penetration resistances of the case histories used to calibrate it, uncertainty in penetration resistance is not treated explicitly in the following derivation. The hazard curve for vertical strain in the i^{th} sublayer of a soil profile can then be computed as

$$\lambda_{\varepsilon_{vi}} = \sum_{m=1}^{N_{CSR}} P[\varepsilon_{vi} > \varepsilon_{vi}^* | CSR_i, N_i] \Delta \lambda_{CSR} \quad (\text{F.4})$$

The right side of Equation (F.4) consists of two parts. The conditional probability term describes a fragility relationship for volumetric strain, which was discussed in the preceding section. The second part is a function of the cyclic stress ratio seismic hazard curve. Computation of these two quantities is described in the following subsections.

Calculation of Cyclic Stress Ratio Hazard Curve

Development of a hazard curve for cyclic stress ratio requires careful examination of the manner in which CSR is calculated and the terms that compose it. The value of CSR_i depends on peak acceleration, magnitude, and depth, as indicated by the standard definition

$$CSR = 0.65 \frac{a_{\max}}{g} \cdot \frac{\sigma_{vo}}{\sigma'_{vo}} \cdot \frac{r_d}{MSF} \quad (F.5)$$

Letting $PGA = a_{\max}/g$, the cyclic stress ratio can be rewritten as

$$CSR = 0.65 PGA_M \cdot \frac{\sigma_{vo}}{\sigma'_{vo}} \cdot r_d \quad (F.6)$$

where $PGA_M = PGA/MSF$ can be interpreted as a magnitude-corrected peak acceleration.

By using the basic framework of performance-based earthquake engineering, the cyclic stress ratio hazard curve can be computed as

$$\lambda_{CSR} = \sum_{m=1}^{N_{CSR}} P[CSR > CSR^* | PGA_M] \Delta \lambda_{PGA_M} \quad (F.7)$$

The right side of Equation (F.8) consists of two parts. The conditional probability term describes a fragility relationship for cyclic stress ratio. The second part is a function of the magnitude-corrected peak acceleration hazard curve. Computation of these two quantities is described in the following two subsections. Defining the cyclic stress ratio as in Equation (F.6), the uncertainty in $CSR|PGA_M$ can come from two sources: the ratio of total to effective vertical stress, σ_{vo}/σ'_{vo} , and the depth reduction factor, r_d .

Uncertainty in σ_{vo}/σ'_{vo} is likely to be small because (a) the information required to evaluate stresses is usually measured relatively accurately, (b) soil densities generally fall within a relatively narrow range, and (c) errors in densities tend to affect both total and effective stresses similarly, so the ratio is less sensitive to those errors.

The depth reduction factor, r_d , however, is uncertain, primarily because of record-to-record variability and differences between specific soil profiles and the average profile

used to develop r_d . For the Cetin et al. (2004) model, the mean value of r_d can be computed as

$$r_d = \begin{cases} \left[1 + \frac{-23.013 - 2.949a_{\max} + 0.999M_w + 0.0525V_{s,12m}^*}{16.258 + 0.201 \exp(0.341(-d + 0.0785V_{s,12m}^* + 7.586))} \right] & d \leq 20 \\ \left[1 + \frac{-23.013 - 2.949a_{\max} + 0.999M_w + 0.0525V_{s,12m}^*}{16.258 + 0.201 \exp(0.341(0.0785V_{s,12m}^* + 7.586))} \right] & m \end{cases} \quad (\text{F.8a})$$

$$r_d = r_d(d = 20 \text{ m}) - 0.0046(d - 20) \quad \begin{matrix} d > 20 \\ m \end{matrix} \quad (\text{F.8b})$$

The standard deviation of r_d was given by Cetin et al. (2004) as

$$\sigma_{r_d} = 0.0198d^{0.85} \quad d \leq 20 \text{ m} \quad (\text{F.9a})$$

$$\sigma_{r_d} = 0.0198(12)^{0.85} \quad d > 20 \text{ m} \quad (\text{F.9b})$$

Dividing the standard deviation of r_d by the mean value gives the dimensionless coefficient of variation, which varies with depth as

$$COV_{r_d}(d) = \frac{\sigma_{r_d}(d)}{r_d(d)} \quad (\text{F.10})$$

As a result, the mean cyclic stress ratio can be expressed as

$$\overline{CSR} = 0.65PGA_M \cdot \frac{\sigma_{vo}}{\sigma_{vo}} \cdot \overline{r_d} \varepsilon_{r_d} \quad (\text{F.11})$$

where ε_{r_d} is a random variable with unit mean and standard deviation, $\sigma_{\varepsilon_{r_d}} = COV_{r_d}$.

Then the cyclic stress ratio fragility relationship can be described by

$$P[CSR > CSR^* | PGA_M] = \Phi \left[\frac{\overline{CSR} - CSR^*}{\sigma_{\varepsilon_{r_d}}} \right] \quad (\text{F.12})$$

where $\Phi(\cdot)$ is the standard normal cumulative distribution function.

Magnitude-Corrected Peak Acceleration Hazard Curve

The design peak acceleration value is typically obtained for some desired return period by using a peak acceleration hazard curve. However, magnitude-corrected peak acceleration is a function of the peak acceleration itself and the magnitude scaling factor, which acts as a proxy for duration in liquefaction analyses. For consistency with the procedures used for performance-based evaluation of the initiation of liquefaction, the cyclic stress ratio is determined by using the definitions of Cetin et al. (2004). However, the *CSR* term in the Cetin et al. (2004) procedure for initiation of liquefaction does not include a magnitude scaling factor (*MSF*), since magnitude is a separate term in the expression for cyclic resistance ratio (*CRR*) in that procedure. However, it is possible to manipulate the Cetin procedure to determine the form of *MSF* that is implied by that procedure. The Cetin expression for the mean value of *CRR* can be written as

$$\begin{aligned}
 \overline{CRR} &= \exp\left[\frac{f(N_{1,60}, FC, \sigma'_{vo}) - 29.53 \cdot \ln M_w}{13.32}\right] & (F.13) \\
 &= \exp\left[\frac{f(N_{1,60}, FC, \sigma'_{vo})}{13.32} - 2.217 \cdot \ln M_w\right] \\
 &= \frac{\exp\left[\frac{f(N_{1,60}, FC, \sigma'_{vo})}{13.32}\right]}{\exp[2.217 \cdot \ln M_w]} \\
 &= \exp\left[\frac{f(N_{1,60}, FC, \sigma'_{vo})}{13.32}\right] M_w^{-2.217}
 \end{aligned}$$

This expression can be reformulated to produce a term that has a value of unity when $M_w = 7.5$, which is the standard form of a magnitude scaling factor. The resulting expression is

$$\overline{CRR} = \exp\left[\frac{f(N_{1,60}, FC, \sigma'_{vo})}{13.32} - 4.467\right] \left(\frac{7.5}{M_w}\right)^{2.217} \quad (F.14)$$

which indicates that

$$MSF_{C_{ein}} = \left(\frac{7.5}{M_w} \right)^{2.217} \quad (F.15)$$

With an expression for the magnitude scaling factor in hand, a seismic hazard curve for PGA_M can be obtained from a seismic hazard curve for peak ground acceleration (PGA) and the underlying deaggregation data. By using the USGS's interactive online PSHA analyses, the total seismic hazard curve for PGA_M (Figure F.7) can be obtained. This hazard curve reflects all sources and all combinations of magnitude and distance that contribute to peak acceleration hazard at the site of interest.

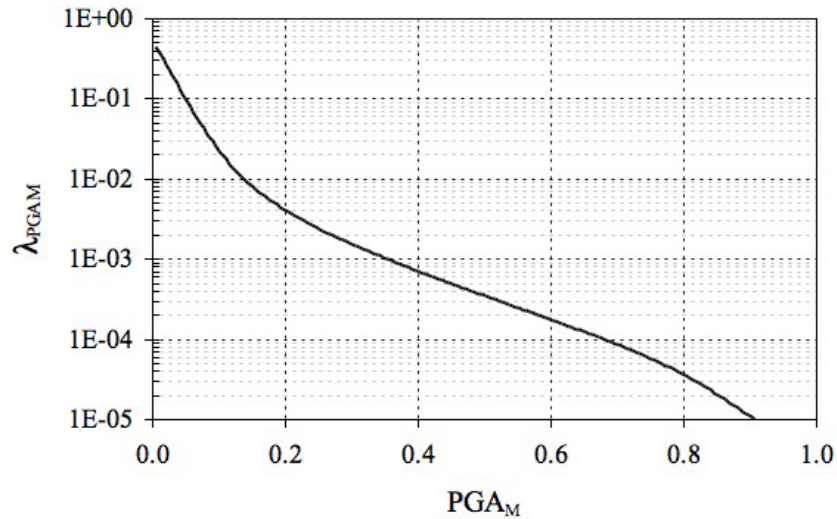


Figure F.7. Seismic hazard curve for magnitude-corrected peak ground acceleration, PGA_M , at site in Seattle.

CALCULATION OF EFFECTIVE THICKNESS HAZARD CURVE

The potential for initiation of liquefaction is accounted for in the performance-based settlement model through the use of an effective thickness defined as

$$t_i^{eff} = P[L_i]t_i \quad (F.16)$$

If the probability of liquefaction in a given sublayer is low, the effective thickness will be low and, therefore, the settlement of that sublayer will be small. The probability of liquefaction is

$$P[L_i] = P[N_{req} > N_i] \quad (F.17)$$

which can be computed by using Cetin's model. The probability of liquefaction will be low for weak motions (short return periods) and high for strong motions (long return periods); therefore, t_i^{eff} will vary with return period. The hazard curve for t_i^{eff} can be calculated as

$$\lambda_{t_i} = \sum_{j=1}^{N_M} \sum_{k=1}^{N_{a_{max}}} t_i P[N_{req} > N_i | a_{max,k}, m_j] \Delta \lambda_{a_{max,k}, m_j} \quad (F.18)$$

Figure F.8 illustrates effective thickness (normalized by actual thickness) hazard curves for a two-layer profile located in Seattle. The upper bound of $t_i^{eff} = t_i$ can clearly be seen at long return periods.

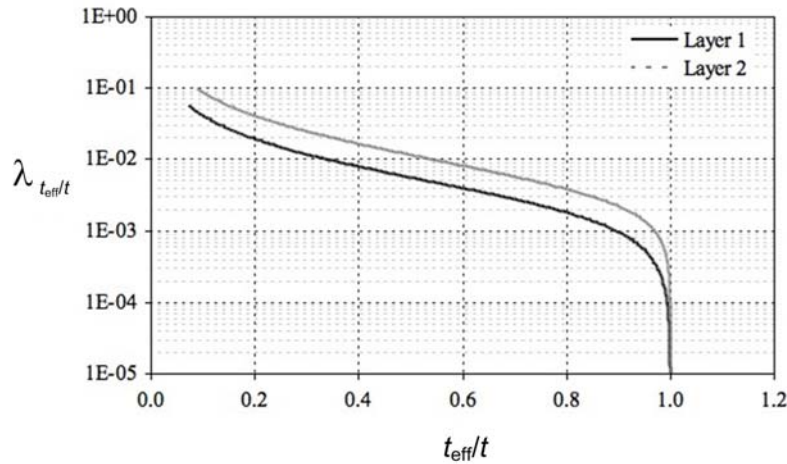


Figure F.8. Illustration of effective thickness hazard curves (Huang, 2008).

IMPLEMENTATION OF PERFORMANCE-BASED SETTLEMENT MODEL

After the previously described components have been assembled, the performance-based settlement calculations are relatively straightforward. The process involves development of sublayer settlement hazard curves followed by the use of those hazard curves to compute a profile settlement hazard curve. The steps involved in this procedure are as follows:

1. Divide the soil profile of interest into a series of sublayers – the accuracy of the calculations will increase with increasing number of sublayers, but the time required to complete the calculations will also increase.
2. Select a return period of interest, T_R .
3. Use the vertical strain hazard curve for sublayer i to determine the vertical strain for the return period of interest, $\varepsilon_{vi}(T_R)$.
4. Use the t_i hazard curve to determine the effective thickness for the return period of interest, $t_i^{eff}(T_R)$.
5. Compute the sublayer settlement for the return period of interest as

$$\Delta h_i(T_R) = t_i^{eff}(T_R) \varepsilon_{vi}(T_R). \quad (F.19)$$

6. Plot $\Delta h_i(T_R)$ vs. $\lambda_{\Delta h_i} (=1/T_R)$, which represents one point on the settlement hazard curve for sublayer i .
7. Repeat for other T_R values until Δh_i hazard curves are completed for all sublayers. Usually, 7 to 10 points will provide an adequate description of a sublayer settlement hazard curve.
8. Repeat Steps 2 through 7 for all sublayers.

The preceding series of steps will result in settlement hazard curves for all sublayers in the soil profile. These sublayer settlements then must be combined to obtain a hazard curve for ground surface settlement. This simple process requires that the user do the following:

1. Select a return period of interest, T_R .
2. Obtain all sublayer settlements at that return period, $\Delta h_i(T_R)$ from sublayer hazard curves.
3. Sum the sublayer settlements to obtain the ground surface settlement,

$$\Delta H(T_R) = \sum_{i=1}^n \Delta h_i(T_R)$$

4. Repeat for other T_R values until ΔH hazard curve is completed.

REFERENCES

- Cetin, K.O., Seed, R.B., Der Kiureghian, A., Tokimatsu, K., Harder, L.F., Kayen, R.E., and Moss, R.E.S. (2004). "Standard penetration test-based probabilistic and deterministic assessment of seismic soil liquefaction potential," *Journal of Geotechnical and Geoenvironmental Engineering*, ASCE, 130(12), 1314-1340.
- Huang, Y.-M. (2008). "Performance-Based Design and Evaluation for Liquefaction-Related Seismic Hazards," Ph.D. Dissertation, University of Washington, 376.pp.
- Ishihara, K. and Yoshimine, M. (1992). "Evaluation of settlements in sand deposits following liquefaction during earthquakes," *Soils and Foundations*, Vol. 32, No. 1, pp. 173-188.
- Shamoto, Y., Zhang, J.-M., and Tokimatsu, K. (1998). "Methods for evaluating residual post-liquefaction ground settlement and horizontal displacement," *Soils and Foundations*, Special Issue No. 2, 69-83.
- Tokimatsu, K. and Seed, H.B. (1987). "Evaluation of settlements in sand due to earthquake shaking," *Journal of Geotechnical Engineering*, ASCE, Vol. 113, No. 8, pp. 861-878.
- Wu, J. and Seed, R.B. (2004). "Estimation of liquefaction-induced ground settlement (case studies)," *Proceedings*, Fifth International Conference on Case Histories in Geotechnical Engineering, New York, pp. 1-8.

Appendix G

Residual Strength of Liquefied Soil

Liquefaction resulting from static or dynamic loading can cause large permanent deformations of soil masses. In cases of earthquake-induced liquefaction, permanent deformations most often occur primarily during the period of ground shaking; these deformations are driven by high dynamic shear stresses and result from the mechanism of cyclic mobility. In some cases, however, the liquefied soil is weak enough that the static shear stresses can drive permanent deformations, which can become very large as in cases of flow slides. In still other cases, delayed slope failures, i.e., failures in which pore pressures generated by cyclic mobility are redistributed in a manner that leads to flow liquefaction, can occur. The specific mechanism(s) that produce a particular flow failure are virtually impossible to distinguish based on the appearance of the failure.

This paper reviews the physical processes that lead to liquefaction-induced permanent deformations, previous procedures for estimation of residual strength, and issues in the interpretation of case histories. It then describes a hybrid model for estimation of residual strength based on the results of backanalyses that account for uncertainties in the inputs to case history analyses. Recommendations for deterministic and probabilistic estimation of residual strength are presented.

SHEAR STRENGTH OF LIQUEFIED SOIL

The excess porewater pressures generated during liquefaction generally reduce the stiffness and strength of coarse-grained soils. Castro (1969) investigated the response of triaxial specimens of loose to medium dense sands under stress-controlled triaxial loading conditions and observed three primary types of behavior. Very loose specimens were observed to reach a peak shearing resistance at a low strain level after which the shearing resistance dropped to a constant, lower value at large strain. Dense specimens were observed to dilate and reach high shearing resistances that were still increasing when the capacity of the loading equipment was reached. Specimens of intermediate density were observed to mobilize a peak shearing resistance at low

strain levels followed by a reduction in shearing resistance, followed in turn by an increase in shearing resistance. Eventually, all specimens reached a constant shearing resistance at large strain levels; Castro and Poulos (1977) and Poulos (1981) defined the state in which a soil is shearing with constant shearing resistance, constant effective stress, constant volume, and constant strain rate as the steady state of deformation, and postulated that the steady state is a unique function of void ratio. The condition in which a local minimum shearing resistance is observed at moderate strain levels in specimens of intermediate density (marked by an 'x' in Figure 1), is commonly referred to as the quasi-steady state (QSS) of deformation (Alarcon-Guzman, 1988). The shearing resistance at very large strains (marked by solid circles in Figure 1) has been referred to as the ultimate steady state (USS) of deformation (Yoshimine and Ishihara, 1998). If the soil is loose enough, the QSS and USS may coincide, a condition referred to as the critical steady state (CSS) by Yoshimine and Ishihara (1998), and no dilatancy following the initial peak resistance is observed.

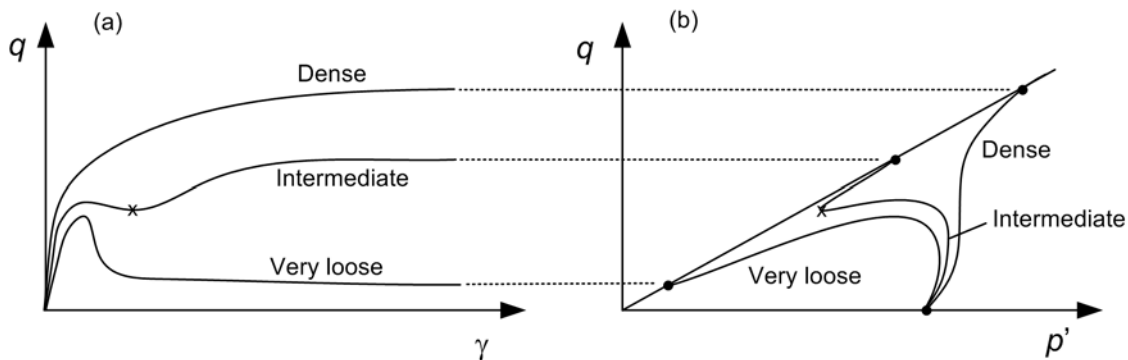


Figure G.1. Schematic illustration of (a) stress-strain and (b) stress path behavior of sands of different densities under monotonic loading.

Yoshimine and Ishihara (1998) presented a framework that clearly describes the relationship between the QSS and USS at different soil densities. Figure G.2 illustrates this framework schematically, and also shows the relative position of the isotropic consolidation line (ICL) as typically observed in laboratory tests on liquefiable soils. The highly contractive behavior shown in Case A of Figure G.2 occurs when the soil is loose enough (or effective stress high enough) that the QSS and USS coincide, a condition referred to as the critical steady state (CSS) by Yoshimine and Ishihara (1998); no dilatancy following the peak resistance is observed in the critical steady state. The dilative behavior shown in Case C occurs when the soil is

sufficiently dense (or effective stress sufficiently low) that the initial state plots well below the USSL. In intermediate cases, such as Case B, contractive followed by dilative response can be observed. Figure G.2 also shows that the USSL and QSSL are generally steeper than the ICL.

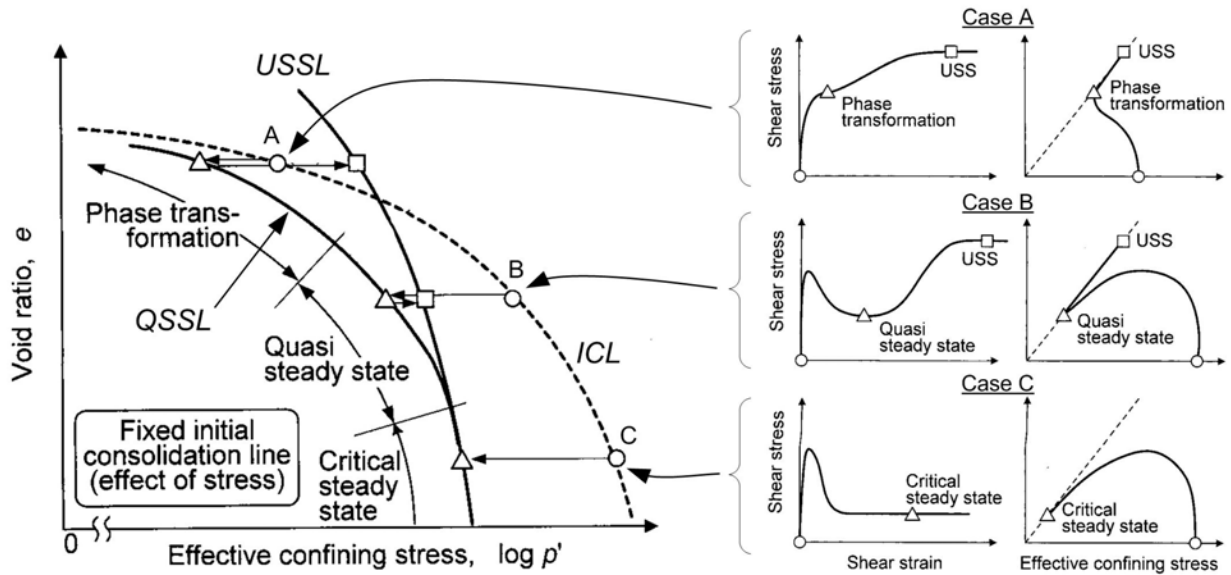


Figure G.2 Schematic illustration of typical relationships between ICL, USSL, and QSSL and effects on stress-strain and stress path behavior (redrawn with modified notation from Yoshimine and Ishihara, 1998).

Laboratory Testing-Based Approach

The roots of modern understanding of the mechanics of liquefiable soil come from early laboratory investigations such as those of Seed and Lee (1966) and Castro (1969). While most of these investigations were oriented toward the issue of liquefaction triggering under cyclic loading, the work initiated by Castro (1969) illuminated the issue of the shear strength of liquefied soil.

Poulos et al. (1985) proposed a method for evaluation of ultimate steady state strength based on laboratory testing of carefully retrieved undisturbed specimens and testing of reconstituted specimens of the same soil. The procedure involves determining the insitu void ratio from one or more undisturbed specimens, measuring the steady state strength of undisturbed specimens consolidated to confining pressures sufficiently high to ensure contractive behavior, determining the slope of the steady state line by testing specimens reconstituted at

different void ratios, and correcting the measured steady state strengths of the undisturbed specimens by assuming the steady state line of the undisturbed specimens in parallel to that of the reconstituted specimens.

Numerous laboratory investigations of the steady state behavior of sands have been undertaken (Castro, 1969; Alarcon-Guzman et al., 1988; Vaid et al., 1990; Been et al., 1991; Verdugo and Ishihara, 1996). These investigations have involved different soils prepared in different manners and tested at different rates using different types of equipment, and have greatly advanced the profession's understanding of liquefiable soil behavior. In a number of instances, however, they have produced conflicting and/or inconsistent results, which have identified important issues in liquefiable soil behavior. For example, DeGregorio (1990), Marcuson et al. (1990), Vaid et al. (1999), and Naeim and Bazier (2000) all found the position of the steady state line to be affected by method of sample preparation. Vaid et al. (1990), Reimer and Seed (1997), and Yoshimine et al. (1998) found undrained behavior to be strongly influenced by stress path.

Case History-Based Approach

Given the difficulties encountered in practical application of laboratory-based procedures for evaluation of ultimate steady state strength, Seed (1987) proposed a case history-based approach to address the problem. The case history-based approach involves identification of flow slide case histories, backanalysis of the shear strength of the liquefied soil in each case history, and correlation of the backanalyzed strengths to a measure of the density of the liquefied soil. Penetration resistance, most commonly standard penetration test (SPT) resistance, is used as the measure of insitu density. In recognition of the fact that actual flow slides frequently involve drainage, pore pressure redistribution, mixing, and other conditions that violate the assumptions of the steady state of deformation, the shear strength backanalyzed from flow slide case histories will be referred to hereafter as the residual strength.

The case history-based approach has generally been implemented in the form of two basic models – “classical” models in which residual strength is predicted directly from penetration resistance alone, and “normalized strength” models in which residual strength is assumed to be proportional to initial vertical effective stress.

Classical Models

Based on the ultimate steady state concept of strength depending solely on soil density and implicitly assuming a unique relationship between density and corrected SPT resistance, one could conclude that the shear strength of liquefied soil at large strain levels should be a unique function of SPT resistance.

Seed (1987) backanalyzed the apparent residual strength from 12 case histories involving liquefaction with substantial soil deformations. The residual strength was backanalyzed by varying the residual strength in a zone considered to have liquefied until limit equilibrium procedures produced a factor of safety of unity. The post-failure slope geometry was analyzed for most of the case histories, but the pre-failure geometry was analyzed for some. The backanalyzed residual strength was plotted against a “representative” clean sand SPT resistance, $(N_1)_{60\text{-cs}}$, which was defined as

$$(N_1)_{60\text{-cs}} = (N_1)_{60} + \Delta(N_1)_{60} \quad (\text{G.1})$$

where $\Delta(N_1)_{60}$ is the fines correction (Table G.1). The procedures by which the representative SPT resistance or the fines correction were obtained were not explicitly described; the representative SPT resistance appears to be based on SPT measurements (adjusted for post-earthquake densification) where available, correlations to relative density where possible, and estimation based on previous performance in other cases. Only three of the case histories (Calaveras Dam, Fort Peck Dam, and Lower San Fernando Dam) were from case histories with clean sand SPT resistances greater than 10. Seed (1987) noted the significant scatter in the results of the backanalysis analyses and that considerable judgment was involved in establishing the SPT resistance and residual strength values for each case history. In recognition of this uncertainty, Seed (1987) presented lower and upper bounds (Figure G.3) to the residual strength data. These bounds cover a wide range of residual strengths, particularly at lower SPT resistances.

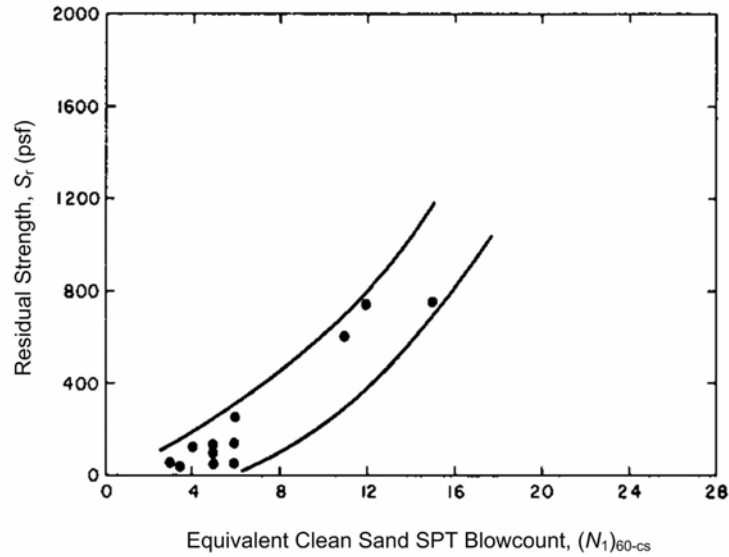


Figure G.3 Variation of residual strength with representative clean sand SPT resistance (after Seed, 1987).

Table 1 Fines corrections recommended by Seed (1987).

Fines Content, FC (%)	SPT Correction, $\Delta(N_1)_{60}$
0	0
10	1
25	2
50	4
75	5

Seed and Harder (1990) expanded and re-interpreted the case history database and developed an updated relationship for residual strength estimation. Backanalyzed residual strengths from 17 case histories were correlated to a representative clean sand SPT resistance, with a fines correction identical to that of Seed (1987). The expanded database had more cases with moderately high SPT resistances – seven with clean sand SPT resistance of 10 or more. Seed and Harder (1990) also noted the significant scatter in the results of the backanalyses and presented lower and upper bounds (Figure G.4) to the residual strength data. In a manner similar to that of Seed (1987) these bounds also cover a wide range of residual strengths, particularly at lower SPT resistances. Seed and Harder (1990) recommended use of “the lower-bound, or near

lower-bound relationship” between residual strength and SPT resistance “owing to scatter and uncertainty, and the limited number of case studies back-analyzed to date.”

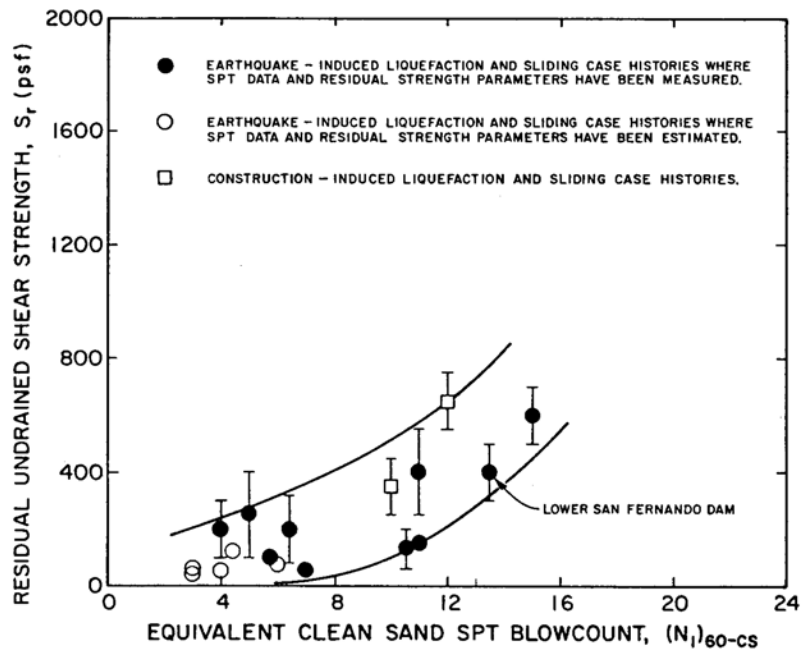


Figure G.4 Variation of residual strength with representative clean sand SPT resistance (after Seed and Harder, 1990).

Idriss (1998) re-interpreted the case history database of Seed and Harder (1990) and presented a graphical model for estimation of residual strength (Figure G5). The Idriss model removed a good deal of the ambiguity in determining a “representative” SPT resistance in previous models by explicitly correlating residual strength to median SPT resistance. Rather than provide a range of residual strengths, Idriss (1998) provided a single curve with error bars that give an indication of the general level of uncertainty in the estimated residual strengths of the different case histories. While the Idriss (1998) curve was expressed graphically, it is consistent with a residual strength computed as

$$S_r \text{ (atm)} \approx 0.0236 \exp[0.16(N_1)_{60}] \quad (\text{G.2})$$

The Idriss (1998) curve is of similar shape to the upper and lower bound curves of Seed and Harder (1990) and is closer to the Seed and Harder lower bound curve than to the upper bound curve. The Idriss (1990) curve extends to median clean sand SPT resistances of nearly 16 after

which it is shown as a dashed line that presumably indicates extrapolation beyond the SPT range that is not supported by observational data.

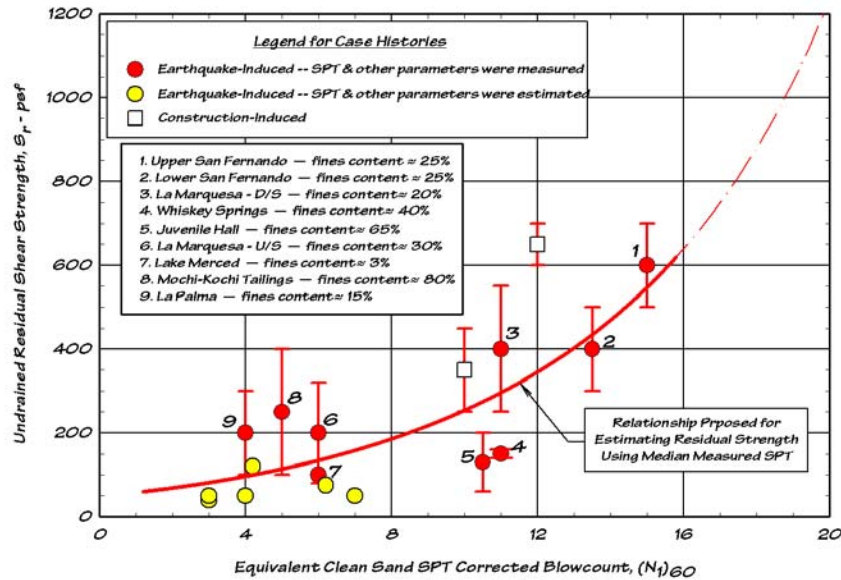


Figure G.5 Variation of residual strength with median clean sand SPT resistance (after Idriss, 1998).

Normalized Strength Models

Castro (1987) observed that the density of a given soil increased with increasing initial effective stress and that residual strength increased with increasing density, and concluded that the steady state strength should be related to initial effective stress. Assuming that the rate of change of void ratio and steady state strength with effective stress is equal, which is equivalent to assuming the consolidation curve and steady state line to be parallel (on an e -log σ' plot), the ratio of steady state strength to effective stress should be constant for a given soil. Castro (1987), Castro and Troncoso (1989), and Castro (1991) investigated several tailings dams in South America and reported ratios of steady state strength to initial major principal effective stress, S_{us}/σ'_{1c} , ranging from 0.12 – 0.19.

Building on the concepts of Castro (1987), Stark and Mesri (1992) parameterized effective stress using the initial vertical effective stress, and developed a database of 20 case histories for which the ratios of residual strength to initial vertical effective stress were

computed. These stress ratios were found to correlate better to a representative clean sand SPT resistance when a different fines correction (Table G.2) than that of Seed (1987) was used.

Table G.2 Fines corrections recommended by Stark and Mesri (1992).

Fines Content, <i>FC</i> (%)	SPT Correction, $\Delta(N_1)_{60}$
0	0
10	2.5
15	4
20	5
25	6
30	6.5
35	7
50	7
75	7

Noting that the strength of a liquefied soil should increase with factors (e.g., gradation, particle angularity, particle roughness) that also increase SPT resistance, Stark and Mesri (1992) related the ratio of critical strength to initial vertical effective stress, hereafter referred to as the normalized residual strength ratio, S_r/σ'_{vo} , to representative clean sand SPT resistance. Plots of the case history data, however, remained significantly scattered. Supplementing the case history database with interpreted laboratory test results, Stark and Mesri (1992) proposed that the normalized residual strength ratio could be estimated as

$$S_r/\sigma'_{vo} = 0.0055(N_1)_{60-cs} \quad (G.3)$$

This equation represented a conservative interpretation (Figure G.6) of the available case history data, particularly at low SPT resistances.

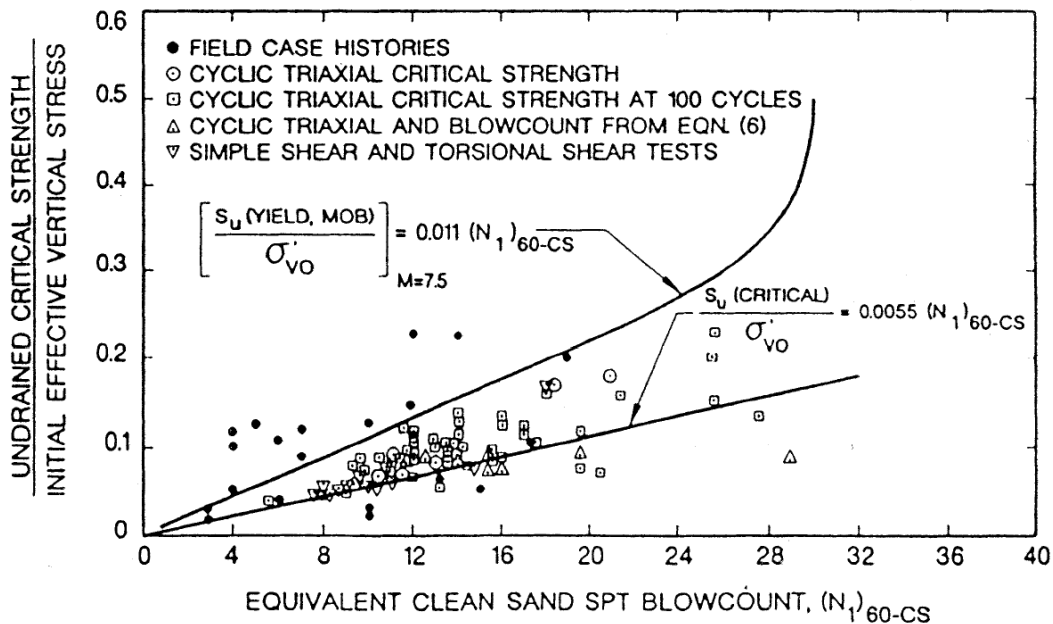


Figure G.6 Recommended relationship for estimation of normalized residual strength ratio as function of clean sand SPT resistance (after Stark and Mesri, 1992).

Olson (2001) and Olson and Stark (2002) expanded the case history database to a total of 33 flow slide case histories and performed detailed residual strength backanalysis analyses on a number of them. These analyses accounted for inertial effects and variable initial vertical effective stresses within the liquefied zone of each case history. Other case histories were not investigated or documented in sufficient detail to warrant detailed analyses and were analyzed using a simple, infinite slope approach. Based on these analyses, Olson and Stark (2002) proposed that the normalized residual strength ratio could be estimated as

$$S_r / \sigma'_{vo} = 0.03 + 0.0075(N_1)_{60} \pm 0.03 \quad (G.4)$$

for $(N_1)_{60} \leq 12$, a relationship that produces substantially higher strengths than that of Stark and Mesri (1992). The Olson and Stark (2002) model is shown graphically in Figure G.7.

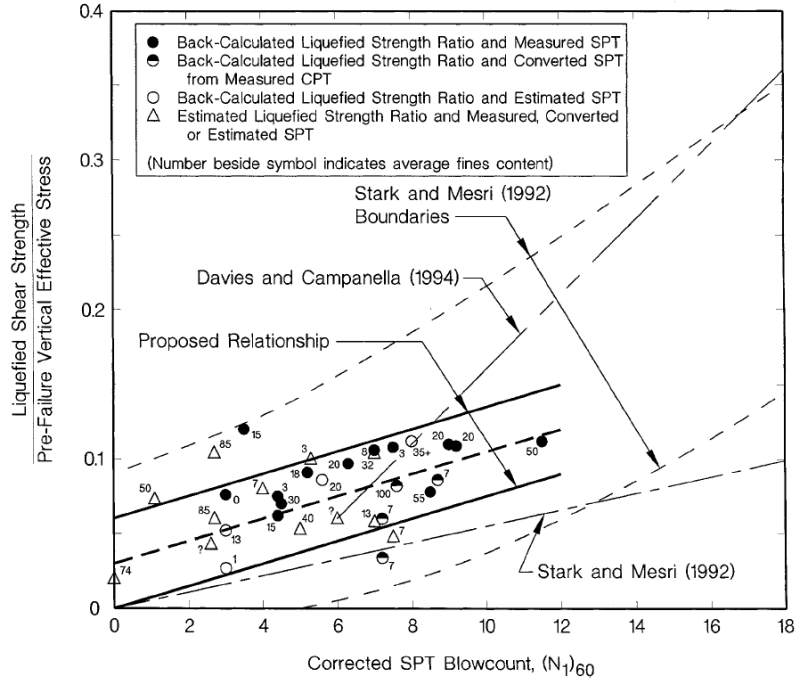


Figure G.7 Recommended relationship for estimation of normalized residual strength ratio as function of SPT resistance (Olson and Stark, 2002). Numbers adjacent to data points represent fines contents (%).

Idriss and Boulanger (2007) considered a subset of 18 flow slides from the case history database compiled by Olson and Stark (2002). This group included 10 of the 12 cases considered by Seed (1987), 13 of the 17 cases considered by Seed and Harder (1990), and 18 of the 33 cases considered by Olson and Stark (2002). The 18 case histories were divided into three groups based on adequacy of insitu measurements (i.e., SPT and/or CPT) and geometric information. Normalizing the average back-calculated strengths (from as many as available) computed by Seed (1987), Seed and Harder (1990), and Olson and Stark (2002) by initial vertical effective stress, Idriss and Boulanger (2007) produced the following relationships for normalized residual strength ratio.

For cases in which void redistribution effects are negligible:

$$\frac{S_r}{\sigma'_{vo}} = \left[\frac{(N_1)_{60-cs}}{16} + \left(\frac{(N_1)_{60-cs} - 16}{21.2} \right)^3 - 3.0 \right] \times \left[1 + \exp \left(\frac{(N_1)_{60-cs} - 6.6}{2.4} \right) \right] \leq \tan \phi' \quad (\text{G.5a})$$

For cases in which void redistribution effects are significant:

$$\frac{S_r}{\sigma'_{vo}} = \left[\frac{(N_1)_{60-cs}}{16} + \left(\frac{(N_1)_{60-cs} - 16}{21.2} \right)^3 - 3.0 \right] \leq \tan \phi' \quad (G.5b)$$

where $(N_1)_{60-cs}$ is computed as in Equation G.1 (i.e., using the Seed (1987) fines correction). The Idriss and Boulanger (2007) relationship is shown graphically in Figure G.8.

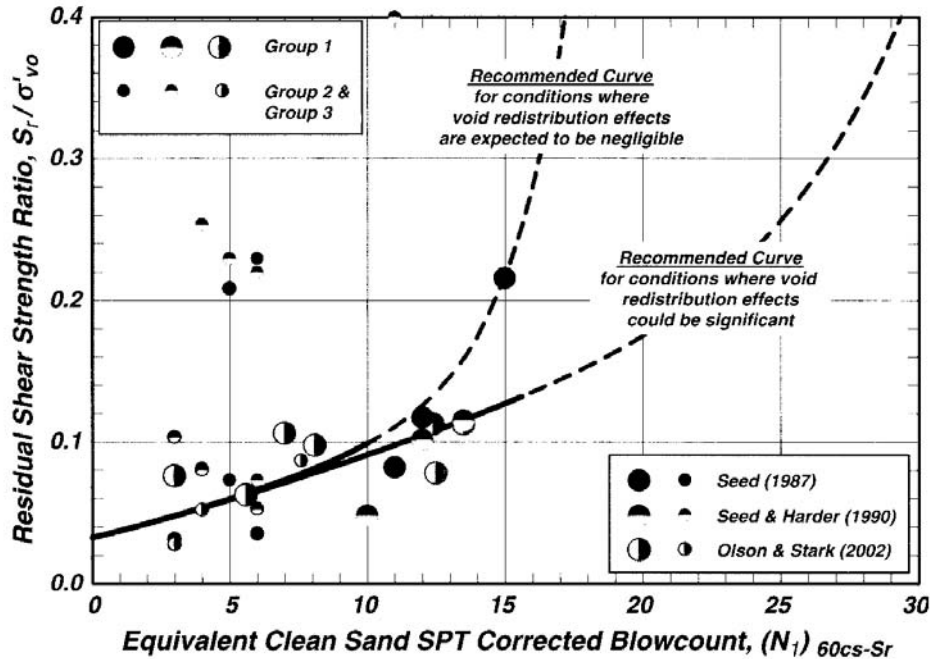


Figure G.8. Recommended relationship for estimation of normalized residual strength ratio as function of SPT resistance (Idriss and Boulanger, 2007).

Discussion

The Seed and Harder (1990) procedure has become the *de facto* standard for estimation of the residual strength of liquefied soil. In practice, it is typically interpreted conservatively, with values closer to the lower than upper bounds generally used for design and evaluation purposes – the Idriss (1999) curve is frequently used as a reasonable representation of the Seed and Harder model. In recent years, the use of normalized residual strength ratios has increased, and it seems likely to increase further with the recent introduction of the Idriss and Boulanger (2007) model.

Figure G.9 shows the residual strengths predicted by the previously discussed models; it should be noted, however, that the SPT values for the different models may be defined differently. The classical models show residual strengths that increase with increasing SPT resistance; the normalized residual strength models increase with increasing SPT resistance, but are also proportional to initial vertical effective stress. Figure G.9(b) shows that residual strengths can be very low, regardless of SPT resistance, at the low effective stress levels corresponding to shallow depths. This aspect of these models suggests that flow sliding should be expected in moderately dense to dense soils subjected to very strong ground shaking – the absence of observations of such events calls this aspect of the normalized strength models into question.

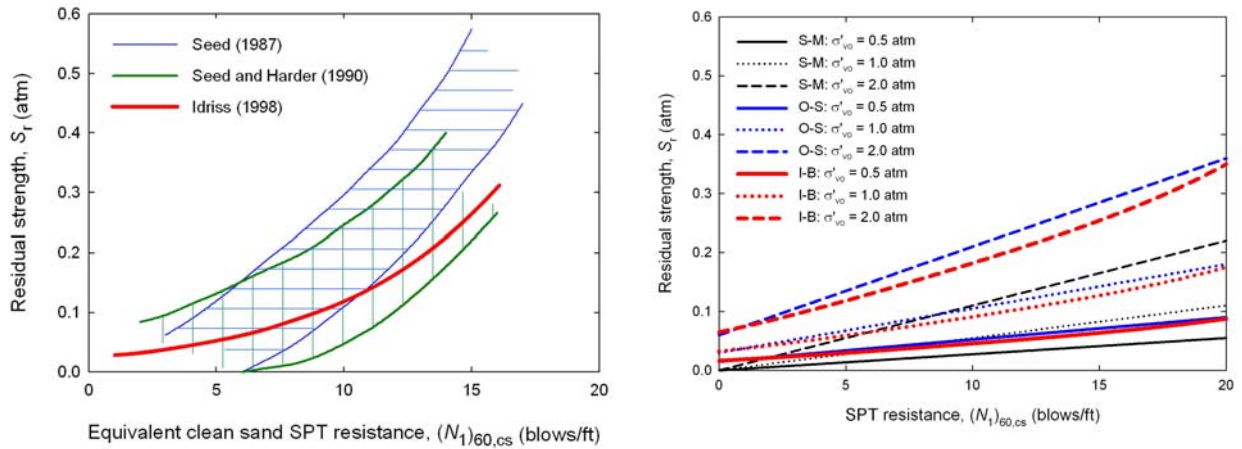


Figure G.9. Variation of residual strengths with SPT resistance for (a) classical models, and (b) normalized residual strength models at different initial effective stress levels (S-M = Stark-Mesri; O-S = Olson-Stark; I-B = Idriss-Boulanger models).

The normalized residual strength ratio models all assume that residual strength is directly proportional to initial vertical effective stress, hence their predicted residual strengths are zero at zero initial effective stress and increase linearly with increasing initial effective stress. The relationship between the slopes of the steady state line and consolidation curve control the variation of normalized residual strength ratio. The steady state strength in the case where the steady state line and consolidation curve are both linear (in e - $\log \sigma'$ space) with slopes λ_{SSL} and λ_c , respectively, can be shown to vary with initial effective stress as

$$S_{su} \propto (\sigma'_{vo})^{\lambda_c / \lambda_{SSL} - 1} \quad (G.6)$$

which is illustrated schematically in Figure G.10(a). Experimental data has shown that steady state lines are generally steeper than consolidation curves (i.e., that $\lambda_c < \lambda_{SSL}$). This behavior implies that the normalized strength ratio should decrease with increasing effective stress as observed in laboratory tests on clean sand (Figure G.10b).

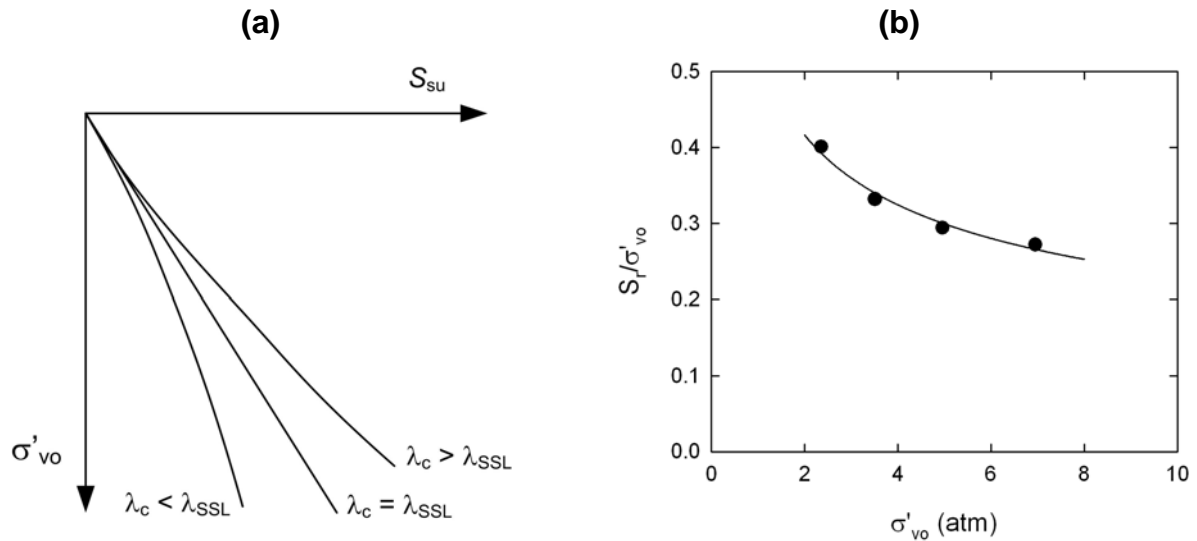


Figure G.10. (a) Effects of relative slopes of steady state and consolidation curves on effective stress dependence of steady state strength, and (b) experimental results consistent with $\lambda_c < \lambda_{SSL}$ (after Riemer and Seed, 1997).

The preceding sections have referred to a number of significant issues that affect estimation of residual strength by backanalysis of flow slide case histories. Previous efforts at residual strength estimation have recognized these issues and dealt with some explicitly, but have either not addressed or made assumptions as the potential effects of others. Most of these estimation procedures have reported a range of residual strength estimates with lower and upper bounds generally corresponding to backanalyzed strengths from post-failure and pre-failure geometries, respectively, and a most likely value obtained by various methods. No information on the (probabilistic) distribution of those residual strengths is available. Furthermore, most previous backanalysis efforts have not evaluated uncertainty in SPT resistance.

ALTERNATIVE APPROACH TO BACKANALYSIS

An alternative approach to the backanalysis of flow slide case histories was developed. The goal of this alternative approach was to develop a predictive model that was consistent with the known mechanics of liquefiable soils, consistent with observed field behavior, and that considered the effects of uncertainties in the inputs to a backanalysis on the uncertainty in backanalyzed residual strength.

The alternative backanalysis procedure was based on (a) estimation of an appropriate slope geometry for backanalysis, (b) characterization of uncertainty of the parameters required for backanalysis in each case history, (c) Monte Carlo simulation of each case history, and (d) backanalysis of residual strength for each Monte Carlo realization. The procedure also accounted for inertial effects for those case histories for which they were important and data was available.

Estimation of Appropriate Slope Geometry

Backanalysis of residual strength based on pre-failure geometry clearly provides an upper-bound strength estimate since the occurrence of failure indicates that the slope was unstable at that strength level. Several researchers (Davis et al., 1988; Olson et al., 2000; Olson and Stark, 2002) have shown that backanalysis based on post-failure geometry provides a lower-bound estimate since a portion of the deformations that produce the post-failure geometry were due to inertial effects. Using the sliding block analogy of Olson and Stark (2002), one can surmise that the most appropriate geometry for residual strength backanalysis would be the geometry in which inertial forces were zero, i.e., the geometry in which the slope has stopped accelerating and begins decelerating. Figure G.11 illustrates the process schematically for a frictional block on a curving plane. The block is unstable at Point A because the slope angle, θ_A , exceeds the friction angle, ϕ . The block then slides down the surface and reaches Point B, the position at which the block would be stable under static loading conditions (since $\theta_B = \phi$), but continues moving to Point C because it has a non-zero velocity at Point B. Backanalyses of the apparent friction angle based on pre- and post-failure positions would give unconservative and overconservative estimates of $\phi_{app} = \theta_A$ and $\phi_{app} = \theta_B$, respectively,

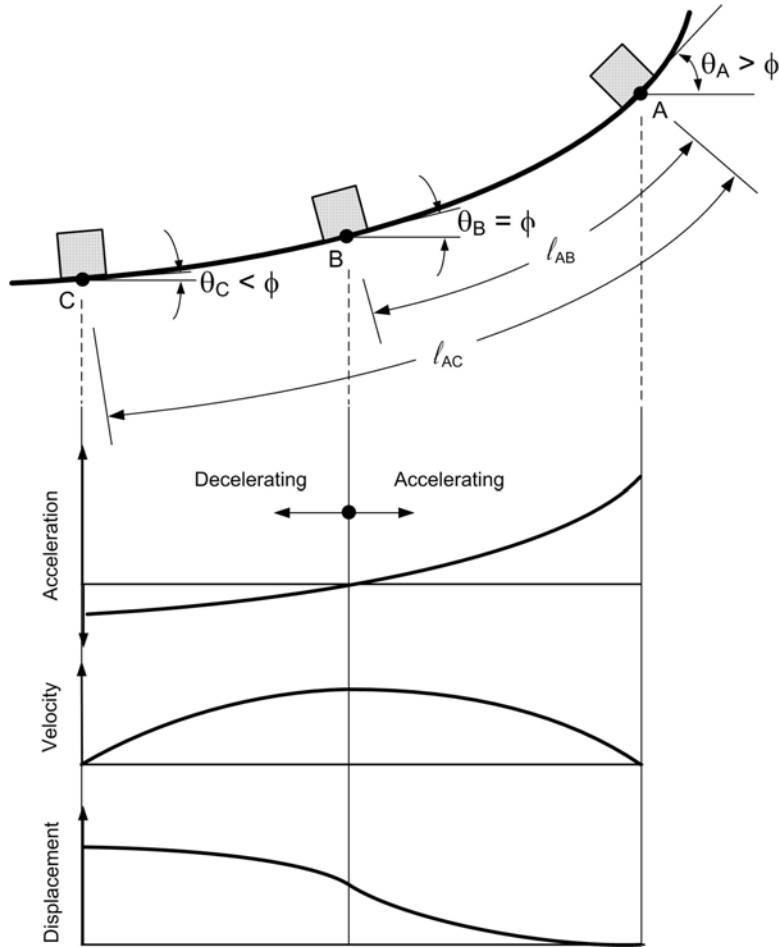


Figure G.11. Schematic illustration of variation of acceleration, velocity, and displacement with position for sliding block model. Inertial forces are zero when acceleration is zero (Point B).

In an attempt to approximate inertial effects more accurately than possible using only sliding block models, a procedure was developed to estimate an inertia-corrected geometry for selected case histories. The procedure involved the following steps:

1. Obtain the most accurate available cross-sections for the pre- and post-failure conditions.
2. Identify, using those cross-sections, both the pre- and post-failure positions of as many specific points as possible.
3. Sketch, considering soil mechanics, kinematics, and all available descriptions of the failure, the anticipated paths taken by the points identified in Step 2 in moving from their pre-failure to post-failure positions.

4. Using sliding block analyses similar to those reported by Olson and Stark (ref), estimate the zero-inertia-ratio for the case history. The zero-inertia-factor, *ZIF*, is defined as the fraction of total displacement corresponding to the zero-inertia position; with reference to the schematic illustration of Figure 4,

$$ZIF = l_{AB} / l_{AC}$$

5. Apply the *ZIF* to each of the kinematic paths developed in Step 3 to estimate the locations of the various points at the zero-inertia state.
6. Construct the zero-inertia slope geometry to be consistent with the positions of the points identified in Step 5 and with the volumes of the various soil zones (i.e., maintaining constant volume).

An example of this procedure is shown in Figure G.12. The procedure was laborious and is recognized as being approximate, a fact that was accounted for in the Monte Carlo analyses described subsequently. It does, however allow backanalysis of residual strength from a geometry that is approximately correct rather than interpolating between residual strength values (those based on pre- and post-failure geometries) that are known to be incorrect.

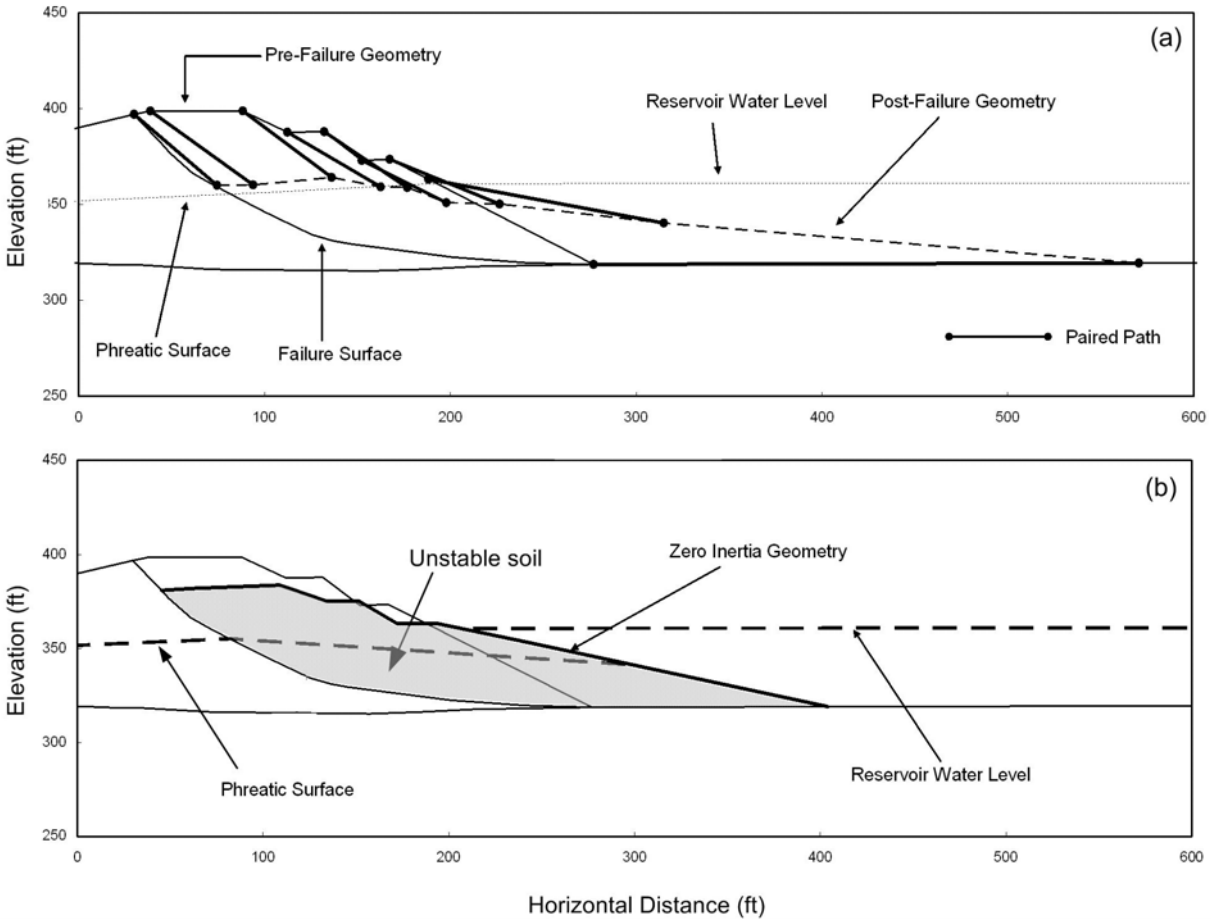


Figure G.12. Illustration of procedure for estimating zero inertia geometry: (a) identification of common points on pre- and post-failure geometries, and (b) construction of zero inertia geometry by interpolating based on ZIF.

Sufficient data to allow correction for inertial effects was not available for some of the case histories, particularly those involving smaller flow volumes.

Characterization of Uncertainty

Because of large differences in the extent and documentation of post-failure investigations, many of the parameters required for backanalyses of residual strength values are not accurately known. Therefore, these parameters were treated as random variables in a series of Monte Carlo backanalyses so that the influence of their distributions on the backanalyzed residual strengths could be accounted for. The randomized variables, and brief descriptions of the manners in which their respective uncertainties were characterized, are listed in Table G.3.

Table G.3 Characterization of uncertainties

Parameter	Description	Uncertainty
Geometric parameters		
Slope geometry points	Locations of points defining exterior topography and interior layers	$\mu = 0$ Exterior $\sigma_H = 0.25 - 0.5$ ft $\sigma_V = 1.0 - 2.0$ ft Interior $\sigma_H = 0.25 - 0.5$ ft $\sigma_V = 1.0 - 2.0$ ft
Zero inertia factor, ZIF	Fraction of total displacement at point of zero acceleration	COV = 0.16 – 0.30
Failure surface	General position of failure surface. Uncertainty modeled by sine offset function with half wavelength equal to length of failure surface.	$\sigma/H = 0.03 - 0.25$
Phreatic surface	Position of phreatic surface within slope	$\sigma_V = 1.0 - 3.3$ ft
Material parameters		
SPT resistance	Value of $(N_1)_{60}$	$\sigma_N = 3.7 - 12$ bpf depending on statistical variability and number of measurements
Strength of non-liquefied soil	Cohesive soils and soils above water table	Coefficients of variation given by Phoon and Kulhawy (1998)

Monte Carlo Backanalyses

Monte Carlo backanalyses were performed by generating suites of randomized input parameters distributed as described in the preceding section. Each realization in the simulation produced a unique slope geometry, failure surface, and phreatic surface, and a unique set of material characteristics. A limit equilibrium backanalysis was performed for each realization to yield a residual strength value for that particular set of parameters. A total of 50,000 simulations were performed for each case history.

The results of the Monte Carlo backanalyses are illustrated in Figure G.13. The mean value of residual strength is 348 psf with a standard deviation of 75 psf; Olson et al. (2000) reported a range of residual strength of 217 psf to 398 psf for this case history. The mean value of $(N_1)_{60}$ was 7.3 bpf; Olson et al. (2000) reported a representative SPT resistance of 8.0 bpf.

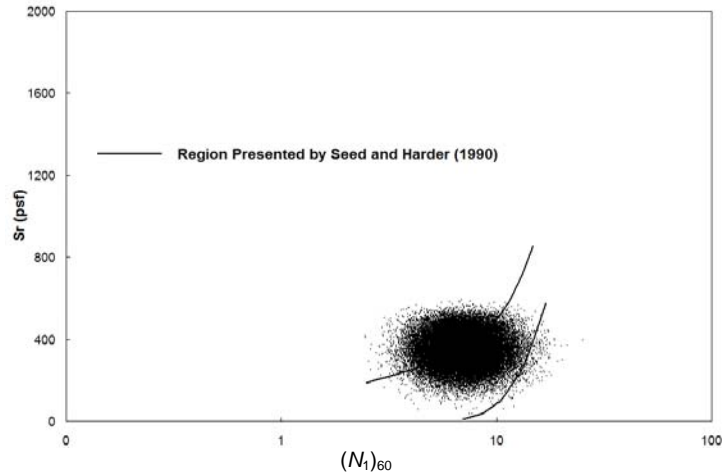


Figure G.13. Results of Monte Carlo simulations for the North Dike of Wachusett Dam. A total of 50,000 data points are shown.

Eight other case histories were analyzed using the Monte Carlo backanalysis procedure. Then, 22 additional case histories for which sufficient data to perform Monte Carlo backanalyses was not available were also considered. For these case histories, distributions of SPT resistance were obtained in the same manner as for the backanalyzed case histories. The mean residual strength was taken as the average of the residual strength values computed for them in previous analyses, an approach justified by the simplicity of the analyses and the general agreement obtained in previous investigations. Uncertainty in the residual strength values was estimated by a procedure that considered the general levels of uncertainty in the nine backanalyzed case histories and a component of modeling uncertainty that reflected the simplified nature of those analyses. A summary of the backanalyzed residual strength values is presented in Table G.4. The backanalyzed residual strength values are plotted as functions of SPT resistance and initial vertical effective stress in Figure G.14.

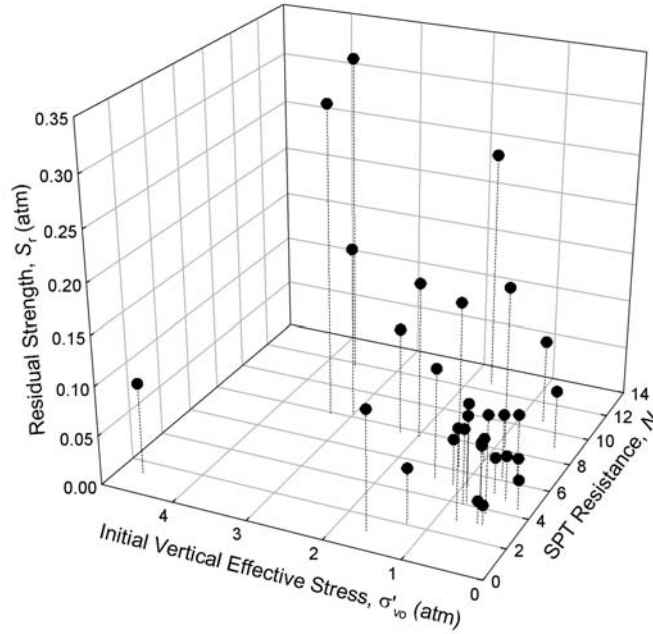


Figure G.14. Three-dimensional view of mean residual strength vs. mean SPT resistance and mean initial vertical effective stress.

Consideration of Quality

Many flow slide case histories are poorly documented. Lack of information leads to increased uncertainty in the parameters that go into a residual strength backanalysis. It seems logical that well documented case histories should produce more reliable estimates of residual strength, and that they should be relied upon more heavily in the development of residual strength estimation procedures.

A procedure to develop weighting factors based on case history quality was developed. The weighting factors, which varied from 0.2 to 1.0, were based on amount and completeness of documentation, number of prior investigations, and consistency of prior investigations. The final weighting factors are listed in Table G.4 and are shown graphically in Figure G.15.

Table G.4 Component values and final weighting factors for all case histories.

Case History	\bar{N}	σ_N	\bar{S}_r	σ_{S_r}	w_{total}
Asele Road	11.0	10.7	163.6	54.6	0.20
Calaveras Dam	10.5	9.7	636.9	223.1	0.55
Chonan Middle School	6.4	6.9	178.7	32.0	0.74
El Cobre Tailings Dam	6.8	0.9	195.2	64.8	0.60
Fort Peck Dam	15.8	0.9	671.6	130.2	0.85
Hachiro-Gata Roadway	5.7	2.8	65.0	24.7	0.55
Helsinki Harbor	5.9	8.0	53.2	19.0	0.39
Hokkaido Tailings	5.1	1.4	250.6	71.9	0.31
Kawagishi-cho Building	4.3	1.2	123.5	56.7	0.50
Koda Numa Embankment	3.6	4.1	48.0	15.9	0.44
Lake Ackerman Roadway	4.8	1.2	98.0	20.4	1.00
La Marquesa Downstream	9.9	3.0	343.5	113.8	0.72
La Marquesa Upstream	6.5	2.8	185.1	82.1	0.76
La Palma Dam	4.2	1.8	193.3	86.3	0.80
Lake Merced Bank	5.9	8.0	139.5	41.4	0.39
Lower San Fernando Dam	14.5	1.1	484.7	111.0	1.00
Metoki Road	2.0	1.5	116.8	53.7	0.39
Mochi Koshi Tailings Dam 1	8.9	0.6	158.9	47.7	0.34
Mochi Koshi Tailings Dam 2	10.0	1.3	233.6	78.0	0.67
Nalband Railway	6.3	5.6	139.9	40.2	0.51
Nerlerk Berm	11.4	7.7	179.1	32.1	0.41
Route 272 Roadway	8.5	2.6	130.5	33.5	0.70
Sheffield Dam	8.2	6.8	100.0	29.8	0.37
Shibecha-Cho Embankment	5.6	2.2	208.9	38.6	0.70
Snow River Bridge Fill	8.5	9.0	50.1	16.6	0.50
Solfatara Canal Dike	4.9	6.9	77.1	25.6	0.42
Soviet Tajik – May 1 Slide	8.9	5.7	334.3	110.9	0.22
Tar Island Dike	8.9	9.7	364.2	115.6	0.32
Uetsu-Line Railway	2.9	4.2	43.7	24.8	0.55
Wachusett Dam	7.3	1.9	348.0	74.8	1.00
Zeeland	8.5	5.5	226.0	75.0	0.39

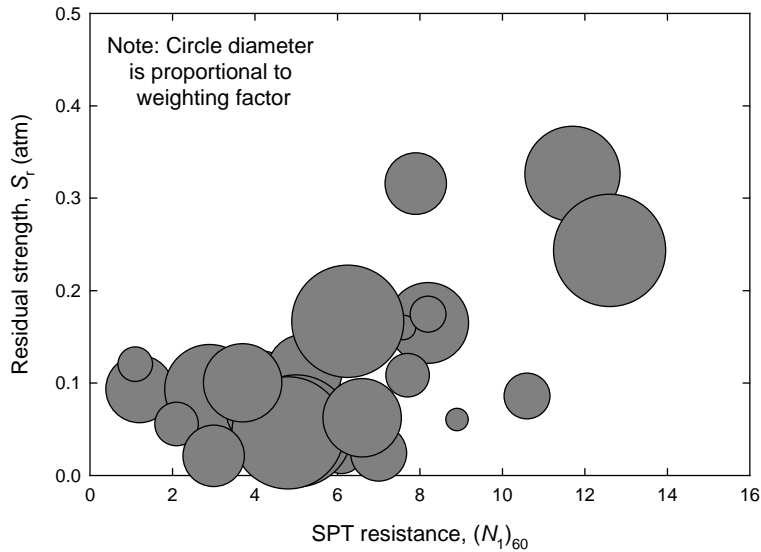


Figure G.15. Variation of backanalyzed residual strength values with mean SPT resistance. Circle diameter is proportional to weighting factor.

DEVELOPMENT OF A HYBRID MODEL

The results of the residual strength backanalyses were used to develop both classical and normalized residual strength ratios. After examining the level of accuracy with which each were able to represent the results of the case history analyses, a hybrid residual strength model was developed. The hybrid model, like the normalized residual strength model, considers residual strength to be dependent on both density and initial effective stress, but the dependence is nonlinear with respect to both of those quantities.

Approach

The hybrid model was recognized as a new approach to prediction of the residual strength of liquefied soil, and its development was guided by several basic criteria:

1. Residual strength should increase with increasing SPT resistance.
2. Residual strength should increase with increasing initial vertical effective stress.
3. The sensitivity of residual strength to SPT resistance should increase with increasing SPT resistance.
4. The sensitivity of residual strength to initial vertical effective stress should decrease with increasing initial vertical effective stress.

5. The model should predict residual strengths at low initial vertical effective stresses that are consistent with shallow flow slide activity observed in actual earthquakes.
6. The predictive model should include all significant predictive variables.
7. The predictive model should be formulated in a manner that allows probabilistic characterization of residual strength.

NLS Analyses

A large number of potential predictive model forms were investigated using nonlinear least squares analysis; nonlinear least squares analyses can be performed relatively quickly. The models were formulated to satisfy as many of the above criteria as possible and then tested against those criteria. The result of these analyses showed that a predictive relationship of the following form could potentially satisfy all of the criteria:

$$S_r = \theta_1 \exp\left[\theta_2 \left(N + \theta_3 S^{\theta_4}\right)\right] \quad (\text{G.7})$$

where, for compactness of notation, $N = (N_1)_{60}$ and $S = \sigma'_{vo}$. The NLS analyses produced parameter values of $\theta_1 = 0.01435$, $\theta_2 = 0.10426$, $\theta_3 = 11.2734$, and $\theta_4 = 0.4$ with a residual standard error of 0.0400. This residual standard error is lower than that of any of the other models tested. Figure G.16 shows the shapes of the residual strength curves predicted by this model.

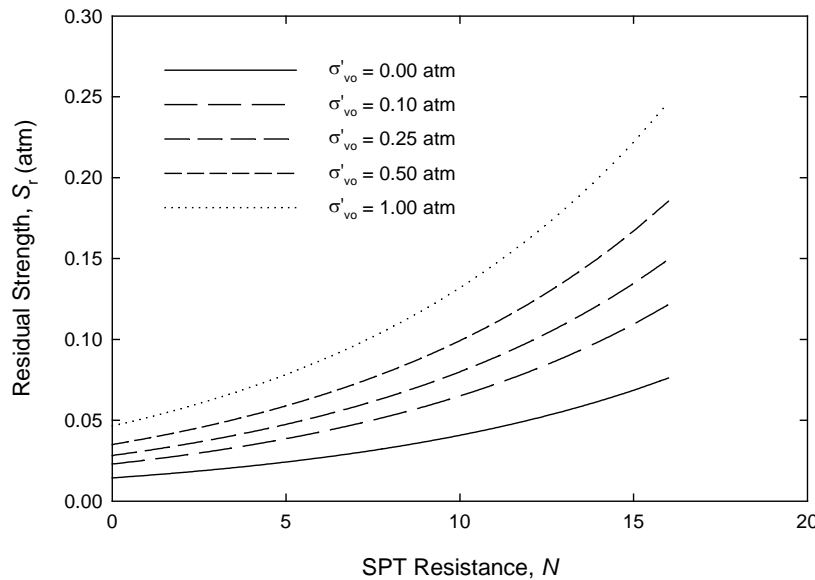


Figure G.16 Variation of mean residual strength with SPT resistance and initial vertical effective stress for NLS hybrid model.

Maximum Likelihood Estimation Analyses

Maximum likelihood estimation is an alternative method for parameter estimation. Consider a random variable, X , with density function, $f(X, \theta)$ where θ is a vector of density function parameters (e.g., mean, standard deviation, etc.). The joint probability distribution of a set of independent samples of X can be expressed, knowing the parameters, θ , as

$$\begin{aligned} f_{X_1, X_2, \dots, X_n}(x_1, x_2, \dots, x_n) &= f_{X_1}(x_1) f_{X_2}(x_2) \cdots f_{X_n}(x_n) \\ &= \prod_{i=1}^n f_X(x_i | \theta) \end{aligned} \quad (\text{G.8})$$

If the sample values are known and θ is not known, however, the right side of Equation G.8 can be interpreted as a likelihood function, i.e., a function that describes the likelihood of observing the sample given the parameters. The likelihood function is frequently expressed as

$$L(\theta | x) = \prod_{i=1}^n f_X(x_i | \theta) \quad (\text{G.9})$$

Then the maximum likelihood estimator of θ is the value, $\hat{\theta}$, that causes the likelihood function to be maximized.

Assuming residual strength to be lognormally distributed, the lognormal parameters, λ and ζ are to be determined. These parameters are related to the mean, μ , and standard deviation, σ , by

$$\mu = \exp\left(\lambda + \frac{1}{2}\zeta^2\right) \quad (\text{G.10})$$

and

$$\sigma = \mu \sqrt{\exp(\zeta^2) - 1} \quad (\text{G.11})$$

Then, a likelihood function can be expressed, using the variable R to represent residual strength, as

$$L(\lambda, \zeta | R_i) = \prod_{i=1}^n \left\{ \frac{1}{\sqrt{2\pi}\zeta R_i} \exp \left[-\frac{1}{2} \left(\frac{\ln R_i - \lambda}{\zeta} \right)^2 \right] \right\} \quad (\text{G.12})$$

where R_i is the residual strength of the i^{th} case history. Put differently, $\lambda = \mu_{\ln R}$ and $\zeta = \sigma_{\ln R}$. The exponential nature of the lognormal distribution makes it convenient to maximize the logarithm of the likelihood function, i.e.

$$\ln L(\lambda, \zeta | R_i) = -n \ln \sqrt{2\pi} - \sum_{i=1}^n \ln \zeta - \sum_{i=1}^n \ln R_i - \frac{1}{2} \sum_{i=1}^n \left(\frac{\ln R_i - \lambda}{\zeta} \right)^2 \quad (\text{G.13})$$

For the proposed hybrid model,

$$\lambda = \ln \theta_1 + \theta_2 (N + \theta_3 S^{\theta_4}) \quad (\text{G.14})$$

and ζ values were handled in one of two ways – first, as an aggregated measure of uncertainty that included the effects of uncertainty in input parameters and model uncertainty, and second, with the uncertainty in input parameters incorporated into the likelihood function.

Aggregated Uncertainty

In the first case, the MLE analyses had to identify five unknown parameters, the values of $\theta_1 - \theta_4$ in Equation 8.23, and the uncertainty variable $\theta_5 = \zeta$. The results of these analyses produced parameter values, $\theta_1 = 63.307$, $\theta_2 = 0.089$, $\theta_3 = -80.348$, $\theta_4 = -0.087$, and $\theta_5 = 0.447$. The value of $\theta_5 = \zeta = \sigma_{\ln R}$ is quite large, indicating substantial uncertainty in residual strength when uncertainties in input parameters are approximately equal to those in the case history database. The residual strength curves produced by this relationship are shown in Figure G.17.

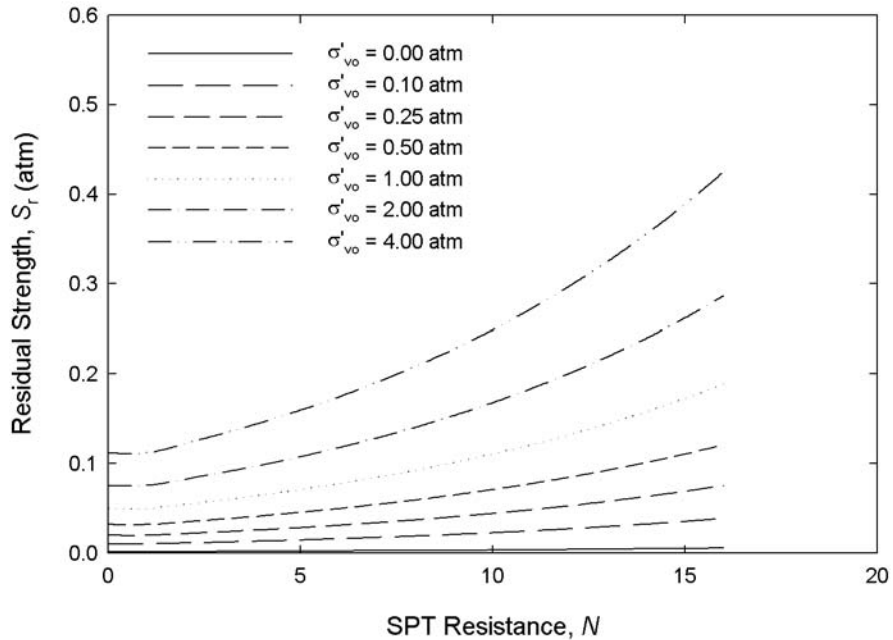


Figure G.17 Residual strength predictions for hybrid model with aggregated uncertainty.

Although the coefficients identified in the MLE analyses produce a good fit to the available case history data, they produce residual strength estimates that are extremely low at very low initial vertical effective stress levels. This aspect of the predicted behavior is similar to that predicted by the normalized residual strength ratio models, and its inconsistency with field observations, i.e., with the lack of very shallow flow slides that would be predicted by such low residual strengths, cannot be ignored. Investigation of this aspect of the model performance revealed it to be most strongly influenced by the low value of the stress exponent, θ_4 .

To identify a reasonable lower bound for θ_4 , i.e., one that would not produce residual strength estimates so low as to predict flow slides for conditions under which flow slides are not observed in the field, the lateral spread case history database of Youd et al. (2002) was utilized. This database provides data on the conditions existing in case histories of lateral spreading under ground slope and free-face conditions for soils with different thicknesses of loose soils and different slope angles. These case histories allow estimation of a conservative, lower-bound residual strength at a particular SPT resistance; since the database contains data on lateral spreads (not flow slides), the residual strengths of the sites in the database must be at least as

large as the highest shear stress in the liquefied zone. The minimum value of this shear stress and the initial vertical effective stress corresponding to it were estimated using the values of ground slope, S_{Youd} , and equivalent thickness, T_{10} , from the database. The ground slope was treated as an infinite slope (using only ground slope spreading case histories), so the minimum shear stress was computed as

$$\tau_{\min} = \gamma_{sat} T_{10} \sin \left[\tan^{-1} \left(\frac{S_{Youd} (\%)}{100} \right) \right] \quad (G.15)$$

where γ_{sat} was the unit weight estimated assuming $e = 0.7$ (approximately 50% relative density for typical uniform sands). The value of T_{10} is the cumulative thickness of soil with SPT resistance, $N \leq 10$. The manner in which the minimum shear stress was estimated implies a water level at the ground surface and that the soils for which $N \leq 10$ are contiguous from the ground surface down; both of these assumptions are conservative in that the actual conditions will produce shear stresses that are greater than the estimated minimum values. Figure G.18 shows data from the lateral spread case history database at initial vertical effective stresses less than 0.6 atm. It was determined that a stress exponent, $\theta_4 \geq 0.1$ would produce reasonable lower bound residual strengths, i.e., for very small initial vertical effective stresses just below the upper range of the minimum strengths inferred from the lateral spread data. For that reason, a lower bound of 0.1 was assigned to θ_4 in subsequent MLE analyses.

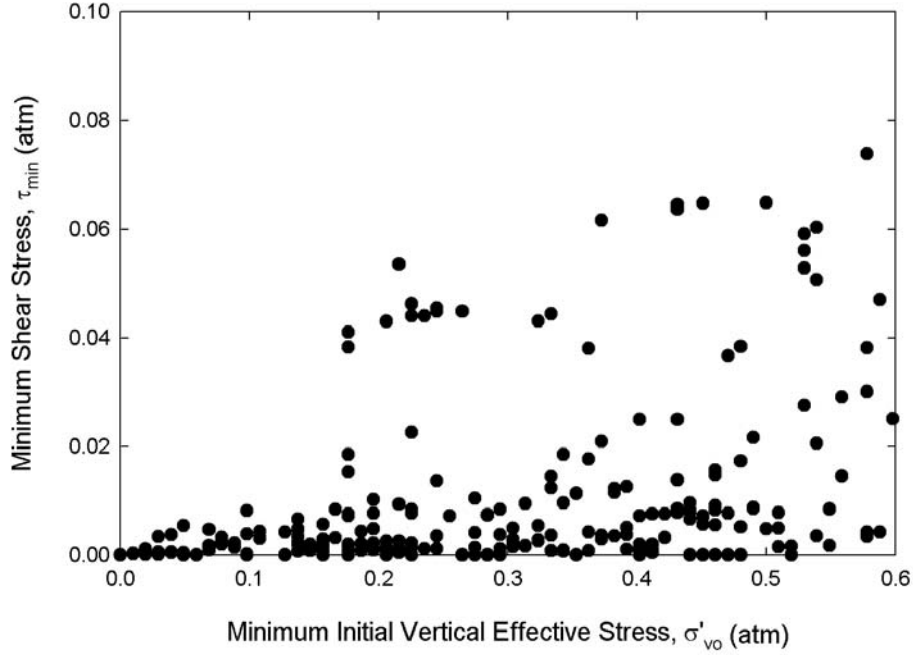


Figure G.18 Combinations of minimum shear stress and minimum initial vertical effective stresses from database of shallow lateral spreading case histories.

Separated Uncertainty

The second case involved estimating the contributions of measurement/estimation errors in the values of N and S on the uncertainty in R . This was accomplished using a first-order, second-moment (FOSM) approximation to the total uncertainty. Taking the natural logarithm of both sides of Equation G.14,

$$\ln R = \ln \theta_1 + \theta_2 (N + \theta_3 S^{\theta_4}) \quad (\text{G.16})$$

Then, assuming uncertainties in N and S are independent,

$$\zeta^2 = \sigma_{\ln R}^2 \approx \sigma_N^2 \left(\frac{\partial(\ln R)}{\partial N} \right)^2 + \sigma_S^2 \left(\frac{\partial(\ln R)}{\partial S} \right)^2 + \sigma_m^2 \quad (\text{G.17})$$

where σ_m is the standard deviation of the model uncertainty. Computing the gradients, the total uncertainty can then be expressed as

$$\zeta^2 = \sigma_{\ln R}^2 \approx \theta_2^2 \sigma_N^2 + \theta_2^2 \theta_3^2 \theta_4^2 S^{2\theta_4-2} \sigma_S^2 + \sigma_m^2 \quad (\text{G.18})$$

For the second set of MLE analyses, then, the dispersion term for each case history was modeled as

$$\zeta_i = \sqrt{\theta_2^2 \sigma_{N,i}^2 + \theta_2^2 \theta_3^2 \theta_4^2 S_i^{2\theta_4 - 2} \sigma_{S,i}^2 + \theta_5^2} \quad (\text{G.19})$$

where θ_5 now represents the standard deviation of model uncertainty.

The results of these MLE analyses produced parameter values, $\theta_1 = 0.000104$, $\theta_2 = 0.089$, $\theta_3 = 68.96$, $\theta_4 = 0.10$, and $\theta_5 = 0.202$. Figure G.19 shows the residual strength curves predicted by this equation. The curves for higher initial vertical effective stresses are similar to those for the previous (aggregated uncertainty) case but the curves for very low initial vertical effective stresses, reflecting the implications of the lateral spreading database, are somewhat higher. The θ_5 term in this analysis, which reflects model uncertainty but not uncertainty in the input parameters, is considerably smaller than in the previous case.

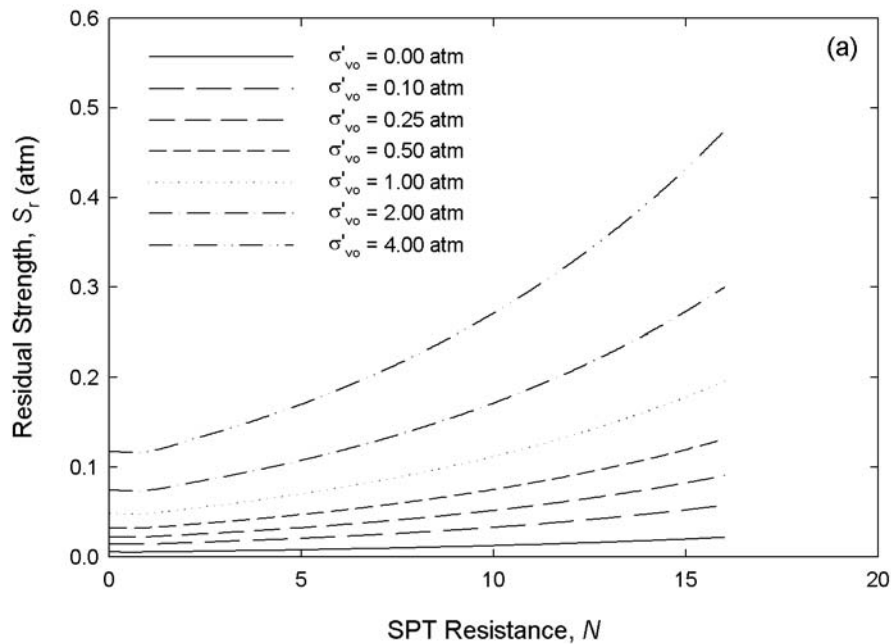


Figure G.19 Residual strength curves for hybrid model with constrained stress exponent, $\theta_4 = 0.1$, from unweighted maximum likelihood analyses.

Weighting Factors

As discussed previously, the flow slide case histories in the database used in this study were investigated and documented in widely varying levels of detail. Because of that, the quality of the case histories was also considered to be highly variable. To reduce the relative influence of case histories that were not thoroughly investigated and well-documented, a weighting factor was assigned to each case history. The weighting factors were scaled so that they summed to the number of case histories and applied in the MLE analyses. The resulting parameters, $\theta_1 = 0.000215$, $\theta_2 = 0.109$, $\theta_3 = 49.35$, $\theta_4 = 0.10$, and $\theta_5 = 0.121$, produced the residual strength curves shown in Figure G.20. These parameters, which reflect the case history data and consider its quality, form the basis of the proposed residual strength model.

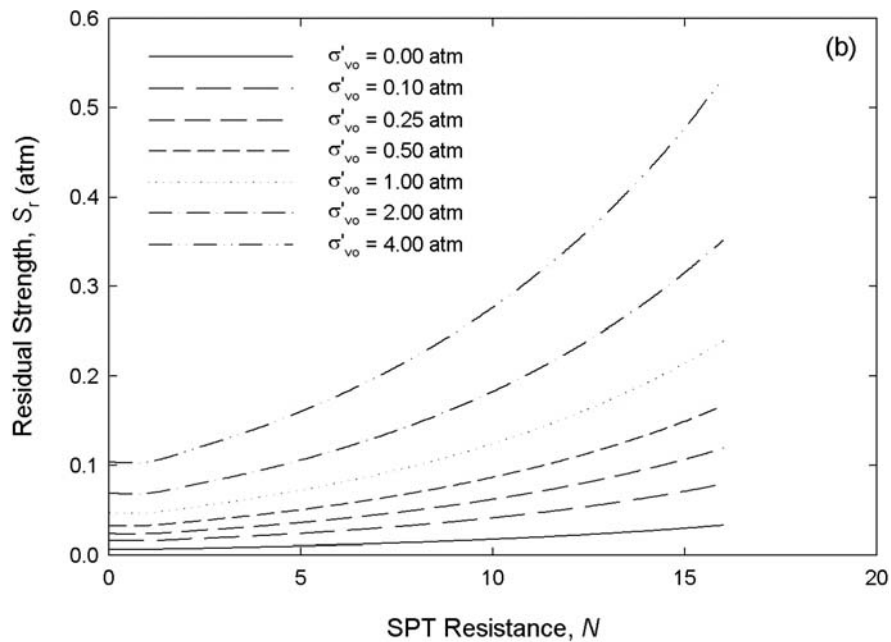


Figure G.20. Residual strength curves for hybrid model with constrained stress exponent, $\theta_4 = 0.1$, from weighted maximum likelihood analyses.

Prediction of Residual Strength

With the calibrated model based on the weighting factors, a predictive model for residual strength can be developed. For this purpose, the predictive model was written in a different form, i.e., as

$$Y = \ln R = A + BN + CS^{0.1} \quad (\text{G.20})$$

The MLE analyses produced mean values, asymptotic standard errors, and correlation values for the unknown parameters A, B, and C. The mean values and asymptotic standard errors are shown in Table G.5, and the correlation matrix in Table G.6.

Table G.5 Mean values and asymptotic standard errors for model parameters.

Parameter	Mean Value	Asymptotic Standard Error
A	-8.444	1.227
B	0.109	0.027
C	5.379	1.273

Table G.6 Correlation coefficients for model parameters.

Parameter	Correlation Coefficient		
	A	B	C
A	1.000	0.293	-0.992
B	0.293	1.000	-0.343
C	-0.992	-0.343	1.000

Recognizing that the coefficients, A-C are uncertain and correlated, and that N and S are not correlated to each other or to A-C, the variance of Y can be estimated as

$$\begin{aligned} \sigma_Y^2 = \sigma_{\ln R}^2 = & \sigma_A^2 \left(\frac{\partial Y}{\partial A} \right)^2 + \sigma_B^2 \left(\frac{\partial Y}{\partial B} \right)^2 + \sigma_N^2 \left(\frac{\partial Y}{\partial N} \right)^2 + \sigma_C^2 \left(\frac{\partial Y}{\partial C} \right)^2 + \sigma_S^2 \left(\frac{\partial Y}{\partial S} \right)^2 \\ & + 2\rho_{AB}\sigma_A\sigma_B \left(\frac{\partial Y}{\partial A} \right) \left(\frac{\partial Y}{\partial B} \right) + 2\rho_{BC}\sigma_B\sigma_C \left(\frac{\partial Y}{\partial B} \right) \left(\frac{\partial Y}{\partial C} \right) + 2\rho_{AC}\sigma_A\sigma_C \left(\frac{\partial Y}{\partial A} \right) \left(\frac{\partial Y}{\partial C} \right) \end{aligned} \quad (\text{G.21})$$

Computing the required gradients and using the asymptotic standard errors and correlation coefficients in Tables G.5 and G.6, the variance of Y can then be estimated as

$$\begin{aligned} \sigma_Y^2 = & 1.627 + 0.00073N^2 + 0.0194N - 0.027NS^{0.1} - 3.099S^{0.1} + 1.621S^{0.2} \\ & + 0.00073\sigma_N^2 + 4.935S^{-1.8}\sigma_S^2 \end{aligned} \quad (\text{G.22})$$

Estimation of the standard deviation of Y (i.e., of $\ln R$) can be simplified by expressing it in the form

$$\sigma_{\ln R} = \sqrt{\sigma_m^2 + 0.00073\bar{N}^2 COV_N^2 + 4.935\bar{S}^{0.2} COV_S^2} \quad (G.23)$$

where the model variance, σ_m^2 , is given by

$$\sigma_m^2 = 1.627 + 0.00073N^2 + 0.0194N - 0.027NS^{0.1} - 3.099S^{0.1} + 1.621S^{0.2} \quad (G.24)$$

\bar{N} is the mean SPT resistance, COV_N is the coefficient of variation of SPT resistance, \bar{S} is the mean initial vertical effective stress, and COV_S is the coefficient of variation of initial vertical effective stress. Values of the model variance are tabulated in Table G.7

Table G.7 Values of model variance, σ_m^2 , for different combinations of SPT resistance and initial vertical effective stress.

SPT Resistance	Initial Vertical Effective Stress, σ'_{vo} (atm)						
	0.01	0.1	0.25	0.5	1	2	4
0	0.317	0.188	0.158	0.147	0.149	0.168	0.206
1	0.320	0.187	0.154	0.142	0.142	0.159	0.195
2	0.325	0.187	0.152	0.138	0.137	0.151	0.186
3	0.331	0.189	0.152	0.136	0.133	0.146	0.178
4	0.338	0.192	0.153	0.135	0.130	0.141	0.171
5	0.347	0.196	0.155	0.136	0.129	0.138	0.166
6	0.357	0.202	0.159	0.138	0.130	0.137	0.163
7	0.369	0.210	0.165	0.142	0.132	0.137	0.161
8	0.383	0.219	0.172	0.147	0.135	0.138	0.160
9	0.397	0.229	0.180	0.154	0.140	0.141	0.161
10	0.414	0.241	0.190	0.162	0.146	0.145	0.163
11	0.431	0.254	0.201	0.171	0.154	0.151	0.167
12	0.450	0.269	0.214	0.182	0.163	0.158	0.172
13	0.471	0.285	0.228	0.195	0.174	0.167	0.178
14	0.493	0.303	0.243	0.209	0.186	0.177	0.187
15	0.517	0.322	0.260	0.224	0.199	0.189	0.196
16	0.542	0.342	0.279	0.241	0.214	0.202	0.207

Proposed Residual Strength Model

The final version of the proposed hybrid model for prediction of residual strength as a function of both SPT resistance and initial vertical effective stress can be expressed as

$$\overline{\ln S_r} = -8.444 + 0.109N + 5.379S^{0.1} \quad (\text{G.25a})$$

$$\sigma_{\ln S_r} = \sqrt{\sigma_m^2 + 0.00073\overline{N}^2 COV_N^2 + 4.935\overline{S}^{0.2} COV_S^2} \quad (\text{G.25b})$$

where $\sigma_m^2 = 1.627 + 0.00073N^2 + 0.0194N - 0.027NS^{0.1} - 3.099S^{0.1} + 1.621S^{0.2}$. The residual strengths produced by this relationship can be used in two ways – to compute a probability distribution of residual strength for given values of SPT resistance and initial vertical effective stress, and to compute a residual strength with a particular probability of non-exceedance. The former can be used as part of a probabilistic flow slide hazard evaluation and the latter for a deterministic evaluation.

Probability Distribution of Residual Strength

Given the assumption of lognormally distributed residual strengths, the probability density function for residual strength, conditional upon SPT resistance and initial vertical effective stress, is given by

$$f_{S_r}(s) = \frac{1}{\sqrt{2\pi}\sigma_{\ln S_r} s} \exp\left[-\frac{1}{2}\left(\frac{\ln s - \overline{\ln S_r}}{\sigma_{\ln S_r}}\right)^2\right] \quad (\text{G.26})$$

For example, consider an element of soil for which $\overline{N} = 10$ and $\overline{S} = 1.0$ atm. From Equation G.25a, $\overline{\ln R} = -1.975$, so the median residual strength is $\exp(-1.975) = 0.139$ atm. With no uncertainty in SPT resistance or initial vertical effective stress, the standard deviation of $\ln R$ would be $\sqrt{0.146} = 0.382$. Figure G.21 shows the probability density functions for this soil with different levels of uncertainty in SPT resistance and initial vertical effective stress.

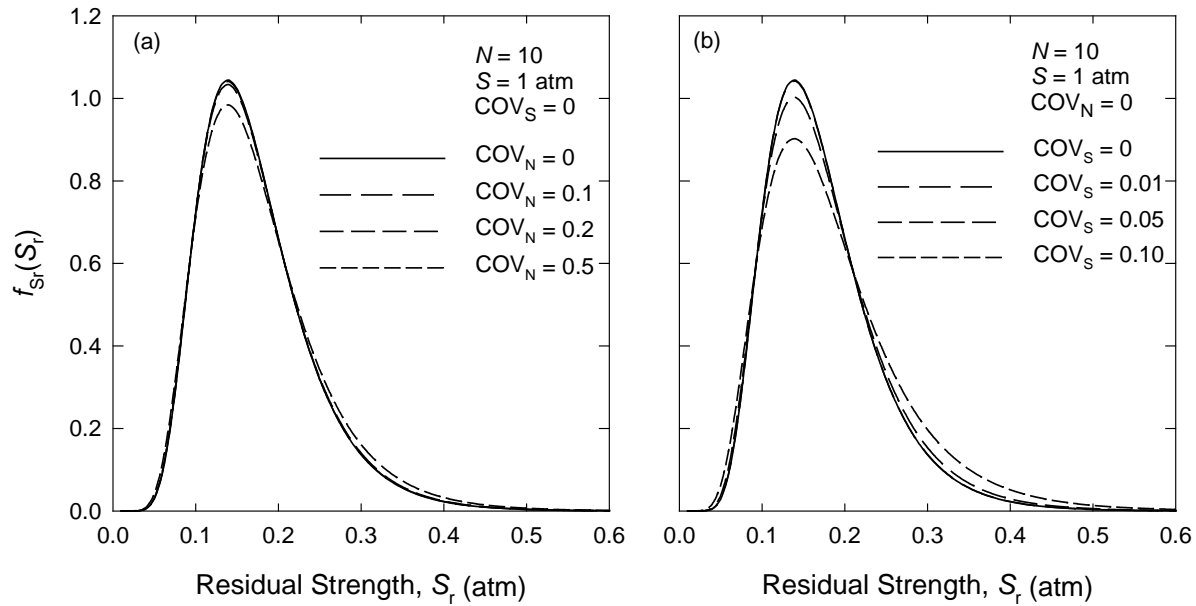


Figure G.21 Probability density functions for residual strength: (a) different uncertainties in SPT resistance, and (b) different uncertainties in initial vertical effective stress.

Figure G.21 shows that the model uncertainty can be expected to dominate the effects of uncertainties in SPT resistance and initial vertical effective stress. As a result, it does not appear necessary to explicitly consider the effects of uncertainties in SPT resistance and initial vertical effective stress in most analyses. The exception to this could be cases of very high uncertainty in initial vertical effective stress, which would likely correspond to cases in which the failure mechanism could not be predicted with confidence in advance. For practical purposes, it is reasonable to assume typical values of COV_N and COV_S ; values of 0.30 and 0.05, respectively, have been used in the following discussions.

The proposed model can also be used to estimate percentile strength values, i.e., values of residual strength with specific probabilities of *non-exceedance*. For a percentile value, P , the corresponding percentile strength is given by

$$S_r(P) = \exp\left[\overline{\ln R} + \Phi^{-1}(P)\sigma_{\ln R}\right] \quad (G.27)$$

where $\Phi^{-1}(P)$ is the inverse standard normal variate for P .

Proposed Deterministic Model

In order to suggest a reasonable procedure for residual strength prediction for deterministic flow slide analyses, it is useful to compare the distributions of residual strength predicted by the hybrid model with the residual strength values from the actual case histories. The mean values of SPT resistance and initial vertical effective stress can be used with the mean residual strength to compute an apparent residual strength percentile for each case history. By virtue of the estimation process, strength percentile values would be expected to fall both above and below the 50th percentile value; the strength percentile value describes the degree to which the mean residual strength for each case history would have been overpredicted (percentiles greater than 50) or underpredicted (percentiles less than 50) by the hybrid model. Figure G.22 shows the residual strength percentiles for each of the case histories. The percentile values can be seen to be well distributed both above and below the 50th percentile. Several of the case histories (e.g., Helsinki Harbor, Koda Numa, Sheffield Dam, Snow River, and Uetsu Line) have very low percentile values indicating that the hybrid model would have predicted median residual strengths considerably greater than the values back-calculated for those case histories.

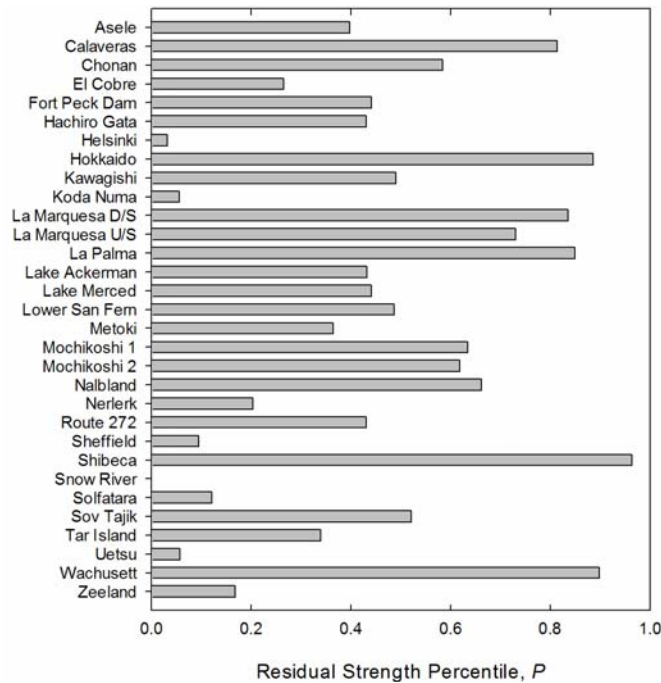


Figure G.22. Residual strength percentile values according to hybrid model for all case histories.

Some useful insight into appropriate percentile levels for deterministic analyses can be obtained by comparing the residual strength percentile values with the weighting factors. Figure G.22 shows the variation of residual strength percentile with weighting factor. Although the data is scattered, there is a general trend of increasing residual strength percentile with increasing weighting factor, which suggests that the poorly investigated and documented case histories would be more likely to have residual strengths that would have been underpredicted by the proposed hybrid procedure. Partitioning the data (Figure G.23) shows that nearly all of the lowest percentile values (percentiles less than 40) are associated with case histories that had weighting factors less than 0.60. Therefore, interpreting case histories with weighting factors greater than 0.60 as reasonably well investigated and well-documented case histories, a residual strength percentile of 40 would produce a predicted residual strength that exceeded the back-calculated residual strength for nearly all case histories.

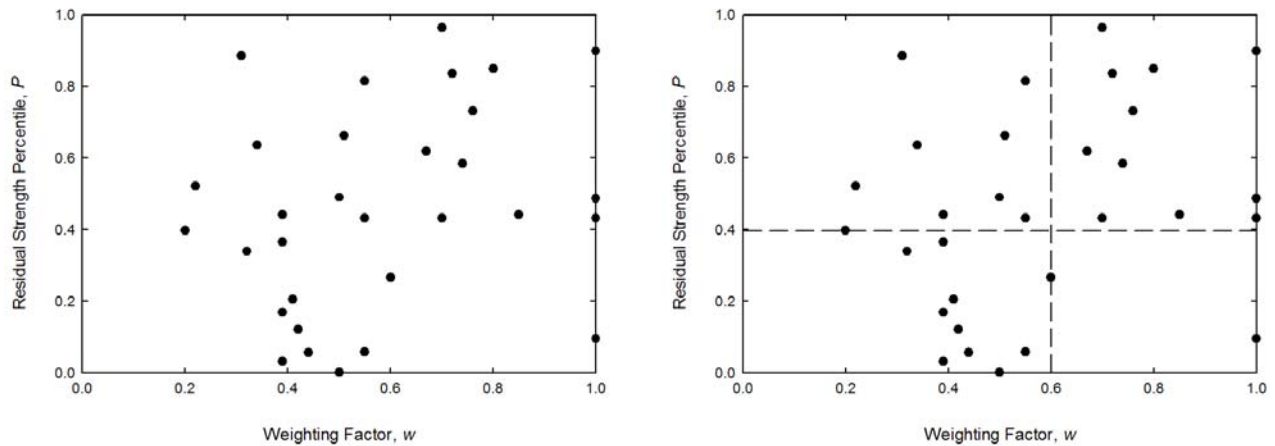


Figure G.23. Relationship between weighting factor and residual strength percentile for each case history: (a) basic data, and (b) partitioned data.

Based on these results, it is recommended that residual strengths for deterministic flow slide analyses at well-investigated sites be based on residual strengths computed using 40th percentile strengths

$$S_r = \exp\left[\overline{\ln S_r} - 0.253\sigma_{\ln S_r}\right] \quad (G.28)$$

where

$$\overline{\ln S_r} = -8.444 + 0.109N + 5.379S^{0.1}$$

$$\sigma_{\ln S_r} = \sqrt{\sigma_m^2 + 0.000066N^2 + 0.0123S^{0.2}}$$

$$\sigma_m^2 = 1.627 + 0.00073N^2 + 0.0194N - 0.027NS^{0.1} - 3.099S^{0.1} + 1.621S^{0.2}$$

With the indicated substitutions, the expression for deterministic residual strength can be expressed in the form

$$S_r = \exp[-8.444 + 0.109N + 5.379S^{0.1} - \tag{G.29}$$

$$0.253\sqrt{1.627 + 0.000796N^2 + 0.0194N - 0.027NS^{0.1} - 3.099S^{0.1} + 1.634S^{0.2}}$$

The recommended residual strength values from this relationship are shown graphically in Figure G.24. The same values are plotted as a function of initial vertical effective stress, in a manner similar to that presented by Baziar and Dobry (1995), in Figure G.25; however, the residual strength values do not increase linearly with increasing initial vertical effective stress as assumed by Baziar and Dobry (1995).

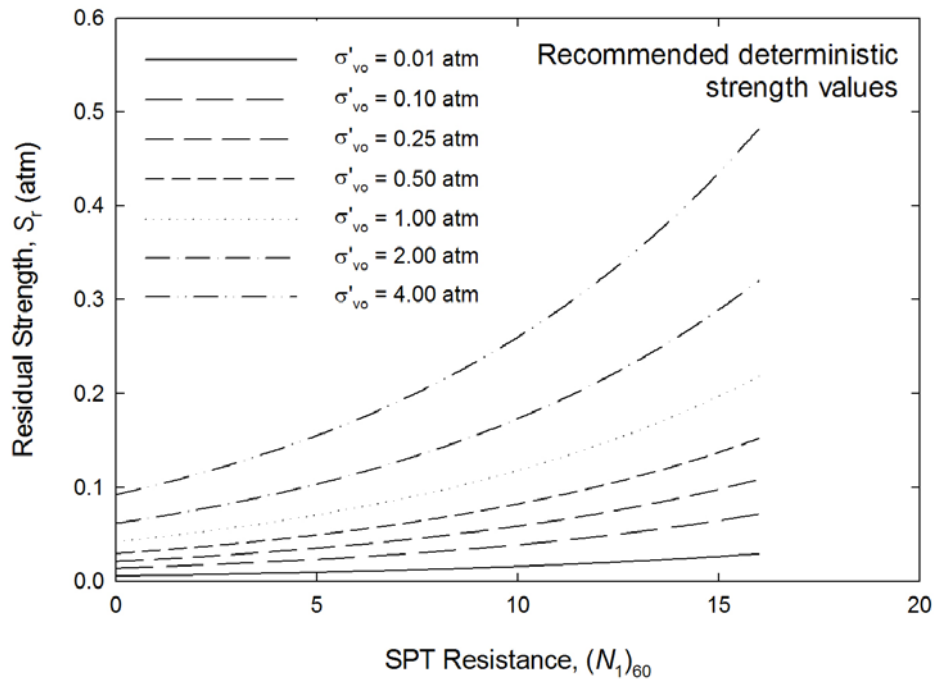


Figure G.24 Recommended residual strength values for use in deterministic stability analyses.

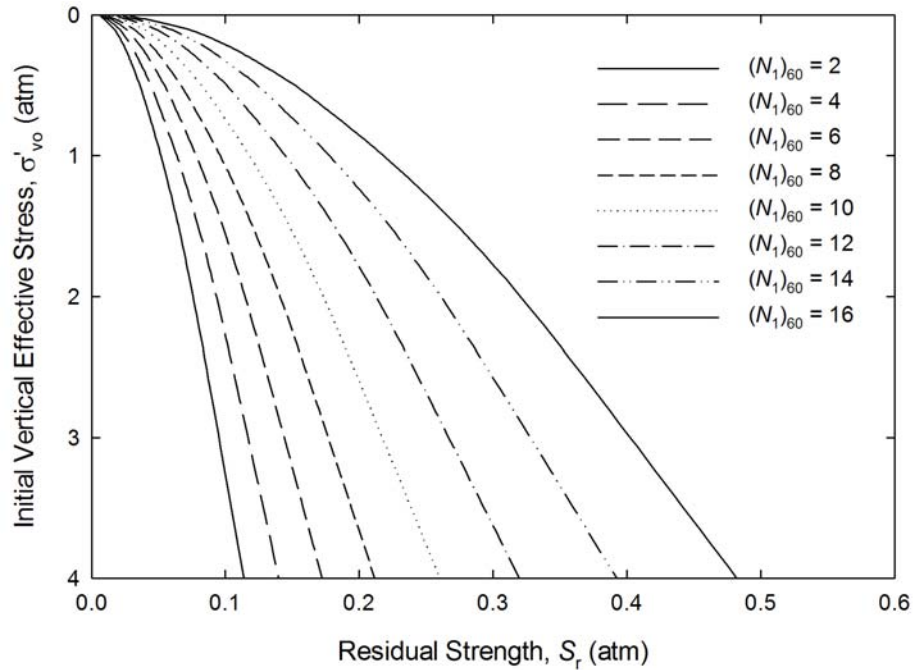


Figure G.25 Variation of recommended deterministic residual strength with initial vertical effective stress.

Comparison with Other Deterministic Residual Strength Models

The recommended deterministic residual strength model can be compared with residual strength predictions from other models. In making these comparisons, however, it is important to recognize that some aspects of the models are expressed differently. For example, the model of Seed and Harder (1990) uses “representative SPT resistance,” Idriss (1998) uses median SPT resistance, and Olson and Stark (2002) and the proposed hybrid model use mean SPT resistance. For lognormally distributed SPT resistances, the mean SPT resistance, μ_N , will exceed the median SPT resistance, m_N , by the ratio

$$\frac{\mu_N}{m_N} = \sqrt{1 + COV^2} \tag{G.30}$$

Assuming $COV = 0.30$, the mean value for lognormally distributed SPT resistances will be 1.044 times greater than the median value. Using this relationship to convert the median values of SPT resistance assumed by Idriss (1998) to approximately equivalent mean values, the residual strengths predicted for each of the case histories by the Idriss, Olson-Stark, and deterministic hybrid models are as shown in Figure G.26. The residual strength values predicted by the Idriss model (Figure G.26a) are generally consistent with the back-calculated residual strengths at lower residual strength levels (≤ 0.1 atm) and are moderately conservative at higher strength levels. The residual strength values predicted by the Olson-Stark model (Figure G.26b) are systematically lower than the back-calculated residual strengths at lower residual strength levels and systematically higher at higher strength levels. The residual strength values predicted by the deterministic hybrid model (Figure G.26c) are generally consistent with the back-calculated residual strengths at very low residual strength levels (≤ 0.05 atm) and are slightly conservative at higher strength levels. The residual strengths predicted by the Idriss and deterministic hybrid models are shown in Figure G.27(a). The two models can be seen to agree well at low and high strength levels, although there is some scatter in the relationship. relatively low residual strength levels ($S_r \leq 0.1$ atm), but the deterministic hybrid model predicts higher residual strengths at higher levels; the difference is due to the initial vertical effective stress dependency in the hybrid model. The residual strengths predicted for the case histories by the deterministic hybrid model and the Olson-Stark model are illustrated in Figure G.27(b). Figure G.27(b) must be viewed carefully to avoid concluding that the procedures produce very similar residual strength estimates; although the relationship has less scatter than the relationship between the deterministic hybrid and Idriss models, the Olson-Stark strengths are systematically lower at low residual strength levels and systematically higher at higher levels; the difference is due to differences in the stress scaling of residual strength assumed by the models.

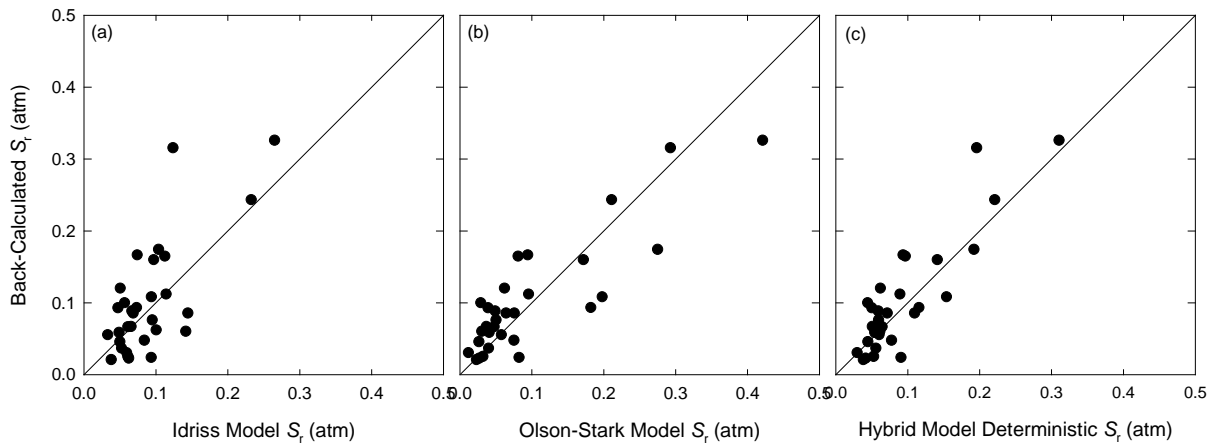


Figure G.26. Comparison of back-calculated residual strengths with residual strength values predicted by: (a) Idriss model, (b) Olson-Stark model, and (c) deterministic hybrid model.

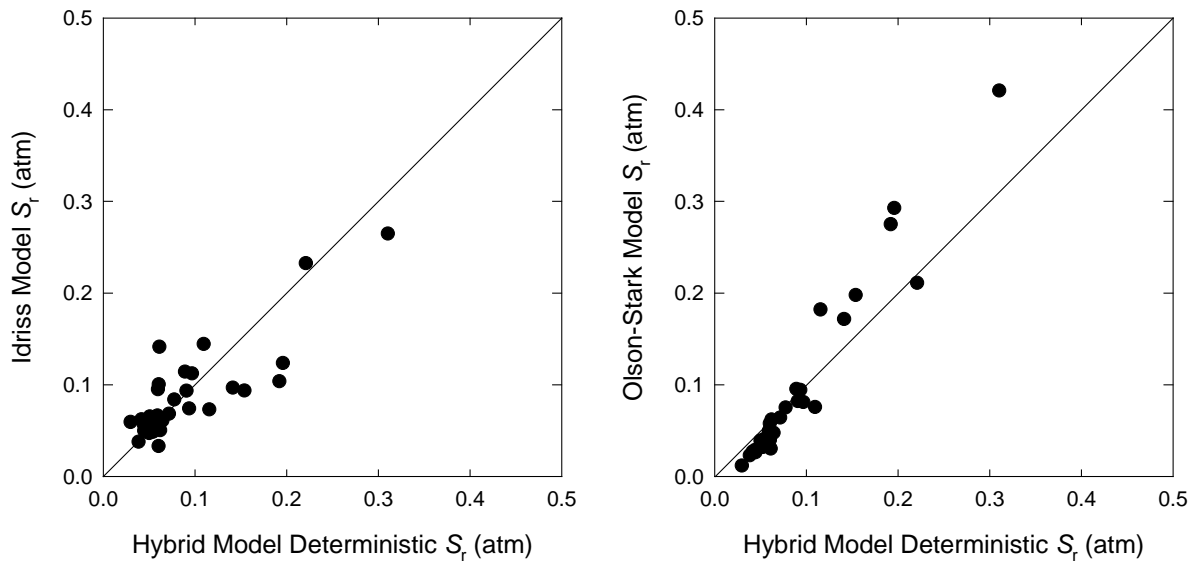


Figure G.27. Residual strength values predicted by deterministic hybrid model and (a) Idriss model, and (b) Olson-Stark model.

The deterministic hybrid model can also be compared with the residual strength interpretation of Baziar and Dobry (1995). Baziar and Dobry showed that a set of case histories were bounded by residual strength values ranging from 4% to 20% of the initial vertical effective stress. Figure G.28 shows how the residual strength values predicted by the deterministic hybrid model compare with the bounds of Baziar and Dobry. The predicted residual strengths generally fall

within the range indicated by Baziar and Dobry, although soils expected to be highly dilative (denser soils at low initial vertical effective stress) are predicted by the deterministic hybrid model to have residual strengths that exceed the Baziar and Dobry upper bound curve. The predicted residual strengths at lower initial vertical effective stresses fall considerably above the upper bound of Olson and Stark; this result is considered to be consistent with the known dilative behavior of granular soils and with field observations of flow sliding and lateral spreading during earthquakes.

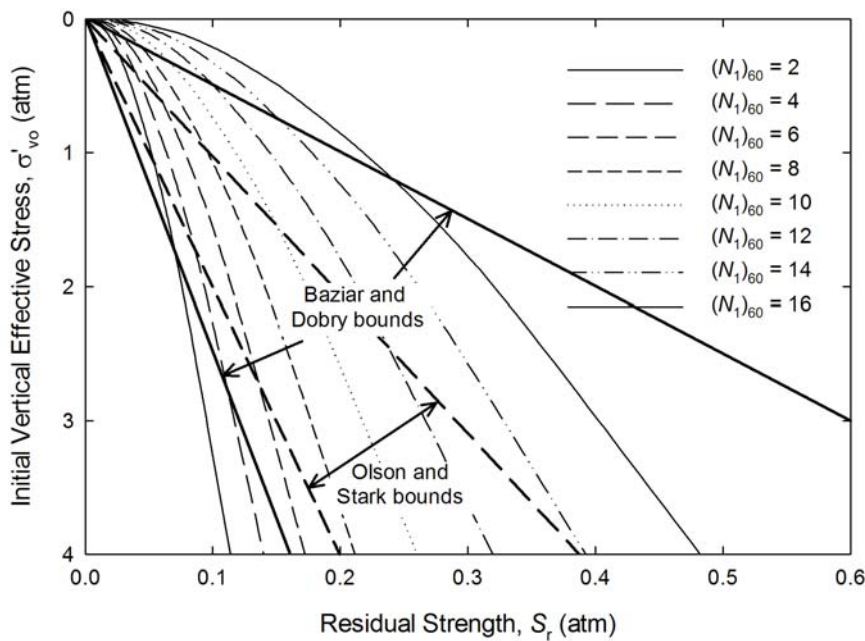


Figure G.28 Comparison of residual strengths from deterministic hybrid model with upper and lower bounds proposed by Baziar and Dobry (1995) and Olson and Stark (2002).

SUMMARY AND CONCLUSIONS

Development of a procedure for estimation of the residual strength of liquefied soil is a difficult task requiring a balance between what is understood about the mechanical behavior of liquefiable soils and what has been observed in actual earthquakes. Because the nature and amount of data that is available from field observations is not sufficient to conclusively define residual strength behavior, principles of soil mechanics have been used to guide the identification

of variables that influence residual strength and the relationship between residual strength and those variables.

Steady state principles indicate that the residual strength of a liquefied soil should depend only on the density of the soil. Elementary soil mechanics indicates that the density of the soil should depend on the effective stress acting on the soil. Basic soil mechanics also indicates that, all other things being equal, the shearing resistance of a well-graded soil is greater than that of a uniformly graded soil, and that the shearing resistance of a soil with angular particles is greater than that of a soil with rounded particles. Geotechnical experience indicates that, all other things being equal, the penetration resistance of a well-graded soil is greater than that of a uniformly graded soil, and that the penetration resistance of a soil with angular particles is greater than that of a soil with rounded particles. Taken together, these facts suggest that the residual strength of liquefied soil should increase with increasing penetration resistance and with increasing initial effective stress.

A number of researchers have investigated the residual strength problem and proposed models for estimation of residual strength. Some of these procedures estimate residual strength as a function of penetration resistance and some as a function of penetration resistance and initial effective stress. The data produced by the residual strength back-calculation analyses described in Chapter 7 were analyzed in detail and found to support a model in which residual strength was influenced by both penetration resistance and initial effective stress. The interpretation of case histories in which soils liquefied but did not flow, i.e., of lateral spreading case histories, provided insight into the stress-dependency of residual strength. A hybrid model, so named because it incorporates elements of soil behavior consistent with different prior residual strength models, was found to be more consistent with available case history data than previous models.

The hybrid model was expressed in both probabilistic and deterministic forms. The probabilistic form allows estimation of a probability distribution (conditional upon SPT resistance and initial vertical effective stress) for residual strength. The probabilistic form can easily be implemented into a performance-based flow slide evaluation. The deterministic form allows estimation of what is judged to be a moderately conservative residual strength for cases in which sufficient investigation has taken place to allow reasonable estimation of mean SPT

resistance and initial vertical effective stress. The deterministic hybrid model was compared with previous residual strength models.

REFERENCES

Alarcon-Guzman, A., Leonards, G.A., and Chameau, J.L. (1988). "Undrained monotonic and cyclic strength of sands," *Journal of Geotechnical Engineering*, ASCE, 114(10), 1089-1109.

Baziar, M.H. and Dobry, R. (1995). "Residual strength and large-deformation potential of loose silty sands." *Journal of Geotechnical Engineering*, ASCE, 121(12), 896-906. Been, K. and Jefferies, M.G. (1985). "A state parameter for sands." *Geotechnique*, 35(2), 99-112.

Been, K., Jefferies, M.G., and Hachey, J. (1991). "The critical state of sands." *Geotechnique*, Volume 41, Number 3, pp. 365-381.

Boulanger, R. W., and Truman, S. P. (1996). "Void redistribution in sand under post-earthquake loading." *Canadian Geotechnical Journal*, 33, 829-834.

Castro, G. (1969). "Liquefaction of sands," *Harvard Soil Mechanics Series, Number 88*, Harvard University, Cambridge, MA, pp. 112.

Davis, A.P. Jr., Poulos, S.J., and Castro, G. (1988). "Strengths backfigured from liquefaction case histories." *Proc., 2nd Int. Conf. on Case Histories in Geotechnical Engineering*, June 1- 5, St. Louis, MO, 1693-1701.

DeGregorio, V.B. (1990). "Loading systems, sample preparation, and liquefaction," *Journal of Geotechnical Engineering*, ASCE, 116(5), 805-821.

Hamada, M., H. Sato, T. Kawakami, 1994, "A consideration for the mechanism for liquefaction-related large ground displacement," *Proceedings of the 5th U.S. Japan Workshop on Earthquake Resistant Design of Lifeline Facilities and Countermeasures for Soil Liquefaction*, NCEER Report 94-0026, T. D. O'Rourke and M. Hamada, Eds., pp. 217-

Hanzawa, H. (1980). "Undrained strength and stability of quick sand," *Soils and Foundations*, 20(2), 17-29.

Kramer, S.L. (1989). "Uncertainty in steady-state liquefaction evaluation procedures," *Journal of Geotechnical Engineering*, ASCE, 115(10), pp. 1402-1419.

Kuerbis, R.H., Negussey, D., and Vaid, Y.P. (1988). "Effect of gradation and fines content on the undrained response of sand," *Proceedings of Specialty Conference on Hydraulic Fill Structures*, GSP No. 21, 330-345.

- Kulasingam, R., Malvick, E. J., Boulanger, R. W., and Kutter, B. L. (2004). "Strength loss and localization at silt interlayers in slopes of liquefied sand." *Journal of Geotechnical and Geoenvironmental Engineering*, ASCE, 130(11), 1192-1202.
- Miuri, S. and Toki, S. (1982). "A sample preparation method and its effect on static and cyclic deformation-strength properties of sand," *Soils and Foundations*, 22(1), 61-77.
- Olson, S.M. and Stark, T.D. (2002). "Liquefied strength ratio from liquefaction flow failure case histories," *Canadian Geotechnical Journal*, 39(5), 629-647.
- Olson, S.M., Stark, T.D., Walton, W.H., and Castro, G. (2000). "Static liquefaction flow failure of the North Dike of Wachusett Dam." *Journal of Geotechnical and Geoenvironmental Engineering*, ASCE, 126(12), 1184-1193.
- Seed, H.B. and Lee, K.L. (1966). "Liquefaction of saturated sands during cyclic loading," *Journal of the Soil Mechanics and Foundations Division*, ASCE, SM6(11), 105-134.
- Vaid, Y.P., Chung, E.F.K., and Kuerbis, R.H. (1990). "Stress path and steady state," *Canadian Geotechnical Journal*, 27(1), 1-7.
- Vaid, Y.P., Sivathayalam, S., and Stedman, D. (1999). "Influence of specimen reconstituting method on the undrained response of sand," *Geotechnical Testing Journal*, ASTM, 22(3), 187-195.
- Wride, C.E. (Fear), Hofmann, B.A., Segoo, D.C., Plewes, H.D., Konrad, J.-M., Biggar, K.W., Robertson, P.K., and Monahan, P.A. (2000). "Ground sampling program at the CANLEX test sites," *Canadian Geotechnical Journal*, 37(3), pp. 530-542.
- Yoshimi, Y., Hatanaka, M., and Oh-Oka, H. (1978). "Undisturbed Sampling of Saturated Sands by Freezing," *Soils and Foundations*, Japanese Society of Soil Mechanics and Foundation Engineering, Tokyo, Japan, 18(3), pp 59-73.
- Kutter, B.L. and Voss, T. (1995). "Analysis of data on plow resistance in dense, saturated, cohesionless soil," *Contract Report CR95.004*, Naval Facilities Engineering Service Center, Port Hueneme, California.
- Palmer, A.C. (1999). "Speed effects in cutting and ploughing," *Geotechnique*, 49(3), 285-294.
- Riemer, M.F. and Seed, R.S. (1997). "Factors affecting apparent position of steady-state line," *Journal of Geotechnical and Geoenvironmental Engineering*, 123(3), 281-288.
- Uzuoka, R., Sento, N., and Kazama, M. (2005). "Numerical analysis of rate-dependent reaction of pile in saturated or liquefied soil," *Seismic Performance and Simulation of Pile Foundations in Liquefied and Laterally Spreading Ground*, R.W. Boulanger and K. Tokimatsu, eds., Geotechnical Special Publication No. 145, ASCE, 204-217.

Vaid, Y.P., Chung, E.K.F., and Kuerbis, R.H. (1990). "Stress path and steady state," *Canadian Geotechnical Journal*, Volume 27, Number 1, pp. 1-7.

Verdugo, R. and Ishihara, K. (1996): "The steady state of sandy soils," *Soils and Foundations*, Vol. 36, No. 2, pp. 81-92.

Yoshimine, M. (2003). "Liquefied soil-pile interaction and its rate effects," *First Japan-U.S. Workshop on Testing, Modeling, and Simulation in Geomechanics*, Boston.

Appendix H

WSliq User's Manual

This appendix presents a description of how the WSliq program can be used to perform a variety of important liquefaction hazard analyses. The WSliq program was created as part of an extended research project supported by the Washington State Department of Transportation (WSDOT). The WSliq program is intended to allow WSDOT engineers to evaluate liquefaction hazards more accurately, reliably, and consistently, and to do so more efficiently than is possible even with the more limited procedures commonly used in contemporary geotechnical engineering practice.

The WSliq program should be used only after the user has read the report within which this User's Manual is contained. The report provides important information on the procedures used to perform the various liquefaction hazard analyses possible with WSliq, and it is essential that users be familiar with those procedures and the information required to complete them before using WSliq.

WSliq is organized in a manner similar to that with which a liquefaction hazard evaluation would normally be conducted. In such an evaluation, an engineer would generally be required to answer three questions:

1. Is the soil *susceptible* to liquefaction?
2. If so, is the anticipated earthquake loading strong enough to *initiate* liquefaction?
3. If so, what will be the *effects* of liquefaction?

The WSliq interface, therefore, is divided into three main tabs devoted to susceptibility, initiation, and effects. Along with tabs that facilitate entry of soil profile data and examination/documentation of results, these define the basic user interface.

This User's Manual is graphically oriented, i.e., it presents the required data by reference to the locations at which that data are entered on the various WSliq forms.

Welcome Tab

The Welcome tab provides two primary functions: a place for entry of global information—i.e., information potentially required for all desired analyses—and an introduction to the purpose of the WSliq program. The required global data consist of information required to identify the site and ground motion hazards at the site. A screen shot of the Welcome tab is shown in Figure H.1.

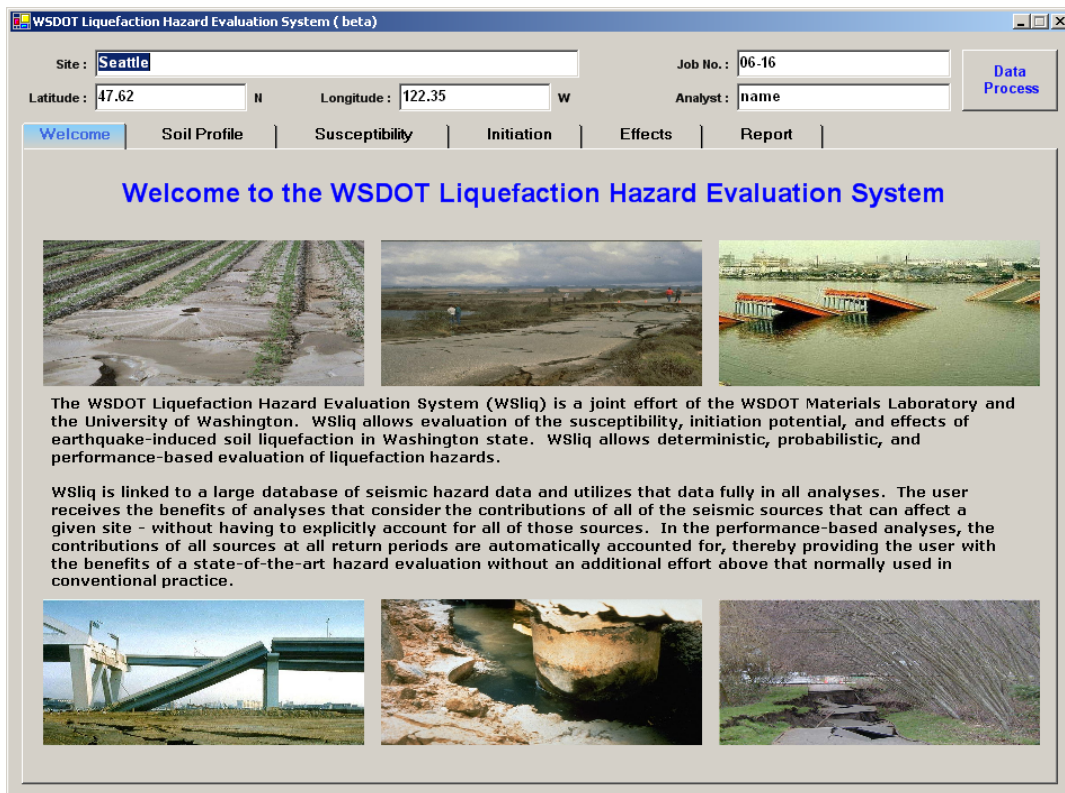


Figure H.1 WSliq Welcome tab.

The global information requested on the Welcome form, and the purpose of the Data Process button found on that form, are described in Table H.1:

Table H.1. Required information and buttons on the Welcome screen.

Text Box Information	
Item	Comments
Site:	Enter an alphanumeric description of the site. This information will be written to the Report to help identify the site.
Job No.:	Enter an alphanumeric description of the job/project number. This information will be written to the Report to help identify the site.
Latitude:	Enter latitude in decimal degrees. All latitude values must exist within Washington State.
Longitude:	Enter longitude in decimal degrees. All longitude values must exist within Washington State.
Analyst:	Enter an alphanumeric description (name) that describes the person performing the analyses.
Buttons	
Item	Comments
Data Process:	Used to specify the location (path) of the ground motion hazard data files or to add to the ground motion hazard database. Only needed if the user wishes to add more hazard locations or store ground motion hazard databases in locations other than the default locations defined during program installation.

Soil Profile Tab

The Soil Profile tab (Figure H.2) allows entry of data that define the soil profile, for the purposes of liquefaction hazard evaluation, at the site of interest. The soil profile is defined by a series of sublayers, within which all properties are assumed to be constant, and information required for the various analyses is entered on a sublayer-by-sublayer basis.

WSDOT Liquefaction Hazard Evaluation System (beta)

Site : Seattle Job No. : 1
 Latitude : 47.620 N Longitude : 122.350 W Analyst : name Data Process

Welcome **Soil Profile** Susceptibility Initiation Effects Report

No. of Soil Layers: 12 GWT at top of layer: 3 GWT Depth, m: 2.00 SPT ER: 60.00 % Amp. Factor Pore Pressure

Ground Surface
 Elevation : 0.00 m Level Infinite Slope : 3 % Free-face ratio : 1.0 % Units
 lbs, ft kN, m Calculate

Add/ Drop	#	Description	Thickness (m)	DTC (m)	Unit Wt (kN/m ³)	Meas. SPT	FC (%)	D50 (mm)	Init. Vert. Eff. Stress (kPa)	(N1)60	Vs (m/sec)
+/-	1	Silty sand	1	0.50	15.40	10	15	0.100	7.70	17.00	196.12
+/-	2	Silty sand	1	1.50	15.40	10	10	0.100	23.10	17.00	196.12
+/-	3	Loose sand	1	2.50	19.66	12	0	0.100	35.73	20.21	206.77
+/-	4	Loose sand	1	3.50	19.80	14	0	0.100	45.65	20.86	216.23
+/-	5	Sand	1	4.50	19.94	16	0	0.100	55.70	21.58	224.76
+/-	6	Sand	1	5.50	20.07	18	0	0.100	65.90	22.32	232.57
+/-	7	Silty sand	1	6.50	20.20	20	14	0.100	76.22	23.06	239.79
+/-	8	Sand	1	7.50	20.33	22	0	0.100	86.68	23.79	246.51
+/-	9	Silty sand	1	8.50	20.46	24	22	0.100	97.27	24.50	252.81
+/-	10	Dense sand	1	9.50	20.58	26	0	0.100	107.98	25.19	258.74
+/-	11	Dense sand	1	10.50	20.70	28	0	0.100	118.81	25.86	264.37
+/-	12	Dense sand	1	11.50	20.81	30	0	0.100	129.75	26.51	269.71

Plot with Depth Elevation Open Data File ... Save Data File ... Plot Soil Profile Batch

Figure H.2 WSliq Soil Profile tab.

Table H.2. Required information and buttons on the Soil Profile tab.

Upper Level Text Box Information	
Item	Comments
No. of Soil Layers:	Enter the integer number of soil layers used to define the subsurface profile
GWT at top of layer:	Enter the layer number corresponding to the groundwater table. Note that sublayers must be arranged so that the groundwater table coincides with the top of some sublayer.
SPT ER:	Enter the SPT energy ratio, E_R , in percent. This value is used to correct measured SPT resistance.
Ground surface elevation	Enter the elevation of the ground surface in appropriate units.
Infinite slope:	For ground slope geometries (lateral spreading analysis), enter the ground slope, S , in percent.
Free-face ratio:	For free-face geometries (lateral spreading analysis), enter the free-face ratio, W , in percent.
Units:	Select the desired units for data.

Soil Profile Data Text Box Information	
Item	Comments
Description:	Enter an alphanumeric soil description (up to 30 characters)
Thickness:	Enter the sublayer thickness
DTC:	Depth to the center of the layer (computed from sublayer thicknesses)
Unit Wt:	Enter the sublayer unit weight (not density)
Meas. SPT:	Enter the measured SPT resistance
FC:	Enter the measured fines content in percent. Estimate if not available.
D50:	Enter the mean grain size (used for Youd et al. lateral spreading analysis). Estimate if not available.
Init. Vert. Eff. Stress:	Vertical effective stress at the center of the layer (computed from unit weight, thickness, and water table data)
(N₁)₆₀:	Value of $(N_1)_{60}$ computed from the initial vertical effective stress and energy ratio. This value is NOT fines-corrected.
Vs:	Shear wave velocity (computed from $(N_1)_{60}$ and vertical effective stress by using the Ohta and Goto relationship; used in Cetin et al. liquefaction model)
Buttons	
Item	Comments
+/-	Allows insertion of new layer above or below the layer for which the button was clicked.
Amp. Factor	Opens new form on which the PGA amplification factor (relative to NEHRP B/C boundary) can be entered. The amplification factor value can be entered directly, or in terms of the a and b coefficients used in the indicated Stewart-type relationship.
Pore Pressure	Opens a window in which the initial pore pressures can be entered. The window should open with the hydrostatic pore pressure values shown; the values can be changed, if necessary, to accommodate a perched water table or other situations that can produce a non-uniform initial pore pressure profile.
Calculate	Uses the entered soil profile data to compute the initial vertical effective stress, corrected SPT resistance, and shear wave velocity.
Open Data File	Allows an existing soil profile data file to be entered into WSliq.
Save Data File	Allows the entered soil profile data to be saved in a data file.
Plot Soil Profile	Produces plots of initial vertical effective stress, measured and corrected SPT resistance, fines content, and plasticity index with depth.
Batch	Opens a window allowing batch analysis to be specified. A susceptibility analysis must be performed before the parameters of the batch analysis are specified. The user can decide in advance which analyses (liquefaction initiation, lateral spreading, post-liquefaction settlement, etc.) are to be performed.

Susceptibility Tab

The Susceptibility tab (Figure H.3) allows convenient computation of the Susceptibility Index (*SI*) and use of the *SI* to evaluate the susceptibility of each layer in the soil profile. The *SI* provides a quantitative measure of liquefaction susceptibility that allows a user to compare the relative susceptibilities of different layers. The *SI* value is also used in subsequent calculations to account for epistemic uncertainty in liquefaction susceptibility. In those calculations, the user can choose to consider only soil layers judged to be susceptible to liquefaction or to consider all layers with their contributions weighted by the *SI* value; in that case, the *SI* value is treated as a subjective probability, or degree of belief, of susceptibility.

WSDOT Liquefaction Hazard Evaluation System (beta)

Site: Job No.:

Latitude: N Longitude: W Analyst:

Layer	Description	DTC	PI	wc/LL	Boulanger Idriss	Bray Sancio	Susceptibility Index	Susceptible?
1	Silty sand	0.50	Unsat	Unsat	0.00	0.00	0.00	NO
2	Silty sand	1.50	Unsat	Unsat	0.00	0.00	0.00	NO
3	Loose sand	2.50	N.P.	N.P.	1.00	1.00	1.00	YES
4	Loose sand	3.50	N.P.	N.P.	1.00	1.00	1.00	YES
5	Sand	4.50	N.P.	N.P.	1.00	1.00	1.00	YES
6	Sand	5.50	N.P.	N.P.	1.00	1.00	1.00	YES
7	Silty sand	6.50	14	0.8	0.01	0.26	0.14	NO
8	Sand	7.50	N.P.	N.P.	1.00	1.00	1.00	YES
9	Silty sand	8.50	22	0.8	0.00	0.05	0.02	NO
10	Dense sand	9.50	N.P.	N.P.	1.00	1.00	1.00	YES
11	Dense sand	10.50	N.P.	N.P.	1.00	1.00	1.00	YES
12	Dense sand	11.50	N.P.	N.P.	1.00	1.00	1.00	YES

Threshold SI: Weighting Factors: B-I B-S

Figure H.3. Liquefaction Susceptibility tab

Table H.2. Required information and buttons on Soil Profile tab.

Text Box Information	
Item	Comments
PI:	Enter the plasticity index for each layer. The notation 'N.P.' (non-plastic) will appear in this box for all layers with zero fines, and the notation 'Unsat' will appear for layers above the water table. Non-plastic soils will be assigned $SI = 1.0$, and unsaturated soils will be assigned $SI = 0.0$.
wc/LL:	Enter the ratio of water content to liquid limit in decimal form. The notation 'N.P.' (non-plastic) will appear in this box for all layers with zero fines, and the notation 'Unsat' will appear for layers above the water table.
Threshold SI:	Enter the threshold value of the Susceptibility Index for judgment of the soil as liquefiable. Entering a threshold value of 0.0 will cause all layers to be treated as susceptible to liquefaction in subsequent calculations.
Weighting factors:	Enter the elevation of the ground surface in appropriate units
Infinite slope:	For ground slope geometries (lateral spreading analysis), enter the ground slope in percent.
Free-face ratio:	For free-face geometries (lateral spreading analysis), enter the free-face ratio in percent.
Slider control	
Item	Comments
Weighting factors:	Use the slider to select weighting factors to be applied to the Boulanger-Idriss and Bray-Sancio procedures for evaluation of liquefaction potential. The weighting factor values will automatically add up to 1.0.
Buttons	
Item	Comments
Evaluate	Computes susceptibility index values for Boulanger-Idriss and Bray-Sancio models, computes Susceptibility Index according to weighting factors, and denotes susceptibility (in yes/no manner).

The results of the susceptibility evaluation are expressed in terms of SI values for both the Boulanger-Idriss and Bray-Sancio procedures, as described in Chapter 4. A weighted average SI value is then compared with the threshold SI value selected by the user to judge whether or not the soil is susceptible to liquefaction.

The user should note that many of the subsequent calculations (liquefaction potential, lateral spreading, etc.) do not include non-susceptible layers. All layers can be forced to be susceptible by setting the threshold SI value to zero; the results of any analyses performed in this manner should be reviewed and interpreted carefully.

Initiation Tab

The Initiation tab has a series of three sub-tabs that allow entry of data for single-scenario, multiple-scenario, and performance-based analyses of liquefaction potential. The required data are described below.

Single-Scenario Analyses

Single-scenario analyses can be performed in two basic ways: by inputting any desired combination of peak ground surface acceleration and magnitude, or by inputting peak ground surface acceleration values associated with a particular return period and the corresponding (mean or modal) magnitude values. In the latter case, the program determines the appropriate a_{\max} and M values from the hazard database. Figure H.4 shows the single-scenario sub-tab, and Table H.3 describes the input required to perform single-scenario analyses.

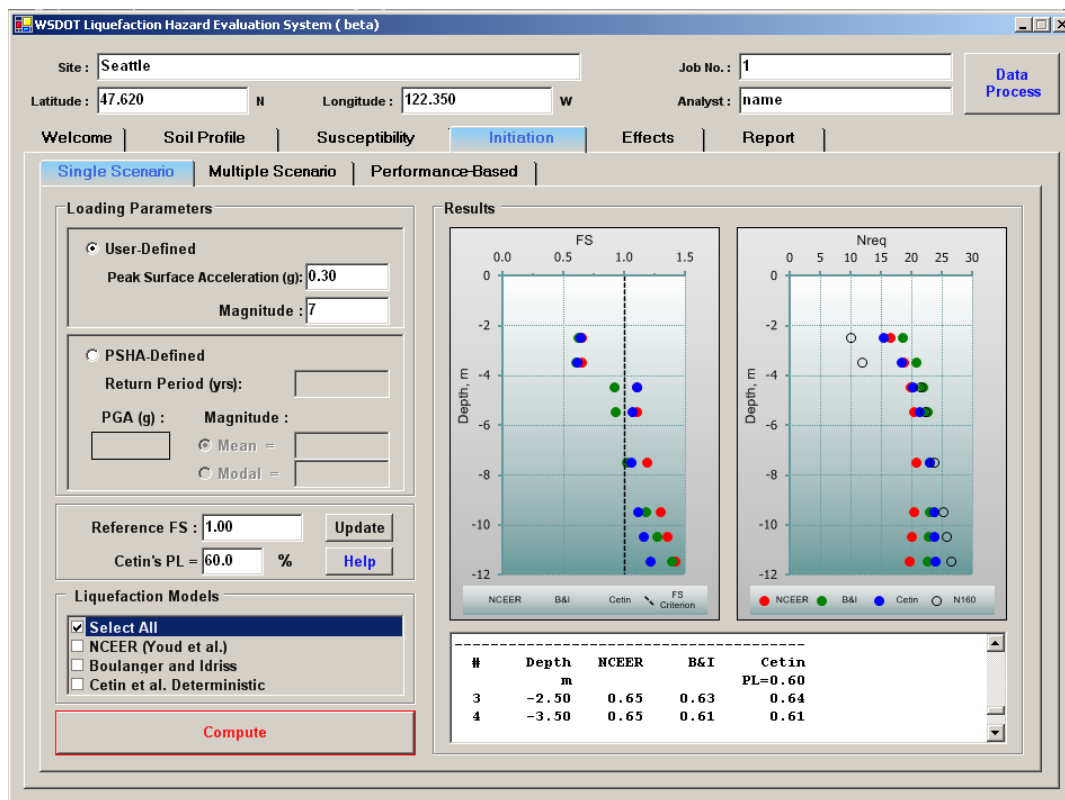


Figure H.4 WSliq Single-Scenario Liquefaction Initiation tab.

The results of single-scenario analyses are displayed graphically as plots of FS_L and N_{req} vs. depth and numerically in tabular form in the window below the plots. Clicking on either of the plots will produce a larger version of the plot. Right-clicking on any plot will allow various characteristics of the plot to be edited. The numerical data can be accessed within the single-scenario tab or on the Report tab; they can also be saved on the Report tab.

Table H.3. Required information and buttons on Single-Scenario Liquefaction Initiation tab.

User-Defined Loading Parameter Information	
Item	Comments
Peak acceleration:	Enter the peak ground surface acceleration in g's. Note that this acceleration value should account for local site conditions (e.g., amplification of rock acceleration values).
Magnitude:	Enter the magnitude to be used in the single-scenario analysis.
PSHA-Defined Loading Parameter Information	
Item	Comments
Return Period:	Enter the desired return period in years. Loading data are interpolated from the ground motion hazard database.
Magnitude:	Select the mean or modal magnitude.
Additional Input	
Item	Comments
Reference FS:	Enter a factor of safety value of interest. This option plots a line at that factor of safety to allow easy comparison of calculated factors of safety with user-defined criteria.
Cetin's PL:	The probability of liquefaction (P_L) to be used in Cetin et al. deterministic analysis. A value of 0.6 has been found to produce results similar to the NCEER model at shallow depths.
Liquefaction Models	
Item	Comments
Select All	Select to compute FS_L and N_{req} using the NCEER, Idriss-Boulanger, and Cetin et al. procedures.
NCEER Idriss- Boulanger Cetin et al.	Select individually as desired to compute FS_L and N_{req} values.
Buttons	
Item	Comments
Update	Plot the reference FS.
Help	Display a brief description of P_L for Cetin's model.
Compute	Computes FS_L and N_{req} with selected procedures.

Multiple-Scenario Analyses

Multiple-scenario analyses are easily performed with WSliq. The user is simply required to provide a return period of interest, and the program obtains the required data from the ground motion hazard database. Figure H.5 shows the multiple-scenario sub-tab, and Table H.4 describes the input required to perform multiple-scenario analyses.

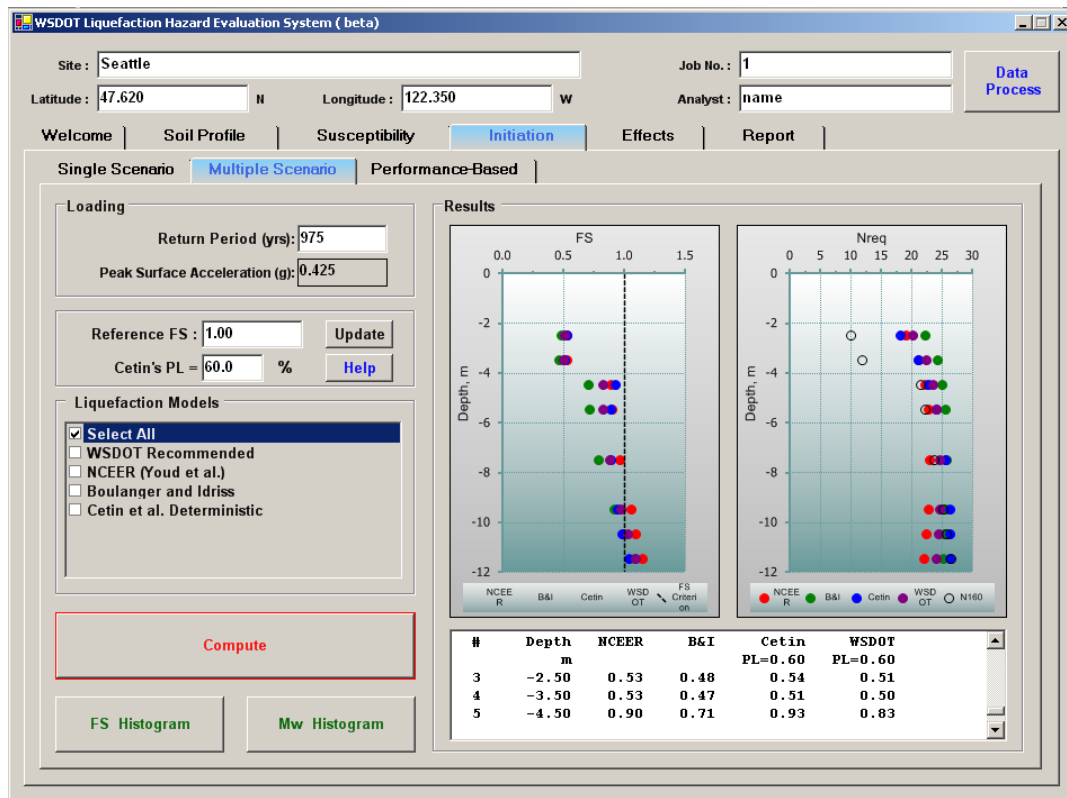


Figure H.5 WSliq Multiple-Scenario Liquefaction Initiation tab.

The results of multiple-scenario analyses are displayed graphically as plots FS_L and N_{req} vs. depth and numerically in tabular form in the window below the plots. The N_{req} plot will also include the *in situ* $(N_1)_{60}$ values for comparison with the computed N_{req} values. Clicking on either of the plots will produce a larger version of the plot. The numerical data can be accessed within the multiple-scenario tab or on the Report tab; they can also be saved on the Report tab.

Table H.4. Required information and buttons on Multiple-Scenario Liquefaction Initiation tab.

Loading Parameter Information	
Item	Comments
Return Period:	Enter the desired return period in years followed by a carriage return to display the corresponding peak ground acceleration.
Additional Input	
Item	Comments
Reference FS:	Enter a factor of safety value of interest. This option plots a line at that factor of safety to allow easy comparison of calculated factors of safety with user-defined criteria.
Cetin's PL:	The probability of liquefaction (P_L) to be used in the Cetin et al. deterministic analysis. A value of 0.6 has been found to produce results similar to the NCEER model at shallow depths.
Liquefaction Models	
Item	Comments
Select All	Select to compute FS_L and N_{req} using the NCEER, Idriss-Boulanger, and Cetin et al. procedures.
WSDOT Recommended	Select to compute FS_L and N_{req} as a weighted average of values given by the NCEER, Idriss-Boulanger, and Cetin et al. procedures. The weighting factors are 0.4, 0.4, and 0.2, respectively.
NCEER Idriss-Boulanger Cetin et al.	Select individually as desired to compute FS_L and N_{req} values.
Buttons	
Item	Comments
Update	Plot the FS criterion, drawing a dashed line at the specified FS value.
Help	Display a brief description of P_L for Cetin's model.
Compute	Computes FS_L and N_{req} with selected procedures.
FS Histogram	Displays a histogram of the computed FS_L values reflecting the variability in magnitudes contributing to the PGA ground motion hazard at a selected return period.
Mw Histogram	Displays a histogram of the magnitudes contributing to the PGA ground motion hazard for a selected return period.

Performance-Based Analyses

Performance-based analyses are also easily performed with WSliq. As discussed in Section 5.6.3, the Cetin et al. liquefaction potential model was used for performance-based analyses. The user is simply required to provide a return period for plotting purposes, and the program obtains the required data from the ground motion hazard

database. Figure H.6 shows the performance-based analysis sub-tab, and Table H.5 describes the input required to perform performance-based analyses.

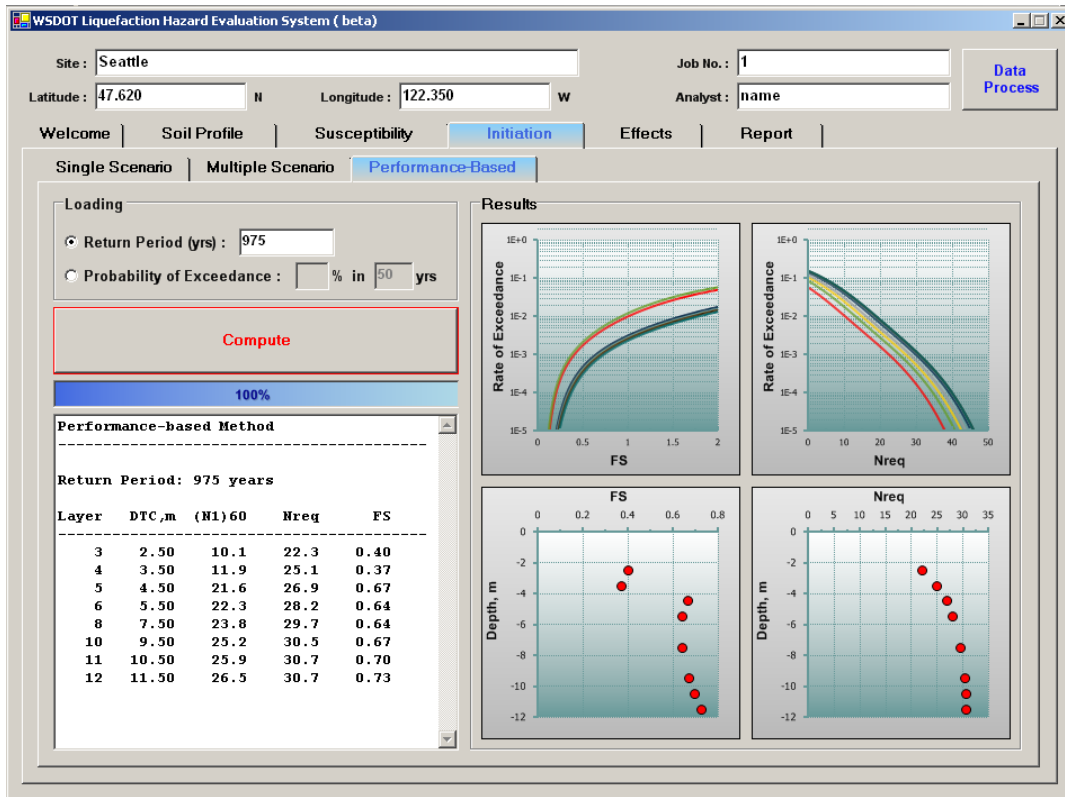


Figure H.6 WSlq Performance-Based Liquefaction Initiation tab.

Table H.5. Required information and buttons on Performance-Based Liquefaction Initiation tab.

Loading Parameter Information	
Item	Comments
Return Period:	Enter the desired return period in years. The return period does not influence the liquefaction hazard curves but is used to produce the FS_L and N_{req} vs. depth profiles.
Exceedance Probability Information	
Item	Comments
Probability of Exceedance:	Select a probability of exceedance and an exposure period of interest. WSliq will plot the results for the corresponding return period. Note that the performance-based calculations are not repeated; rather, the already computed curves are used to obtain the FS_L and N_{req} values at the indicated hazard level.
Buttons	
Item	Comments
Compute	Computes FS_L and N_{req} hazard curves and profiles of FS_L and N_{req} corresponding to the return period of interest. The performance-based calculations are voluminous and will take a couple minutes to complete; a progress bar below the Compute button will display the progress of the calculations. Do not attempt to move to another tab while these calculations are being performed – it could cause the program to crash.

The results of performance-based analyses are displayed graphically as plots of FS_L and N_{req} hazard curves, and plots of FS_L and N_{req} vs. depth for the return period of interest. The results are presented numerically in tabular form in the window below the exceedance probability box. Clicking on any of the plots will produce a larger version of the plot. The numerical data can be accessed within the performance-based tab or on the Report tab; they can also be saved on the Report tab.

Effects Tab

The Effects tab has a series of four sub-tabs that deal with the alteration of ground motions, lateral spreading, post-liquefaction settlement, and the residual strength of liquefied soil. The lateral spreading and post-liquefaction settlements tabs each have three sub-tabs that allow entry of data for single-scenario, multiple-scenario, and performance-based analyses of lateral spreading and settlement.

Response Spectrum

The occurrence of liquefaction is known to alter the temporal and frequency characteristics of ground surface motions. Research on the effects of liquefaction on ground surface motions (which was beyond the scope of the WSDOT-funded study) is continuing at the University of Washington. The preliminary results of that research have been implemented into a simple model for response spectrum modification.

The response spectrum tab allows estimation of a response spectral ratio, defined as the ratio of spectral acceleration from an effective stress analysis (which accounts for pore pressure generation) to the spectral acceleration from a total stress analysis (which does not). The response spectrum produced by a total stress (e.g., SHAKE) analysis can be multiplied by the response spectral ratio to produce an improved estimate of the spectral accelerations that would be produced at a site underlain by potentially liquefiable soils.

This tab provides some general guidance on the anticipated average relationship between the response spectrum with pore pressure effects and the response spectrum without pore pressure effects. Note that the research on which it was based showed high levels of uncertainty in this relationship for specific input motions and soil profiles; interpretation of these results should consider that fact.

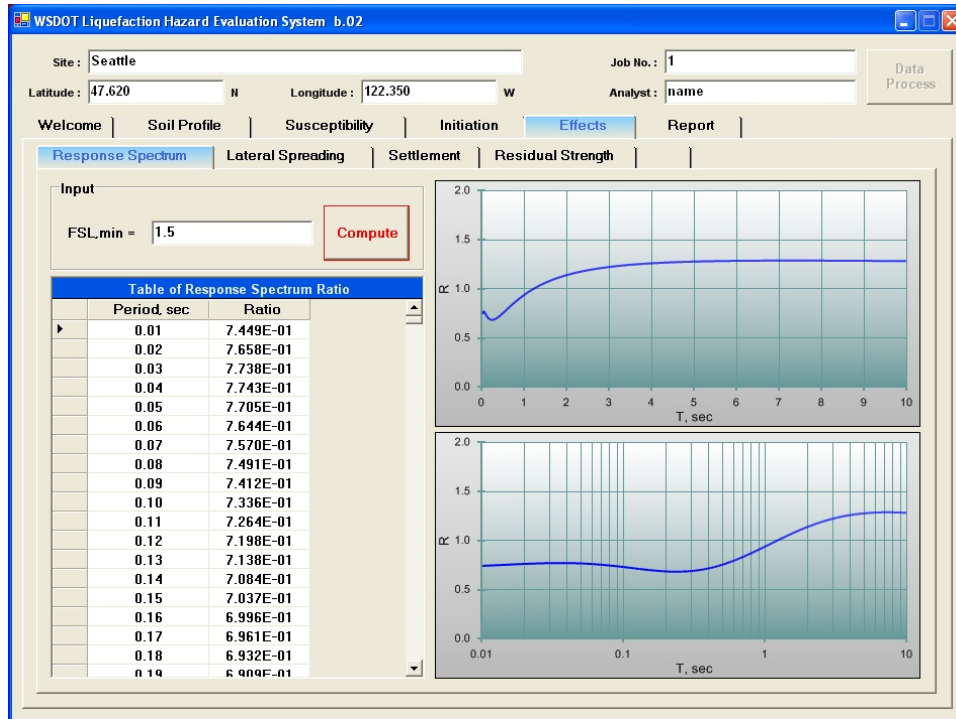


Figure H.6 WSlq Response Spectrum tab.

Table H.5. Required information and buttons on Response Spectrum tab.

Input Information	
Item	Comments
FSL _{min} :	The minimum <i>FS</i> against liquefaction, found from all soil layers.
Buttons	
Item	Comments
Compute	Computes the median response spectral ratio at periods ranging from 0.01 to 1.0 sec.

The results of these analyses show the response spectral ratio plotted on both arithmetic and logarithmic period scales.

Lateral Spreading

The Lateral Spreading tab has a series of three sub-tabs that allow entry of data for single-scenario, multiple-scenario, and performance-based analyses of lateral spreading. Prior to the performance of any lateral spreading analysis, however, it is important to make sure that the ground slope or free-face ratio has been entered on the

Soil Profile tab (Figure H.2). The required data for each type of analysis are described below.

Single-Scenario Analyses

As in the case of Initiation, single-scenario lateral spreading analyses can be performed in two basic ways. Because the inputs to empirical lateral spreading models consist of magnitude and distance, the scenarios are defined by magnitude and distance. Therefore, scenarios can be defined by the user inputting any desired combination of magnitude and distance, or by inputting a particular return period and selecting the corresponding (mean or modal) magnitude and distance values. Figure H.7 shows the single-scenario sub-tab and Table H.6 describes the input required to perform single-scenario analyses.

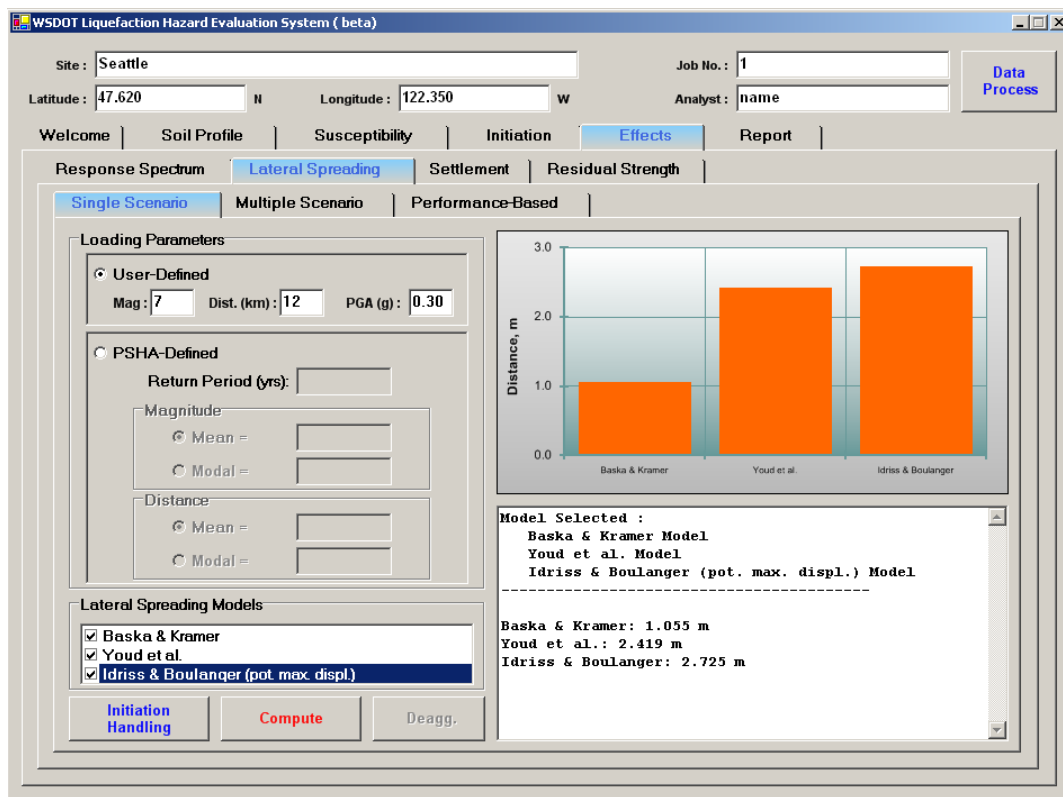


Figure H.7 WSlq Single-Scenario Lateral Spreading tab.

The results of single-scenario analyses are displayed graphically in a bar chart and numerically in tabular form in the window below the plots.

Table H.6. Required information and buttons on Single-Scenario Lateral Spreading tab.

User-Defined Loading Parameter Information	
Item	Comments
Mag.:	Enter the magnitude to be used in the single-scenario analysis.
Dist.:	Enter the distance to be used in the single-scenario analysis in km.
PGA:	Enter the peak ground surface acceleration in g's. Note that this acceleration value, which is used to compute the FS_L value required by the Idriss and Boulanger model, should account for local site conditions (e.g., amplification of rock acceleration values).
PSHA-Defined Loading Parameter Information	
Item	Comments
Return Period:	Enter the desired return period in years, followed by a carriage return (to display the corresponding mean and modal magnitudes and distances). Loading data are interpolated from the ground motion hazard database.
Magnitude:	Select the mean or modal magnitude.
Distance:	Select the mean or modal distance.
Lateral Spreading Models	
Item	Comments
Select All	Select to compute the lateral spreading displacement with the Baska-Kramer, Youd et al., and Idriss-Boulanger procedures.
WSDOT Recommended	Select to compute the lateral spreading displacement as a weighted average of values given by the Baska-Kramer, Youd et al., and Idriss-Boulanger procedures.
Baska-Kramer Youd et al. Idriss & Boulanger	Select individually as desired to compute the lateral spreading displacements. Note that Idriss & Boulanger computes maximum <i>potential</i> displacements.
Buttons	
Item	Comments
Initiation Handling	Allows consideration of the potential for initiation of liquefaction in lateral spreading computations. The user can specify a threshold factor of safety against liquefaction for inclusion/exclusion of individual soil layers, or can choose to have individual layer contributions weighted by the probability of liquefaction.
Compute	Computes the lateral spreading displacement with selected procedures.
Deagg.	Plots the deaggregation of peak ground acceleration by contributions from all magnitudes and distances.

Multiple-Scenario Analyses

Multiple-scenario analyses are easily performed with WSliq. The user is simply required to provide a return period of interest, and the program obtains the required data from the ground motion hazard database. Figure H.8 shows the multiple-scenario sub-tab, and Table H.7 describes the input required to perform multiple-scenario analyses.

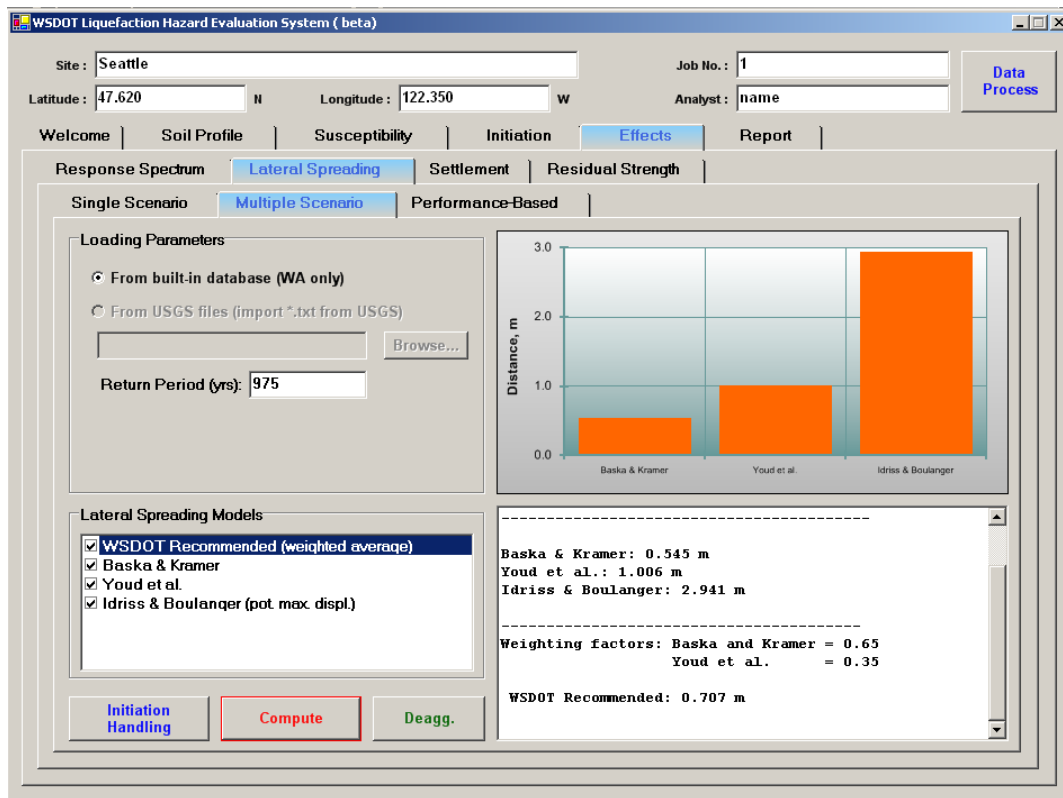


Figure H.8 WSliq Multiple-Scenario Lateral Spreading tab.

The results of multiple-scenario analyses are displayed graphically in a bar chart and numerically in tabular form in the window below the plots. The numerical data can be accessed within the multiple-scenario tab or on the Report tab; they can also be saved on the Report tab.

Table H.7. Required information and buttons on Multiple-Scenario Lateral Spreading tab.

Loading Parameter Information	
Item	Comments
Return Period:	Enter the desired return period in years.
Liquefaction Models	
Item	Comments
WSDOT Recommended	Select to compute the lateral spreading displacement as a weighted average of values given by the Baska-Kramer and Youd et al. procedures. The weighting factors are 0.65 and 0.35, respectively.
Baska-Kramer Youd et al. Idriss & Boulanger	Select individually as desired to compute the lateral spreading displacements. Note that Idriss & Boulanger computes maximum <i>potential</i> displacements.
Buttons	
Item	Comments
Initiation Handling	Allows consideration of the potential for initiation of liquefaction in lateral spreading computations. The user can specify a threshold factor of safety against liquefaction for inclusion/exclusion of individual soil layers, or can choose to have individual layer contributions weighted by the probability of liquefaction.
Compute	Computes the lateral spreading displacement with selected procedures.
Deagg.	Plots the deaggregation of peak ground acceleration by contributions from all magnitudes and distances.

Performance-Based Analyses

Performance-based lateral spreading analyses are also easily performed with WSliq. As described in Section 6.6.3, the Kramer-Baska model is used in performance-based lateral spreading predictions. The program obtains the required data from the ground motion hazard database. Figure H.9 shows the performance-based analysis sub-tab, and Table H.8 describes the input required to perform performance-based analyses.

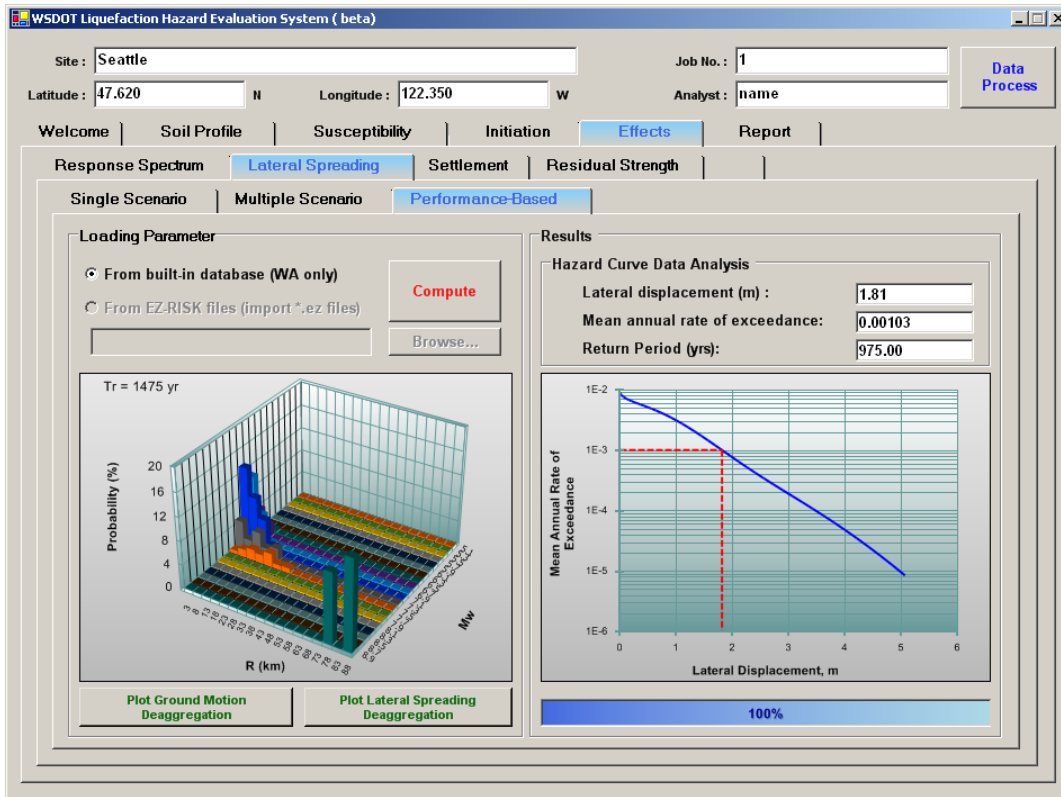


Figure H.9 WSliq Performance-Based Lateral Spreading tab.

The results of performance-based analyses are displayed graphically as a lateral displacement hazard curve. Numerical values of the hazard curve can be obtained by entering data in the text boxes above the hazard curve plot, followed by a carriage return.

Table H.8. Required information and buttons on Performance-Based Lateral Spreading tab.

Loading Parameter Information	
Item	Comments
Loading Parameter	Enter the source of ground motion hazard data. For sites in Washington, the built-in database should be used.
Results	
Item	Comments
Lateral displacement:	Enter a lateral spreading displacement value, followed by a carriage return, to obtain the corresponding mean annual rate of exceedance and return period from the hazard curve.
Mean Annual Rate of Exceedance:	Enter a mean annual rate of exceedance value to obtain the corresponding lateral spreading displacement and return period from the hazard curve.
Return Period:	Enter a return period to obtain the corresponding lateral spreading displacement and mean annual rate of exceedance from the hazard curve.
Buttons	
Item	Comments
Compute	Computes the lateral displacement hazard curve.
Plot Ground Motion Deaggregation	Plots the deaggregation of peak ground acceleration by contributions from all magnitudes and distances.
Plot Lateral Spreading Deaggregation	Plots the deaggregation of lateral spreading displacement by contributions from all magnitudes and distances.

Settlement

The Settlement tab has a series of three sub-tabs that allow entry of data for single-scenario, multiple-scenario, and performance-based analyses of post-liquefaction settlement. The required data for each type of analysis are described below.

Single-Scenario Analyses

As in the case of Initiation, single-scenario settlement analyses can be performed in two basic ways. Because the loading-related input to lateral spreading models is in the form of cyclic stress ratio, the scenarios are defined by peak acceleration and magnitude. Therefore, scenarios can be defined by the user inputting any desired combination of peak acceleration and magnitude, or by inputting a particular return period and selecting the corresponding (mean or modal) magnitude value. Figure H.10 shows the single-

scenario sub-tab, and Table H.9 describes the input required to perform single-scenario analyses.

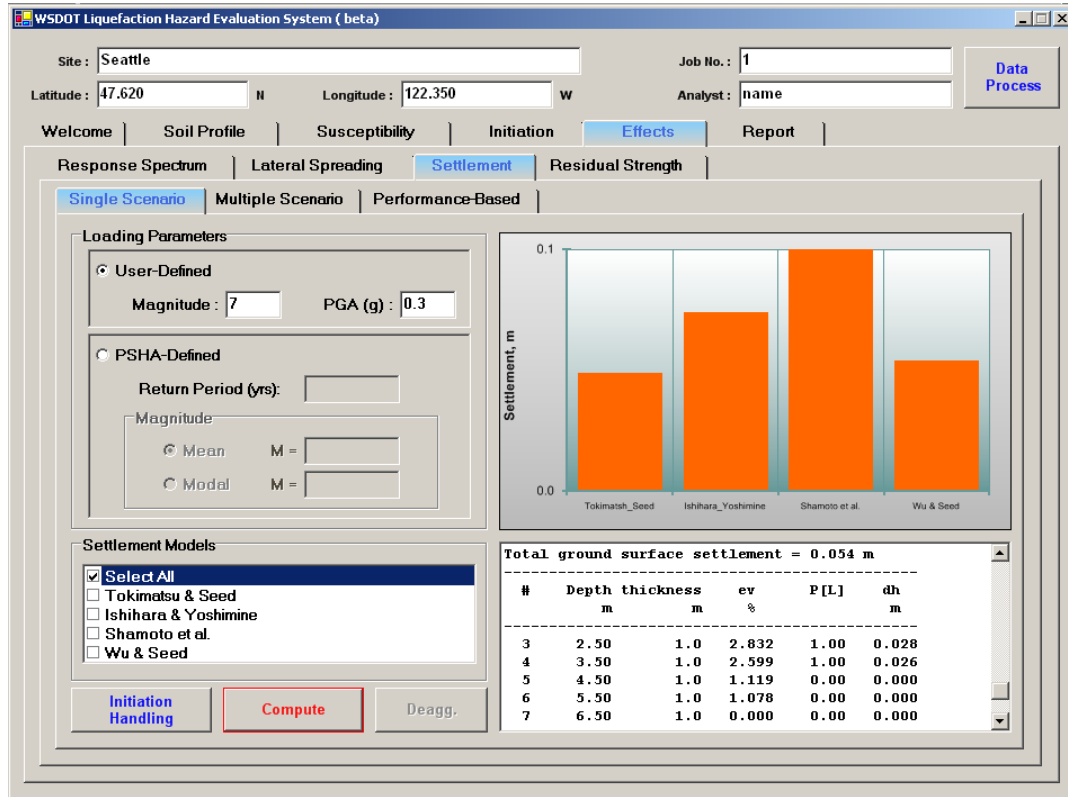


Figure H.10 WSliq Single-Scenario Settlement tab.

The results of single-scenario analyses are displayed graphically in a bar chart and numerically in tabular form in the window below the plots. The numerical data can be accessed within the single-scenario tab or on the Report tab; they can also be saved on the Report tab.

Table H.9. Required information and buttons on Single-Scenario Settlement tab.

User-Defined Loading Parameter Information	
Item	Comments
Magnitude:	Enter the magnitude to be used in the single-scenario analysis.
PGA:	Enter the peak ground surface acceleration in g's. Note that this acceleration value should account for local site conditions (e.g., amplification of rock acceleration values).
PSHA-Defined Loading Parameter Information	
Item	Comments
Return Period:	Enter the desired return period in years, followed by a carriage return (to display the corresponding mean and modal magnitudes and distances). Loading data are interpolated from ground motion hazard database.
Magnitude:	Select the mean or modal magnitude.
Settlement Models	
Item	Comments
Select All	Select to compute the lateral spreading displacement with the Tokimatsu-Seed, Ishihara-Yoshimine, Shamoto et al., and Wu-Seed procedures.
Tokimatsu-Seed Ishihara-Yoshimine Shamoto et al. Wu-Seed	Select individually as desired to compute lateral spreading displacements.
Buttons	
Item	Comments
Initiation Handling	Allows consideration of the potential for initiation of liquefaction in settlement computations. The user can specify a threshold factor of safety against liquefaction for inclusion/exclusion of individual soil layers, or can choose to have individual layer contributions weighted by the probability of liquefaction.
Compute	Computes the settlement using selected procedures.
Deagg.	Plots the deaggregation of peak ground acceleration by contributions from all magnitudes and distances.

Multiple-Scenario Analyses

Multiple-scenario analyses are easily performed with WSliq. The user is simply required to provide a return period of interest, and the program obtains the required data from the ground motion hazard database. Figure H.11 shows the multiple-scenario sub-

tab, and Table H.10 describes the input required to perform multiple-scenario settlement analyses.

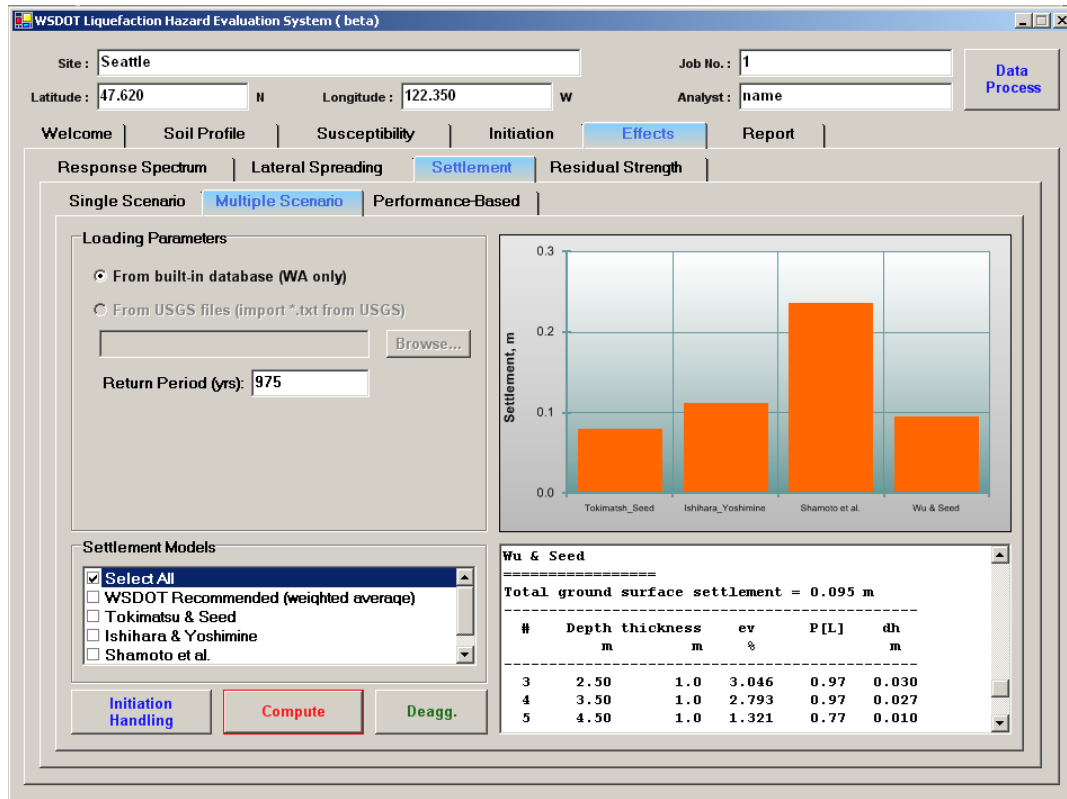


Figure H.11 WSliq Multiple-Scenario Settlement tab.

The results of multiple-scenario analyses are displayed graphically in a bar chart and numerically in tabular form in the window below the plots. The numerical data can be accessed within the multiple-scenario tab or on the Report tab; they can also be saved on the Report tab.

Table H.10. Required information and buttons on Multiple-Scenario Settlement tab.

Loading Parameter Information	
Item	Comments
Return Period:	Enter the desired return period in years.
Liquefaction Models	
Item	Comments
Tokimatsu-Seed Ishihara-Yoshimine Shamoto et al. Wu-Seed	Select individually as desired to compute the post-liquefaction settlements.
WSDOT Recommended	Select to compute the settlement as a weighted average of values given by all four procedures. The values are weighted equally.
Buttons	
Item	Comments
Initiation Handling	Allows consideration of the potential for initiation of liquefaction in settlement computations. The user can specify a threshold factor of safety against liquefaction for inclusion/exclusion of individual soil layers, or can choose to have individual layer contributions weighted by the probability of liquefaction.
Compute	Computes the settlement using selected procedures.
Deagg.	Plots the deaggregation of peak ground acceleration by contributions from all magnitudes and distances.

Performance-Based Analyses

Performance-based post-liquefaction settlement analyses are also easily performed with WSliq. As discussed in Section 7.6.3, the Wu and Seed model was used to develop the performance-based model. The Wu and Seed model was modified, however, to include a limiting volumetric strain for the performance-based settlement calculations. The program obtains the required data from the ground motion hazard database. Figure H.12 shows the performance-based analysis sub-tab, and Table H.11 describes the input required to perform performance-based analyses.

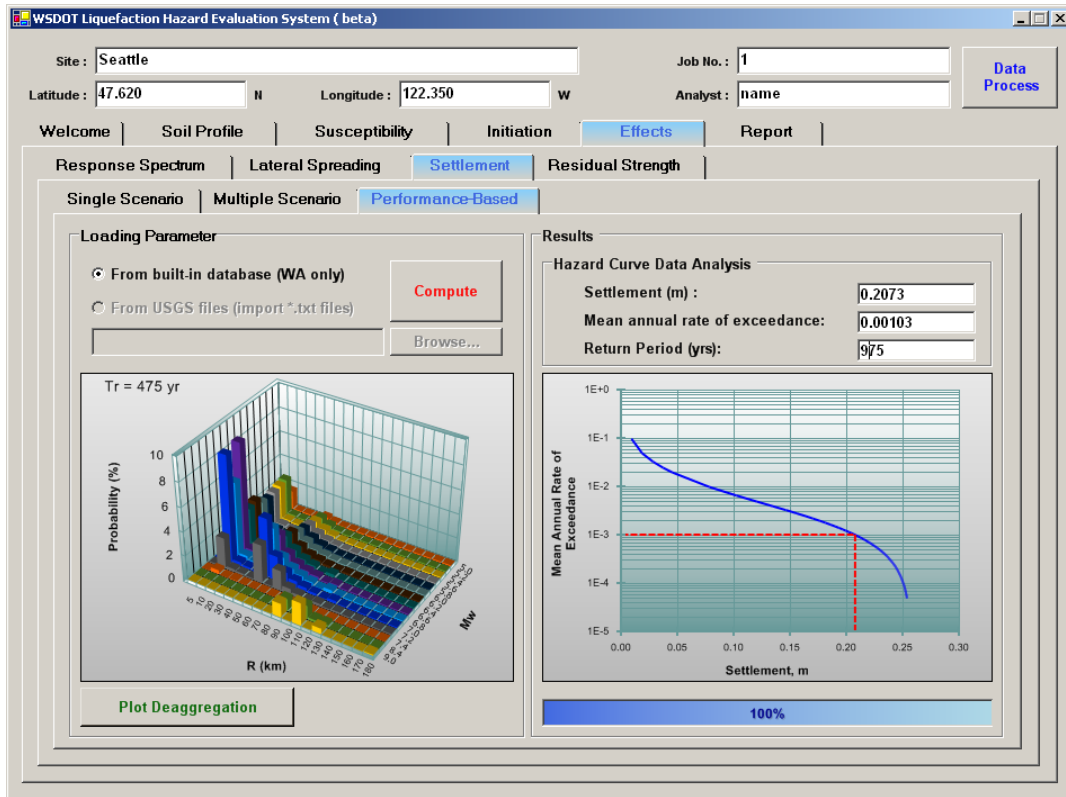


Figure H.12 WSlq Performance-Based Settlement tab.

The results of performance-based analyses are displayed graphically as a lateral displacement hazard curve. Numerical values of the hazard curve can be obtained by entering data in the text boxes above the hazard curve plot, followed by a carriage return.

Table H.11. Required information and buttons on Performance-Based Settlement tab.

Loading Parameter Information	
Item	Comments
Loading Parameter	Enter the source of the ground motion hazard data. For sites in Washington, the built-in database should be used.
Results	
Item	Comments
Settlement:	Enter a settlement value, followed by a carriage return, to obtain the corresponding mean annual rate of exceedance and return period from the hazard curve.
Mean Annual Rate of Exceedance:	Enter a mean annual rate of exceedance value to obtain the corresponding settlement and return period from the hazard curve.
Return Period:	Enter a return period to obtain the corresponding settlement and mean annual rate of exceedance from the hazard curve.
Buttons	
Item	Comments
Compute	Computes the settlement hazard curve.
Plot Deaggregation	Plots the deaggregation of settlement by contributions from all magnitudes and distances.

Residual Strength

WSliq allows estimation of residual strength by using a variety of residual strength models and allows the computation of a user-defined weighted average residual strength. Figure H.13 shows the residual strength tab, and Table H.12 describes the input required to estimate residual strength.

The results of residual strength analyses are displayed graphically as plots of residual strength vs. depth and numerically in tabular form in the window below the plots. The residual strength plots use solid circles to represent strengths based on corrected SPT resistances that are within the range of each model, and open circles for strength values extrapolated to higher SPT resistances. Extrapolated strengths should be interpreted carefully. The numerical data can be accessed within the Residual Strength tab or on the Report tab; they can also be saved on the Report tab.

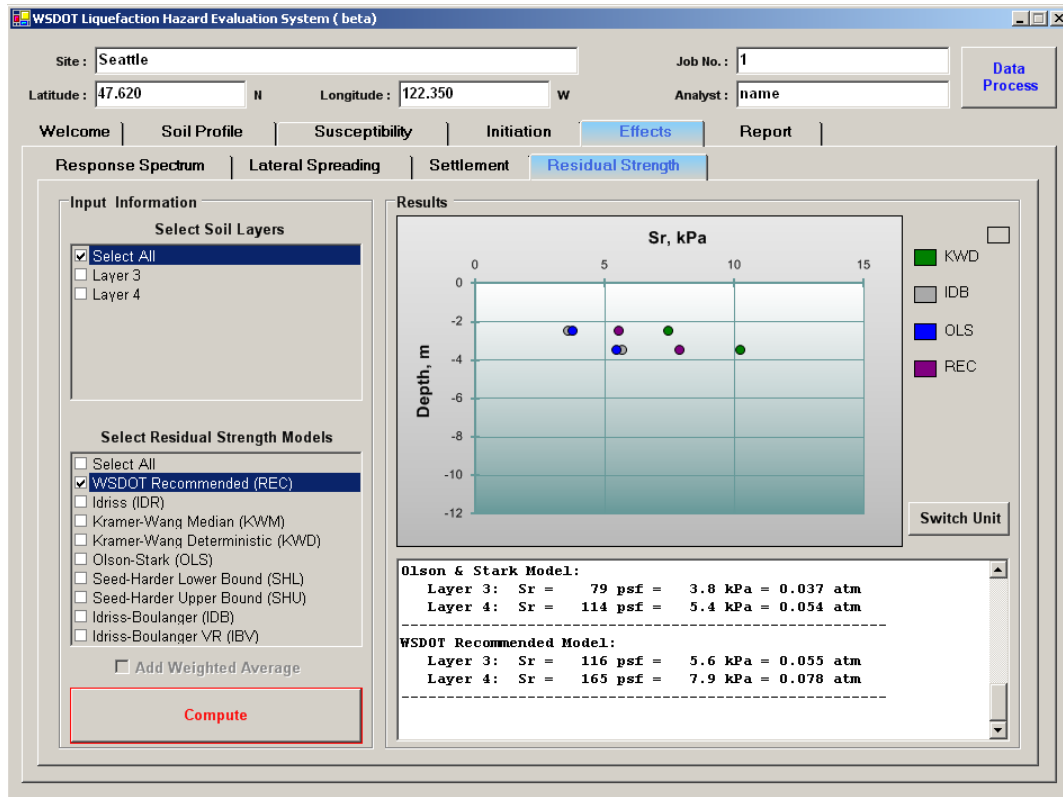


Figure H.13 Residual Strength tab.

Table H.12. Required information and buttons on Residual Strength tab.

Input Information	
Item	Comments
Select Soil Layers	Check boxes corresponding to the layers for which estimated residual strengths are desired. Only layers that liquefy are considered.
Select Residual Strength Models	Check boxes corresponding to the models for which estimated residual strengths are desired. Checking the WSDOT Recommended box will produce results for the Idriss, Kramer-Wang hybrid, and Olson-Stark models, as well as the weighted average (Table 8.2) of those results.
Add Weighted Average	Check to apply user-defined weighting factors for residual strength estimation.
Buttons	
Item	Comments
Compute	Computes the residual strength using selected procedures.
Legend	The legend immediately to the right of the residual strength plots is interactive – clicking on any of the boxes that indicate the color of each residual strength model will highlight the results of that model. Clicking on the blank box above and to the right of the legend will clear all highlighted curves
Switch Unit	Toggles residual strength units between kPa and psf.

Report Tab

The Report tab provides the means for documenting the results of WSliq analyses in a simple text file. As shown in Figure H.14, the Report tab contains a series of check boxes for each of the various analyses that can be performed with WSliq. By selecting the desired check boxes, the user can write the results of the corresponding analyses to an RTF (rich text file) file. These data can then be further processed by using spreadsheets or other graphics programs. Copies of the plots generated by WSliq are also written directly to the file, from which they can be copied and pasted into other documents.

The screenshot shows the 'Report' tab of the WSDOT Liquefaction Hazard Evaluation System (beta). The interface includes a header with site information (Seattle, Job No. 1, Analyst: name) and a 'Data Process' button. Below the header are tabs for 'Welcome', 'Soil Profile', 'Susceptibility', 'Initiation', 'Effects', and 'Report'. The 'Report' tab is active and contains several sections:

- Report:** A list of analyses with checkboxes: Soil Profile, Susceptibility Index, Initiation, and Effects.
- Initiation:** A sub-section with checkboxes: Select All, Single Scenario, Multiple Scenario, and Performance-Based.
- Lateral Spreading:** A sub-section with checkboxes: Select All, Single Scenario, Multiple Scenario, and Performance-Based.
- Settlement:** A sub-section with checkboxes: Select All, Single Scenario, Multiple Scenario, and Performance-Based.
- Effects:** A sub-section with checkboxes: Select All, Response Spectrum, Lateral Spreading, Settlement, and Residual Strength.
- Report File:** A section with a text box for 'Report File Name' (Results.txt) and a 'Save to' field (C:\) with an 'OPEN' button.
- Buttons:** A large 'Generate Report' button and a smaller 'Preview' button.
- Status Log:** A text area on the right showing progress: 'Checking folders...', 'Checking report file...', 'Soil Profile data is done...', 'Susceptibility Index is done...', 'Initiation: Multiple Scenario text is done...', 'Lateral Spreading text is done...', 'Settlement text is done...', and 'Report is done.'

Figure H.14 Report tab.

Table H.13. Required information and buttons on Report tab.

Buttons	
Item	Comments
Generate Report	Generates a report file based on the selected text, picture, and file format options.
Preview	Opens a report in a small window (Figure H.15).

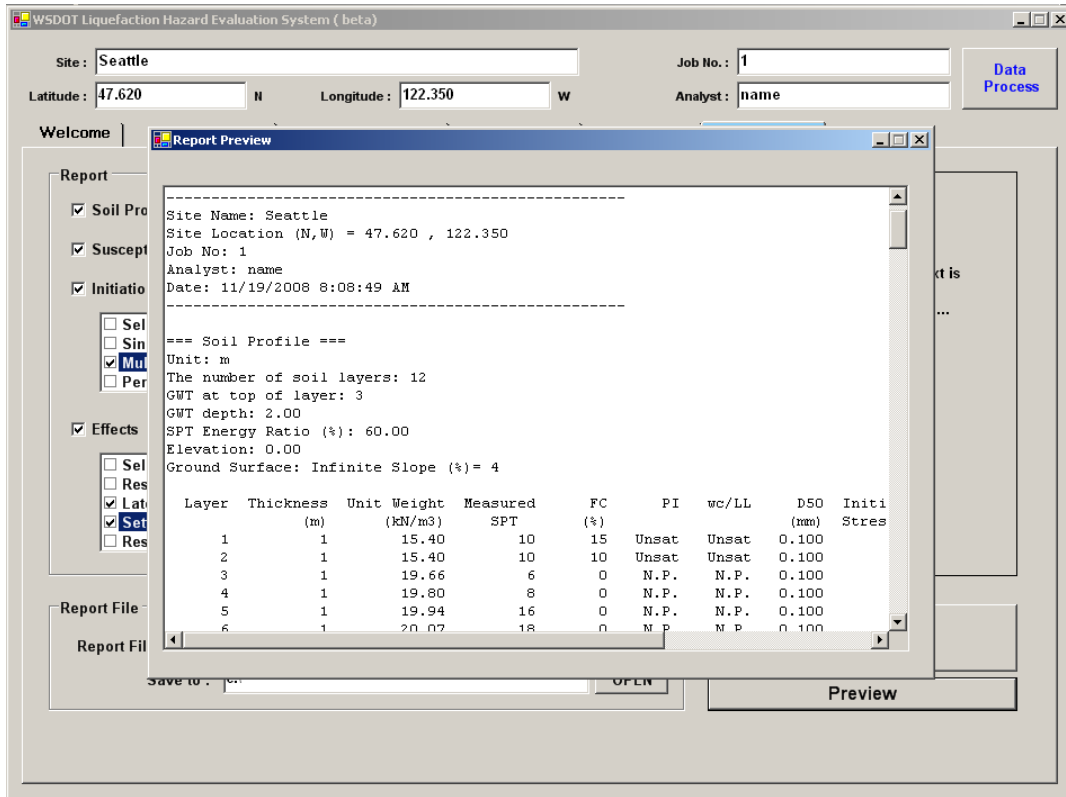


Figure H.15 Report Preview window.

Appendix I

WSliq Database Update Instructions

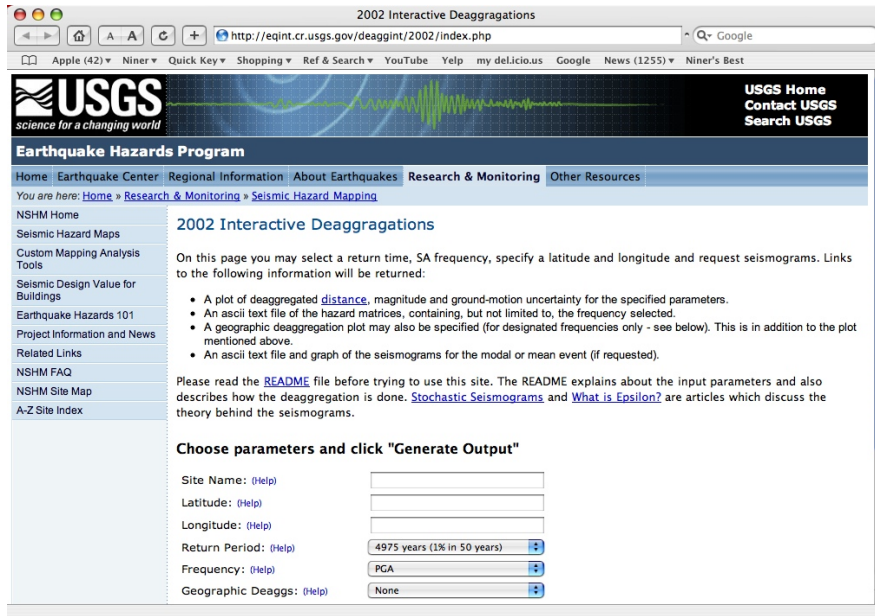
The seismic hazard database that comes with the WSliq program was created by downloading seismic hazard data on a grid across Washington State from the USGS website. When a user enters an arbitrary latitude and longitude, the program interpolates the seismic hazard data for the site of interest by using an inverse distance weighting procedure (i.e one in which the contributions of the nearby grid points are weighted in inverse proportion to their distance from the site).

For particularly important projects, and for projects near faults where seismicity may change rapidly over relatively short distances, more accurate results may be produced by downloading data for the site latitude and longitude and adding them to the database. Also, the USGS hazard mapping procedures change periodically, for example when new attenuation relationships are developed or when new sources are added, so that it may be necessary to update the database. This appendix provides instructions for expanding and/or updating the seismic hazard database.

Two procedures are required to update the seismic hazard database for the *WSliq* analysis program. The first procedure involves downloading the raw seismic hazard data from the USGS website, and the second one imports the downloaded files to the WSliq seismic hazard database.

Downloading USGS Files

1. Go to the 2002 Interactive Deaggregations page at the USGS Seismic Hazard Mapping website. (<http://eqint.cr.usgs.gov/deaggint/2002/index.php>). As of the date of this report, the following page will appear.



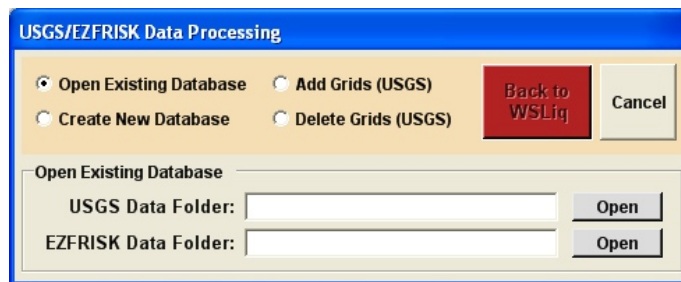
2. Input the site info in the corresponding text boxes. The site latitude and longitude must be input in decimal format (two digits), and the longitude is a negative number for locations in America. A convenient latitude and longitude converter (from degree-minute-second to decimal degrees) can be found at <http://www.fcc.gov/mb/audio/bickel/DDMMSS-decimal.html>
3. Choose one Return Period of interest. There are six return periods from which to choose, and this process will be repeated for each.
4. Set the Frequency selection to 'PGA.'
5. Leave the last two options (Geographic Deaggs and Stochastic Seismograms) as their defaults.
6. Press the Generate Output button to produce the deaggregation file.
7. A new Web page will appear. Click on the link for Report, and a text file will open in the web browser. Save this file (use File --> Save As) in a temporary folder on your hard drive with the specific filename determined by using the following rules:
 - a. The file has the name "Latitude_Longitude_xx.txt" (underscore characters required).
 - b. The 'Latitude' and 'Longitude' in the filename should be replaced with the numerical coordinates corresponding to the site's location, and 'xx' should be replaced by the 50-year exceedance probability (to identify the return period). The table below indicates the required 'xx' values.

Value of xx	Return Period, yr
01	4975 (1% in 50 yrs)
02	2475 (2% in 50 yrs)
05	975 (5% in 50 yrs)
10	475 (10% in 50 yrs)
20	225 (25% in 50 yrs)
50	108 (50% in 75 yrs)

- c. For example, if the site of Test #1 is located at (47.53N, 122.50W), and the deaggregation data correspond to a return period of 4975 years, then the data should be saved in a file called: 47.53_122.50_01.txt . Save this file to a temporary folder (e.g., “NewGrid”) on the hard drive.
8. Repeat steps 3 through 8 for all other return periods. For each location, six deaggregation data files will be downloaded and saved to the hard drive.

Importing and Processing USGS Files

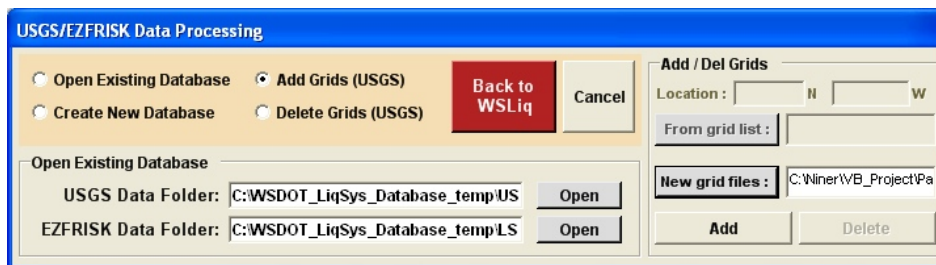
1. Open the WSLiq program. The button labeled “Data Process” in the upper-right corner will do the work of importing the new deaggregation files created in last procedure.
2. If the button is not active (not shadowed), it means that the Washington database has been installed in the default location (c:\WSDOT_LiqSys_Database) or the database is installed at the location given in the “DatabasePath.txt” file defined during installation (See the ReadMe file when downloading the WSLiq program). Simply move the database folder to a different hard drive, or change the folder’s name, then close WSLiq and re-open it. This will activate the Data Process button.
3. Click the Data Process button. A Data Processing window will pop up. This window provides the option to add the new grid points (downloaded in the previous procedure) to the database.



4. Select “Add Grids (USGS)” in the USGS/EZFRISK Data Processing window.



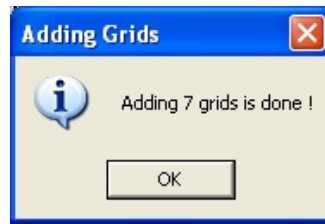
5. Assign the data folder of the existing database under the USGS Data Folder: in the Open Existing Database area of the window. This should be the folder you moved (or named) in Step 2.
6. In the Add/Del Grids panel, click on “New grid files”. A folder browser will pop up. Choose the folder in which you saved the downloaded USGS files (the temporary folder in Step 7 of the previous procedure). **Note: just choose the folder, not the file itself.**



7. Click the Add button and the program will process the USGS files and add the new grid points into the Washington database. If the database has the same grid points as the ones you try to add, a warning message will appear and ask if you want to overwrite the data with the new files.



8. When the “Adding grids is done” message pops up, the data processing job is finished. Click OK to close the message.



9. Click the Back to WSLiq button to go back to the WSLiq program.

